UNIVERSITY OF SOUTHAMPTON

FACULTY OF ENGINEERING AND THE ENVIRONMENT

School of Civil Engineering and the Environment

The influence of suction changes on the stiffness of railway formation

by

Louise Otter, B.Eng

A thesis submitted in partial fulfillment of the degree of Doctor of Philosophy
in the Faculty of Engineering and Environment
at the University of Southampton

December 2011

For my parents and brother

UNIVERSITY OF SOUTHAMPTON

ABSTRACT

FACULTY OF ENGINEERING AND ENVIRONMENT
School of Civil Engineering and the Environment

Doctor of Philosophy

THE INFLUENCE OF SUCTION CHANGES ON THE STIFFNESS OF RAILWAY FORMATION

by Louise Otter

Despite compacted soils being unsaturated, geotechnical design is predominantly based on saturated soils, despite it being known that differences exist between the behaviour of saturated and unsaturated soils. Suction in soils has been shown to increase its strength and stiffness with the increase dependent on the degree of suction, soil type and particle arrangement. Future climate change predictions suggest an increase in average global temperatures leading to longer drier summers and wetter winters resulting in seasonal fluctuations in suction, such that unsaturated soil behaviour will become more important.

Transport infrastructure such as railway tracks, founded at shallow depths, are likely to be unsaturated and influenced by variations in suction. A key parameter in assessing the performance of soils is stiffness; in particular shear modulus, however, although suction affects shear modulus, limited research has been conducted into its influence. This research, therefore, considers how variations in suction influence the small strain shear modulus of railway formation material.

Soil water characteristic curves were determined, using the pressure plate apparatus and filter paper technique, for four materials covering the spectrum of railway formation materials encountered on the COALlink line in South Africa. Shear modulus measurements of specimens prepared from two of these materials were determined using a Stokoe resonant column apparatus. Suction was controlled by preparing specimens at different water contents, with the suction independently measured using the filter paper technique.

Results showed that shear modulus was significantly influenced by suction and exhibited a complex behaviour. For specimens tested at their preparation water content shear modulus increased with increasing suction up to an optimum value, and then reduced as suctions exceeded this optimum value forming a bell-shaped curve. The influence of suction was seen to be greater at lower net normal stresses. Although this behavioural pattern was similar for both materials tested in the resonant column apparatus, the peak value of shear modulus increased with clay content. Importantly, the marked changes in shear modulus due to suction coincided with the suction range predicted in-situ.

Tests were also conducted on specimens prepared at different water contents but the same density, air-dried to very low water contents. The shear moduli of these air dried specimens were markedly higher than those of the dry and unsaturated specimens tested at their preparation water contents. Variation in measured shear modulus between specimens led to the conclusion that different particle arrangements between the specimens may have also contributed to the changes in shear modulus and were dependent on the preparation water content. At high water contents the clay particles became evenly distributed around the sand particles when the specimen was prepared, whilst, at low water contents the clay formed lumps during preparation of the material mix and became embedded with the sand particles during formation. CT scanning undertaken to look at the particle arrangement highlighted regions throughout the specimen where sand particles were embedded in lumps of clay and silt particles.

These results are the first to demonstrate the importance of suction and its variation on the small strain shear modulus behaviour of railway formation material.

Content

List of Tables

List of Figures

List of Symbols

a, n, m	curve fitting parameters
d	specimen diameter
e	void ratio
f_r	resonant frequency
g	gravitational acceleration at the earth's surface
i	hydraulic gradient
k	coefficient of permeability
k	stiffness
k_a	top platen stiffness
$k_{equipment}$	equipment stiffness
$k_{specimen}$	specimen stiffness
k_{stem}	central stem stiffness
q	volumetric flow rate of water
r	radius of specimen
r_s	radius of curvature
$s, s*$	soil water characteristic curve fitting descriptors
u_a	pore air pressure
u_c	material viscosity
u_w	pore water pressure
$\bar{u}_v$	partial pressure of pore water vapour
$\bar{u}_{vo}$	saturation of pore water over a flat surface of pure water at room temperature
v_{w0}	specific volume of water
w	water content
w_1	mass of flask and disc
w_2	mass of flask, disc and dry soil
w_3	mass of flask, disc, dry soil and water
w_4	mass of flask, disc and water
x	distance to accelerometer from central axis of specimen

A	cross sectional area of flow
Acc	acceleration amplitude
G	shear modulus
G_0	maximum shear modulus
G_s	specific gravity
G_T	specific gravity of distilled water
I	mass polar moment inertia
I_a	mass polar moment of top platen
I_{am}	mass polar moment of added masses
I_0	mass polar moment of the drive plate
I_p	polar moment of inertia
L	length of specimen
M_1	mass of the wet specimen and weighing container
M_2	mass of the dried specimen and weighing container
M_3	container mass
R	universal gas constant
Sr	degree of saturation
T	absolute temperature
T_r	torque
T_s	surface tension
V_{RMS}	root mean squared voltage
V_s	shear wave velocity
γ	shear strain
ΔN	change in capillary force
θ	angle of rotation
θ_r	residual water content
θ_s	saturation water content
θ_w	water content
λ	pore size distribution index
π	osmotic suction
ρ	specimen density
σ	total normal stress
σ'	effective stress
χ	Bishop's (1959) material parameter
ψ	total suction
ψ_i	suction at inflection point

ψ_p	soil water characteristic curve fitting descriptor
ψ_r	suction at residual water content
ω_d	damped natural frequency
ω_n	natural circular frequency
ω_v	molecular mass of water vapour
$\frac{\partial^2\theta}{\partial t^2}$	angular acceleration
$\frac{\partial\theta}{\partial x}$	angular of twist

List of abbreviations

AEV	air entry value
CT	computerised tomography
LB	Leighton Buzzard (sand)
LVDT	linear variable differential transformer
SWRC	soil water retention curve
SWCC	soil water characteristic curve
U.K.	United Kingdom

Declaration of Authorship

I, Louise Otter declare that this thesis, **'The influence of suction changes on the stiffness of railway formation'**, and the work presented in it are my own and has been generated by me as the result of my own original research. I confirm that:

- This work was done wholly or mainly while in candidature for a research degree at this University;
- Where any part of this thesis has previously been submitted for a degree or any other qualification at this University or any other institution, this has been clearly stated;
- Where I have consulted the published work of others, this is always clearly attributed;
- Where I have quoted from the work of others, the source is always given. With the exception of such quotations, this thesis is entirely my own work;
- I have acknowledged all main sources of help;
- Where the thesis is based on work done by myself jointly with others, I have made clear exactly what was done by others and what I have contributed myself;
- None of this work has been published before submission.

Signed:……

Date:……

Acknowledgements

In order to complete this project the author would like to thank and recognise the following people:

I would like to thank my parents for all their love and support, their belief in a good education, to aim for the seemingly impossible, and teaching me never to give up. My brother for doing what brothers do and always making me laugh.

My supervisors Prof. Christopher Clayton and Dr. Jeffery Priest for providing this opportunity, their knowledge, guidance and advice, perseverance with my writing skills and pushing me to succeed and always improve.

Harvey Skinner for his help in the laboratory and patience whilst teaching me basic DIY. Karl Scammell who definitely will not miss searching for American fittings, and the other members of the laboratory technical team.

Andrew Ridley (Geotechnical Observations) for his advice and undertaking tensiometer measurements.

Iain Sinclair, Dmitry Grinev and Mark Mavrogordato with all their help and guidance with CT scanning.

Jane Warren for also helping improve my writing skills.

My friends for listening, distracting me and for some great times.

For financial support I would like to thank EPSRC (Engineering and Physical Sciences Research Council) where the funding formed part of Rail Research UK and the School of Civil Engineering and the Environment (University of Southampton).

Chapter 1

Introduction

1.1 Background

Saturated and unsaturated soils are known to behave differently due to the development of suction within unsaturated soils. Dependent on the magnitude of this suction, increases in strength and stiffness of the soil is likely to occur (Vanapalli et al., 1998, Mancuso et al., 2002). Geotechnical design currently considers the soil as saturated, but unsaturated soils cover about a third of the earth's surface and during dry periods most soils located close to the surface (Fredlund and Rahardjo, 1993). By not considering the unsaturated state, geotechnical designs may be too conservative adding unnecessary cost. Furthermore, behavioural changes in the soil from suctions due to seasonal fluctuations, and its implications may not be fully understood nor considered.

Understanding unsaturated soil behaviour will become increasingly important in the future, owing to predictions of increasing global temperatures which are likely to result in lower water table levels, increasing the global distribution of unsaturated soils (IPCC, 2007). In the U.K., current climate change predictions will result in longer drier summers and more intense rainfall in the winter (Murphy et al., 2009). This could lead to saturation of soils in winter, and unsaturated conditions in summer months. Therefore understanding the influence of suction (degree and variation) on soil behaviour is important.

Infrastructure, such as road and rail pavements, is fundamental to a country's economy through providing a reliable means of transporting goods or personnel. As pavements are located at shallow depths, usually above the water table, or at ground level, and are constructed of engineered soil, they are likely to be in an unsaturated state and are therefore likely to be influenced by suction. It is therefore important to understand if variations in suction are detrimental to the structural performance, since temporary closures or speed restrictions may have to be implemented to allow remedial action.

Railway pavements are a special case: as they do not have an impermeable top layer, their variations in water content, and hence suction, are likely to be greater than other pavement infrastructure. They comprise two distinct parts (Figure 1.1): the superstructure (rails, sleepers and fasteners) and the substructure (ballast, sub-ballast and subgrade levels), each having a significant role in distributing the applied load and maintaining structural integrity (Selig and Waters, 1994). Both Selig and Waters (1994) and Gräbe (2002) suggest that substructure is the most important factor in regard to infrastructure cost, but is the least understood. Subgrade failure, although relatively uncommon, can be potentially serious and costly, requiring closure of the line to repair or rebuild the track. This is also costly to the wider economy.

A commonly used parameter to assess structural performance is stiffness (specifically resilient modulus in pavement (Brown, 1996)) (Clayton et al., 2006). Research by Gräbe (2002) on saturated specimens replicating railway formation found that the stiffness determined in the laboratory was less than that back-calculated from field monitoring. It was hypothesised that this may be due to the influence of suction in the field. Therefore, research is needed to understand the influence of suction and its variation on the behaviour of railway infrastructure, thus leading to better understanding of in-situ soil behaviour. Implementation of preventative measures and altered maintenance regimes, could lead to significant cost savings. Additionally, this research also contributes to the wider understanding of unsaturated soils and the influence of suction on stiffness behaviour.

1.2 Research aim and methodology

The aim of this research was, therefore, to understand the influence of suction changes on the stiffness of railway pavements. The focus was on the behaviour of the substructure (formation layers), due to its importance in maintaining tack geometry and adequate ride quality, and the cost and difficulty of undertaking remedial action in this region.

This aim was met through laboratory testing of reconstituted specimens of four materials representative of railway formation. Gräbe (2002) formulated these material mixes to represent the formation material found on the COALlink line in South Africa. Completed in the 1970s, this heavy haul coal export line running from Broodsnyerplass to Richards Bay transports over 60 million tonnes per year with a maximum axle load of 26tonnes/axles (Gräbe, 2002). Importantly these material mixes are also representative of formation material found on other lines (Selig and Waters, 1994, Indraratna and Wadud, 2005).

Stiffness was determined using a resonant column apparatus. Although the resonant column was initially adapted to control and vary a specimen's suction, suction was controlled by varying the specimens' preparation water content. In order to understand the influence of suction changes with water content, the soil water characteristic curves were determined for each material. As the research developed, it became clear that the stiffness and suction relationship was highly dependent on particle arrangement. Therefore, tests were conducted to see if there was variation in particle arrangements between specimens of a given material constructed at different water contents but to the same density. CT-scanning was also used to see if the specimen preparation procedure led to density variation.

1.3 Thesis overview

Chapter One gives a brief background as to why considering the unsaturated soil state is important especially with current climate change predictions. Focusing on its influence to infrastructure, particularly railway pavements. It then details how this lead to this research project, the research aim and the methodology followed.

Chapter Two presents a comprehensive literature review. This firstly details the basic concepts of unsaturated soils, and the techniques for measuring suction. A research summary of small strain shear modulus of unsaturated soil is given, and then other factors which can influence the shear modulus are described.

Chapter Three describes the laboratory equipment and test methodology. Along with the properties of the materials tested.

Chapter Four presents and discusses the experimental results. It includes the implications of these findings to railway formation and current understanding of unsaturated soil behaviour.

Chapter Five draws the findings of this research together, presenting the conclusions and suggesting areas requiring further research.

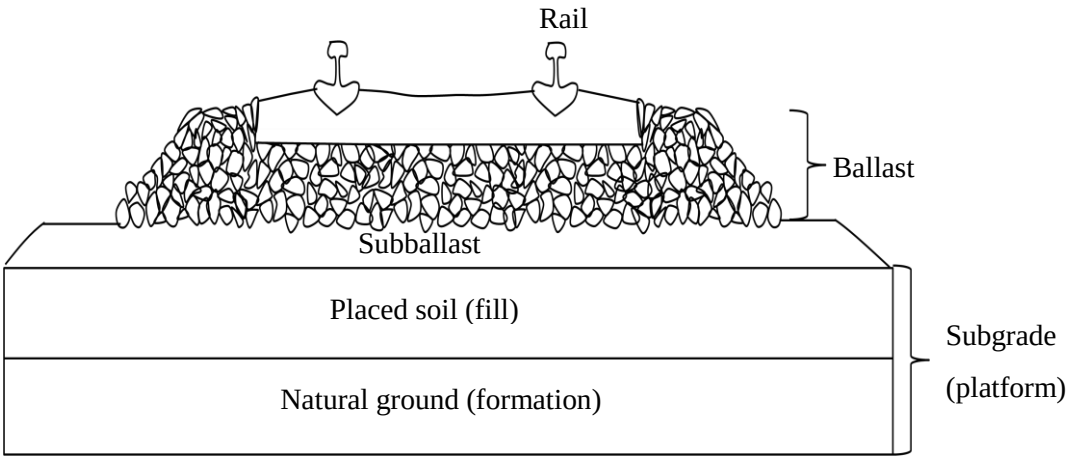

Figure 1.1: Components of railway pavement. Redrawn from Selig and Waters (1994).

Chapter 2

Literature Review

Unsaturated soil refers to a soil which comprises three phases. The solid phase, which is the soil particles, and the liquid and gas phases (usually water and air respectively). Unsaturated soils can be found naturally above the water table (vadose zone) or can be made-man, for example through compaction of fill (Fredlund and Rahardjo, 1993, Lu and Likos, 2004, Ng and Menzies, 2007).

The volume of water relative to the gas filling the pore space determines whether these phases are continuous or discontinuous throughout the soil specimen, influencing the mechanical behaviour of the soil. The capillary fringe refers to the region were the liquid phase is continuous and the gas phase discontinuous, thus presenting itself as occluded bubbles, which results in a compressible fluid. As the water content decreases both the liquid and gas phases become continuous, known as the capillary (funicular) region and at a degree of saturation of ≈20% the liquid phase becomes discontinuous, usually absorbed around the solid phase with the air phase remaining continuous, known as the residual (pendular) zone (Lu and Likos, 2004).

At the air-water interface, due to the imbalance of forces between the molecules of water, and to restore equilibrium a tensile pull develops along the water surface, known as surface tension; a phenomena which decreases in magnitude with increasing temperature (Kaye and Laby, 1973). This small region, which is only a few molecular layers deep, is referred to as the contractile skin/meniscus (Fredlund and Rahardjo, 1993). The contractile skin is concave towards the larger pressure, and as soils are three dimensional, applying Laplace equation to the two dimensional force equilibrium, the pressure difference, termed matric suction can be related to the surface tension (T_s) and radius of curvature (r_s) through Equation 2.1, Kelvin's capillary model (Fredlund and Rahardjo, 1993):

$$(u_a - u_w) = \frac{2T_s}{r_s} \quad (2.1)$$

(where u_a is the pore air pressure, u_w is the pore water pressure)

When the air phase is continuous, this contractile skin interacts with the soil particles and to maintain force equilibrium, as seen in Figure 2.1, a normal force develops at the particle contact which acts to pull the particles together and prevent particle slippage. In the 1920s the extent of this capillary force acting between the particles for an idealised soil, (uniform rigid spheres in regular packing with the meniscus idealised as an anchor-ring) was theoretically investigated with the capillary force (ΔN) being attributed to the tension exerted by the air-water interface and the resultant force from the water pressure being lower than the air pressure (Haines, 1925, 1927, Fisher, 1926, 1928). As seen in Figure 2.2, although the normal force increases initially with an increase in meniscus radius, it does not continue indefinitely but reaches a limiting value just below $2\pi T_s r$ (Haines, 1925).

Consideration has been made as to how different particle arrangements and shape would influence the normal force. Particle arrangement may lead to menisci development between particles that are not in contact. The normal force still develops, although reduced in magnitude with increasing particle separation. Should the separation distance be sufficient, rupture of the menisci-water volume during drying (a volume that could have been maintained between the particles if they were in perfect contact) could occur. The larger the separation distance the greater water volume at rupture (Allberry, 1950). Particles are not perfectly spherical and not all particles can be idealised to this shape, for example clay particles are platy. Gili and Alonso (2002) considered this by making the contact area between the spherical particles a flat surface. The menisci-water behaviour then becomes dominated by the narrow slot between the particles (Figure 2.3). As seen in Figure 2.3 the capillary force can be significant. When the suction is sufficient to empty the slot, which is controlled by geometry, the capillary force decreases. Cho and Santamarina (2001) stated that as the menisci-water reduces at this type of contact, either the particles will move closer together or the water recedes into the gap at constant rate relative to the radius of the curvature between the two particles.

Figure 2.2 shows that the normal force reaches an asymptotic value with suction increase however, the menisci-water around a particle will disappear, at very low degrees of saturation and at the dry state. Lu and Likos (2006) consider its reduction, as shown in Figure 2.4, regions III and IV, for both a clay and sand where the suction stress refers to the net force from the menisci-water along with van der Waals, double layer and cementation

forces. Lu and Likos (2006) state menisci-water is only present for suctions of several hundred kPa for sandy soil and several thousand kPa for clayey soil. At which point the water is initially retained by short-ranged hydration mechanism around the particle (region III), and then absorbed water around the particles (region IV). For sand particles residual water gives monolayer coverage which is a small percentage of the particle's mass hence the reduction in the suction stress at low water contents. However, due to high specific surface area of clay particles this water coverage can be multilayer representing 10% to 25% of water content by particle mass hence the suction stress remains (Lu and Likos, 2006).

As emphasised in Wheeler et al. (2003) it is the number of inter-particle contacts affected by the capillary force rather than the value at a particular particle which influences the behaviour of the soil. Depending on the saturation of the soil, the water can act between particles (meniscus-water) or be interconnected around a number of particles (bulk-water) (Figure 2.5). Meniscus-water only influences the normal forces at particle contacts but as bulk-water acts at a number of contacts it permits loading through the soil skeleton, thereby affecting normal and tangential forces. Meniscus-water and external stresses therefore act on a soil in two different ways (Jennings, 1961, Gallipoli et al., 2003, Wheeler et al., 2003).

As unsaturated soils have free phases and different pressures can exist in the water and gas phases an unsaturated soil's behaviour cannot be described using Terzaghi's equation (Terzaghi, 1936) (Equation 2.2).

$$\sigma' = (\sigma - u) \tag{2.2}$$

(where σ' is the effective stress, σ the total normal stress and u the pore water pressure)

Attempts have been made to modify Equation 2.2 to account for the different phases (Croney, 1952, Bishop, 1959, Aitchison, 1961, Jennings, 1961). Bishop's Equation (Equation 2.3), introduces the parameter χ, which is a material parameter related to the degree of saturation (Bishop, 1959).

$$\sigma' = (\sigma - u_a) + \chi(u_a - u_w) \tag{2.3}$$

(where u_a is the pore air pressure, u_w is the pore water pressure and σ the confining pressure)

It was shown through experimental studies to have different values to explain volume change and shear strength behaviour (Jennings and Burland, 1962, Bishop and Blight, 1963, Burland, 1964, Blight, 1965). This, governing stress variables should be independent of

material parameters (Fung, 1994), led to the behaviour of unsaturated soils being commonly described through two separate stress variables, matric suction (Equation 2.4) and net normal stress (Equation 2.5) (Fredlund and Morgenstern, 1977).

$$u_a - u_w \tag{2.4}$$

$$\sigma - u_a \tag{2.5}$$

Matric suction is one of two components of a soil's suction. Soil suction termed total suction (ψ) is defined as the free energy of the soil water (Aitchison et al., 1965) and from the thermodynamic relationship with the partial pressure of the pore water is expressed through Equation 2.6.

$$\psi = -\frac{RT}{v_{w0}\omega_v} \ln\left(\frac{\bar{u}_v}{\bar{u}_{vo}}\right) \tag{2.6}$$

Where R is the universal gas constant, T absolute temperature, v_{w0} specific volume of water, ω_v molecular mass of water vapour, $\bar{u}_v$ partial pressure of pore water vapour and $\bar{u}_{vo}$ saturation of pore water over a flat surface of pure water at room temperature (Aitchison, 1961, Fredlund and Rahardjo, 1993). The other component of total suction (Equation 2.7) is the osmotic (solute) suction (π).

$$\psi = (u_a - u_w) + \pi \tag{2.7}$$

Which is related to the salt concentration of the soil, and unless the concentration is altered, remains constant with water content and is therefore more significant at lower suctions and is also present in saturated soils (Fredlund and Rahardjo, 1993). Therefore, this research focuses on matric suction behaviour.

2.1 Methods for determining soil suction

There are a number of methods available to determine suction (total, matric or osmotic) either directly or indirectly (Fredlund and Rahardjo, 1993). There are however differences between the suctions measured with the different techniques (Chandler and Gutierrez, 1986, Madsen et al., 1986, Marinho et al., 2008, Bittelli and Flury, 2009, Tarantino et al., 2011). For indirect methods there is also dependence on the calibration used to determine the suction (McQueen and Miller, 1968, Leong et al., 2002, Bulut and Wray, 2005, Bulut and

Leong, 2007, Bicalho et al., 2010, 2011). This section focuses only on the techniques used in this research to determine the matric suction of the railway formation material.

2.1.1 Direct methods

Soil suction can be measured directly using tensiometers, or using apparatus which employs the axis translation technique (e.g. Tempe cell, pressure plate apparatus). Direct methods measure or control the pore pressures to determine the matric suction, with the pore air usually atmospheric thus giving a negative pore water pressure.

To measure the air and water pressures these phases must be separated and this is usually achieved by using a high-air-entry disc, a uniformly pore sized ceramic disc (usually sintered kaolin). When fully saturated, due to the surface tension of the contractile skin in its pore spaces, a high-air-entry disc only allows the passage of water provided the difference between the air and water pressure (matric suction) is less than its air entry value. The air entry value is the point at which air can move freely through the disc and is dictated by the largest pore size. The larger the pore size the smaller the air entry and increased permeability of the disc (Fredlund and Rahardjo, 1993). Currently commercially available high-air-entry discs have air entry values of less than 1500kPa, therefore imposing a limitation to the suction that can be measured.

A difficulty with using a high-air-entry disc is the diffusion of air through the disc. The diffusion gradient is greater when the water reservoir around a disc is filled with de-aired water whilst the pore water is not (Ridley et al., 2003). If the volume of diffused air is large enough, it can lead to loss of continuity between the water in the disc and the measuring system. Therefore, the water beneath a ceramic disc has to be regularly flushed (Marinho et al., 2008).

Tensiometer

A tensiometer measures the pore water pressure through a high-air-entry disc with a reservoir of water behind, with a strain device, usually a pressure transducer (Ridley et al., 2003). Water flows into or out of the reservoir through the high-air-entry disc until there is water pressure equilibrium between the soil specimen and reservoir, with the pressure transducer recording the pressure of the reservoir water (Fredlund and Rahardjo, 1993). As the suction measurement is dependent on water exchange between the specimen and tensiometer, sample size is important to ensure that the water exchange does not change the soil's suction (Ridley and Burland 1993).

Measurement of water pressures below -100kPa are problematic with these devices due to cavitation of water (although water has a tensile capacity greater than -500MPa) (Ridley and Burland, 1993). Research by Ridley and Burland (1993) highlighted that it was not the water cavitating at -100kPa, but the ability of the devices to inhibit cavitation. Air is present in water and can reside in small crevices in a device if the walls are not perfectly smooth, and this air will expand when negative pressures are reached, causing cavitation.

Ridley and Burland (1993) found that two main principles were important to preventing/limiting the occurrence of cavitation: correctly saturating the device, and secondly, restricting the volume of water between the high-air-entry device and the transducer where cavitation can occur. Ridley and Burland (1993) developed a high capacity tensiometer, referred to in this research as the 'Ridley suction probe' which overcame these factors, allowing water pressures up to -1500kPa to be measured (Figure 2.6). Ridley and Burland's (1994b) new device did not prevent cavitation but was designed to limit the likelihood of cavitation. The main design features are a small reservoir, about $3mm^3$ between the filter (ceramic disc) and the measuring device (transducer/strain gauge) and careful machining of the reservoir from stainless steel to limit crevices (Ridley and Burland, 1993, Ridley et al., 2003). The design was further improved as detailed in Ridley and Burland (1999), by using a strain gauge rather than an off-the-shelf transducer.

The high-air-entry disc's saturation procedure is just as important as the design in ensuring that all the air is removed from the ceramic disc and is detailed in Ridley and Burland (1999). Saturation is conducted under high pressures as this causes de-nucleation of the water minimising the amount of air which could nucleate.

Tensiometer suction measurements have been found to be both higher and lower than those determined with the filter paper technique, but with good correlation up to suctions of 500kPa for a London clay (Chandler and Gutierrez, 1986, Marinho et al., 2008). An argument put forward for this difference has been that the tensiometer measured matric suction. Ridley and Burland (1994a) illustrated that the tensiometer measures matric suction through comparison with total and matric suction measurements with the filter paper technique on specimens with controlled salt concentrations, and as Laloui and Nuth (2008) highlight, a high-air-entry disc allows the passage of solutes. Hypotheses not yet discounted are the influence of the filter paper's calibration curve; as the variation was only present in compacted and not reconstituted soils, Ridley and Burland (1994a) put forward that it is caused by the micro fabric, with different suctions in the macrostructure than in the individual clods of a clay specimen. The quick measurement time of the tensiometer, usually

hours, means it is unlikely to measure the equilibrium suction between the macrostructure and the clods, whilst the longer equilibrium period with the filter paper technique, usually seven days, means this is more likely.

Axis translation – pressure plate apparatus

The major limitation to measuring soil suction directly is the ability to measure negative water pressures. The axis translation technique introduced by Hilf (1956) overcomes this by elevating the pore water to a positive pressure by raising the pore air pressure which directly influences the pore water pressure (Olson and Langfelder, 1965, Bocking and Fredlund, 1980). This allows pore water pressure to be read in a conventional manner (e.g. pressure transducer) without the risk of cavitation. To maintain constant stress variables, the pore air and confining pressure around the soil are often varied in tandem with each other.

Elevating the pore pressures has however led to criticism; as the soil's pressures are no longer at their in-situ state, usually negative pore water pressure and air at atmospheric pressure. Concerns regarding the effect on the absorbed pore water and problems when the pore air is discontinuous (air is present as occluded bubbles within the soil) as raising the air pressure causes the occluded bubbles to contract and as water is incompressible, the menisci shape will alter (Marinho et al., 2008). The menisci shape will return to its original shape over time as air diffuses through the water and into the air bubble, however as this is reliant on air diffusion this can take a long period of time (Marinho et al., 2008).

Bocking and Fredlund's (1980) modelling of the axis translation technique in the pressure plate apparatus illustrated that when the pore water and air are interconnected, at degrees of saturation less than 0.85, the axis translation technique is valid but that the presence of occluded bubbles leads to an overestimation of the suction value (Bocking and Fredlund, 1980, Delage et al., 2008, Marinho et al., 2008). If the pore water and the water within the high-air-entry disc are in partial contact then the period to equilibrium increases, with Marinho et al. (2008) stating that when continuity is lost, the air pressure acts around the soil specimen causing a no flow condition.

This technique is not only used to measure suction but is predominantly used to control suction. Here the pore water is allowed to drain, either vented to atmosphere or controlled, and the air pressure raised; therefore pore air pressure, to apply a given suction. Suction may be assumed to have been applied when water drainage is less than 0.04% of total water volume change per day (Mancuso et al., 2002). The reliance on water drainage to reach equilibrium requires selection of the correct high-air-entry disc in order that suction

equilibrium is reached in the quickest possible period, due to the reducing permeability of high-air-entry discs with increasing air entry value. For a silty clay material using a 500kPa high-air-entry disc Mancuso et al. (2002) found it took around a week to reach equilibrium.

The pressure plate apparatus uses the axis translation method to control suction. The apparatus consists of a pressure chamber in which high-air-entry disc(s) are placed (Figure 2.7). The high-air-entry disc is vented to atmosphere, therefore the water pressure is assumed zero and suction is induced in the specimen(s) placed on the disc by raising the air pressure within the chamber, usually through a compressed air line. The pressure differential between the pore air causes water to drain from the soil through the high-air-entry disc until the pore air pressure is in equilibrium with the applied vessel pressure. Once suction equilibrium is reached a specimen is then removed and its water content determined. If only one specimen is being tested, its water content can be determined from the water expelled through the water line.

A common issue with using a high-air-entry disc is not achieving proper contact between the soil and the ceramic. If contact is not made between the specimen and ceramic, the water phases are not connected and no flow will occur, preventing the soil from reaching equilibrium. If partial contact is made then the time required to reach equilibrium increases. This has commonly been overcome by placing weights on top of specimens (Olson and Langfelder, 1965, Tinjum et al., 1997, Tarantino et al., 2011). Madsen et al. (1986) also reported the loss of continuity between the pore water and ceramic at high suctions, due to the reduced hydraulic conductivity of the sample as the pore water becomes discontinuous. Another issue is the clogging of the ceramic disc with particles over time. For a brick material Janz (2001) did not find any difference in using kaolin paste to adhere the specimens to the ceramic or the use of a cloth to prevent clogging.

The period to equilibrium, with the specimen's water content at the applied suction has been shown to depend on the saturation of the specimen before undertaking measurements. Hillel and Mottes (1966) found that when specimens were pre-saturated by absorbing water from the plate rather than flooding with water from above, their initial and equilibrium water contents were lower, with a shorter period to reach suction equilibrium. This was attributed to the pre-saturation method altering the specimen's structure and the hydraulic gradient between the specimen and the plate, suggesting that there was a critical hydraulic gradient that must be exceeded before flow occurred; smallest when a plate with low permeability was used and a low suction applied. For both saturation techniques, specimens of alluvial loamy clay reached equilibrium water content, were stable, and then started to increase

again. Based on Ridley and Burland's (1994b) hypothesis of different suctions in the micro and macro pore spaces, this may be an indication of two differing suctions within the specimen and water being drawn from the ceramic plate to balance the exchange of water within a specimen. These findings demonstrate the difficulty in determining equilibrium, and the influence of specimen preparation on results.

An issue which is not as easy to control, affecting the time to reach equilibrium, is the relative humidity of the compressed air applied to the chamber. Marinho (2008) highlighted for a particular soil that a difference in a relative humidity of the air from 99.95% to 99.7% results in a suction difference of 350kPa. Wang and Benson (2004) stated that leakage of the pressure device, around the connections to the ceramic and the pressure vessel can be an issue.

A round robin between eight laboratories, using at least one technique in two laboratories (except osmotic technique which was used in one laboratory), was conducted as detailed in Tarantino et al. (2011) to compare suction determined from the pressure plate, axis–translation oedometer, high capacity tensiometer and osmotic technique. Measurements were conducted on a sand-clayey material with all samples (apart from one set) prepared in the same laboratory. There was good correlation between the suctions determined at each laboratory with the same technique, even though the procedure differed between the laboratories; for example, one laboratory shut off the water line when reducing the air pressure in the pressure plate and also placed weights on top of the specimens to ensure contact between the specimen and ceramic.

Although the different techniques correlated at low suctions, where the specimens were saturated, and in the high suction range (>700kPa), they differed in the middle range (Figure 2.8). The tensiometer suction measurements were lower than both the osmotic and pressure plate techniques at a given water content. However, the suction difference between the osmotic technique and the tensiometer measurements was similar to the difference between the calibration curves used to determine suction with the osmotic technique. In contrast, the difference between the tensiometer measurements and the pressure plate was 200kPa at 0.3% water content. As the pressure plate technique, unlike the tensiometer technique, elevated the pore pressures, Tarantino et al. (2011) suggested that the pressure elevation caused the size of the occluded bubbles to alter. As water is incompressible (its volume remains the same), the change in the volume of occluded bubbles causes the area the water occupies to alter, hence altering the menisci shape and therefore the suction.

The influence of the contact between the ceramic disc and the specimens in the pressure plate was investigated by placing different weights on the specimens, increasing the vertical stress to see if it improved the contact. It was found that the greater the vertical stress, the lower the water content at a given suction, with all specimens subjected to the same equilibrium time. The weights' masses were small in comparison to the specimens' masses and it was therefore assumed that they had no mechanical effect on the specimen, only improving the hydraulic conductivity with the disc by increasing the contact area (Tarantino et al., 2011).

2.1.2 Indirect methods

Suction can also be determined indirectly, through the calibration of suction against another measurable factor, relative humidity (e.g. psychrometer), electrical conductivity (e.g. gypsum block), moisture content (e.g. filter paper) all of which overcome the issue of measuring suctions greater than 1500kPa. These techniques however in general take longer to measure suction than direct methods (Ridley and Burland, 1993).

Filter paper

The filter paper technique, first used by Gardner in 1937, determines a soil's suction through the absorption properties of filter paper (Al-Khafaf and Hanks, 1974). A filter paper will absorb moisture until its moisture content is in equilibrium with its surroundings. If the exchange of moisture is through the vapour phase (i.e. the filter paper is not in direct contact with a soil specimen, as there is no exchange of solutes) total suction is measured. When direct contact is made, moisture exchange is through the liquid phase and therefore as solute exchange occurs the measurement is of matric suction. If partial contact is made than the measurement is a combination of matric and total suction (Fredlund and Rahardjo, 1993).

The corresponding filter paper's water content to a given suction is determined through calibration, usually either through using the pressure plate apparatus (matric) or osmotic solutions in which a given salt concentration corresponds to a given suction (total). Each type and grade of filter paper has different absorptive properties, and Schleicher and Schuell No 589 or Whatman No. 42 are commonly used for this technique. The calibration curve for both of these filter paper's is bi-linear changing at around 47% for Whatman and 57% for Schleicher and Schuell, (Figure 2.9) showing the transition from absorbed film regime at high suctions to capillary absorption at low suctions (McQueen and Miller, 1968, Chandler and Gutierrez, 1986, Fredlund and Rahardjo, 1993, Likos and Lu, 2002, Ng and Menzies, 2007). The calibration curves do show hysteresis between wetting and drying with a marked

difference at suction less than 100kPa (Figure 2.10), and are different for matric and total suction at suctions less than 1000kPa (Figure 2.11) (Leong et al., 2002). Leong et al. (2002) inferred from this that the matric suction measurements beyond this point were in fact total suction measurements with Al-Khafaf and Hanks (1974) previously highlighting that matric suction measurements are difficult at high suctions due to the pore water being absorbed around the soils particle so that water exchange between the specimen and filter paper is through the vapour phase.

The main advantage of this technique is that it is relatively easy to undertake along with being low cost, whilst obtaining relatively accurate results for a wide range of suctions and unlike other techniques allows determination of both matric and total suction. It is however best suited to the laboratory environment with Ridley et al. (2003) detailing that an accuracy of ±10% could be achieved but that accuracy is very dependent on the test technique. Chandler and Gutierrez (1986) illustrates that due to the rapid exchange of moisture between a filter paper and the atmosphere, measurements should occur within thirty seconds. The absolute temperature at which the filter paper is stored does not influence results but temperature fluctuations do (Al-Khafaf and Hanks, 1974, Chandler and Gutierrez, 1986).

Total suction measurements with this technique have compared favourably with psychrometer measurements on shale and clays, however matric suction measurements in-situ do not compare favourably because of the difficulty in ensuring contact, with the problem increasing with depth (Fredlund and Rahardjo, 1993). McQueen and Miller (1968) detailed that they found less variability in measurements undertaken with the filter paper than the pressure plate apparatus. Ridley et al. (2003) reported from comparison with the suction probe, that when a soil has a significant amount of salts present the equilibrium water content of the filter paper for a given suction reduces. Therefore care must be taken as to the calibration curve used for salty soils.

Total suction measurements have been found to be less accurate than the matric measurements. It is assumed to be the influence of varying contact distances and also because the period to reach equilibrium is greater than for matric suction measurements (Leong et al., 2002). Furthermore, measurements are not accurate at high suctions, as small water content changes cannot be adequately measured with the filter paper (Ridley et al., 2003).

2.2 Soil water characteristic curve (SWCC)

The significance of the relationship between a soil's water content and its suction has led to this relationship being expressed through a soil water characteristic curve (SWCC) (also referred to as the soil water retention curve (SWRC)). The relationship of suction (matric or total), is plotted on a logarithmic scale whilst water content (volumetric/gravimetric) or degree of saturation is plotted on a linear scale.

2.2.1 Material dependence

Example soil water characteristic curves are shown in Figure 2.12. The overall pattern is similar for all soils regardless of the material type. The main behavioural patterns and descriptors as shown in Figure 2.13 are:

- Saturation water content (θ_s): The soil is completely saturated and the water content remains constant regardless of suction changes at this low range. Suction here indicates that the air has caused the soil to recede at the outer edges but the soil is still saturated. Throughout this region the soil behaves as a saturated soil, regardless of whether there are measurable suctions (Laloui and Nuth, 2008).
- The air entry value (AEV) is the point at which air enters the pore space. Air enters the larger pores first, and de-saturates the soil with the water receding from the larger to smaller pores (Fredlund and Rahardjo, 1993). Suctions present in this region are predominantly capillary suctions and this region is referred to as the transition zone. The gradient of this proportion of the curve, λ, is the pore size distribution index. A shallower gradient indicates a less uniform particle size distribution.
- The residual water content (θ_r) marks the end of the transition zone and the start of the residual zone where further changes in matric suction lead to minimal changes in water content (Fredlund et al., 1994, Fredlund et al., 1997, Lu and Likos, 2004). The pore water is usually absorbed around the particles (Lu and Likos, 2004).
- Regardless of material type, zero water content has been shown from both theoretical considerations and experimental data to occur at a suction of the order of 1 000 000kPa (Fredlund et al., 1994, Leong and Rahardjo, 1997).

Despite each curve exhibiting the same overall behavioural pattern, as seen in Figure 2.12 the shape and the extent of these regions are material dependent, being influenced by particle size, shape and arrangement (Fredlund and Rahardjo, 1993, Fredlund et al., 2002).

Coarse sand has relatively large size particles in comparison to a clay or silt therefore smaller capillary forces at a given contact and also greater permeability. The steep gradient

of the transition zone also highlights that the particles are all fairly uniform in size (Figure 2.12). The fine particles of a clay material result in a higher air entry value. Due to clay's high surface hydration mechanism (unlike a sand material) pore water remains as absorbed water around the particles and therefore the residual water zone is significant.

Sample preparation, water content and density of the soil affects particle arrangement. This leads to different void volumes and particle interactions affecting drainage and the menisci shape (radius of curvature) and ultimately the magnitude of suction. A soil water characteristic curve is only relevant for the same material at the same state (density and preparation water content) (Ng and Menzies, 2007).

These curves have also been found to be dependent on the stress conditions, with a larger stress causing the air entry value to decrease and the rate of desorption to reduce (Ng and Menzies, 2007). Ng and Pang (2000) state that this is the consequence of the stress resulting in a reduction of the pore space through particle re-arrangement.

2.2.2 Hysteresis

Figure 2.13 shows that there is hysteresis between the wetting and drying branches. The drying branch always overlies the wetting branch, with the wetting curve not returning to the initial saturation water content. This is due to the entrapment of air within the soil as it is re-saturates, hence the effect is more pronounced for less dense specimens (Ng and Menzies, 2007).

The hysteresis is predominantly due to the "ink bottle" effect which occurs because of the non-uniformity of the pore sizes. This effect is illustrated by considering a tube that has a bulge half way up its height, and therefore has larger and smaller radii. When wetting, water advancement at the bulge is controlled by the smaller radii. In contrast when drying, (i.e. the water is already above the bulge), then when it reaches the bulge drainage is controlled by the larger radii. Therefore, for a given suction the water content will be higher during drying.

Secondly, suction is influenced by the contact angle, (the angle formed at the boundary between the solid-liquid-gas boundary by the air-water interface (Laloui, 2010) (Figure 2.14)) which is greater for wetting than drying (Lu and Likos, 2004). Likos and Lu (2004) also indicate that capillary condensation, occluded air, and swelling and shrinkage altering particle arrangement, are also contributing factors. Particle rearrangement is also hypothesised as the reason why the first wetting and drying curves are greater than subsequent cycles (Ng and Menzies, 2007).

The main drying and wetting branches are essentially the extremities of the soil water characteristic curve for a given material. In-situ a soil will not follow the whole of this curve, only partially wetting or drying in-between these branches. As shown in Figure 2.13 these in-between branches are known as scanning curves and also exhibit hysteresis due to the aforementioned reasons.

The differences between the wetting and drying branches mean that it is fundamental that the derived curve is representative of the in-situ conditions with drying curves commonly being obtained.

2.2.3 Curve fitting (Fredlund and Xing equation)

The limited amount, and range, of suctions measured by experiments in deriving the soil water characteristic curve and its use for predicating other phenomena, for example flow behaviour, has led to curve fitting this data in order to define the whole soil water characteristic curve (Fredlund and Xing, 1994, Lu and Likos, 2004).

Although there are a number of equations, Fredlund and Xing (1994) and Van Genuchten (1980) have been found to best represent the experimental data (Leong and Rahardjo, 1997). As Fredlund and Xing (1994) is based upon the same pore distribution function used in Van Genuchten (1980) the results are similar. However, as Van Genuchten's (1980) equation rapidly falls to zero at high suctions, to compensate for this Fredlund and Xing (1994) introduced a correction factor so that there was a linear drop to zero water content at a suction of 1 000 000kPa, after the residual water content (Equation 2.8 (Fredlund and Xing (1994) Equation 36)).

$$\theta_w = C(\psi)\frac{\theta_s}{[\ln[e+(\psi/a)^n]]^m} \tag{2.8}$$

Where θ_w is the volumetric water content, θ_s the saturation volumetric water content, e is the natural number 2.71828, ψ is suction, a, m, n: are curve fitting parameters and $C(\psi)$ is the correction function (Equation 2.9) where ψ_r is the suction at the residual water content (θ_r).

$$C(\psi) = \frac{\ln(1+\psi/\psi_r)}{\ln[1+(1000000/\psi_r)]} \tag{2.9}$$

The curve fitting parameters a, n and m, are estimated from the experimental data as shown in Figure 2.15 by determination of the inflection point by drawing a tangent through the

transition zone and are then calculated using Equations 2.10 to 2.12 (Fredlund and Xing,(1994) Equations 37 to 40). a is usually slightly higher than the air entry value except at low values of suctions and n controls the slope of the transition region.

$$a = \psi_i \tag{2.10}$$

$$n = \frac{1.31^{m+1}}{mC(\psi_i)} 3.72s^* \tag{2.11}$$

$$m = 3.67\ln\left[\frac{\theta_s C(\psi_i)}{\theta_i}\right] \tag{2.12}$$

Where ψ_i is the suction corresponding to the inflection point (Figure 2.15), θ_s is the saturation water content and s^* is calculated as shown in Equation 2.13 where s (Equation 2.14) is the slope of the of the tangent line used to define the inflection point, where ψ_p is it's suction intercept on a semi-log plot (Figure 2.15).

$$s^* = \frac{s}{\theta_s} \tag{2.13}$$

$$s = \frac{\theta_i}{\ln(\psi_p/\psi_i)} - \frac{\psi_i}{1.31^m(\psi_i+\psi_r)\ln\left[1+\left(\frac{1000000}{\psi_r}\right)\right]} \tag{2.14}$$

2.3 Influence of suction on soil stiffness and other factors

Stiffness is a fundamental soil parameter as it quantifies a soils ability to resist deformation, with this research focusing on shear modulus (G). Although it can be measured in-situ from seismic tests (Wu et al., 1984), it is commonly measured in the laboratory using the resonant column apparatus or bender elements.

This section focuses only on resonant column testing. Firstly, looking at the limited number of unsaturated soil studies and how suction influences the shear modulus behaviour and then discussing other factors which influence its magnitude, through research which has been conducted on dry and saturated specimens in this apparatus.

2.3.1 Influence of suction on shear modulus

Limited research has been conducted into the small strain behaviour of unsaturated soils; as unsaturated research has predominantly focused on elasto-plastic modelling complimented by laboratory studies using the triaxial apparatus (Toll, 1990, Romero et al., 1997, Yang et

al., 1998, Wheeler et al., 2003). Suction has been found to influence both soil strength, and stiffness (Figures 2.16 and 2.17). The magnitude of increase, and the suction at which this occurs is material dependent, as the suction at which menisci-water dominate differ between soils due to different soil fabrics (particle shapes and arrangement).

Cohesionless soils

Investigation into the shear modulus of unsaturated sands with the resonant column apparatus began in the 1980's. Although suction increased the shear modulus, its influence was found to be dependent on void ratio, grain shape and size, and degree of saturation (Wu et al., 1984, 1985, Qian et al., 1991, 1993). In addition, the influence of suction was always significant at low confining stresses (Wu et al., 1984, 1985, Qian et al., 1991, 1993). Railway formations are usually subjected to low stresses (Gräbe and Clayton, 2009) therefore implying the need to investigate their behaviour.

The contribution of suction to shear modulus was found to decrease as strain amplitude increased, but this reduction was less pronounced at low effective stresses (Wu et al., 1985). The strain levels induced in railway formation material, 0.01% to 0.05%, although dependent on the stress applied and stiffness of the formation (Brown, 1996), are larger than those applied during resonant column testing, <0.01%. It should therefore be assumed that if resonant column testing of railway formation material shows an increase in shear modulus due to suction, this will be of a larger magnitude than in-situ. However, since Gräbe (2002) observed increased stiffness in-situ, hypothesising that this was due to suction, this suggests that the strain levels induced in railway formations are not sufficient to eradicate the influence of suction on the shear modulus.

Suction's contribution to shear modulus has been defined by dividing the shear modulus of an unsaturated specimen by the shear modulus of the same material tested at a dry state (Wu et al., 1984, 1985, Qian et al., 1991, 1993). The magnitude of suction was not measured, thus the relationship presented in terms of degree of saturation (the relationship of suction and saturation was discussed in section 2.2). As seen in Figure 2.18, the shear modulus of an unsaturated sand was found to rapidly increase, reach a peak and then decrease with increasing saturation. This behavioural pattern occurred regardless of the sand type or particle size. The degree of saturation at which the peak shear modulus occurred (for specimens at the same void ratio for a given grain shape) was not influenced by particle size provided the particles were greater than 37μm. The shear modulus was greater the smaller the predominant particle size. It is assumed the increased number of particles increases the combined total capillary forces acting through the specimen (Wheeler et al., 2003).

When a sand specimen included particles less than 37μm, these were found to influence the degree of saturation at which peak shear modulus occurred. For a given type of sand, it was found that a greater percentage of particles <37μm both influenced where peak shear modulus occurred and also increased its magnitude as suction increased. It is hypothesised that this occurs because only particles <37μm could enter the voids between other larger particles in a specimen. This increases the number of contacts at which menisci-water can form, and reduces the void space between particles, thus reducing the menisci radius acting between particles and hence increasing the normal force. A similar investigation into the influence of particle size on the suction/shear modulus behaviour of cohesive materials has not been conducted. However, as clay particles (particles less than 2μm) and some silt particles (60μm to 2μm) are this size or smaller, it would be expected that they would act in a similar manner. The formation of individual clay particles into aggregates (Thom et al., 2007) may mean that this is not the case for all clay materials.

Grain shape influences shear modulus as it influences both the shape and number of menisci contacts. Wu et al. (1984) observed the shear modulus due to suction was greater for flaky particles than angular shaped particles due to the greater number of contacts that could develop over a planner area. Thus inclusion of clay particles as the fines fraction would increase the shear modulus compared to that of the same percentage and sized fines that were angular.

The shear modulus of a sand of sub-rounded particles was found to be less than a sand of angular particles at the same void ratio for any given degree of saturation (Wu et al., 1985, Qian et al., 1991, 1993). Although both sands exhibited the same overall behaviour, the shear modulus increasing linearly with decreasing void ratio, void ratio changes were less influential to the shear modulus for sub-rounded sand (Qian et al., 1993). Furthermore, the optimum degree of saturation for a given material increased with void ratio (Qian et al., 1993), since a larger pore space required a greater volume of water to produce the same menisci radius as a smaller pore space.

Kim and his co-workers have tested non-plastic sandy road subgrade using two techniques to control suction: compaction-controlled testing, where suction was varied by the water content of a prepared specimen, and suction-controlled testing, varying suction on a single compacted specimen using the axis translation technique, controlling the water and air pressures separately in the resonant column apparatus. These results were then compared with in-situ measurements (Kim and Stokoe II, 1994, Kim et al., 1997, 2003, Kweon and Kim, 2000). The maximum shear modulus (G_0) decreased linearly with increasing water

content (between 6% to 15%) for all testing techniques (Kim et al., 2003). However, the change in shear modulus with any change in water content was larger for the suction-controlled than the compaction-controlled tests. The former also showed better correlation with the in-situ measurements. This led to the conclusion that controlling the suction on a single specimen was a better testing technique and also better represented in-situ conditions (Mancuso et al., 2002, Kim et al., 2003).

However, variation in the resilient modulus due to the state (density and water content) that a specimen was wetted or dried from was observed by Khoury and Zaman (2004), with hysteresis between the wetting and drying cycles. Therefore, even if suction-controlled testing is conducted (either through controlling suction with the axis translation technique or drying a specimen in the air or wetting in a saturation tank) the specimen must be prepared at a state and subjected to suction changes that replicates the in-situ conditions to ensure that the shear modulus measured is representative.

Interestingly, Kim et al.'s (2003) study highlighted that although shear modulus reduced with increasing water content/reducing suction, suction and the specimen's resulting water content had different influences on the maximum shear modulus. The shear modulus at given water content was identical for specimens compacted at the same water content regardless of density, but different for specimens compacted to the same density but at different compaction water contents. In contrast, the shear modulus was only influenced by preparation density and water content at suctions greater than 100kPa, when the shear modulus at a given suction was the same for specimens compacted to the same density but at different preparation water contents, but different for specimens compacted to different densities at the same water content. Kim et al. (2003) gave no explanation for these differences but did state difficulty in measuring the water content changes of the specimens during testing, which may have influenced the relationship. The finding does, however, suggest that although the specimens may have been at the same water content or measurable suction, the contribution from menisci-water and bulk-water differed (Wheeler et al., 2003).

Cohesive soils

A number of different cohesive soils have been tested, using resonant columns adapted to control suction during testing by axis translation to control the pore air pressure and pore water pressure separately (Mancuso et al., 1993, 2002, Vassallo et al., 2007a, 2007b, Casini et al., 2008, Biglari et al., 2010, 2011). It has been observed that as the plasticity of these soils increased, the strains at which the maximum shear modulus occurred (linear elastic region) also increased (Kim et al., 2003).

Kim et al. (2006) studied the maximum shear modulus/water content relationship for a cohesive subgrade with a plasticity index of 14%, using both the compaction-controlled test technique and suction-controlled testing, finding little difference between these. Merchán et al. (2010) concurred with this for a Boom clay, but controlled a specimen's suction by air drying and then allowing its suction to homogenise. This suggests that the relationship is different for cohesive and cohesionless specimens and the testing technique is less important for the former. Unlike the cohesionless specimens, which were prepared at optimum, and greater and less than optimum, water contents, the cohesive specimens were compacted wet of optimum water content (Kim et al., 2006).

For a clayey silty sand (16% clay content, plasticity index 13.7%) used for the core of dams, tested in a suction-controlled resonant column, Mancuso et al. (2002) found that the maximum shear modulus increased due to suction. It varied in an s-shape manner in relation to suction, reaching an asymptotic value (Figure 2.17). This figure shows that although the overall behavioural pattern was the same for specimens prepared, using the Proctor technique (section 3.2.1), at different states (density and water content), at any given suction the shear modulus was smaller for the wet of optimum specimen. This occurred regardless of the net normal stress that the specimens were tested at, which varied between 100kPa and 400kPa. This difference highlights that the suction/shear modulus relationship is not only dependent on the type of material but also on the preparation state (density and water content) (Vinale et al., 2001).

This s-shape relationship contrasts with the bell-shaped curve observed by Qian et al. (1991) and Wu et al. (1984). However, Vassallo et al. (2007a) state that other researchers have observed the s-shape relationship, although measured using bender elements, with suction-control through either axis translation or air drying, for both highly plastic soil and coarse-grained materials (Mancuso et al., 2003). The latter suggested that Qian et al.'s (1991) and Wu et al.'s (1984) results were due to different testing techniques: Qian et al.'s (1991) use of different compaction energies and water contents for each specimen resulted in different particle arrangements and therefore could not be used to compare the suction/shear modulus relationship (Mancuso et al., 2003).

Underlying Mancuso et al.'s (2003) hypothesis is that suction-controlled testing has minimal influence on a specimen's particle arrangement. Recent studies using mercury intrusion on clay specimens (Thom et al., 2007, Monroy et al., 2010, Sivakumar et al., 2010) have highlighted that suction changes on a given specimen lead to particle re-arrangement, dependent on the initial consolidation pressure of the specimen (Thom et al., 2007). For a

London clay this only occurred at full saturation, with very small changes within the smallest sized particle fraction during hydration (Monroy et al., 2010). In contrast, for a Boom clay, void ratio altered during the initial drying of the specimen. At suctions greater than 1000kPa, no such change was detected, suggesting that at these large suctions, water is only held within the clay aggregates (Pineda et al., 2008). Mercury intrusion porosimetry studies on a silty-clayey material at various suctions are needed to understand if suction-controlled testing alters a specimen's particle arrangement.

The justification for the s-shape behaviour is related to the transition between bulk-water and menisci-water (Mancuso et al., 2002). At low suctions, at or near saturation, bulk-water effects dominate, with the influence of suction less than that of net normal stress. As suction increases, air enters the specimen and the dominant behaviour moves from bulk-water to menisci-water. When menisci-water dominates, it follows Fisher's model (Figure 2.2) in tending to an asymptotic value (Mancuso et al., 2002, D'Onza et al., 2008).

This s-shape relationship was based on shear modulus measurements where suctions had only been controlled up to 400kPa. Although Mancuso et al. (2003) did consider the results of other researchers, no consideration was made as to how the shear modulus would vary with further suction changes between the last reported value at the partially saturated state and at the dry state. In contrast, Wu et al.'s (1984) observation had been made across the complete range of saturations for a material and therefore the suction magnitudes investigated were likely to be greater. It could therefore be argued that as suction-controlled testing provides data over a limited range of suctions, it is insufficient to justify the s-shape relationship and assume the asymptotic shear modulus value.

Later suction-controlled testing on a Po silt (27% clay, 40% silt content, plastic limit 32.5%) illustrated the difficulty in interpreting the behaviour over a limited suction range as a threshold shear modulus value was not reached (Vassallo et al., 2006). Vassallo et al. (2007a), however, stated that this did not discount the previous findings as the changes in shear modulus with suction reduced at higher suctions; the s-shape curve shifted in position as the material was finer than those tested previously so the asymptotic value would occur at higher suctions (Vassallo et al., 2007a).

Cho and Santamarina (2001) measured the shear wave velocity (directly related to shear modulus section 3.4) of both cohesionless and cohesive soils using bender elements during drying. As seen in Figures 2.19 (a to d) the shear modulus was dependent upon the volume of small and platy particles within the specimens. Although these measurements were

conducted on a single specimen for each soil type, the relationship differs from that found by Mancuso et al. (2002) since an asymptotic shear modulus value was not reached. Furthermore, the behaviour of a glass bead specimen (Figure 2.19 (a)) was similar to Wu et al.'s (1984) and Qian et al.'s (1991, 1993) bell curve (Figure 2.18). However, when Cho and Santamarina (2001) compared peak saturation values with those predicted from Wu et al. (1984) and Qian et al. (1991, 1993) the degree of saturation at which peak shear modulus occurred was lower. They hypothesised that this was because of the different methods of menisci development. When suction is controlled through compaction (Wu et al., 1984, Qian et al., 1991, 1993), menisci location is dependent on a sufficient water film at a particle contact, whilst when suction is controlled through drying from saturation, menisci develop due to receding of the water. Although the behavioural pattern is similar, the measurements are related to different menisci behaviours (location and radius) and are therefore not directly comparable.

Figure 2.19 (a) is the only specimen without a significant amount of platy or fine particles and shows a reduction in strength as the degree of saturation reduces further from 0.007, where it reached maximum shear wave velocity. The other specimens' shear wave velocities increased with a reduction in saturation, reaching maximum at zero saturation (Figure 2.19 (b to d)). Hence, a reduction in shear wave velocity at low degrees of saturation is a phenomenon likely to occur only with granular materials. Cho and Santamarina (2001) state that maximum shear wave velocity for the glass specimen was reached before the dry state and then reduced, arrangement of the particles may have led to separation between some of the particles. This resulted in the menisci between the glass beads rupturing before the specimen was completely dried. Furthermore, when the kaolinite and glass bead specimen was sectioned after drying, it was observed that the clay particles had moved to surround the glass bead contacts (Cho and Santamarina, 2001). The increased strength of the cohesive specimens was therefore postulated as the clay retreating with the menisci-water and forming buttresses around the glass beads.

Vassallo et al. (2007a) observed that shear modulus increased significantly if a specimen was subjected to its first drying path, due to strain hardening, with minimal change for further wetting or drying cycles. If it had not been subjected to the suction previously it returned to the initial shear modulus value. Biglari et al. (2011) showed that this shear modulus was completely independent of previous stress history (both net normal stress and suction). This behaviour is similar to a saturated material subjected to loading and unloading. These observations indicate that the stress history of the specimen must be considered. Additionally, as the largest changes in shear modulus due to suction occur with

the first reduction in suction it is important to investigate this state during testing. In railway formations, suction changes predominantly arise due to climate change, resulting in cycling of the suctions. This indicates that if suction is controlled and varied on a test specimen, provided changes in suctions have not occurred previously, this data relates to the worst case that will occur within a railway formation.

2.3.2 Influence of factors other than suction on shear modulus

The shear modulus of a soil has also been found to be influenced by other parameters: strain amplitude, confining pressure, void ratio, number of loading cycles, time, saturation ratio, strain rate, overconsolidation ratio, particle shape and size and also natural cementation.

Strain amplitude

Shear modulus magnitude is dependent upon strain amplitude, as seen in Figure 2.20. At strains less than 0.001%, it remains fairly constant with strain, and as Clayton (2011) states it is sufficiently constant in this region to measure the very small-strain 'reference' shear modulus (G_0) (Clayton, 2011). In this research this was taken as the maximum shear modulus occurring in this region. At higher strains between 0.01% to 0.2% shear modulus significantly reduces with increasing strain (Hardin and Black, 1968, Hardin and Drnevich, 1972b, Hardin et al., 1994, Clayton, 2011). However, the shear modulus is recoverable in the small and medium strain region (<0.1%) (Mitchell, 2005, Dyvik, 2010). The relationship is both material and environment dependent and is also commonly expressed through G/G_0 vs. shear strain. Damping on the other hand increases with strain amplitude (Hardin and Drnevich, 1972a, 1972b).

Confinement period

Previous studies had identified that for a given pressure the shear modulus increased with confinement period in the linear elastic region. Anderson and Stokoe II (1977) showed that there are two distinct stages of shear modulus behaviour with time when the specimen is subjected to stains less than 0.001%. An initial rapid increase in shear modulus occurs with time due to void ratio changes known as primary consolidation; then a linear increase in shear modulus occurs when plotted against the logarithm of time, which is termed secondary consolidation (long term effects). It is postulated that it is due to the strengthening of physical-chemical bonds in cohesive soils and particle contacts in cohesionless soils (Anderson and Stokoe II, 1977). The extent of these regions and the magnitude of changes is material dependent. Primary consolidation occurs rapidly for clean sands with slow

secondary consolidation, compared to days or weeks for primary consolidation before secondary consolidation is reached for cohesive materials.

Measurements within the primary consolidation region should be avoided as the shear modulus can be underestimated and secondly the effective stress may be unknown because the excess pore pressures may not have dissipated. Although measurements at the same time within the secondary consolidation region can be taken, Anderson and Stokoe II (1977) detail a correction equation to account for the changes within this region.

Hardin and Black (1968) concluded that raising the confining pressure eradicates the influence of secondary consolidation as long as the change in confining pressure is sufficient for all the particles to rearrange. Hence, if the confining pressure is raised sufficiently, the increase in shear modulus due to secondary consolidation during the previous testing stage does not need to be considered.

The number of loading cycles is less significant for cohesionless specimens with only an initial reduction in shear modulus with the first few loading cycles. In contrast cohesive soils show a continued decrease in maximum shear modulus with loading cycles (Hardin and Drnevich, 1972b).

Confining pressure

Shear modulus increases with effective confining pressure (Kim and Novak, 1981, Chung et al., 1984, Hardin et al., 1994). For a specimen at constant void ratio, shear modulus changes by the square root of the confining pressure (variations observed between approximately 0.4 to 0.6 for pluviated sands (Clayton, 2011)), the constant b in Equation 2.15 (Clayton et al., 2010):

$$G_0 = a\left(\frac{\sigma'}{1\text{kPa}}\right)^b \tag{2.15}$$

(where a and b are constants).

Except at large strains, >0.05%, where the b exponent tends to one (Hardin and Black, 1968, Hardin and Drnevich, 1972b).

Railway formation is located at shallow depths (Burrow et al., 2007) and therefore confining pressures are very small. There is no standard design method for railway formations (Burrow et al., 2007), but Selig and Waters (1994) state that the subgrade starts within a

metre of the sleeper bottom. In the UK Burrow et al. (2007) details that the ballast, subballast and prepared subgrade thickness is usually 0.85m to 1m with a minimum ballast thickness of 0.2m to 0.3m and on the COALlink line the prepared formation extended 800mm beneath 300mm of ballast (Gräbe, 2002, Gräbe and Clayton, 2009). Therefore confining pressures are low. However, a train's passage momentarily increases the vertical stress and as the COALlink line is a heavy haul line it provides the extreme loading case, with a vertical stress increase ranging from 10kPa to 50kPa during a train's passage. Gräbe (2002) through finite element modelling confirmed this stating that if the ground was subjected to a confining pressure of 30kPa the train loading caused the vertical stress to rise by 40kPa to 50kPa using the model to illustrate that the confining pressure of the formation was between 20kPa to 40kPa (Gräbe and Clayton, 2009).

Void ratio, particle shape and size

Void ratio, influences shear modulus at a given confining pressure, with G_0 increasing with reducing void ratio. For cohesive materials particle arrangement (dispersed or flocculated structure) and clay mineralogy is also a contributing factor (Hardin and Richart, 1963, Hardin and Black, 1968, Hardin and Drnevich, 1972b). For sand specimens, Hardin and Richart (1963), found that grain shape and particle size had no influence other than on the void ratio of the material. Equation 2.16 is Hardin (1978) correction factor to normalise for the influence of void ratio for granular materials and low surface activity clays.

$$F(e) = 0.3 + 0.7e^2 \tag{2.16}$$

In recent years it has been postulated that particle shape and size are contributing factors to shear modulus (Bui, 2009, Clayton et al., 2010). This is clearly illustrated in Clayton et al. (2010) who directly compared different fractions of a quartz sand correcting for void ratio differences between specimens. They found that a specimen of larger sized sand particles (1mm), but also a more rounded sand, had a greater shear modulus at any given confining pressure than a specimen of smaller sized sand particles (0.1mm). Specimens based on larger particle sand were constructed where 10% of their weight was replaced either with the smaller sized particles or with mica. Mica was used as although its particle size is similar to the smaller sized sand particles it is a platy material. The shear modulus for both these specimens lay between those obtained for the two sand specimens, with the shear modulus lower for the specimen with 10% mica than the specimen with 10% smaller sized sand particles.

Bui (2009) extensively studied the influence of particle shape and size on the shear modulus behaviour of granular material, finding that shear modulus increased with increasing particle diameter, but that it also increased the linear elastic region. Different percentages of mica were also investigated and despite reducing void ratio with increasing mica content the shear modulus reduced. Bui (2009) found by testing similar sized particles but with different grain shapes that shear modulus increased with sphericity and roundness. Formation material comprises granular particles with different percentages of silt and clay present. Based on this study it can be hypothesised that as clay particles are platy like mica, the higher percentage of clay in the formation material the lower the shear modulus. However, this does not consider the influence of the absorbed mechanism acting around clay particles when partially saturated, which affects their arrangement (Thom et al., 2007, Murray and Sivakumar, 2010).

2.4 Summary

The literature review has highlighted the basic concepts for unsaturated soils, showing that the presence of suction significantly increases strength and stiffness, but that the magnitude of this increase and the range of suctions at which it occurs is dependent on material and construction state (water content and density), along with stress and drying/wetting history. As the influence of suction on shear modulus is most pronounced at low confining pressures, the effect on the stiffness of railway formations needs research.

It has been shown that limited research has been conducted into unsaturated shear modulus behaviour. The focus has been on cohesionless or low plasticity materials, with two different techniques used to control and investigate the influence of suctions on shear modulus: controlling and varying the suction on a single specimen during testing (suction-controlled testing), or testing a variety of specimens of a material prepared at different water contents but the same density to vary suction (compaction-controlled testing).

Suction-controlled testing has been found to better correlate with in-situ measurements. Mancuso et al. (2003) also considered that this was a better testing technique, as testing a single specimen avoids differences between the particle arrangements of specimens. Shear modulus variations can therefore be assumed to be dependent on suction changes only. Mercury intrusion porosimetry studies provide conflicting views as to whether particle re-arrangement occurs within a specimen during suction-controlled testing. The water content and density that suction-controlled specimens are prepared at has, however, been shown to influence the shear modulus at a given suction.

Suction-controlled testing by drying from a saturated state and measuring the shear modulus with bender elements (Cho and Santamarina, 2001) showed a similar suction-shear modulus behavioural pattern to compaction-controlled testing (Wu et al., 1984, Qian et al., 1991). Cho and Santamarina (2001) stated that the results were not directly comparable because of the different methods of menisci development in compaction-controlled and suction-controlled specimens. In compaction-controlled testing, menisci location is dependent on there being a sufficient water film at a particle contact during compaction, whilst for suction-controlled testing it depends on the way in which the water recedes, controlled by particle size and arrangement.

Unlike suction-controlled testing in the resonant column apparatus, neither Cho and Santamarina (2001) or Wu et al. (1984, 1985) and Qian et al. (1991, 1993) testing techniques reached an asymptotic shear modulus value at large suctions, although they did cover the whole saturation range of the tested material. Suction-controlled testing in the resonant column therefore provided a limited perspective to the suction-shear modulus behavioural pattern which may have led to the wrong conclusion.

Given that the behaviour of unsaturated soils is dependent on material type, particle arrangement and suction, the lack of research into materials similar to railway formation leads to the need to conduct research on these types of materials. This will not only contribute to the understanding of the suction-shear modulus behaviour but the wider understanding of unsaturated soils.

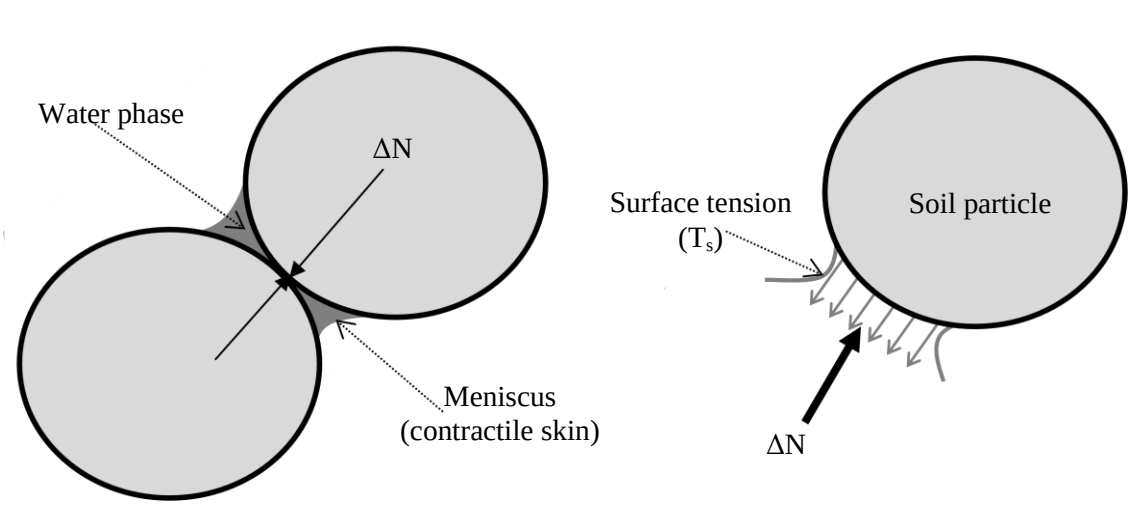

Figure 2.1: Idealisation of surface tension between two spherical particles.

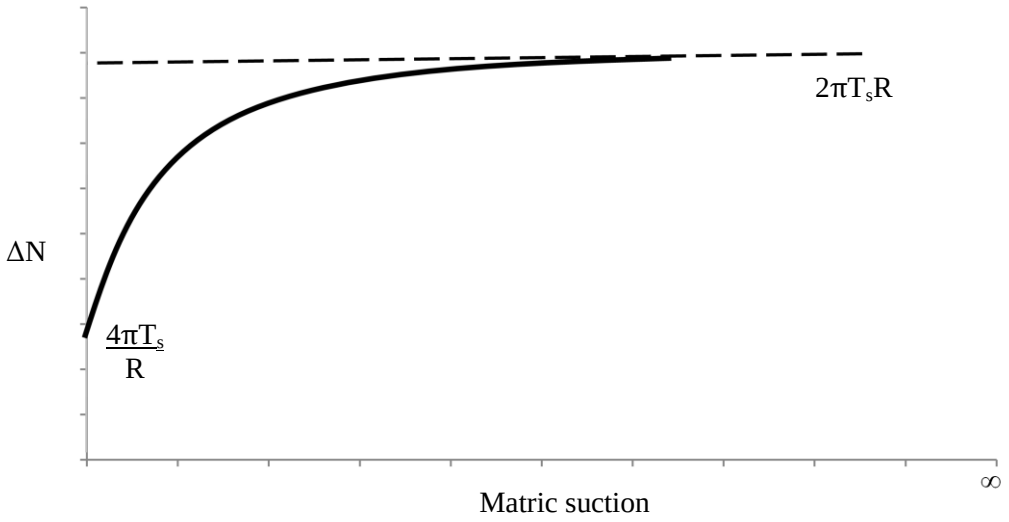

Figure 2.2: Change in normal force versus matric suction between spherical particles.

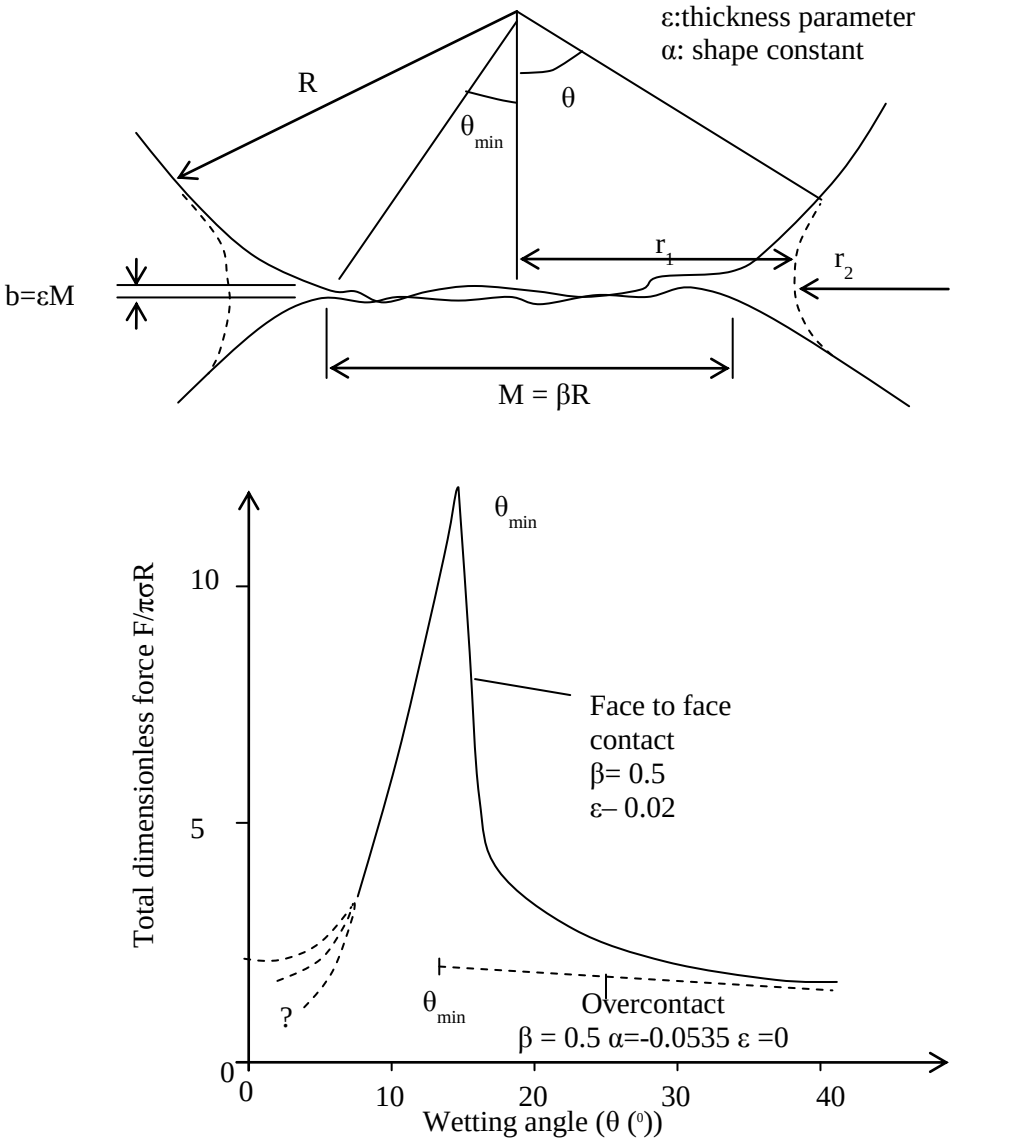

Figure 2.3: Normal force due to planar contact. Redrawn from Gili and Alonso (2002).

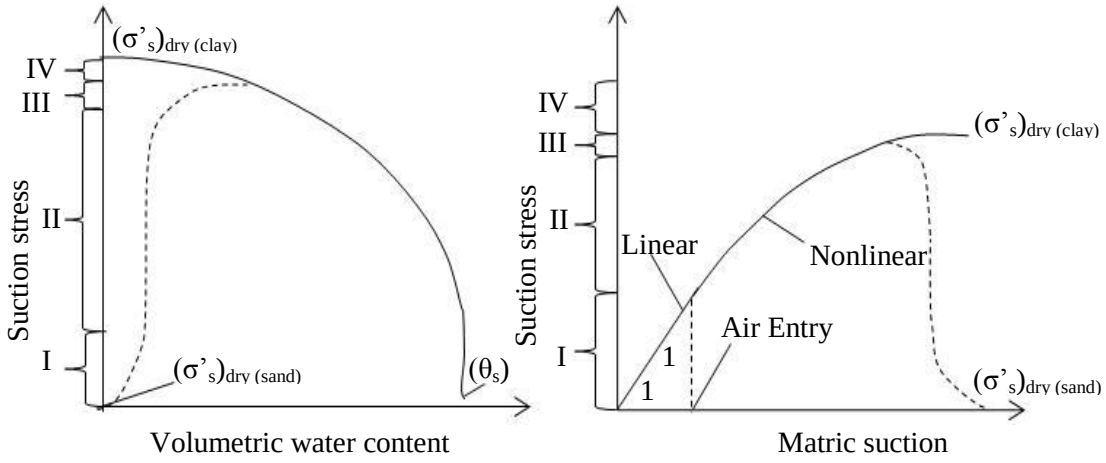

Figure 2.4: Conceptual illustration of normal force development with volumetric water content and matric suction. Redrawn from Lu and Likos (2006).

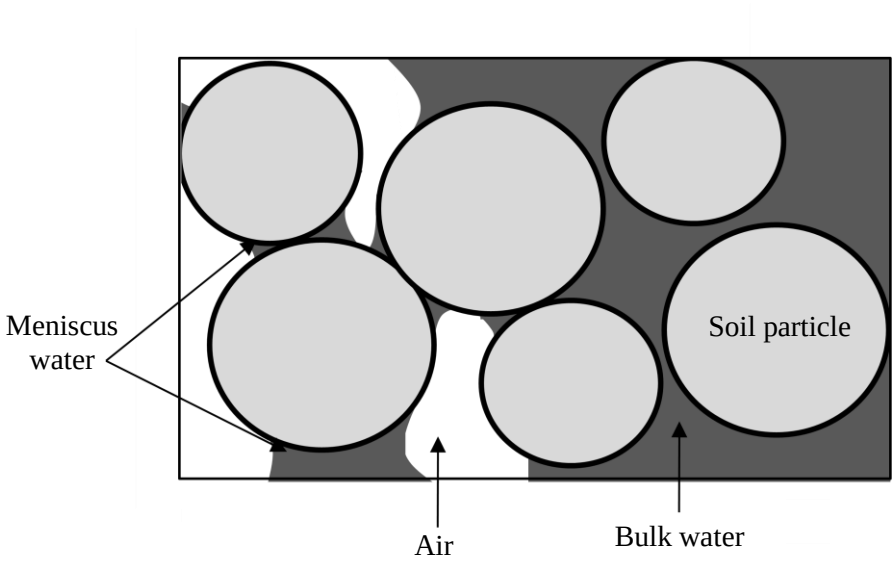

Figure 2.5: Idealisation of bulk-water and menisci- water.

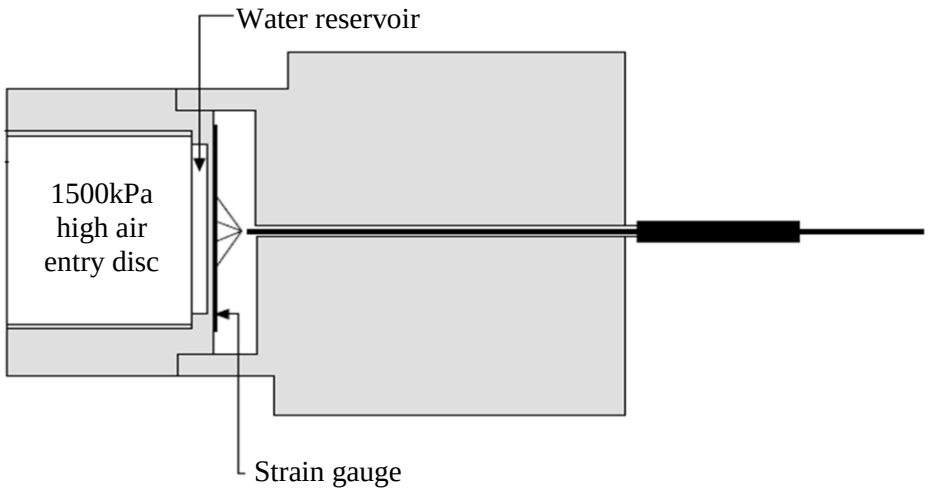

Figure 2.6: Ridley suction probe. Redrawn from Ridley et al. (2003).

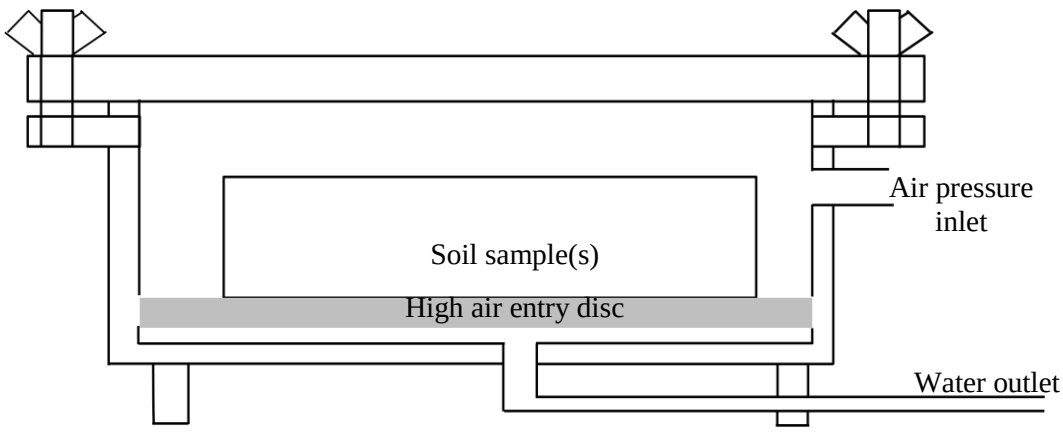

Figure 2.7: Pressure plate apparatus.

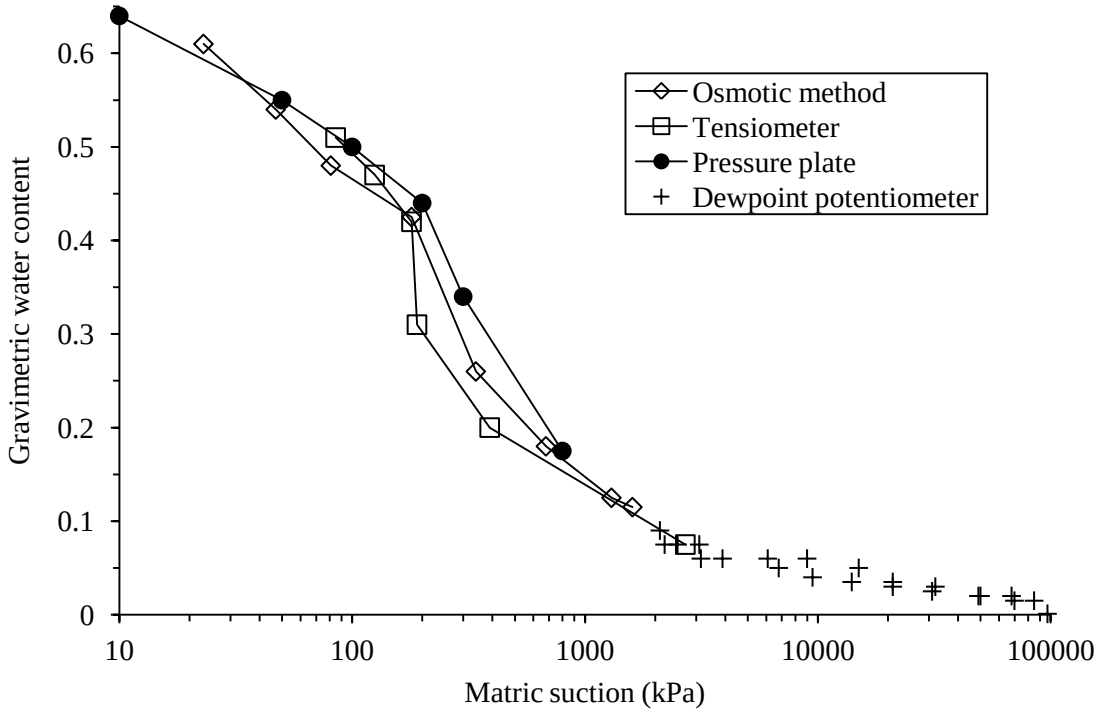

Figure 2.8: Comparison between pressure plate, osmotic method, tensiometer and dewpoint potentiometer matric suction measurements. Redrawn from Tarantino et al. (2011).

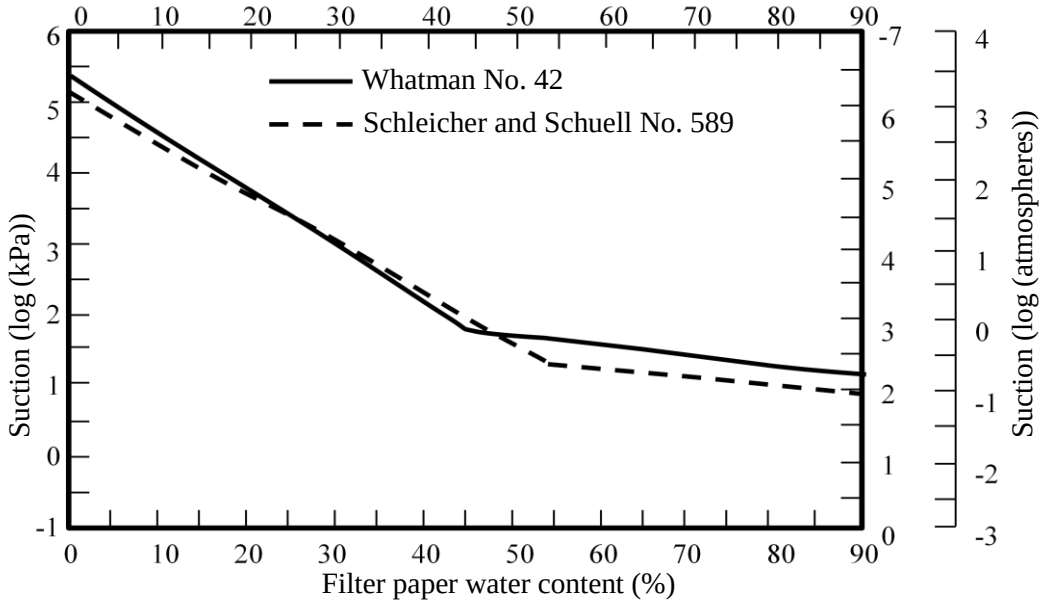

Figure 2.9: Whatman No 42 and Schleicher and Schuell No. 589 calibration curves. Redrawn from ASTM D 5298 -94 (1994).

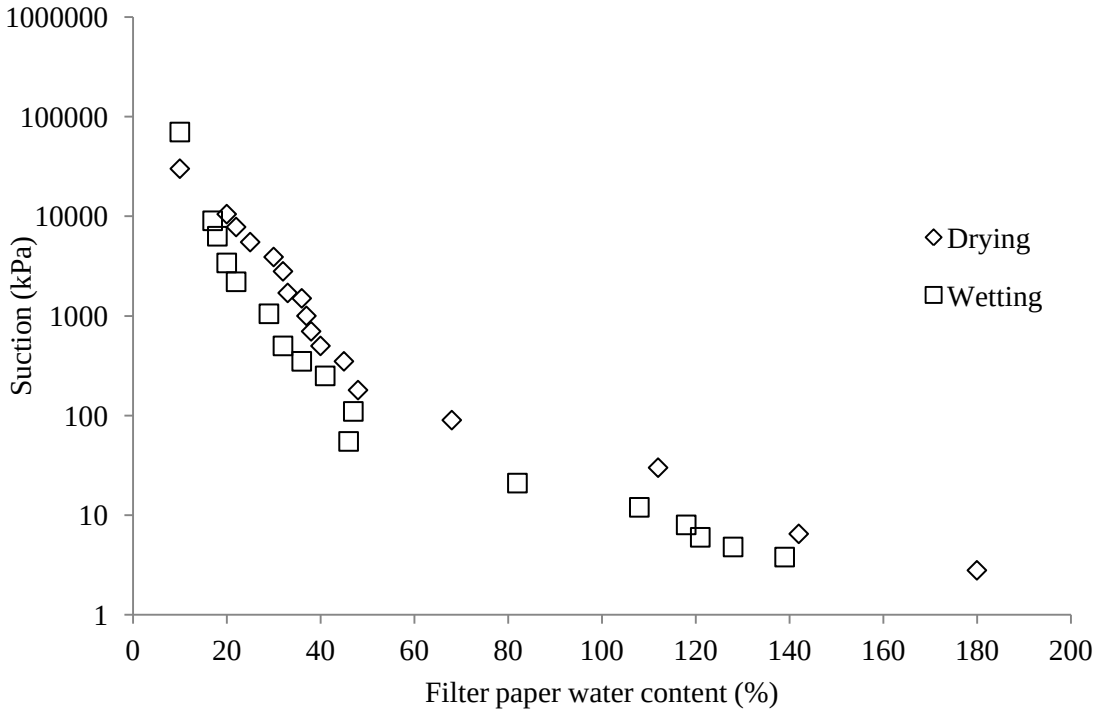

Figure 2.10: Whatman No 42 calibration data points for wetting and drying. Based on Munoz-Castelblanco et al. (2011).

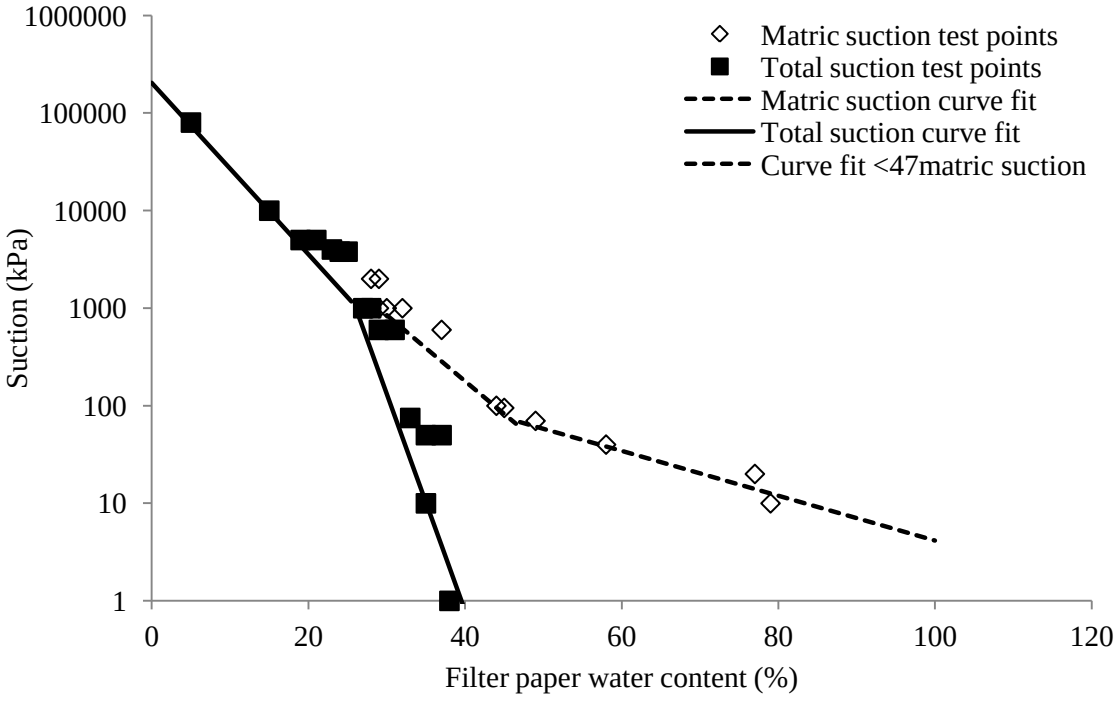

Figure 2.11: Whatman No. 42 calibration data points for total and matric suction. Based on Leong et al. (2002).

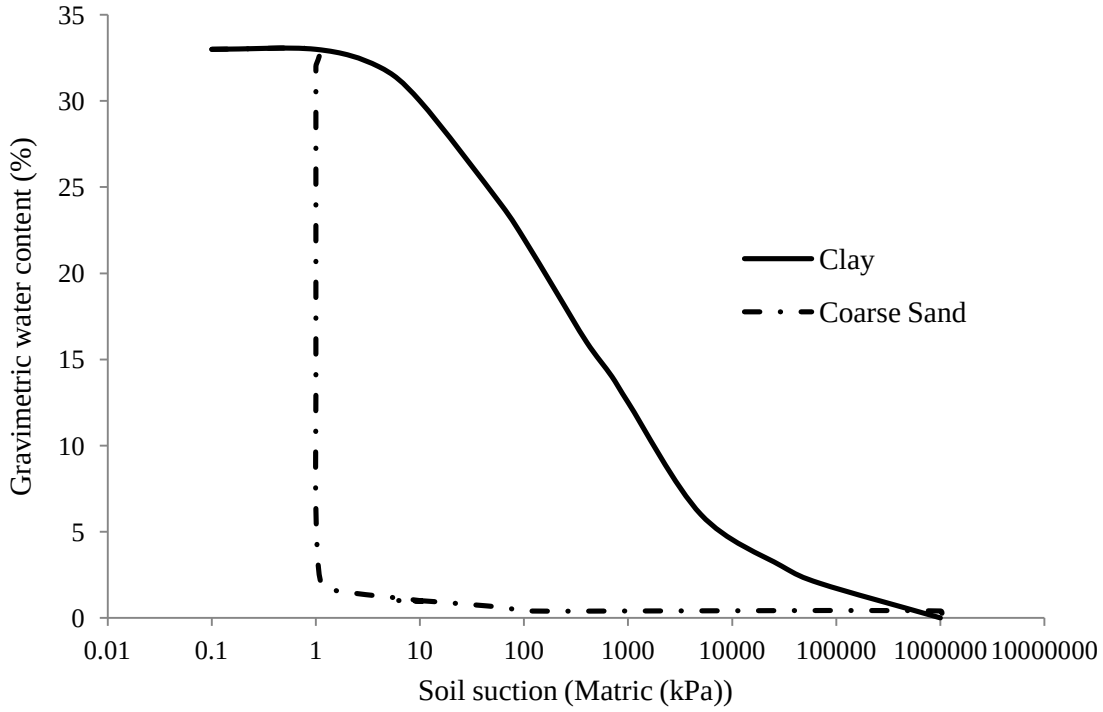

Figure 2.12: Typical soil water characteristic curve for clay and coarse sand. Redrawn from Fredlund (2002).

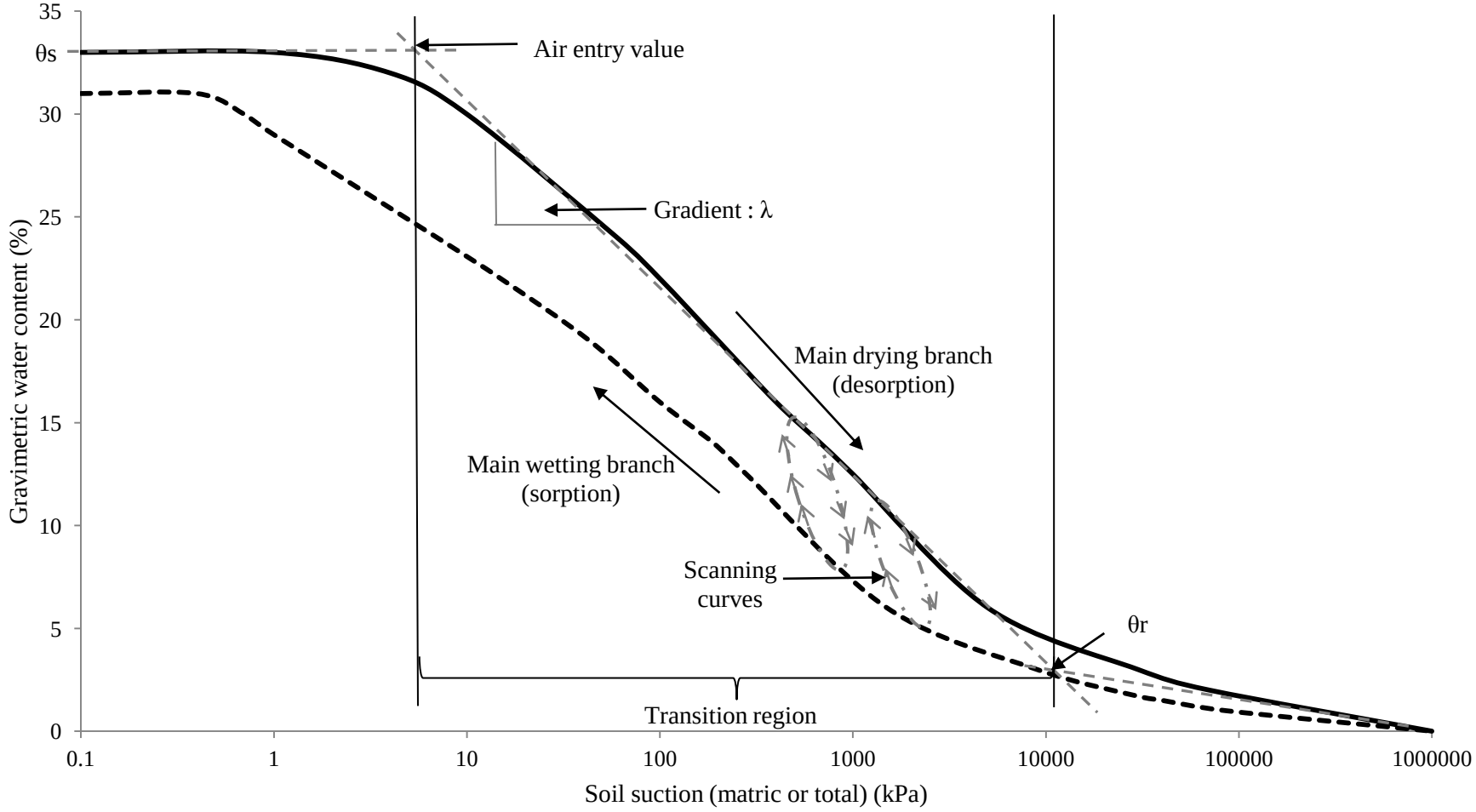

Figure 2.13: Soil water characteristic curve descriptors.

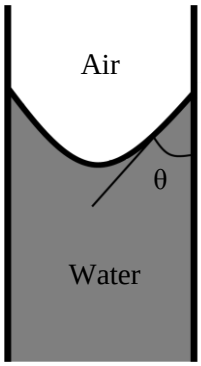

Figure 2.14: Illustration of the contact angle (θ) formed by the air-water interface. Based on Laloui, (2010).

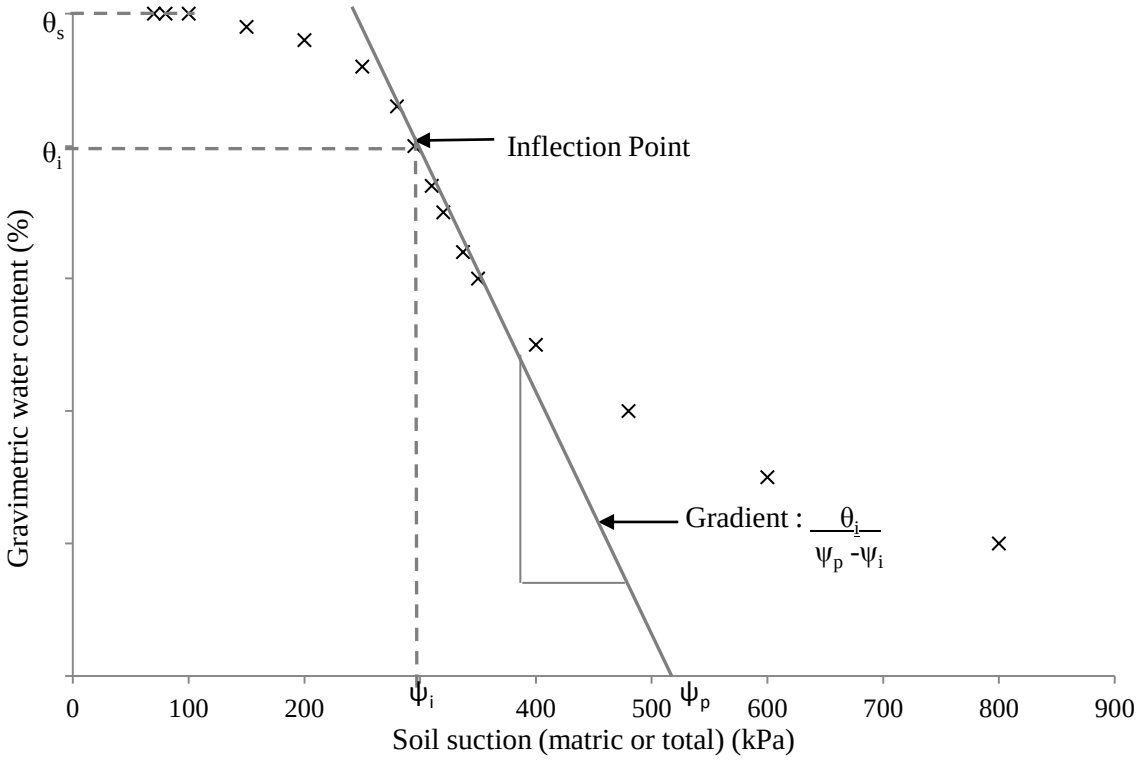

Figure 2.15: Deriving fitting parameters for Fredlund and Xing (1994) equation.

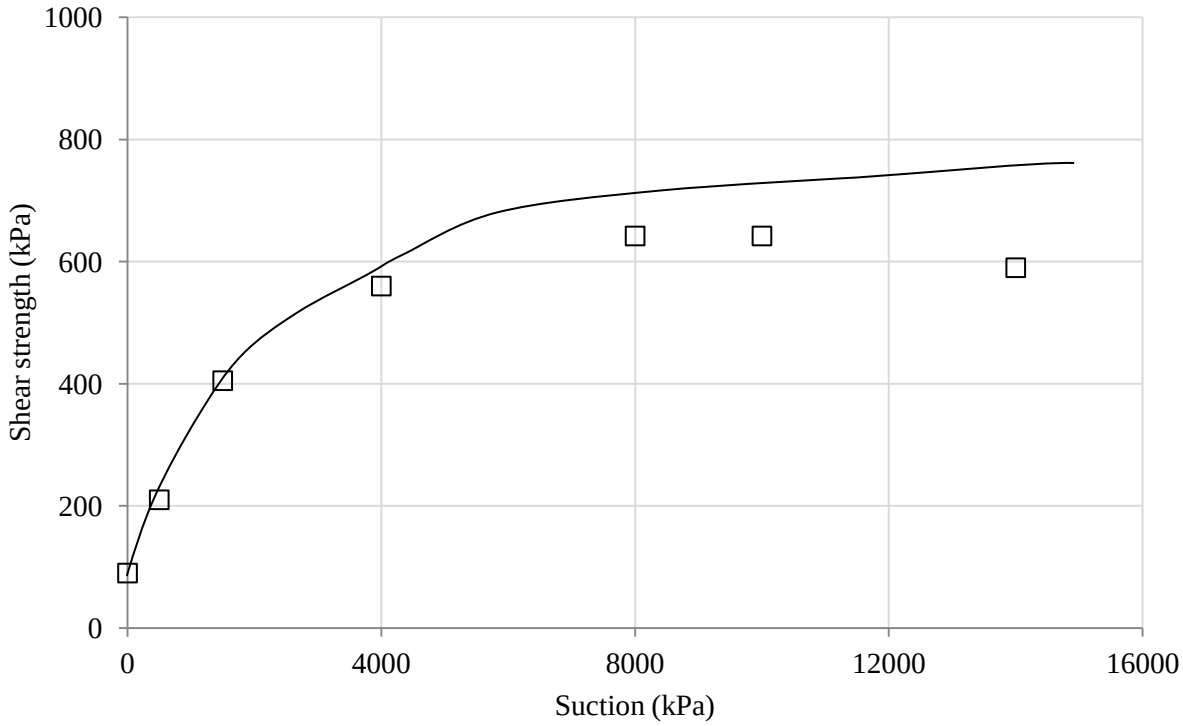

Figure 2.16: Shear strength changes with suction for a Guadalix red silty clay at a net normal stress of 120kPa. Redrawn from Vanapalli et al. (1998).

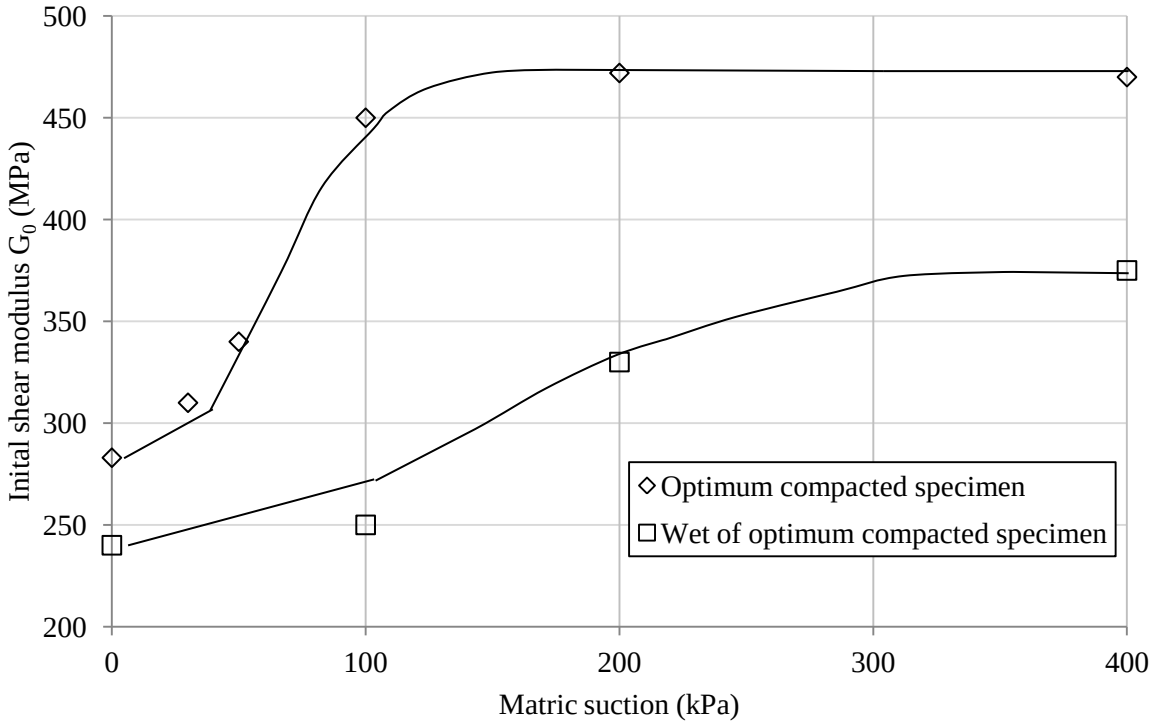

Figure 2.17: Variation in shear modulus with suction for silty sand specimen's tested from compaction state at various suction levels at a net normal stress of 400kPa. Redrawn from Mancuso et al. (2002).

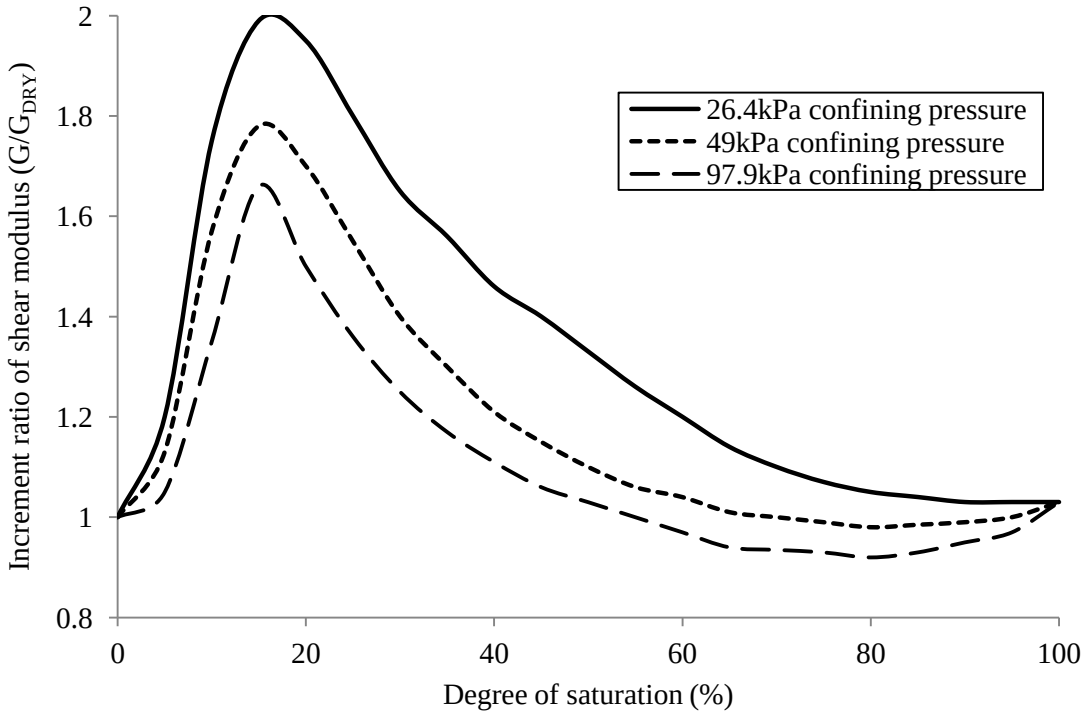

Figure 2.18: Ratio of shear modulus increase due to suction versus degree of saturation for a Glazier Way silt, e = 0.65 at various confining pressures. Redrawn from Qian et al. (1993).

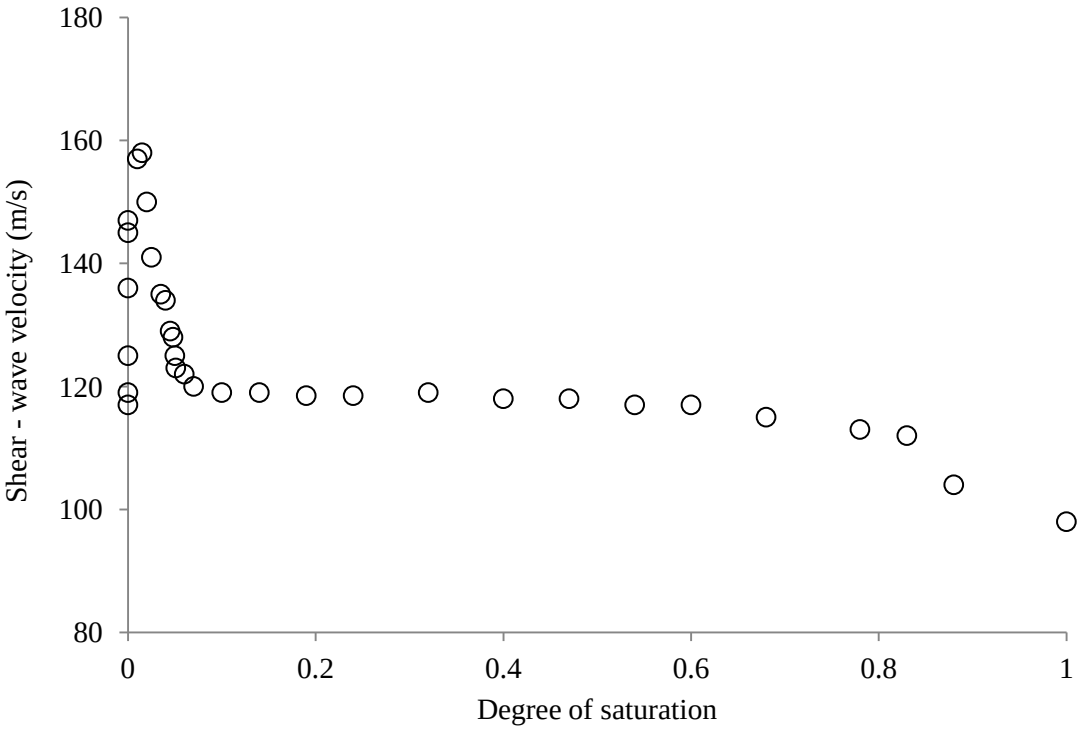

Figure 2.19 (a): Shear-wave velocity versus degree of saturation for clean glass beads. Redrawn from Cho and Santamarina (2001).

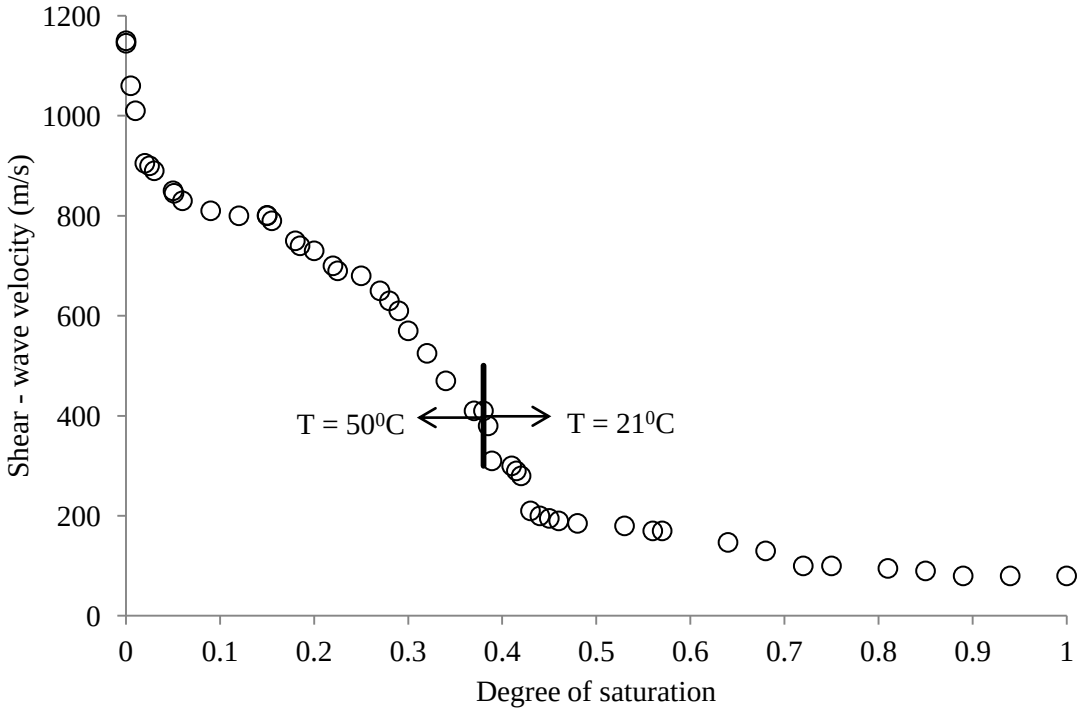

Figure 2.19 (b): Shear-wave velocity versus degree of saturation for kaolinite and glass beads. Redrawn from Cho and Santamarina (2001).

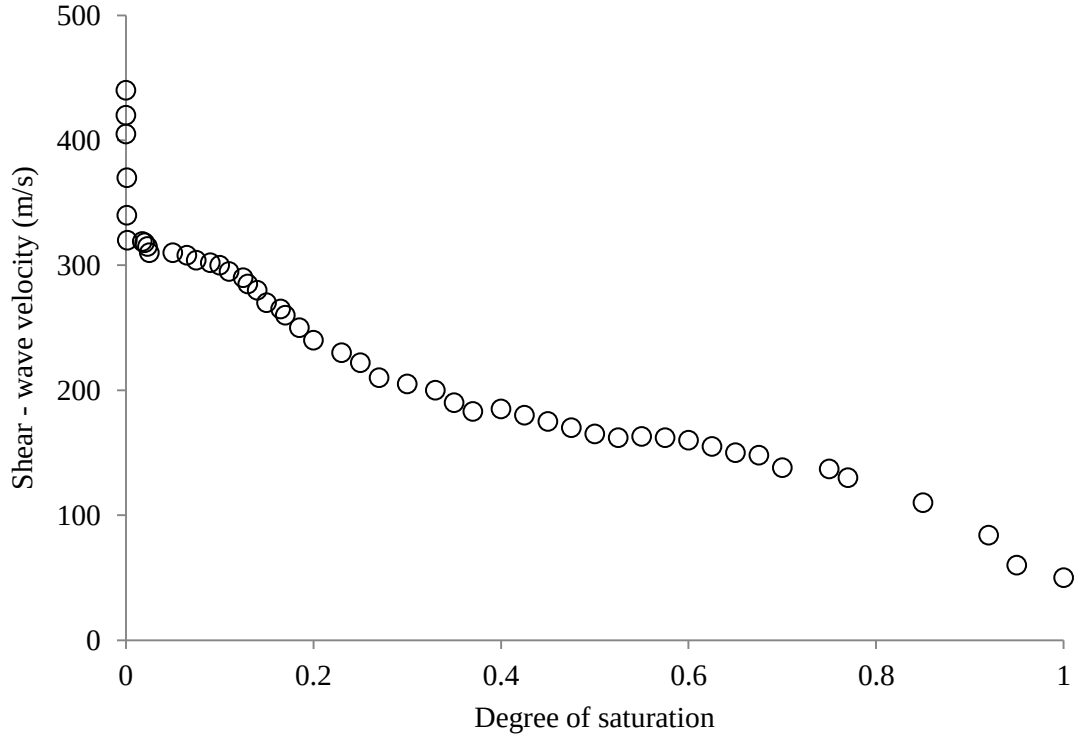

Figure 2.19 (c): Shear-wave velocity versus degree of saturation for granite powder. Based on Cho and Santamarina (2001).

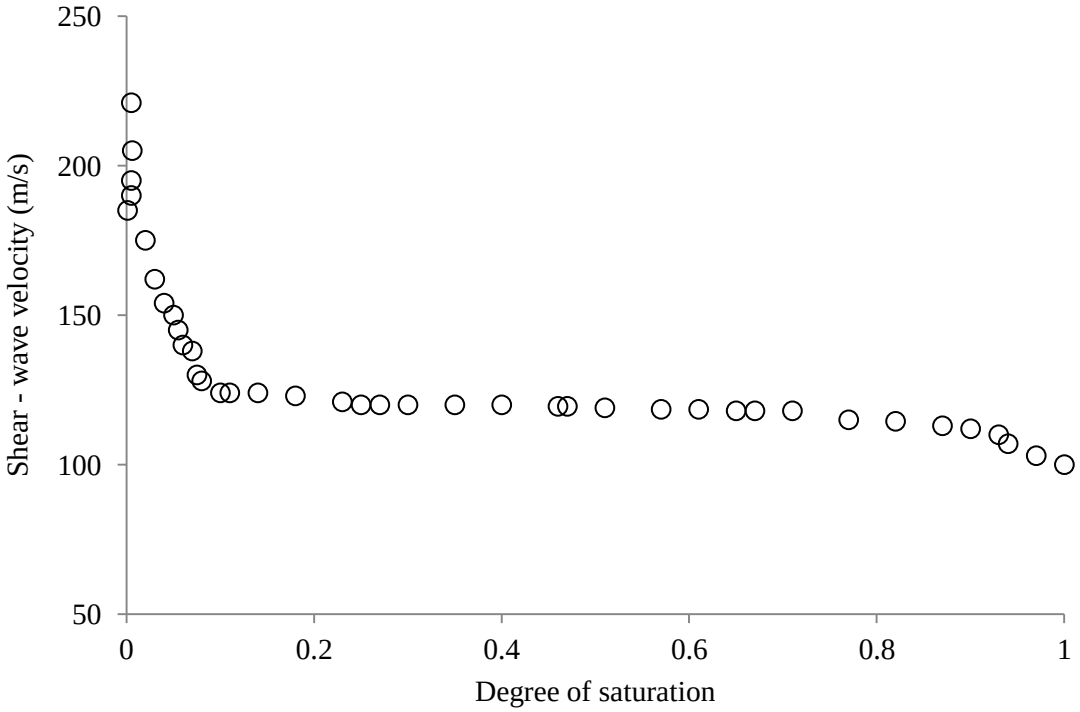

Figure 2.19 (d): Shear-wave velocity versus degree of saturation for sandboil sand. Redrawn from Cho and Santamarina (2001).

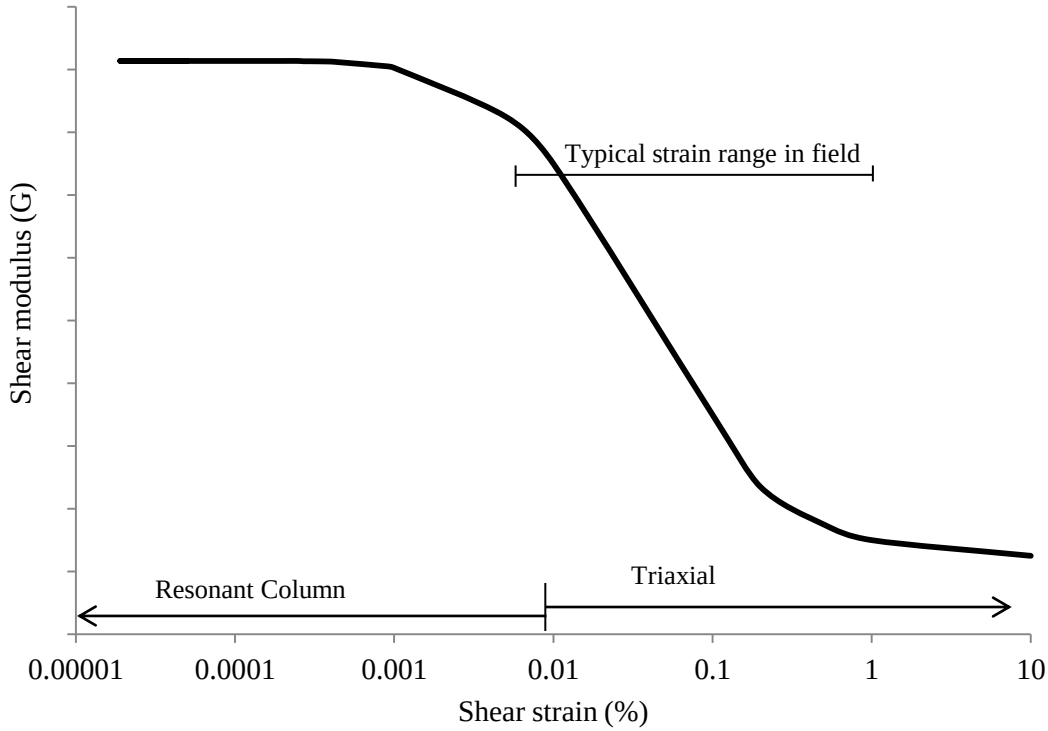

Figure 2.20: Shear modulus behaviour with strain amplitude. Based on Atkinson and Sallfors (1991).

Chapter 3

Material Properties, Laboratory Equipment and Testing Methodology

To understand how the stiffness behaviour of railway formation material is influenced by suction changes, specimens that replicated railway formation were tested in the laboratory. This chapter discusses their material properties and the laboratory equipment used to determine the stiffness and suction of these specimens.

3.1 Material properties

Information regarding the composition of the formation material on the heavy haul COALlink Line in South Africa is available, with Gräbe (2002) detailing soil specimens made with different particle size distributions which replicated the range of formation material found on this line. These materials are representative of both the material specified for construction of new formation and current in-situ formation material (Gräbe, 2002). Importantly, the soil of this line is similar to that found on other lines (Selig and Waters, 1994, Indraratna and Wadud, 2005). There is also data relating to field trials conducted on this line measuring soil behaviour, and laboratory testing on saturated specimens made from these mixes (Gräbe, 2002, Gräbe and Clayton, 2003, 2009, Gräbe et al., 2005, Clayton et al., 2006, Priest et al., 2010). Therefore, similar soil components to that used by Gräbe (2002) were used in this research. The following sections discuss the properties of the different soil mixes.

3.1.1 Particle size distribution

Four different mixes were used (known as materials A, B, C and D[1]) with their particle distribution as shown in Figure 3.1. The materials mixes were made up of: sand (Leighton Buzzard sand: fractions B, C and D, with the particles of these fractions ranging between

[1] The mixes are given the same material names as detailed in Gräbe (2002)

1.18mm and 90μm and are rounded to subrounded), silt (Oakamoor HPF5 silica flour with a particle size ranging between 250μm and 5μm (Sibelco Minerals and Chemicals LTD, 2000b)) and clay (Hymod Prima (ball clay) a fine grained highly plastic sedimentary clay predominately consisting of kaolinite but also mica and quartz (The kaolin and ball clay association UK, 2011)), with the constituent mass of each detailed in Table 3.1 a and b. Gräbe (2002) specified the use of HPF4, however, this is no longer commercially available. Therefore, HPF5, which has slightly greater proportion of larger sized fraction particles, as seen in Figure 3.2 was chosen as a replacement.

3.1.2 Atterberg values

The plastic and liquid limits for material's A to D were determined following BS 1377-2 (1990). The plastic limit ranged between 14% and 17%, and the liquid limit between 23% and 36%, as shown in Table 3.2, which also includes the values obtained by Gräbe (2002), and a sample of material D sent out for commercial testing.

Plastic limit determination is highly subjective as it is dependent on operator judgement as to when cracking is observed in the material. Comparing the plastic limit and liquid limit results on three sets of materials tested at over 40 UK based laboratories, Sherwood (1970) detailed variation of 11%, 18% and 19% between the maximum and minimum plastic limit determined between the laboratories for the three soils, with Clayton et al. (1995) detailing the standard deviation/coefficient of variation as 2.4%/13.1; 3.2%/12.8; 3.1%/12.7 for these soils.

Sherwood (1970) also looked at the liquid limit variation. However, it was determined using the Casagrande apparatus which is susceptible to user judgement, hence the British Standard now specifies the alternative cone penetration method which requires the user to repeat the operation to specified limits at each moisture content (BS1377-2, 1990). Sherwood and Ryley (1968) investigated the repeatability within given laboratories using this technique reporting variability but improved repeatability compared with the Casagrande apparatus.

The Atterberg values obtained for the formation material (Table 3.2) are therefore within the expected variation between users. In this thesis those determined by the author are used.

3.1.3 Specific gravity

Specific gravity (G_s) (particle density) determination was initially undertaken on each material using the gas jar technique (BS1377-2, 1990), with the obtained values shown in

Table 3.3. The values obtained for material A and C are lower than the 2.64 quoted for all materials by Gräbe (2002). Specific gravity determination is dependent on completely de-airing the water and soil (Krawczyk, 1969). Although de-aired water was used in the gas jar, specific gravity determination was repeated using the vacuum method. In this method, shaking of the gas jar whilst under vacuum was carried out in the hope that the contents would be completely de-aired.

The effectiveness of de-airing is dependent on the time that the vacuum is applied; although shaking does reduce this period (Clayton et al., 1995). The vacuum method was therefore run for different periods of times, leaving the saturated soil to de-air from between 15 minutes to around 6 hours. This had no affect on the results and for these materials and constituents it was found that applying the vacuum for 30 minutes was sufficient. The vacuum method was conducted using the following procedure.

- Using two flasks (Figure 3.3), place a known amount of the material in flask B, and enough de-aired water in flask A to completely fill flask B (if the flasks are the same size half fill flask A).
- Connect the flasks and attach flask A to the vacuum. Apply the vacuum and shake flask B to ensure the soil is de-aired.
- Slowly transfer the water from flask A to flask B until the soil is fully covered.
- Slowly swirl flask B until the material is completely de-aired (no air bubbles can be seen).
- Only when the fully saturated material is de-aired, slowly add the rest of the water from flask A to completely fill flask B.
- Once flask B is full, turn off the vacuum and disconnect from flask A. Top up the flask with de-aired water until completely full (water menisci should just protrude above the top of the flask), slide a flat plastic disc onto the flask top and weigh (the plastic disc should sit completely flat with the flask top, without trapping any air bubbles).
- Empty the contents of flask B and completely fill with de-aired water and reweigh, and then repeat with the flask completely dry (include the plastic disc).
- Calculate G_s using Equation 3.1:

$$G_s = \frac{(w_2 - w_1)G_T}{(w_4 - w_1) - (w_3 - w_1)} \tag{3.1}$$

where w_1 is the mass of flask and disc, w_2 the mass of flask, disc and dry soil, w_3 the mass of flask, disc, dry soil and water, w_4 the mass of flask, disc and water

and G_T the specific gravity of distilled water.

As shown in Table 3.3 the values are again lower than those quoted by Gräbe (2002). In order to understand the reason for the error, accepted published values were obtained for each constituent aggregate with a theoretical value for the mix determined using the percentage weight for a given material. Using this method, a specific gravity of 2.64 was obtained for each material (Table 3.3). This theoretical value has been used in all calculations in this research.

To understand why the theoretical values could not be obtained experimentally, the specific gravity was determined for each of the constituents using the vacuum technique. Table 3.3, clearly shows difficulty in determining the specific gravity for the Hymod Prima clay. This has the smallest particle size, and it is hypothesised that this led to difficulties in completely de-airing the material. Visually it was seen that difficulty arose in keeping all the particles completely in suspension rather than forming clay clumps, which might not be completely de-aired.

Sherwood's (1970) report also investigated repeatability of determining the specific gravity between the laboratories, finding a variation of 1.1% between the maximum and minimum values for three clays.

3.1.4 Proctor compaction curves

During formation of the railway line the material (A to D detailed above) is placed and compacted. In 1933 Proctor, devised a technique to replicate the compactive effort used for earth-filled dams when forming specimens in the laboratory. This technique involves compacting soils at a known moisture content using a metal hammer with a defined mass which is dropped a set number of times from a known height to compact the soil with a compaction mould. From the mass of the soil used to fill the mould, and the mould volume the dry density of the soil can be calculated and plotted as a function of moisture content. The resulting 'Proctor' curve can then be used to determine the optimum water content (water content that gives the highest dry density) as illustrated in Figure 3.4 (Proctor, 1933). This test has been modified to replicate current compaction techniques and use of standard units of mass and volume, and is known as the modified Proctor technique (Clayton et al., 1995).

The Proctor compaction curve for each material used in this research was determined following the modified Proctor technique detailed in BS1377-4 (1990) with a 2.5kg hammer

(Figure 3.5). The differences between the curves for different materials are a common characteristic of the 'Proctor compaction curve'. Material A has a low clay content in contrast to material C. A flatter Proctor compaction curve indicates a fine graded soil and a pronounced curve a coarse graded soil (Transport and Road Research Laboratory, 1973).

The technique used to derive the Proctor compaction curve is important. Shape and position of the Proctor compaction curve is dependent on the technique used and also the compaction effort. If the compaction effort is increased, the maximum dry density tends to increase and the water content at which it occurs reduces, essentially shifting the whole curve upwards and to the left (Clayton et al., 1995). Sherwood (1970) highlighted that for different laboratories the optimum water content can vary between 4% and 8% and the maximum dry density varied by up to 0.19Mg/m^3. Therefore, the position of the maximum dry density should act only as a guide.

Designs usually specify that a material is compacted at its maximum dry density and optimum water content. The derived curves were therefore used as a guide to identify this position for each material and to help specify the construction state for the laboratory specimens. From Figure 3.5, the maximum dry density and optimum water content for materials A to D are, 2.15Mg/m^3 and 7.7% for material A; 2.05Mg/m^3 and 9% for material B, 1.97Mg/m^3 and 11% for material C, and 2.1Mg/m^3 and 8% for material D. The curves also showed the consequence of minor changes in water content on dry density. As an example, for material A around the optimum water content and using the same compaction effort, a significant dry density variation between specimens could result for minor changes in water content. In contrast, minimal dry density variation would occur for material C. The derived curves also acted as a guide to the compactive effort required to reach a specific dry density at given water content and whether construction states were viable based on the zero air void line position.

3.2 Specimen preparation

The specimens used in this research were 'reconstituted', meaning that they were made from constituent parts to replicate the in-situ material. Therefore, not only must the material properties be representative, as discussed in section 3.1, but the formation of these specimens must result in the interaction of the particles, i.e. the fabric of the soil, representing the in-situ state. The following sections discuss how this criterion was met and the specimen preparation procedure.

When a railway is constructed, the formation material is compacted; therefore the laboratory specimens should be prepared using a compaction technique. The two most common compaction methods for constructing specimens in the laboratory are moist tamping using the undercompaction technique (Ladd, 1978) or the Proctor method (BS1377-4, 1990).

Moist tamping although devised for granular soils is suitable for other soil types, with the specimen formed in a mould by compacting the soil in a number layers. If the same compactive effort is applied to each layer, compaction of an above layer results in densification of the underlying layers. To overcome the non-uniformity in specimen density, Ladd (1978) proposed the undercompaction technique, where lower layers have lower compactive effort applied initially; as subsequent layers are applied and compacted, the lower layers are further densified. The resulting densification of these layers during formation results in a specimen of more uniform density.

Through analysis of radiographs of Ottawa sand specimens constructed using the undercompaction technique, Frost and Park (2003) found that uniform density was not achieved. Not only did it vary throughout a specimen, but also reduced with increasing height within a construction layer, which resulted in significant density changes at the boundaries between the layers. As the present research was concerned with measuring stiffness, and the method used influenced by density changes, it was originally perceived that the undercompaction technique, which limits density variation, was a more suitable technique than the Proctor technique, which ignores the densification of underlying layers with compaction effort. However, in the light of Frost and Park's (2003) findings there was no longer an advantage to using the undercompaction technique, and as the author had experience of the Proctor technique it was decided to use the latter to construct the specimens.

3.2.1 Adapted Proctor technique

The modified Proctor technique, BS 1377-4 (1990), specifies the construction of specimens in a 1L mould which gives a specimen of 105mm diameter, and a height of 115.5mm. However, in this research the use of the resonant column apparatus to determine stiffness requires that specimens are 70mm diameter by 140mm high. Specimens of these dimensions could be extruded from the 1L mould specimen constructed following the modified Proctor technique, or by trimming. Both these techniques can lead to sample disturbance altering the specimen's soil structure. This can lead to changes in the apparent suction within the specimen, leading to changes in specimen stiffness which cannot be quantified. Thus, obtaining a specimen in this manner was discounted.

The modified Proctor technique is based on replicating the compaction effort in-situ. Based on the specific energy for the modified Proctor test, as defined in BS 13286-2 (2004), the equivalent number of blows required to form a specimen with a diameter of 70mm and a height of 140mm using the same 2.5kg hammer (as used for the modified Proctor technique) at the same dry density was calculated. For example to construct material D at the optimum dry density in three layers required fifteen blows per layer compared to twenty five blows per layer in the 1L mould. As the compactive effort and technique is the same for both moulds the material Proctor compaction curves shown in Figure 3.5 were assumed to be the same for the specimens constructed in the smaller mould. The formation technique using the smaller mould will be referred to herein as the adapted Proctor technique.

The only issue arising from constructing specimens in the smaller mould was the use of the 2.5kg hammer designed for the larger mould. The hammer's diameter (47mm) is designed to ensure there is no overlap between each blow in the central and outer regions. However, in the 70mm mould there was significant overlap between the central and outer regions which meant that some parts of the soil were subjected to an unintentional higher compactive effort and therefore the density in this region of the specimen was likely to be greater. This was investigated through CT scanning.

3.2.2 Computerised tomography (CT-scanning)

CT-scanning is a non-destructive image analysis technique which reconstructs a number of two dimensional (2D) radiographs using software (CT Pro in this research) to recreate a three dimensional (3D) image. The radiographs are taken of the object at different rotations. The object is then analysed using computer software which can be undertaken through either two dimensional slices through the object or three dimensional blocks. Image J and VG studio respectively were used in this research.

The radiographs that are obtained highlight the degree of attenuation of the x-rays as they pass through the specimen, with the degree of attenuation related to the density of the specimen. CT-scanning therefore was used in this research to gain an understanding of the density variation that might occur throughout a specimen. The technique would allow the effect of the hammer overlap during construction to be seen, In addition, the effect of constructing a specimen in three layers in regard to changes in vertical density through the specimen could also be considered. Secondly the high resolution of the x-ray scanner was sufficient to consider the interaction of the different particle fractions. As the clay tended to clump during mixing, a high resolution scan could assess how evenly this was distributed and how the clay interacted with other particles.

Nikon/Metris custom designed x-ray machine (225kV X-TEK/Nikon Metrology HMX ST) at the University of Southampton was used to scan a specimen of material D (dry density 2.10Mg/m^3, bulk density 2.18Mg/m^3 and water content 4.22%). The scan was conducted under the following conditions: 160keV; 175µA; gain and binning set at 1, with a 2.5mm copper filter. For each scan 3142 projections with two frames per-projection with a four second exposure was used. The voxel resolution was 44.6µm.

The x-ray attenuation of the object is related to a digital number, which CT computer programs usually display in relation to grey scale. A low digital number indicates low density (black on CT-scan and white/light grey on radiograph) and high digital number indicates high density (white/light grey on CT-scan and black on radiograph). In order to calibrate the digital number with density, a lump of dried hymod prima clay and a lump of quartz were placed at the bottom of the specimen mould. The mean digital number for these, the mould's plastic tube and the surrounding air were analysed. As the densities of these components were known the linear best fit between the digital number and density was established for each CT-scan (Figure 3.6 a and b). This relationship was then used to convert the mean digital number values from the CT-scan to density.

The same specimen was re-scanned at a later date once the specimen was completely dried to ascertain whether the drying process altered the soil structure. The specimen was dried by removing the lid of the mould which it was constructed in. Therefore, the specimen dried from the top downwards. Drying occurred over a two month period, for the middle couple of weeks the specimen was placed in a 70^{0}C oven to ensure it was fully dry.

Figure 3.7 shows a typical segment of a radiograph of the specimen, clearly illustrating that vertical density variation occurred, with each construction layer forming a distinct band. To investigate the density variations, a centralised 40mm^2 region was taken, and further subdivide into 10mm^2 regions, as shown in Figure 3.8. For each region the mean digital number was determined and converted to density. This was replicated down the whole length of the specimen in 1mm slices using ImageJ. The analysis did not include the first few millimetres at the top of the specimen due to surface irregularities, nor the bottom region, where the clay and gravel lumps were placed, as these would lead to skewed results. In the analysis's presented, 0mm depth relates to the top of the specimen with construction from the bottom upwards.

The average density of the specimen was calculated from the average digital number to be 2.16Mg/m^3 for the unsaturated specimen and 2.15Mg/m^3 when dried. From the specimen's

dimensions before scanning and the water content of the mix used to prepare the specimen, the bulk density was calculated as 2.18Mg/m^3 with a dry density of 2.10Mg/m^3. This suggests that although the dried specimen had reached a stable weight and despite being place in an oven not all of the water had been removed. The density from the CT-scan cannot therefore be referred to as the dry density.

Drying is dependent upon drying paths throughout the specimen. When the specimen's material mix was made, due to clay's affinity for water (Lambe and Whitman, 1969), the added water was attracted to the clay particles, and lumps formed within the mix, leaving dry regions in the mix. Figure 3.9 shows a horizontal slice through the specimen, visual checking of different slices down the length of each specimen scan suggested that Figure 3.9 was representative of particle arrangement throughout the specimen regardless of depth, with no discernible clustering of the clay or sand particles throughout. Within a slice it can be seen that there are regions around sand particles where there is greater infill, creating areas with low void space possibly leading to zones of lower permeability. This creates different drying paths within the specimen. The larger void space where the water surrounds the sand particles and clay drying first, due to greater permeability, whilst the water bound to the clay within the in-filled regions dries at a slower rate.

Figures 3.10 to 3.13 show the results of the analysis for a number of different sub-regions for the specimen when wet and dry. The results show that density increased within the specimen, from the top to bottom. The dashed line on each figure represents the base of each compacted layer. Although the mean density of each layer varied, typically density was greatest at the base of each layer compared to the top of each layer, with the difference decreasing with increasing construction height, concurring with Frost and Park (2003) findings for the undercompaction technique on sand specimens. As a smaller layer depth minimises variation in density it was decided to compact the test specimens using shallower layer depths giving a height for each layer ≈14mm.

From Figures 3.10 and 3.11 the maximum variation in the wet specimen's density is about 0.5Mg/m^3 with the majority of values within 0.35Mg/m^3. For the dry specimen the variation is about 0.6 Mg/m^3, this larger range of variation in density is due to some particles drying so that their density reduces whilst those particles where the water remains stays at the higher density.

When considering the density variation for the dry specimen, its overall density increases with depth similar to the wet specimen. However, the change in the density for the layers at

the bottom of the specimen are less than at the top. This possibly suggests that more water remained at the bottom of the specimen. Given that the drying front was from the top of the specimen towards the bottom of the specimen, the hydraulic gradient driving the drying process would have been less near the bottom, hence drying is slower than the top layers.

Comparing the density of the central and outer regions of the specimen (Figure 3.11), it can be seen that a small density increase occurred in the outer regions (1 and 16) compared with the central regions (6 and 11) throughout the specimen height. Although relatively small, it is suggested that this is a consequence of the central region receiving less compactive effort than the outer region during the specimen formation. As the hammer blows were spread evenly over a layer surface there was less overlap between each hammer blow in this region. The use of a smaller diameter hammer might reduce this density contrast; it was felt that this small difference was not significant to the soil stiffness.

As previously mentioned, visual checking of both CT-scans found no significant clustering of the clay or sand particles in the specimen. Therefore the variation in density down the length of the specimen was assumed to relate only to the increased compaction effort applied to the lower layers caused by the compaction of the above layer.

3.2.3 Specimen construction procedure

The following outlines the procedure used for preparing and constructing specimens in the 70mm diameter mould using the adapted Proctor technique.

- Dry constituents for a given material were weighed and mixed together.
- The required de-aired water was then measured and slowly added evenly over the surface of the mix in small quantities whilst continually mixing. The next quantity of water was only added once the previous amount had been completely mixed with the material.
- The mixed material was then transferred to an air tight bag and left in a temperature control room (20ºC) for the water content to equalise throughout the mix [Twenty four hours was sufficient for materials A, B and D with material C being left for forty eight hours].
- Based on the specified water content and relative density the amount of material required per layer was calculated and this amount of material was then weighed out into pots (a pot for each layer). The pots were then sealed until use (maximum period of half an hour) to prevent loss of water through evaporation.

- When constructing the specimen, the split mould was lined internally with plastic film. The plastic was required to stop the specimen adhering to the mould sides and the specimen being damaged when the mould was removed.
- The material for a layer was transferred from the pot into the mould, evenly spread and compacted with the Proctor hammer. Once the layer was compacted the top surface was scarified and the next layer constructed.
- Once the whole specimen was constructed, the protection cap of the mould was removed, excess material removed and weighed, with the top surface completely levelled. The soil and mould were then weighed before the mould was removed and the specimen's height and diameter measured.

For the construction of the dry specimens the split mould also fitted the base platen of the resonant column apparatus allowing the specimen to be constructed in-situ. This only occurred for the dry specimen mixes as the soils strength for these was not sufficient to support its own weight once constructed. As a high-air-entry disc was located in the base platen the Proctor hammer could not be used. Instead a rubber bung on a stick was used to construct these specimens to the required density.

3.3 Suction determination

Having devised a methodology for forming the specimens at a known water content, the suctions within these specimens needed to be quantified. The soil water characteristic curve allows the relationship between suction at different water contents to be identified. As the literature review highlighted, this curve can be used to provide an understanding of the likely suction-stiffness behaviour of a material as previous testing had found that the most significant changes in stiffness due to suction coincided with the transition region of the soil water characteristic curve. The curve was therefore also beneficial to scoping the water contents at which to construct the specimens for stiffness determination, as these could be selected to coincide with this region.

The following sections detail the methodology for both the filter paper technique and pressure plate apparatus which were used to derive the soil water characteristic curves for each material. The 'Ridley suction probe' is then discussed; this was used to measure the suction of specimens of material D prepared at the same density and water content as those used to determine stiffness.

3.3.1 Filter paper

In this research, filter paper in direct contact with the soil specimen was used to measure matric suction. The procedure was undertaken using Whatman No. 42 (55mm diameter) filter paper. Leong et al. (2002) have suggested that Whatman No. 42 is a better quality filter paper than Schleicher and Schuell No 589 because of the greater consistency between the calibration curves obtained using different techniques and by different authors.

The general consensus is that although this technique is simple and straight forward, its accuracy for determining suction is dependent on following a standard procedure that is based on a comprehensive understanding of the principles of the filter paper technique and also the calibration curve used (Leong et al., 2002, Bulut and Wray, 2005). The fact that there was little variation between different calibration curves on different batches of this manufactured filter paper (Hamblin, 1981) meant it was not felt necessary to conduct an independent calibration of the filter paper for this research.

The calibration curve used for deriving suction must relate to whether the filter paper is being wetted or dried due to the hysteresis which occurs when wetting or drying a filter paper (section 2.2.2). There is some debate in literature as to whether the calibration curves are different for total or matric suction measurements although Leong et al. (2002) argue that this is due to the time that the filter paper is left to equalise (Ridley, 1995, Leong et al., 2002, Bulut and Wray, 2005). In the procedure outlined below the filter paper was used from an air dry state and then wetted, therefore a wetting calibration curve was used. Due to its successful use at Imperial College London (Ridley et al., 2003), and consistency with previous calibration curves, the Chandler et al. (1992) calibration curve was used in this research.

The filter paper technique procedure is standardised in ASTM D 5298-4 (1994), and was followed in this research. To prevent inaccurate measurements of the filter paper's water content due to contamination and or transfer of moisture, gloves were worn throughout, the filter paper and moisture tins handled only with tweezers, all moisture tins and containers were sterilised and all surfaces cleaned.

- A number of specimens were constructed following the procedure detailed in section 3.2.3. Once constructed, each specimen was wrapped in alternating layers of cling film and tin foil to prevent water content changes until the procedure below was conducted.

- The protection around the specimen was partially removed whilst two sections 20mm long were cut from it. It was then re-covered. The surfaces of the cut sections were made level. This was to ensure that when the two sections eventually sandwiched the filter paper was in complete contact with the soil surfaces and also not in contact with the original cutting surface where small changes in particle arrangement may have occurred. These combined sections (referred to as the filter paper specimen) were then weighed. The specimens used for the filter paper tests were constructed in an identical manner to those specimens used in the resonant column apparatus for determining stiffness, rather than modifying the construction procedure to construct smaller specimens, which may have resulted in different particle arrangements between the two specimen sizes hence suction.
- The filter paper specimen was then dried or wetted to the desired water content. Drying was conducted by leaving all surfaces equally exposed in the temperature controlled laboratory. It was assumed that this led to drying occurring at a constant rate. Wetting was conducted in a purpose built saturation tank[2] partially filled with distilled water and a pond fogger. A pond fogger was used as it creates a constant mist within the tank without creating a temperature gradient.
- Once the filter paper specimen had reached the desired water content the two halves of the specimen were split and on one half of the soil section three filter papers were placed centrally using tweezers.
- The other section was then placed on top and the two halves taped around the middle at the joint with electrical tape to prevent moisture lost.
- The formed specimen was then transferred to a glass container with a lid secured into position and sealed with electrical tape to prevent moisture entering or leaving the container. The glass container was large enough to fit the specimen but sufficiently small for the specimen's water content not to alter during the filter paper equalisation period through the vapour phase of free air and specimen coming into equilibrium with each other (McQueen and Miller, 1968). The glass container was then placed in an insulated polystyrene box and left at 20^0C for seven days, to allow the water content of the filter paper and soil specimen to equalise.

After seven days the specimen was removed from the box and the water content of the filter paper determined. As a filter paper's mass is small and the amount of water it absorbs to reach saturation is small, Bulut and Wray (2005) detail that Schleicher and Schuell No. 589 –WH filter paper weighs 0.2g, and absorbs just 0.1g of water to reach full saturation, small

[2] Its design was based on the saturation tank used at Durham University

errors in determining a filter paper's weight can have a significant influence on its water content, hence the determined suction. To accurately measure its water content, weighing must be conducted on an analytical balance with a resolution of 0.0001g. Its water content can also change during weighing due to equalising with the moisture content of the surrounding air (Chandler and Gutierrez, 1986). Therefore, exposure to the atmosphere during weighing must be minimised. Chandler and Gutierrez (1986) suggest weighing should be completed within thirty seconds. The filter paper's mass was determined as follows:

- The mass of an empty moisture tin including its lid was weighed on the analytical balance.
- The filter paper specimen was then removed from the container split in half and the top and bottom filter paper discarded with the middle filter paper placed in the moisture tin. The moisture tin with lid was then weighed immediately on the analytical balance. [The top and bottom filter paper were used to prevent contamination of the middle filter paper with soil particles, if this did occur the soil particles were gently tapped from the filter paper].
- The two sections were then placed in a pre-weighed tin and weighed. Both tins were placed in a 105^0C oven for twenty-four hours. The lid of moisture tin was kept open slightly.
- After drying the moisture tin with filter paper was removed from the oven and the lid immediately put on the moisture tin. The moisture tin was then left to cool for thirty seconds on an aluminium block and then weighed. The filter paper was removed from the moisture tin and the moisture tin reweighed. The filter paper specimen and tin were also weighed. Desiccators were not used to transfer the tins from the oven to the balance as McQueen and Miller (1968) reported this affected the results.

The water content of the filter paper specimen and the filter paper were than calculated and the filter paper's water content used to determine the specimen's suction curve using Chandler et al. (1992) calibration curve (Table 3.4).

3.3.2 Pressure plate

The pressure plate allows a measure of the soil suction directly by using the axis translation technique. The procedure is standardised in ASTM D6836-02 (2003) and was summarised in section 2.1.1.

A specimen is assumed to have reached suction equilibrium when water is no longer draining from the pressure plate after the application of a positive air pressure (considered equal to the assumed suction in the specimen). Accurate results are reliant on the assessment that water has stopped draining. However, despite monitoring the water flow from the pressure plate apparatus by continually logging the weight of water collected, fluctuations in the balance readings caused by temperature changes and water evaporating from the container made assessment of when equilibrium was reached difficult and subjective.

Consequently, it was decided to remove specimens at regular intervals from the pressure plate (section 4.2.1) and weigh them. Two different pressure plates manufactured by Soilmoisture Equipment Corporation were used in this research with a pressure rating of 500kPa and 1500kPa and containing 500kPa and 1500kPa high-air-entry disc(s) respectively. The manufacturer quoted a permeability of 1.21×10^{-9}m/s and 2.59×10^{-11}m/s for the 500kPa and 1500kPa high-air-entry discs respectively. Following a private conversation with the manufacturer variation in permeability were given ranging between 1.60×10^{-10}m/s and 7.20×10^{-10}m/s with a typical value of 6×10^{-10}m/s for a new 500kPa high-air-entry disc and between 5×10^{-10}m/s and 6.25×10^{-11}m/s with a typical value of 1.88×10^{-11}m/s for a 1500kPa high-air-entry disc. This research used two 500kPa high-air-entry discs with measured average permeability's of 4.18×10^{-10}m/s and 2.15×10^{-10}m/s, and one 1500kPa with measured average permeability of 4.22×10^{-11}m/s. For each pressure step the specimens were left to reach equilibrium for twenty four hours in the 500kPa pressure plate and due to the lower permeability of the high-air-entry disc four days in the 1500kPa pressure plate.

The pressure plate test is usually conducted on initially saturated specimens where suctions are assumed to be zero and in equilibrium with the saturated porous disc of the pressure plate. However, saturation from the constructed state could result in a change in fabric (particle arrangement) in the specimen. This research was concerned with measuring the suction behaviour at a given dry density and water content. Therefore, specimens were placed on the saturated porous disc after being formed at a given water content. As the specimens would have a higher initial suction than the pressure plate, water would migrate from the pressure plate into the specimen increasing its weight. However, due to the low permeability of the specimens and the short time steps for each rise in pressure, the increase in weight was deemed to be small. When the air pressure applied was greater than the suction within the specimen the specimen's weight started to reduce. Therefore, a change in slope in the soil water characteristic curve can be used to define the in-situ suction at the given water content and density that the specimen was prepared at. The points derived up

until this change in slope are not representative of the materials soil water characteristic curve, and are a consequence of this testing procedure adopted and are referred to as the construction points of the soils water characteristic curve.

Before each test the high-air-entry disc(s) in the pressure plate were saturated. The assumption of complete saturation was assessed by measuring their permeability and comparing with the manufacturers published value. A disc was saturated by submerging it in de-aired water in the pressure plate and applying pressure, either equal to the air entry value of the ceramic for the 500kPa pressure plate or the maximum air supply pressure for the 1500kPa pressure plate. The pressure plate was left under this pressure for a complete working day, continually flushing water through the porous disc, and then left with no pressure overnight but covered in de-aired water. The following day a known pressure was applied and the water flowing out of the pressure plate was collected for a given duration (a minute). This was repeated five times, the volume of water measured and the permeability then calculated using Darcy's Law (Equation 3.2):

$$q = Aki \tag{3.2}$$

(where A is the cross sectional area of flow, q is the volumetric flow rate of water, i is the rate of decrease of total head with distance in the direction of flow and k is the coefficient of permeability)

The average permeability was then compared with the manufacturers published value. If this indicated that the disc was not saturated the procedure was repeated. Once saturated, a disc remained submerged in de-aired water until use. To prevent air entering the disc during the procedure its outlet drainage line was submerged in water.

A number of specimens were then constructed as outlined in section 3.2.3. These were then cut into segments slightly longer than specially made rings. The ring was pushed through a segment to extrude a specimen, with the excess soil removed and the surfaces trimmed level with the top and the bottom of the ring. [Achieving level surfaces was crucial to achieving good contact between the specimen and the high-air-entry disc: suction equilibrium is reliant upon water exchange between the specimen and the porous disc to give accurate results. If only part of the specimen's surface is in contact with the high-air-entry disc the period to reach equilibrium increases, and if no contact is made then the specimen does not reach suction equilibrium as there is no water exchange].

Once all the specimens had been constructed the de-aired water was removed from the apparatus and the specimens placed on the high-air-entry disc(s) as quickly as possible. A weight was placed centrally on each specimen to ensure contact between the specimen and the high-air-entry disc. (The size of the weights were smaller than the specimen's diameter to ensure that the air was able to interact with the soil specimen and not act as an impermeable boundary restricting the specimens coming to suction equilibrium).

The apparatus was then sealed and the air pressure raised to the desired pressure. The apparatus was then left for the set time interval of twenty four hours for the 500kPa pressure plate and four days for the 1500kPa pressure plate.

Once the time interval to reach suction equilibrium was reached, the air pressure was reduced, the apparatus opened, a specimen removed and immediately resealed and the next pressure applied. The specimen was placed in a pre-weighed tin, and weighed immediately and then placed in a 105^0C oven for twenty four hours. After which it was reweighed and its water content determined. This was repeated until no specimens were left in the pressure plate.

3.3.3 Ridley suction probe

Geo-observations[3] (Geotechnical Observations Limited) undertook suction measurements using the Ridley Suction Probe with a 1500kPa ceramic filter (Ridley and Burland, 1993, Geo-observations, 2011) on a number of specimens of material D that were prepared at the same dry density and water content as those tested in the resonant column apparatus.

The specimens were prepared based on the adapted Proctor technique (section 3.2.1), but constructed into plastic tube moulds with a specimen's diameter 77mm and 120mm high, with the mould having removable ends to allow insertion of the suction probe. In addition the use of a plastic tube allowed the side walls to be drilled to access the specimen at different heights to measure suctions if necessary.

The principle of the suction probe is discussed in section 2.1.1, and the preparation of the suction probe prior to taking measurements is detailed in Ridley and Burland (1993). The suction probe was mounted, in a base platen, with the probe protruding slightly. The top lid of the mould was removed and this exposed surface was then placed on the base platen making direct contact with the suction probe. Kaolin paste was used to ensure good contact

[3] Geotechnical Observations Limited, The Peter Vaughan Building, 9 Avro Way, Brooklands, Weybridge, Surrey, KT13 0YF United Kingdom. Website www.geo-observations.com

between the suction probe and the soil specimen. The response of the suction probe was then measured for at least twenty four hours.

The first specimen tested with the suction probe did not have a completely flat top surface, which caused difficulty in obtaining good contact between the specimen and the probe. Initially, kaolin paste which has the same properties of the ceramic of the probe was used to form a connection between the specimen and the probe. To check the measurement a probe was inserted into the side of the specimen.

Although the author did not undertake the measurements directly with this device, the equilibrium suction value was determined from the results.

3.4 Measurement of stiffness

The resonant column apparatus was chosen to determine the stiffness of railway formation material, not only because of its simplicity and quick determination of shear modulus (G), but primarily as its operation in the small strain region (10^{-5}% to 10^{-3}%,) permits non destructive testing (Anderson and Stokoe II, 1977). Therefore, a specimen can be tested at a variety of different confining pressures, or alternatively if controlling suction, different suctions.

There are a number of resonant column devices with different configurations (fixed-free, free-free, fixed-spring top) available. Stiffness is determined through torsional excitation based on the analysis of propagation of waves in a cylindrical specimen. A fixed-free 'Stokoe' resonant column apparatus was used in this research and only the principals of operation related to this device are discussed in the subsequent sections.

3.4.1 Principal of operation

The fixed-free configuration assumes that the specimen is perfectly fixed at the base and free to move at the top. At the free end a drive mechanism consisting of four sets of magnets located within a pair of coils is attached to the specimen (Figure 3.14).

Shear modulus is determined using torsional vibration. A sinusoidal signal (voltage) is applied to the coils, which induces an electro-motive force in the magnets causing the specimen to oscillate. The response of the specimen is measured by an accelerometer (DCB A20) attached to the drive head. The frequency of excitation applied at a given torque (i.e. voltage) is varied and from the 'frequency sweep' (Figure 3.15), the maximum amplitude of

vibration is determined. The frequency at which this occurs, assuming the damping is small, is referred to as the resonant frequency.

Ideally the drive voltage should be applied to each coil set at exactly the same time to ensure that the magnets move in phase. The drive mechanisms of Stokoe resonant column's when manufactured are wired in series which can lead to minute time differences in when the voltage reaches each coil. To ensure that the voltage was applied at the same time, the drive mechanism was re-wired by the author in parallel.

Shear wave propagation in an elastic medium

Data reduction is based on shear wave propagation in an elastic medium, and the assumption that the specimen obeys Hooke's law. Idealising the specimen as a solid elastic cylinder subjected to torsional vibration (Figure 3.16), by considering a segment, dx, and applying Newton's second law of motion the angular motion can be defined as:

$$\frac{\partial T_r}{\partial x} = \rho I_p \frac{\partial^2 \theta}{\partial t^2} \tag{3.3}$$

Where ρ is specimen density, I_p the polar moment of inertia and $\frac{\partial^2 \theta}{\partial t^2}$ the angular acceleration. The applied torque acting on the segment's cross section is then:

$$T_r = G I_p \frac{\partial \theta}{\partial x} \tag{3.4}$$

Where G is the shear modulus and $\frac{\partial \theta}{\partial x}$ the angle of twist. Differentiating Equation 3.4 and substituting into Equation 3.3 leads to:

$$\frac{\partial^2 \theta}{\partial x^2} = V_s^2 \frac{\partial^2 \theta}{\partial t^2} \tag{3.5}$$

The wave equation where

$$V_s = \sqrt{\frac{G}{\rho}} \tag{3.6}$$

Equation 3.5 is a linear partial differential equation, and can be solved through separation of variables and applying the boundary conditions (for the fixed-free configuration it is assumed that the specimen is completely rigid at the base and that the drive mechanism and

top cap can be idealised as a rigid non-deformable solid mass). This leads to Equations 3.7 and 3.8 the fundamental resonant column equations.

$$\frac{I}{I_0} = \beta\tan\beta \tag{3.7}$$

with

$$\beta = \frac{\omega_n L}{V_s} \tag{3.8}$$

Where I is the mass polar moment inertia of the specimen, I_0 is the mass polar moment of the drive plate, and ω_n the natural circular frequency given by:

$$\omega_n = 2\pi f_r \tag{3.9}$$

Where f_r is the resonant frequency. Although the resonant frequency is in fact the damped natural frequency (ω_d), as the damping in a specimen is low (<20%) there are no significant errors by assuming that they are equal (Priest, 2004). Once the shear wave velocity is found (Equation 3.8), then the shear modulus is determined by rearrangement of Equation 3.6.

Strain measurement

The magnitude of shear modulus, and therefore resonant frequency is dependent on the shear strain level. In pure torsion, the shear strain within a cross section is:

$$\gamma = \frac{r\theta}{L} \tag{3.10}$$

Where r is the radius of the specimen, L the specimen length and θ the angle of rotation assumed constant per unit length. Strain is zero at the axis of rotation and maximum at the perimeter (Figure 3.16). ASTM D4015 (1995) states that the average shear strain occurs at 0.8r from the centre of the specimen. Substituting this into Equation 3.10 the average shear strain is:

$$\gamma = \frac{0.8r\theta}{L} \tag{3.11}$$

The angle of rotation (θ), is determined based on the accelerometer's output, the measured resonant frequency and specimen geometry through Equation 3.12:

$$\theta = \frac{y}{x} = \frac{Acc}{(\omega_n)^2 x} \tag{3.12}$$

Where y is the displacement of vibration amplitude; Acc the acceleration amplitude and x is the distance to the accelerometer from the central axis of the specimen. In the apparatus used in this research x was 0.05m. The acceleration amplitude is calculated from the accelerometer's peak output. The accelerometer outputs a charge proportional to the drive systems imposed acceleration that is converted to volts via a charge amplifier. In the apparatus used in this research the charge amplifier was set to 5 volts peak to peak output with the gain set to 1g (where g is the gravitational acceleration at the earth's surface). The computer also converted this to the root mean squared voltage (V_{RMS}), therefore, to convert to volts it was multiplied by $\sqrt{2}$. The peak accelerometer output in this research was therefore:

$$A_{cc} = \frac{2\sqrt{2}V_{RMS}}{5} g \tag{3.13}$$

Substituting into Equation 3.12 the angle of rotation is:

$$\theta = \frac{Acc}{(\omega_r)^2 x} = \frac{(9.81)2\sqrt{2}V_{RMS}}{f_r^2 \pi^2} \tag{3.14}$$

where f_r is the resonant frequency. Substituting into Equation 3.11 the shear strain is then:

$$\gamma\,(\%) = \frac{80 \text{ x } 9.81 x d\sqrt{2}V_{RMS}}{f_r^2 \pi^2 L} = 112.4 \frac{(d)V_{RMS}}{f_r^2 L} \tag{3.15}$$

Where d is the specimen's diameter.

3.4.2 Calibration

To determine the shear modulus, the mass polar moment of inertia of the drive plate must be determined (Equation 3.7), which due to the complex shape of the drive mechanism is determined through calibrating the apparatus using four different aluminium bars (Table 3.5). Aluminium calibration bars are used because aluminium has very low damping. The shear modulus for aluminium was taken as 27GPa (Mondolfo, 1976).

The mass polar moment of inertia of the drive mechanism (I_0) is determined by modelling the system as a torsional pendulum with a single degree of freedom (Priest, 2004, Clayton et al., 2009), where the calibration bar is idealised as a torsional spring of stiffness k and the drive mechanism as the mass then the circular motion is:

$$\omega_n = \sqrt{\frac{k}{I_o}} \tag{3.16}$$

Where ω_n is the natural circular frequency of the calibration bar, k the stiffness of the bar and I_o the mass polar moment of inertial of the drive system. The resonant frequency of the bar is determined and then an additional masses (I_{am}), is added to the drive mechanism and the new resonant frequency determined. Three additional masses were used for each bar during this calibration, with Equation 3.16 becoming:

$$I_{am} = \frac{k}{\omega_n^2} + I_o \tag{3.17}$$

Plotting I_{am} against $\frac{1}{\omega_n^2}$ for each calibration bar, the intercept on the y-axis gives I_o and k the gradient of the best fit line. As seen in Figure 3.17 although the geometric properties of the drive mechanism remain constant, I_o varies with frequency which has also been observed by Priest (2004), Bui (2009), Kumar and Clayton (2007) and Rees (2009). As the derived value of I_o is used to determine the stiffness of the bar (Equation 3.16), this increasing value of I_o, if not accounted for, would lead to inaccuracies in determining G. In order to increase the accuracy, Priest (2004) back-calculated the value I_o (Equation 3.16), using the known properties of the aluminium bar (G=27GPa and $V_{s=}$ 3097m/s) and the measured resonant frequency to derive an equation of best fit, as shown in Figure 3.18, giving I_o(kg/m^2) as:

$$I_o = 1.726 \times 10^{-5}x^2 - 2.437 \times 10^{-3}x + 2.788 \tag{3.18}$$

Where x is the resonant frequency.

Back calculating these calibration values to determine the shear modulus and comparing with the theoretical value, an error of around ±1.5% (maximum variation of 1.70% minimum of 1.37%) occurs over the whole resonant frequency range. Although by back calculating I_o as above corrects for the errors in the calibrated I_o, the discrepancy has been shown to arise due to equipment compliance issues. Compliance of the drive mechanism (fixity of magnets, its connection to the top cap and its stiffness); specimen (fixity between the specimen, top cap and base platen); support frame (sufficient base mass and fixity), and calibration bar (fixity to the base and top cap and end plates not contributing to the angular displacement) (Bui, 2009, Clayton et al., 2009).

Pressure transducers and LVDT

Druck-PDR 810S/N (10bar 10V) pressure transducers were used to measure the pore pressures (air and water) and the cell pressure. These were calibrated over a pressure range of 100kPa to 1000kPa using a Budenberg dead weight calibration equipment and the cell pressure transducer was also calibrated from 0kPa to 100kPa using a Druck Digital Pressure Indicator (DP1-60). Figures 3.19 and 3.20 show the calibration of the transducers with a measurement error of ±1.3kPa and ±1.74kPa obtained for the cell and air pressure transducer respectively between 100kPa to1000kPa. For the cell pressure transducer the accuracy increased to ±0.36kPa between 0kPa to 100kPa. The transducers were recalibrated at regular intervals during the research.

To determine axial displacement of the specimen during testing, a LVDT (linear variable differential transformer) was attached to the drive mechanism. The LVDT was calibrated using a micrometer. The output of the LVDT is given in terms of a voltage which meant that when setting up the LVDT should only be used in the calibrated voltage range of -2.07029V to 3.1931V. As shown in Figure 3.21 the resolution was for this LVDT about 0.05mm with an accuracy of 1.16% (±0.28mm).

3.5 Resonant column testing

The following two sections, discuss the assembly of the resonant column apparatus following specimen construction and then the test procedure followed. At the beginning of this research the resonant column apparatus was adapted to control and measure suction with the axis translation technique as shown in Figure 3.22.

In order to test with the axis translation technique, the pore air and water pressure had to be controlled independently. So that the resonant column boundary conditions were not violated these were both controlled at the base of the specimen using a high-air-entry disc. When fully saturated, the high-air-entry disc (provided the specimen's suction or the air pressure does not exceed the discs air entry value) permits only the passage of water. Therefore a base platen was specially constructed for this apparatus to contain a high-air-entry disc in its centre with the air pressure applied at the outer edge, through a sintered bronze disc. In order that the high-air-entry disc remained saturated during testing, the design included a region beneath the high-air-entry disc for a small water reservoir, with a spiral groove to allow flushing of the water line to remove any diffused air which was collected in a specially designed air trap.

Although the majority of testing did not use the axis translation technique, the apparatus still remained in this configuration for these tests but with the air line disconnected from the GDS controller.

3.5.1 Assembly

Following specimen construction as detailed in section 3.2.3, the specimen was transferred onto the resonant columns base platen. The top cap was fixed using dental plaster ensuring the top cap was level. This helped prevent movement of the top cap during positioning of the drive mechanism, especially when a vacuum could not be applied to the specimen and coupling at low confining pressures. Chung et al. (1984) highlighted underestimation of the shear modulus at a low confining pressure of 10kPa, postulating that this pressure was not significant to ensure proper coupling between the top cap of the resonant column and the specimen of Monterey sand. However, they did not use an adhesive, such as dental plaster, which can be used to give a better coupling between a specimen and the top cap.

A latex membrane was then placed around the specimen and this membrane covered in silicon grease, and another membrane placed on top. Two o-rings were placed on both the top cap and base platen to ensure a good seal. A vacuum was then applied to the specimen. The specimen height and diameter were re-measured, a perspex bath placed around the specimen and filled with silicon oil. Double membranes with grease between and an oil bath were used to prevent air diffusion into or out of the specimen. As whilst investigating the effects of confining pressure Kim and Novak (1981), noted that air diffused through the rubber membrane(s), occurring within two days of applying a higher pressure. They tested with a variety of different confining fluids around the specimen which can limit the rate of diffusion. As this included mercury which has a higher density than silicon oil, a commonly used confining fluid to limit air diffusion, without influencing the shear modulus; it is acceptable to undertake resonant column testing with silicon oil as the confining fluid.

The drive mechanism was then secured into position on the top cap and the magnets aligned so they were central within the coils in both the vertical and horizontal direction. The LVDT was then attached to the drive head, the resonant column cell put in place, the wires connected and the cell sealed.

3.5.2 Test procedures

Shear modulus measurements, unless stated, were measured twenty four hours after the cell pressure was applied. This time period was determined based on the behaviour of a

specimen of material C, as this material required the longest time to reach secondary consolidation (sixteen hours).

Measuring specimen suction and shear modulus in the resonant column apparatus

The initial tests conducted using this apparatus measured the shear modulus and the specimen's suction. For these tests prior to placement of the specimen on the base platen the high-air-disc platen was saturated as follows:

- The perspex bath was placed around the base platen. The water line opened and de-aired water flushed up through high-air-entry disc using the water controllers.
- When water completely covered the top of the high-air-entry disc the water lines were closed and the bath filled to mid height with freshly de-aired water.
- The resonant column apparatus was then sealed, the water lines opened and a pressure applied to the cell up to the air entry value of the disc. The pressure gradient caused water to flow through the high-air-entry disc and diffused air to accumulate in the reservoir beneath the disc.
- One hour after applying the cell pressure it was lowered and the diffused air flushed from the spiral groove and collected in the air trap.
- Following flushing the cell pressure was raised and the last step repeated. Repeating this over an entire day was found to be sufficient to saturate the disc. Once saturated the bath was refilled with freshly de-aired water and left covered until use.

To determine the specimen's suction the specimen's pore water pressure has to be measured. However, at the specimen's prepared state this is negative and therefore cannot be measured by the transducer. As explained in chapter 2, the axis translation technique allows the pore water pressure to be translated to the positive region and once it reaches a positive value it can be read with the transducer.

In order to measure the pore water pressure there must be continuity between the specimen and the water line. However, the pressure differential between the specimen's pore water pressure and the disc causes water to be drawn from the disc into the specimen. Therefore, to measure the correct specimen's suction, the procedure must be conducted as quickly as possible from the specimen making contact with the disc and a positive pore water pressure being applied.

The specimen was set up as detailed in section 3.5.1, with all valves at the base closed. When complete, the water line valves were opened and the air controller volume taken. The cell and air pressure were then raised to reach the desired net normal stress. If the pore water pressure reading was negative, the cell and air pressure were then raised by the same magnitude, to maintain constant stress variables, until a positive water pressure was measured. Although positive water pressure is desired, negative water pressures up to -100kPa can be read with the pressure transducer provided cavitation does not occur. The water line was then flushed to remove any de-aired water and the difference between the pore air and pore water was taken as the specimen's suction.

Assessing the validity of the axis translation technique

A specimen's shear modulus under constant stress should remain constant, neglecting secondary consolidation, if its properties do not alter. Which led to the hypothesis that the apparatus could be used to assess whether the axis translation technique alters the properties of a specimen. For this assessment, the specimen already tested following the procedure above, was then subjected to increases in the magnitude of the cell and air pressure, maintaining a constant net normal stress. As the pore air pressure change was reliant on the diffusion of air into the specimen, for each test stage the cell and air pressure were raised gradually in 10kPa steps. During each test stage the pore water pressure and shear modulus were monitored and a test stage assume complete when both of these were stable.

Shear modulus measurement of specimens for which suction was determined independently of the resonant column apparatus

The majority of resonant column testing in this research was conducted to determine a specimen's stiffness without measuring or controlling suction, at a variety of different net normal stresses. The water line valves remained closed during this testing procedure and the high-air-entry disc remained dry.

Once the specimen was assembled the desired net normal stress was applied to the specimen by raising the cell pressure to this value. When the cell had reached this pressure and a stable reading on the cell pressure transducer was obtained, the vacuum applied to the specimen was removed. The pump was disconnected from the air line and this line vented to atmosphere, the assumption being made that the pore air pressure was in equilibrium with the line and therefore zero.

At a given net normal stress, the specimen was tested at two hour intervals throughout a working day. Testing was conducted at one constant strain value in the linear elastic region, with the LVDT and cell pressure readings taken before and after testing. Following twenty four hours at constant pressure, a full shear modulus strain degradation test was undertaken. Once complete the net normal stress was then increased and the procedure repeated until the test regime for the specimen had been completed. The vacuum pump was then reattached to the air line. A vacuum applied to the specimen, the cell pressure reduced to zero and its pressure recorded along with the LVDT measurement. The cell was then disassembled and the specimen dimensions measured in-situ. The specimen was then removed from the apparatus and immediately placed in a pre-weighed tin, weighed and placed in a 105^0C oven for twenty four hours, re-weighed and its water content determined.

	Sand (%)	Silt (%)	Clay (%)
Material A	78	14	7
Material B	68	18	14
Material C	54	22	24
Material D	73	16	11

Table 3.1(a): Percentage of sand, silt and clay for materials A to D (as a percentage of total sample weight). Materials composition is based on representing the range of material encountered following a survey of the COALlink line (Gräbe, 2002). Reproduced from Gräbe (2002).

	Sand			Silt	Clay
	Leighton Buzzard sand fraction B (%)	Leighton Buzzard sand fraction C (%)	Leighton Buzzard sand fraction D (%)	HPF5 (%)	Hymod Prima (%)
	(particle size 1.18mm to 600um)	(particle size 600um to 300um)	(particle size 300um to 150um)		
Material A	51	11	11	19	8
Material B	43	9	9	23	16
Material C	32	7	7	27	27
Material D	47	10	10	21	13

Table 3.1(b): Different aggregates for materials A to D, (as a percentage of total sample weight) as formulated by Gräbe (2002). Reproduced from Gräbe (2002).

	Plasticity index (%)	Liquid limit (%)	Plastic limit (%)
Material A	9	23	14
Material B	16	30	14
Material C	19	36	17
Material D	15	29	14
Gräbe (2002)			
Material A	11	25	14
Material B	17	31	14
Material C	21	37	16
Material D	14	28	14
Commercial laboratory			
Material D	14	25	11

Table 3.2: Atterberg values determined following BS1377-2 (1990) including those determined by Gräbe (2002) and the results for material D from a commercial laboratory.

	Gas jar	Vacuum method	Theoretical[1]
Material A	2.62	2.57	2.64
Material B	2.64	2.46	2.64
Material C	2.62	2.35	2.64
Material D	2.64	2.58	2.64
LB B		2.64	2.65[a]
LB C		2.63	2.65
LB D		2.62	2.65
HPF 5		2.63	2.60[b]
Hymod Prima		2.39	2.65[c]

[1]Calculated based on published values for aggregate constituents and their percentage weight for each material ([a]Clayton et al.(2004), [b]Adwan Chemicals (2011), [c] Imery-Ceramics (2005))

Table 3.3: Determined specific gravity and theoretical values.

	Range of water content's applicable to	Calibration curve ($\log_{10}$(suction) –kPa)
Whatman No. 42 Filter Paper	<47%	4.842-0.0622w*
	>47%	6.050-2.48 log$w$

* w = water content

Table 3.4: Chandler et al. (1992) calibration curve equations. Reproduced from Ridley et al. (2003).

Aluminium bar number	Stem diameter (mm)	Stem height (mm)	Top platen diameter (mm)	Top platen height (mm)	Measured resonant frequency (Hz)
1	13	175	70	15	61.5
2	18	175	70	15	115.7
3	23	175	70	15	180.2
4	28	175	70	15	257.0

Aluminium bar number	k_{Stem} (Nm/rad)	$k_{Top\ platen}$ (Nm/rad)	Polar moment of inertia (I_a) of top platen (m)
1	433	4.24E+06	2.36E-06
2	1590	4.24E+06	2.36E-06
3	4239	4.24E+06	2.36E-06
4	9310	4.24E+06	2.36E-06

Table 3.5: Calibration aluminium bar properties and measured resonant frequency.

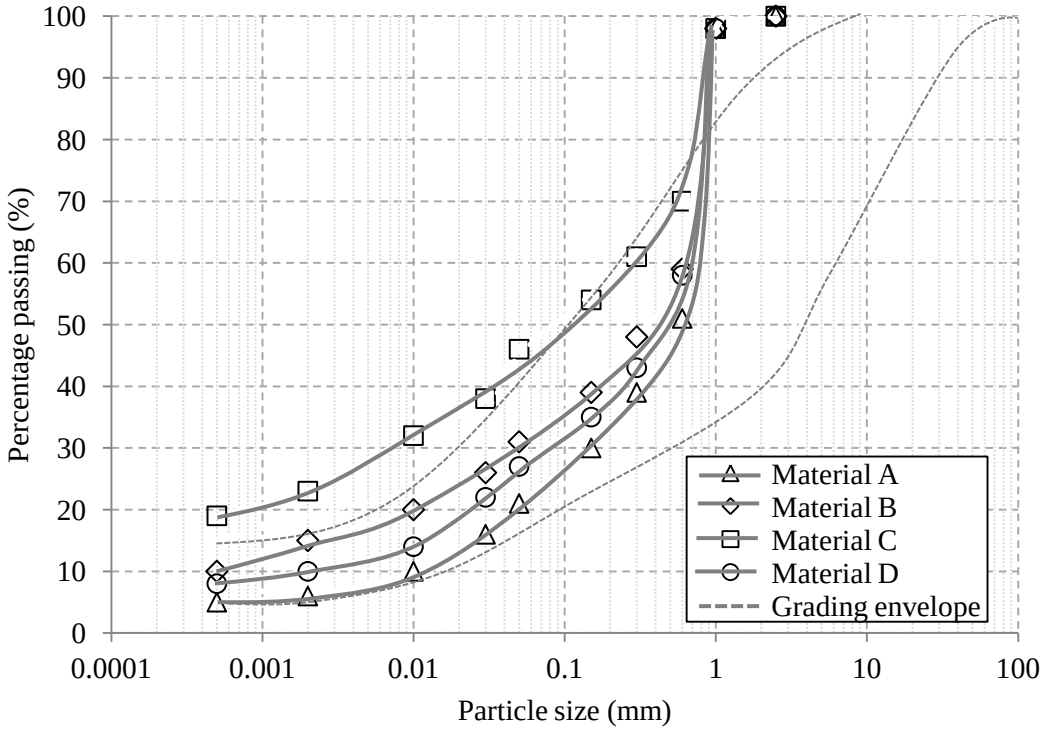

Figure 3.1: Particle size distribution for materials A to D and grading envelope of the formation material on the COALlink line. Redrawn from Gräbe (2002).

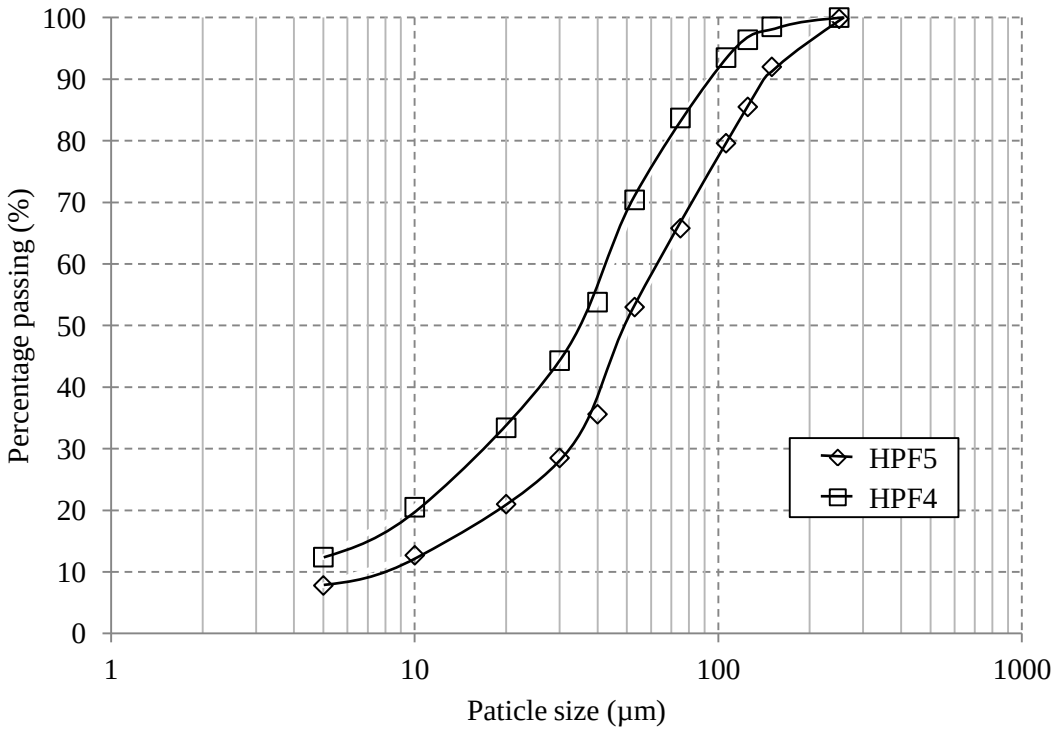

Figure 3.2: Particle size distribution for HPF5 and HPF4 Oakamoor silica flour. Drawn using data from Sibelco Minerals and Chemicals LTD (2000a, 2000b)

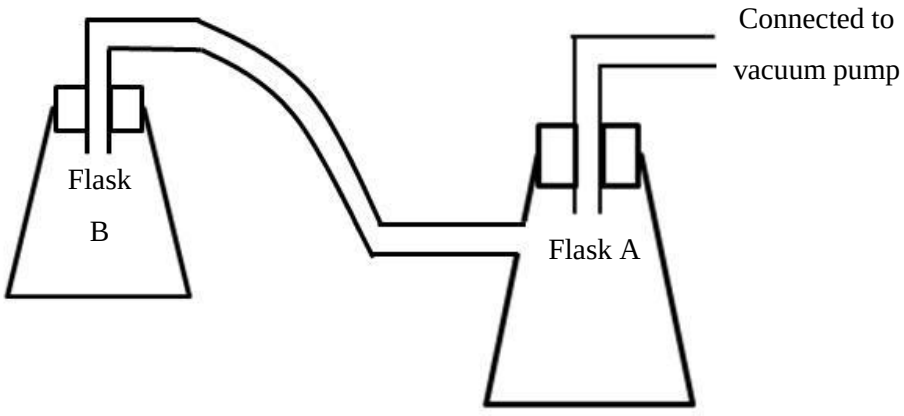

Figure 3.3: Specific gravity determination: Vacuum technique equipment setup.

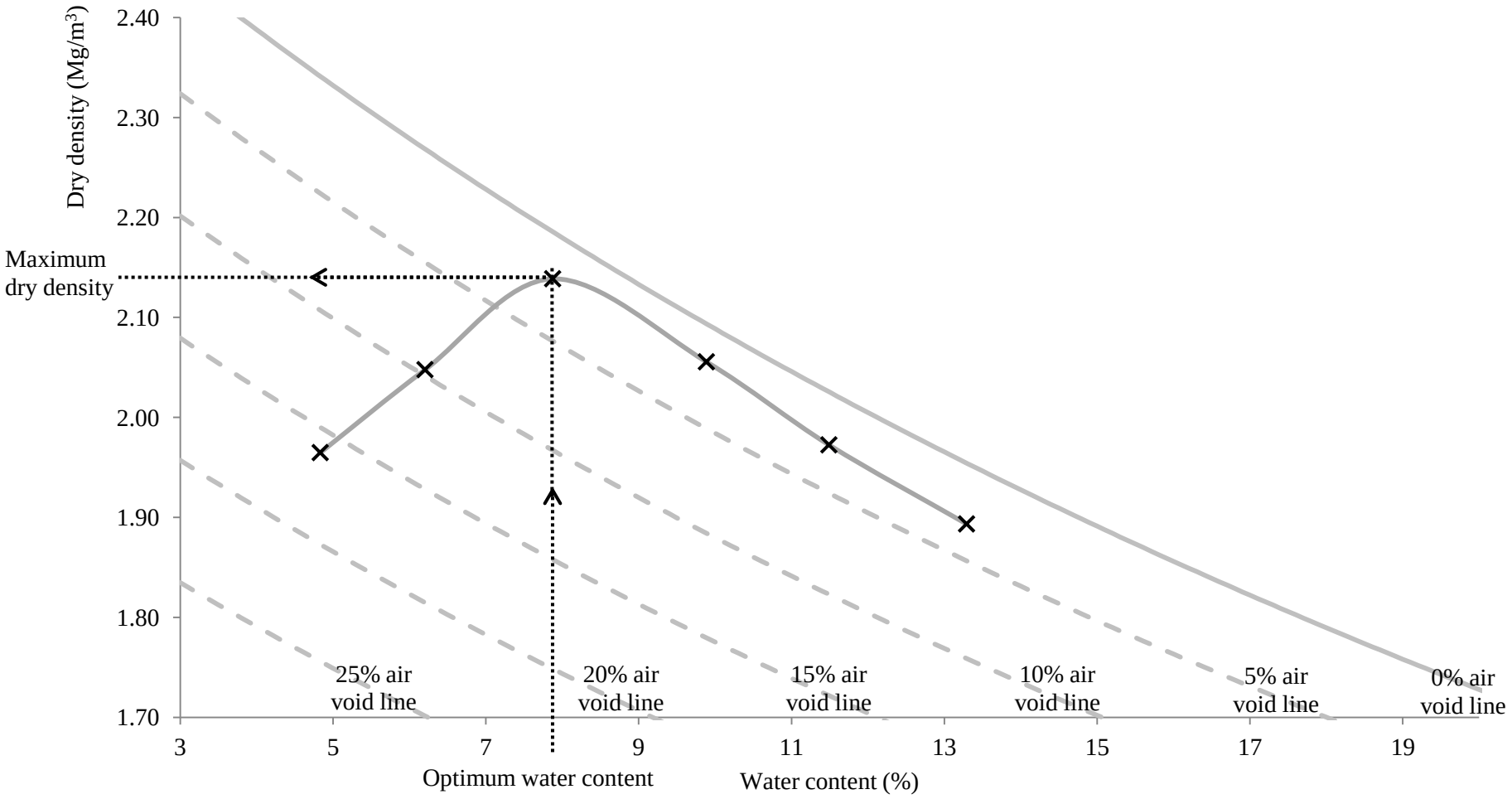

Figure 3.4: Maximum dry density and optimum water content for Proctor compaction curve of material A.

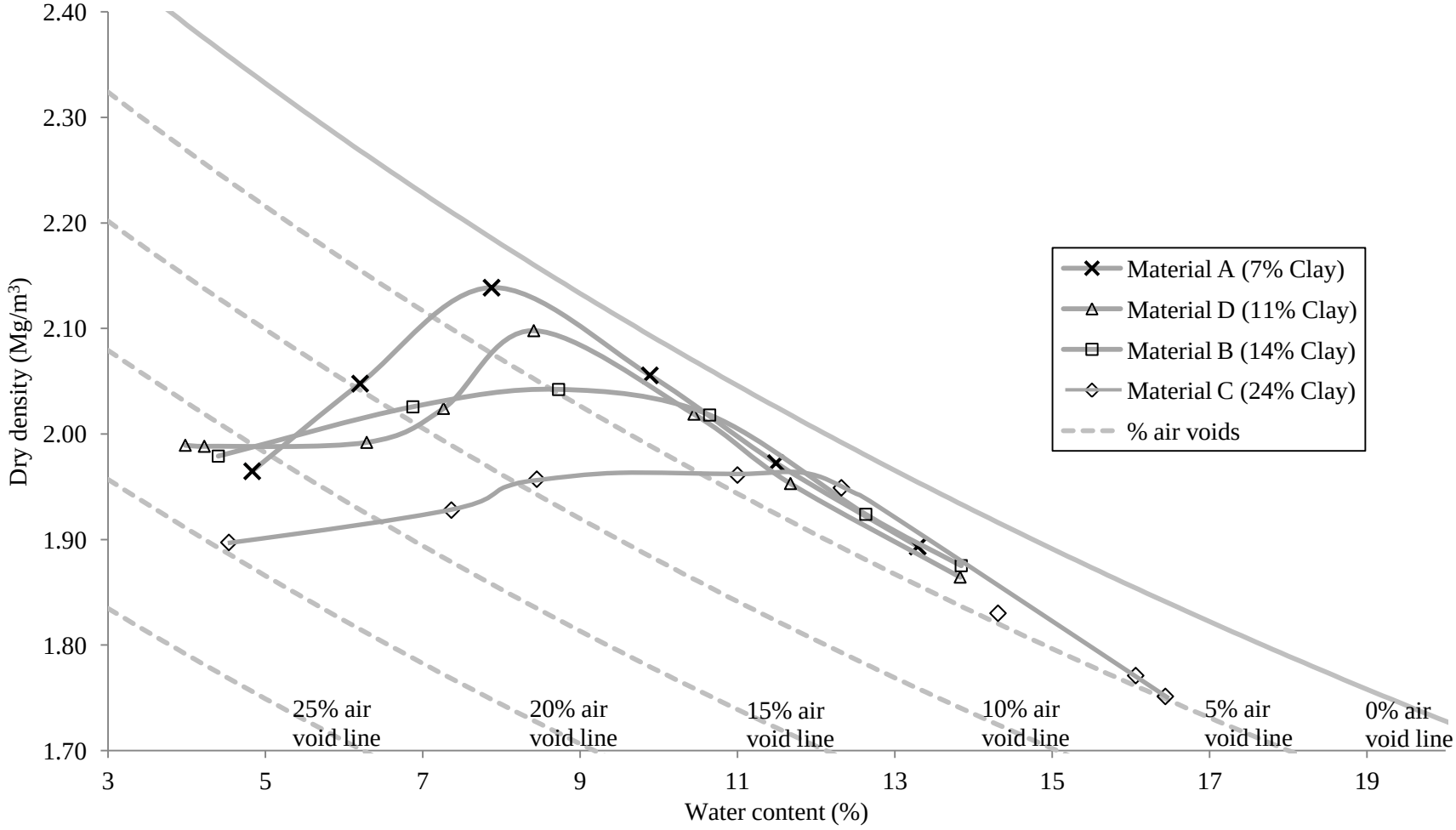

Figure 3.5: Proctor compaction curves for materials A to D.

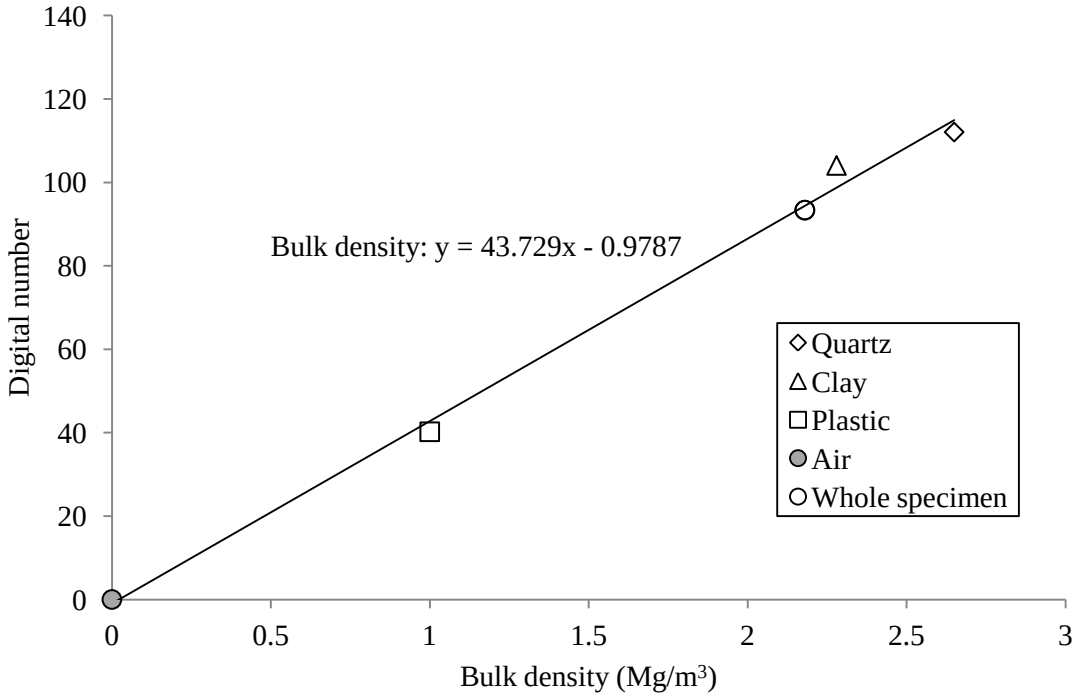

Figure 3.6(a): Calibration of CT digital number to bulk density (wet specimen)

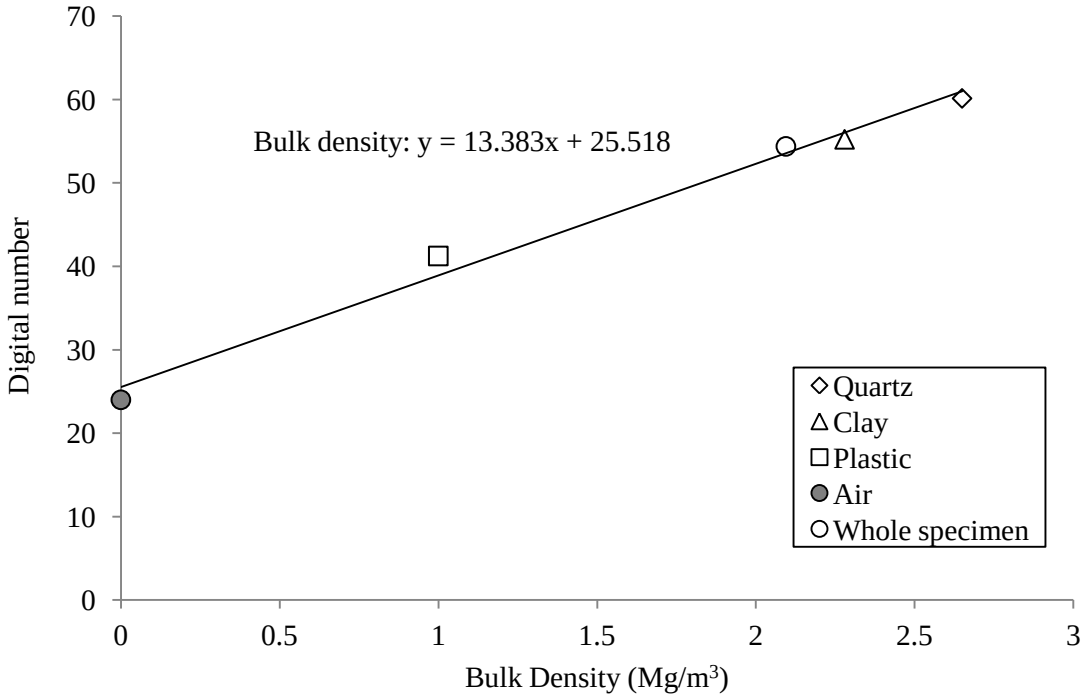

Figure 3.6(b): Calibration of CT digital number to bulk density (partially dried specimen)

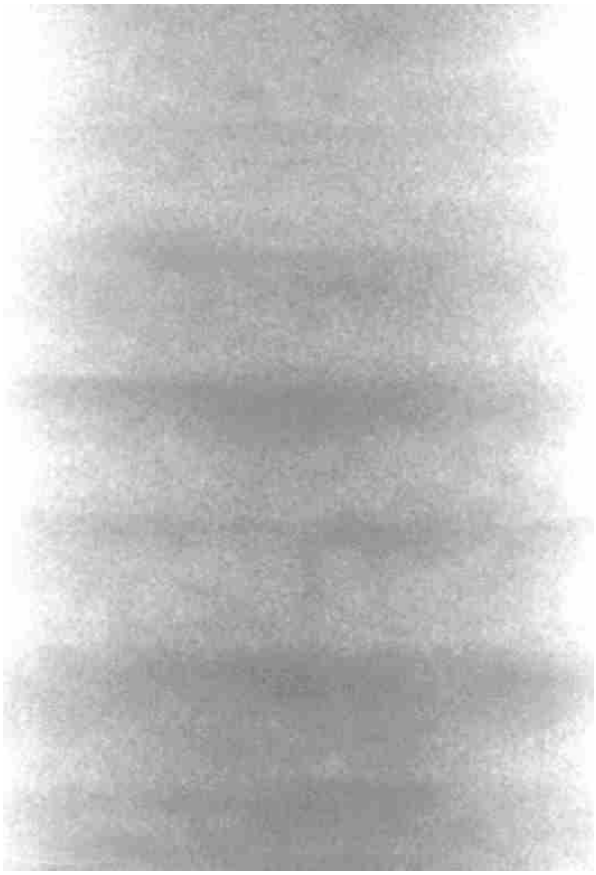

Bottom of specimen

Figure 3.7: Radiograph of the bottom segment of the specimen highlighting vertical density variation (wet specimen). (Due to the specimen's height the CT scan was conducted in two halves and joined together following scanning. Therefore the radiograph shows ¾ of specimen total height).

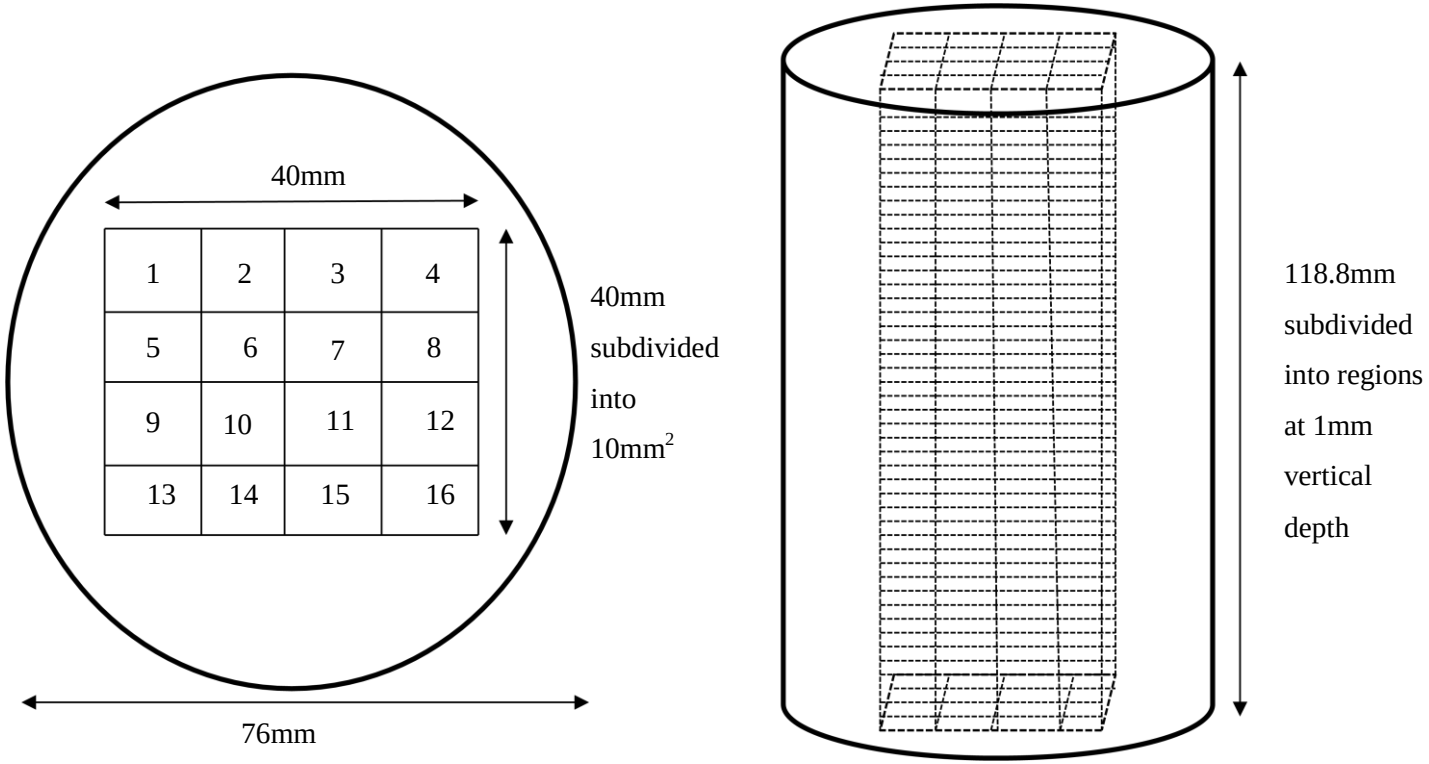

Figure 3.8: CT analysis: Regions of interest (note – figure not to scale).

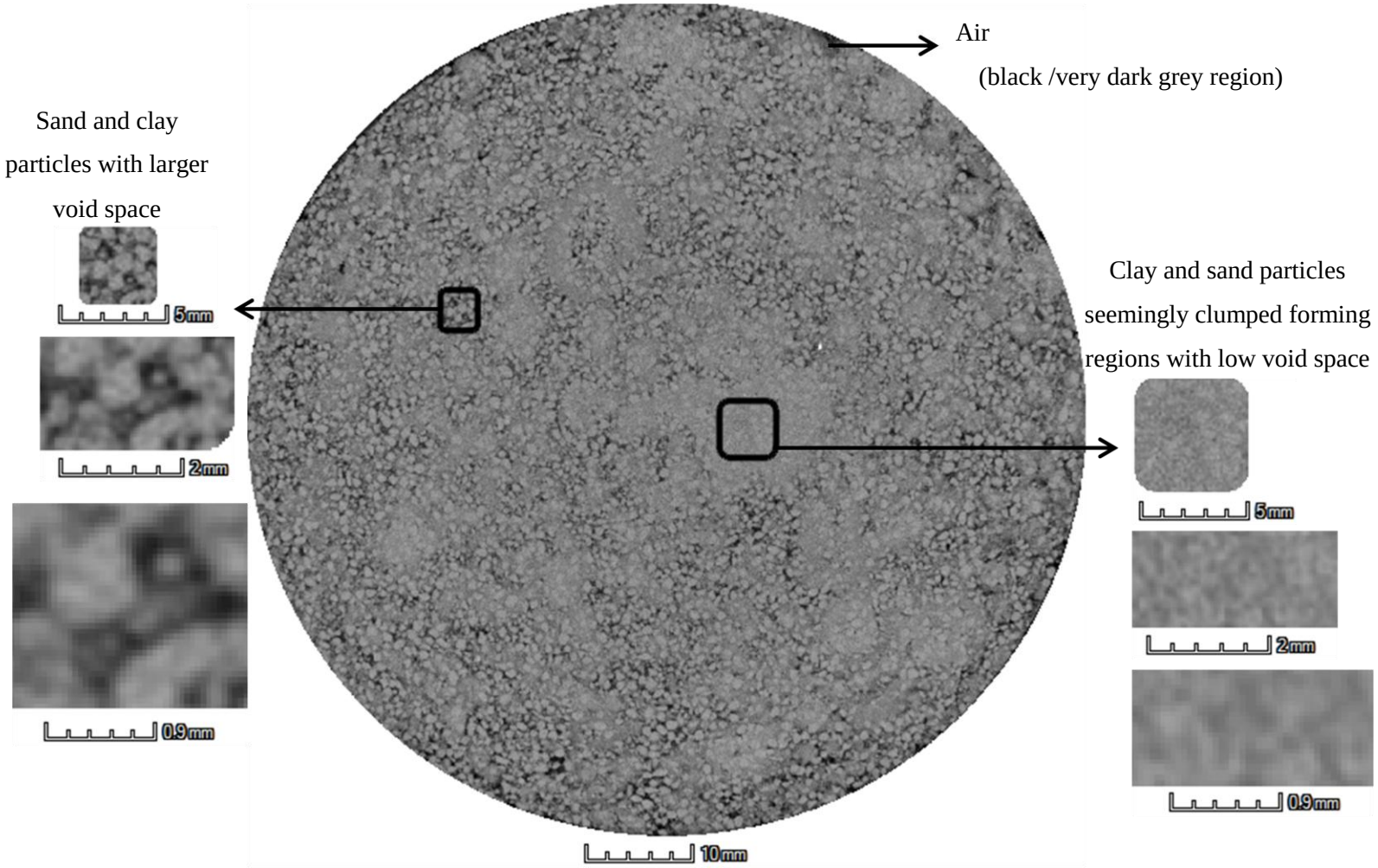

Figure 3.9: Horizontal slice of CT scan of material D dry density 2.10Mg/m^3/ water content4.22% (wet specimen).

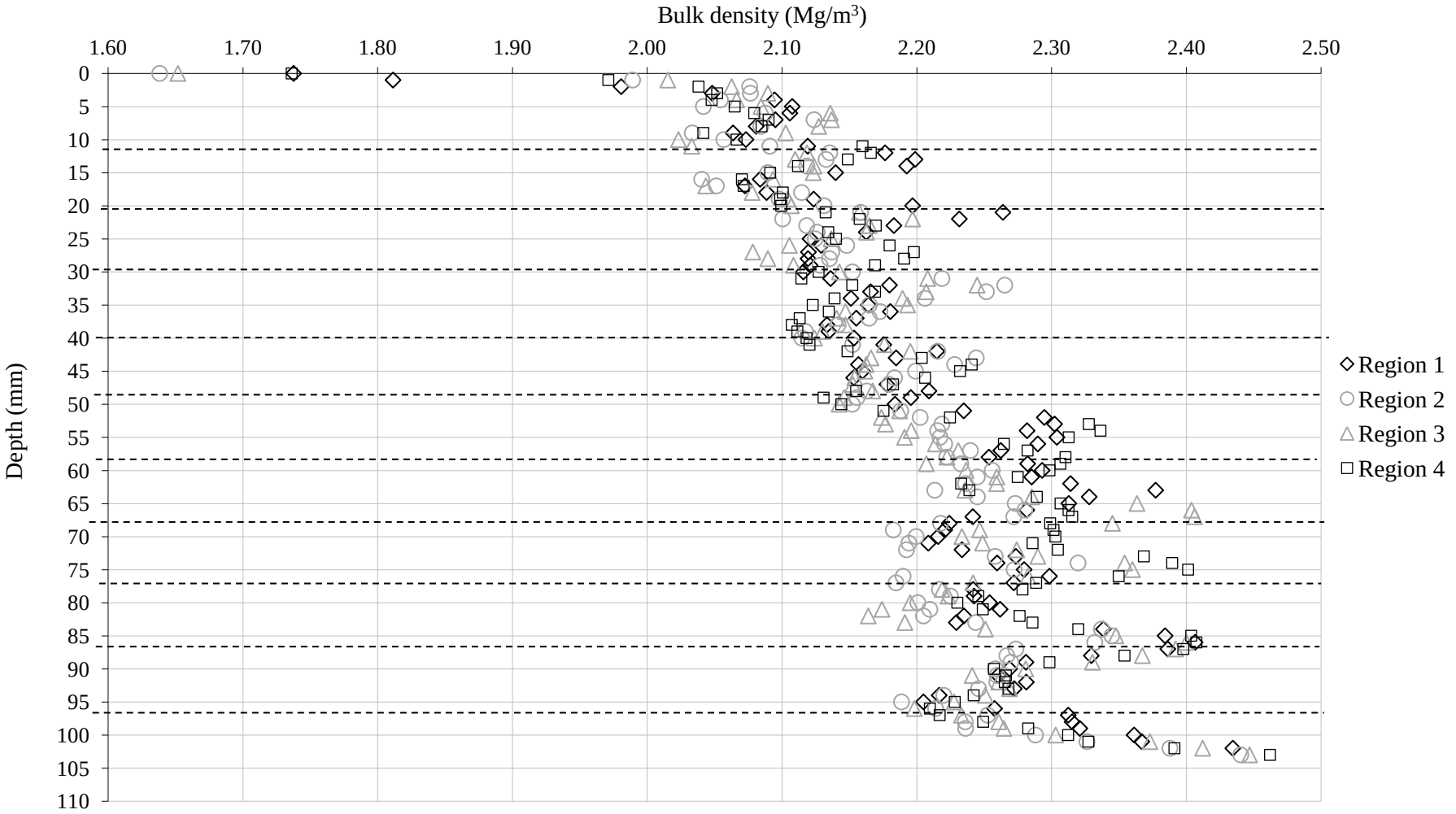

Figure 3.10: CT scan: Density variation for regions 1, 2, 3 and 4 (wet specimen).

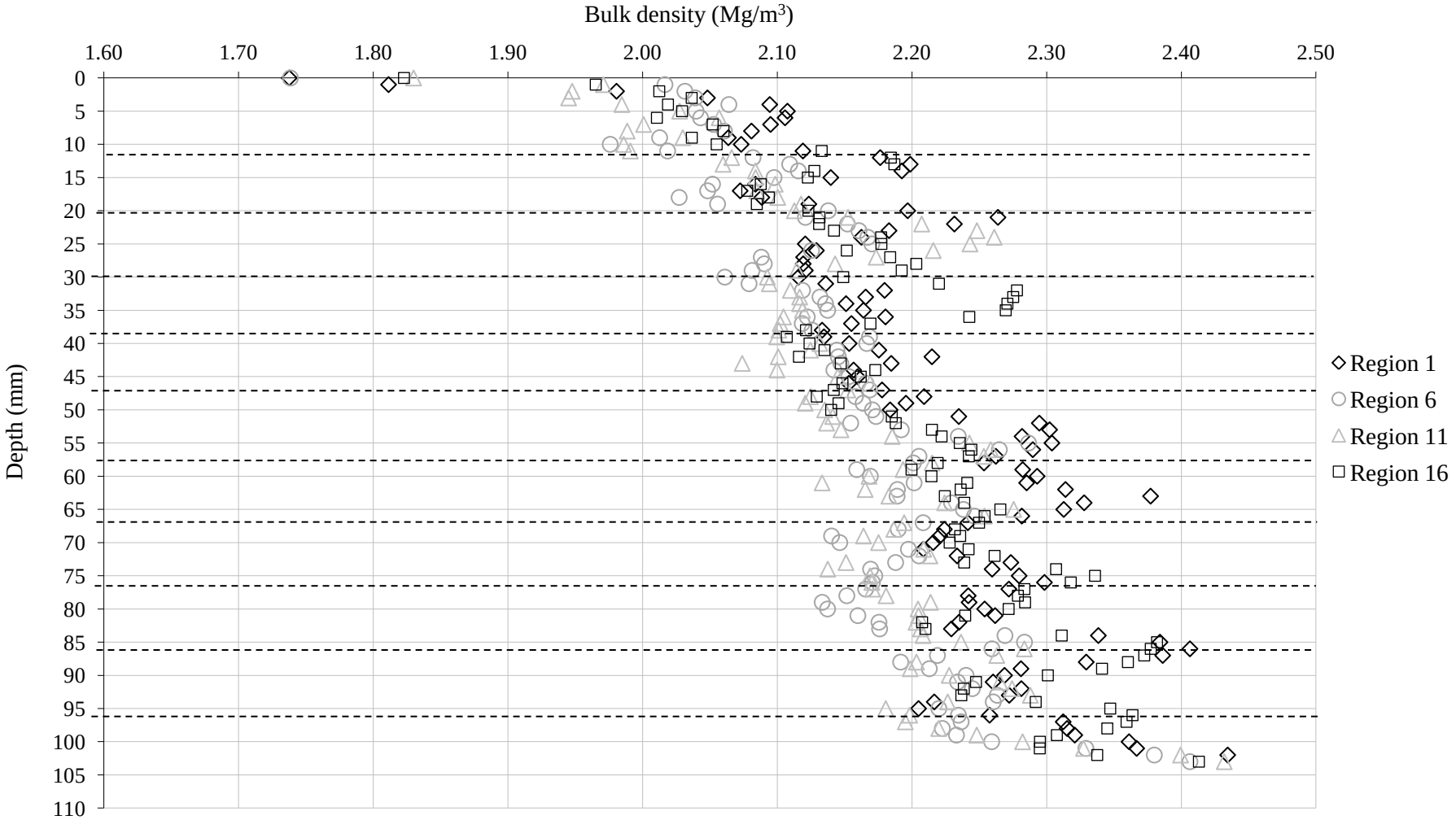

Figure 3.11: CT scan: Density variation for regions 1, 6, 11 and 16 (wet specimen).

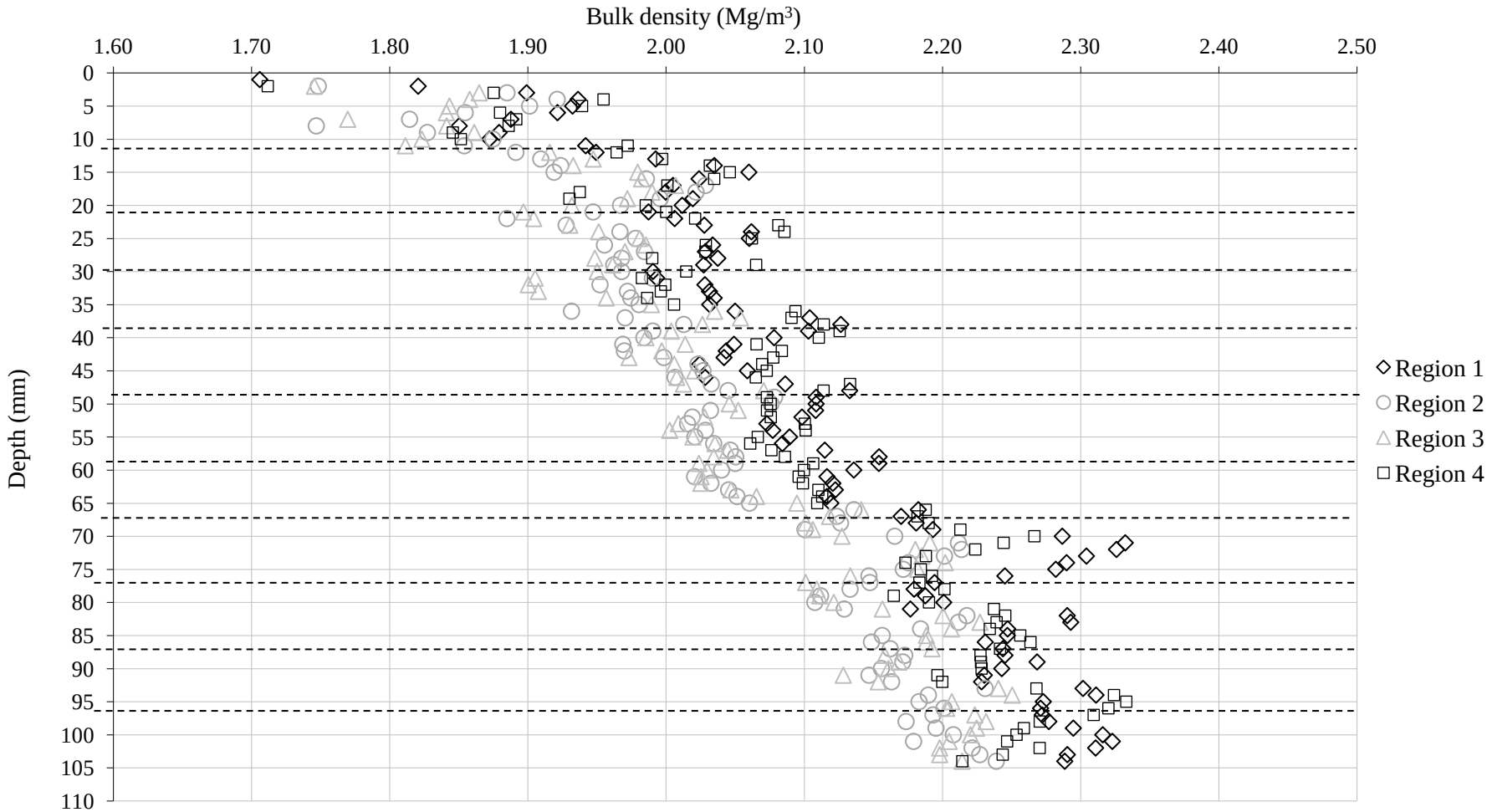

Figure 3.12: CT scan: Density variation for regions 1, 2, 3 and 4 (partially dried specimen).

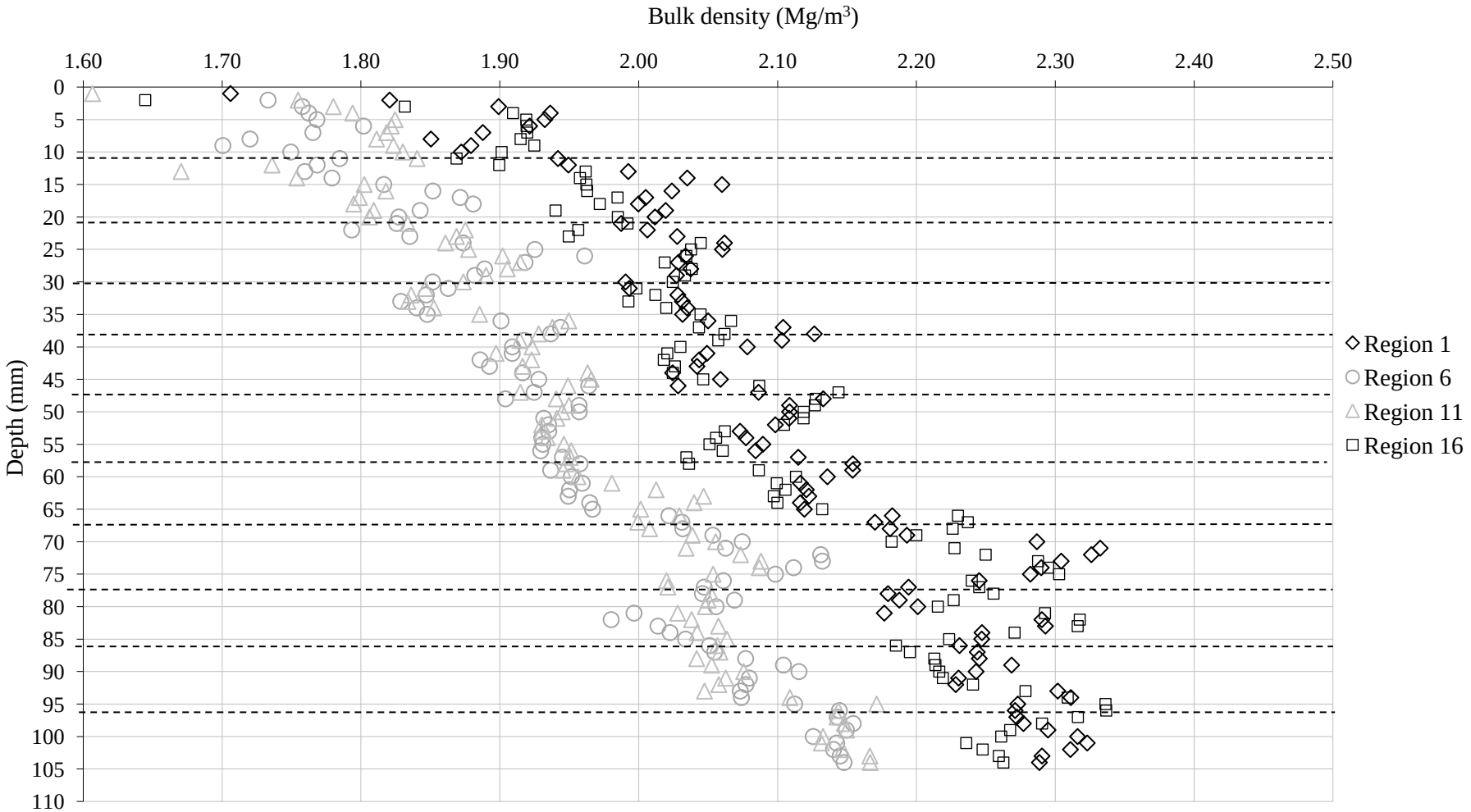

Figure 3.13: CT scan: Density variation for regions 1, 6, 11 and 16 (partially dried specimen).

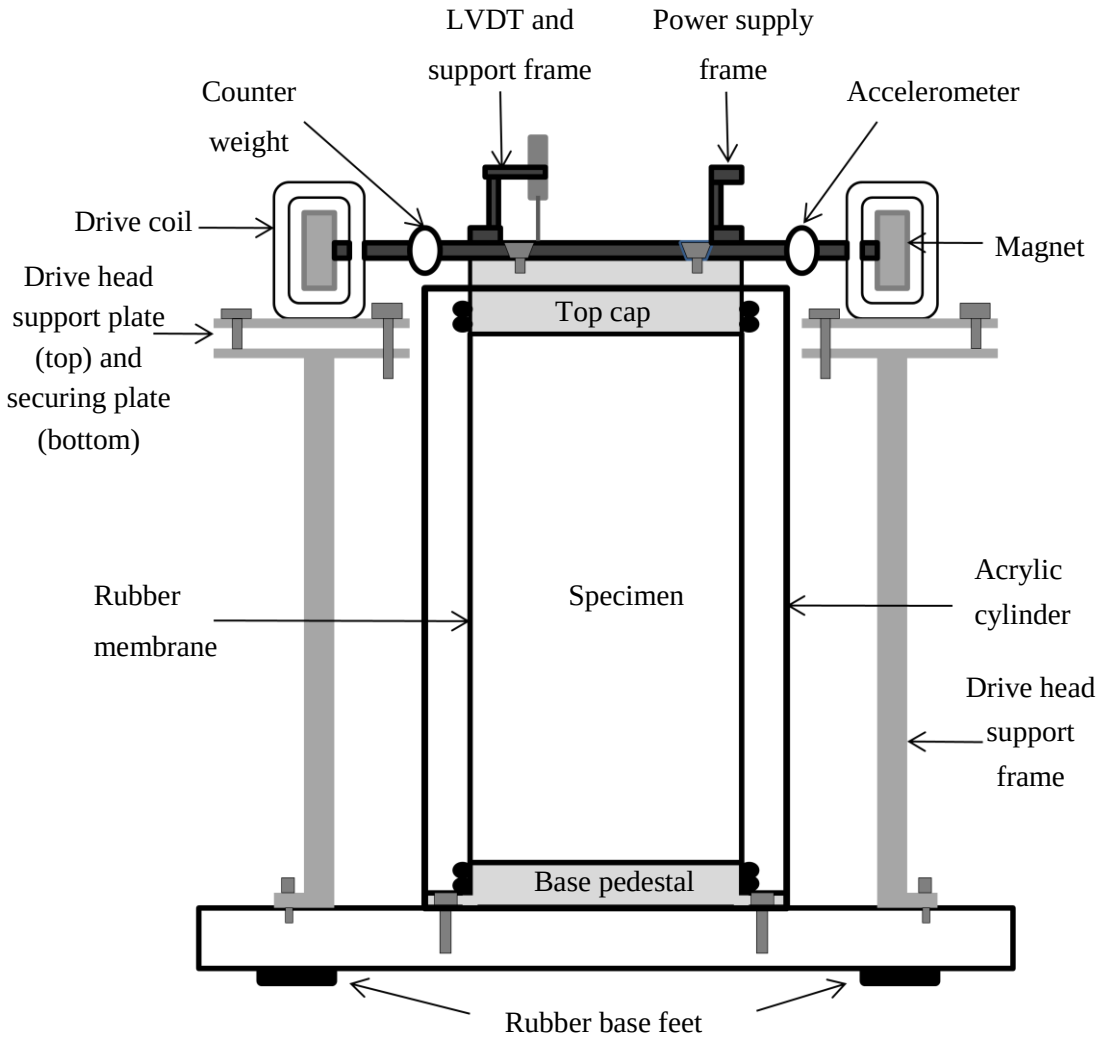

Figure 3.14: Schematic of resonant column apparatus.

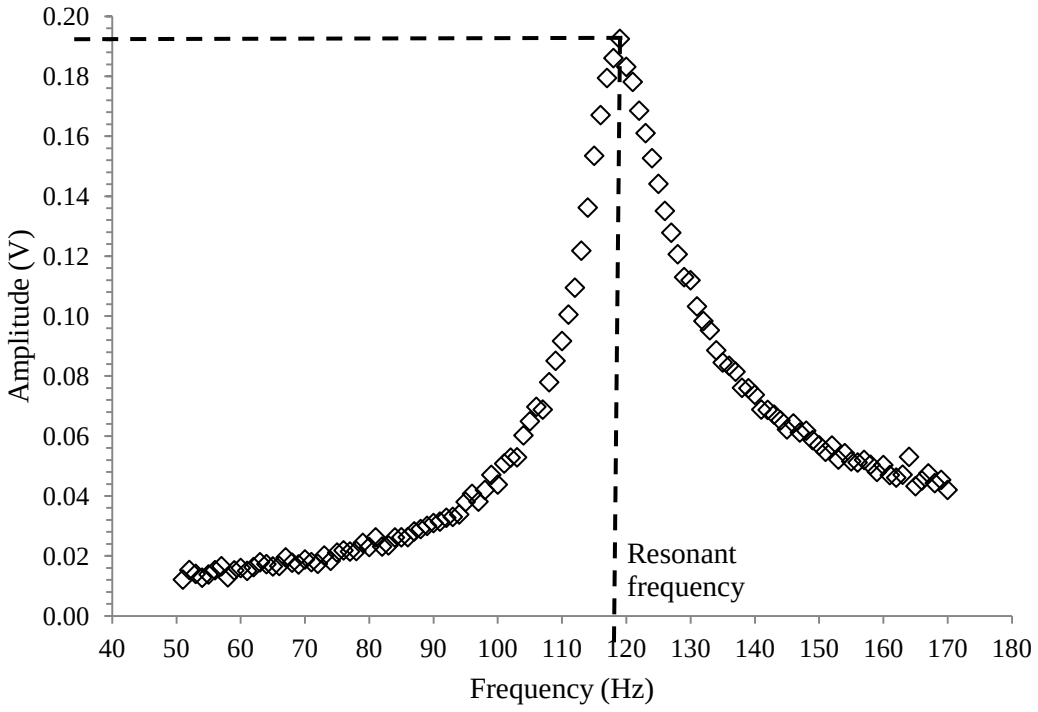

Figure 3.15: Frequency sweep at 10kPa net normal stress (Material D - 4% water content).

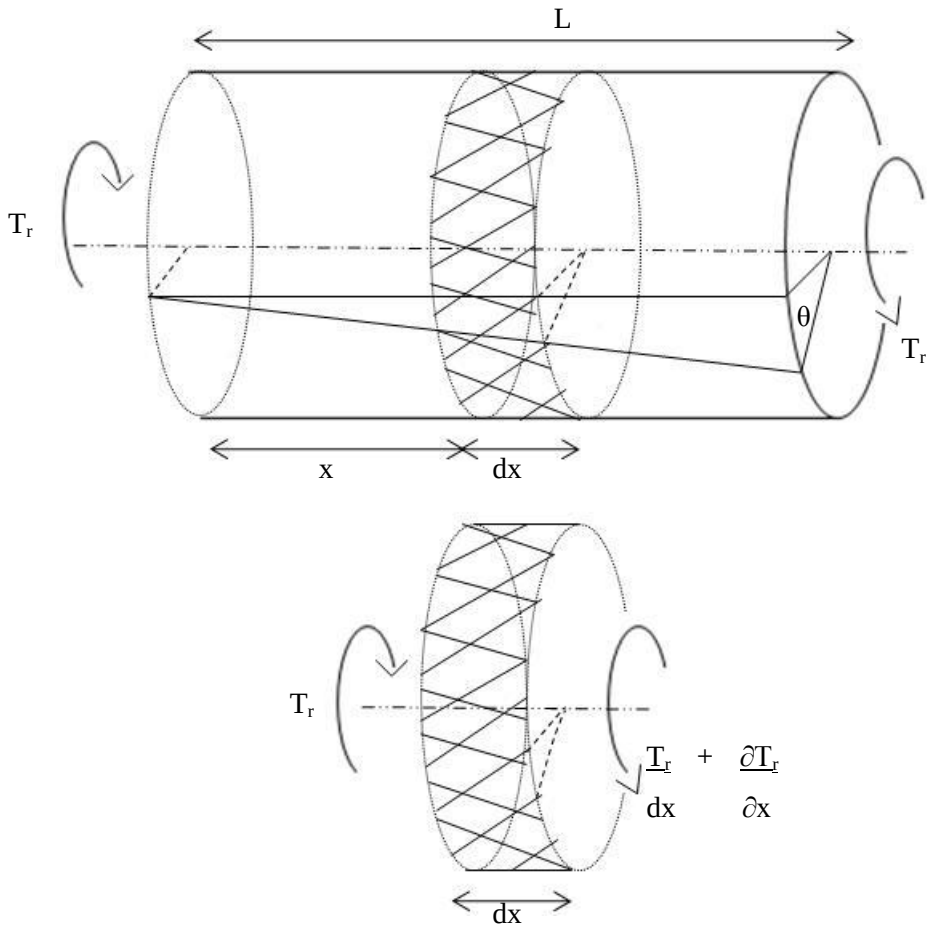

Figure 3.16: Idealisation of wave propagation in a solid elastic cylinder. Redrawn from Priest (2004).

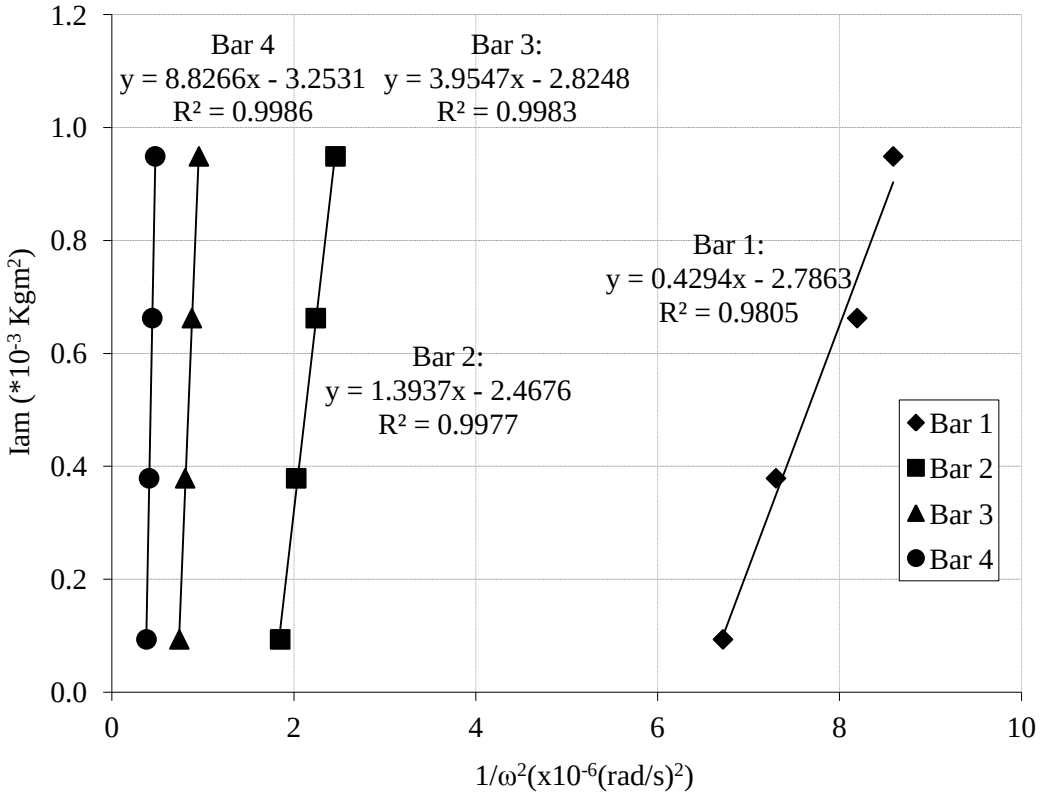

Figure 3.17: Single degree of freedom calibration.

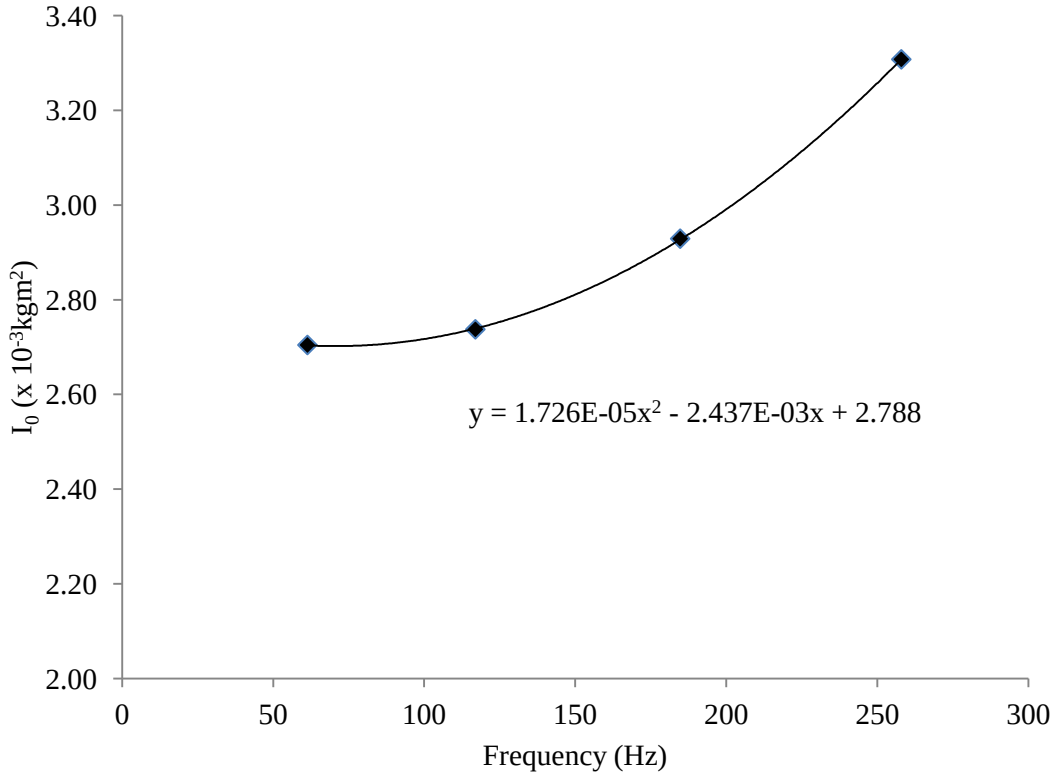

Figure 3.18: Single degree of freedom calibration I_0 from regression analysis.

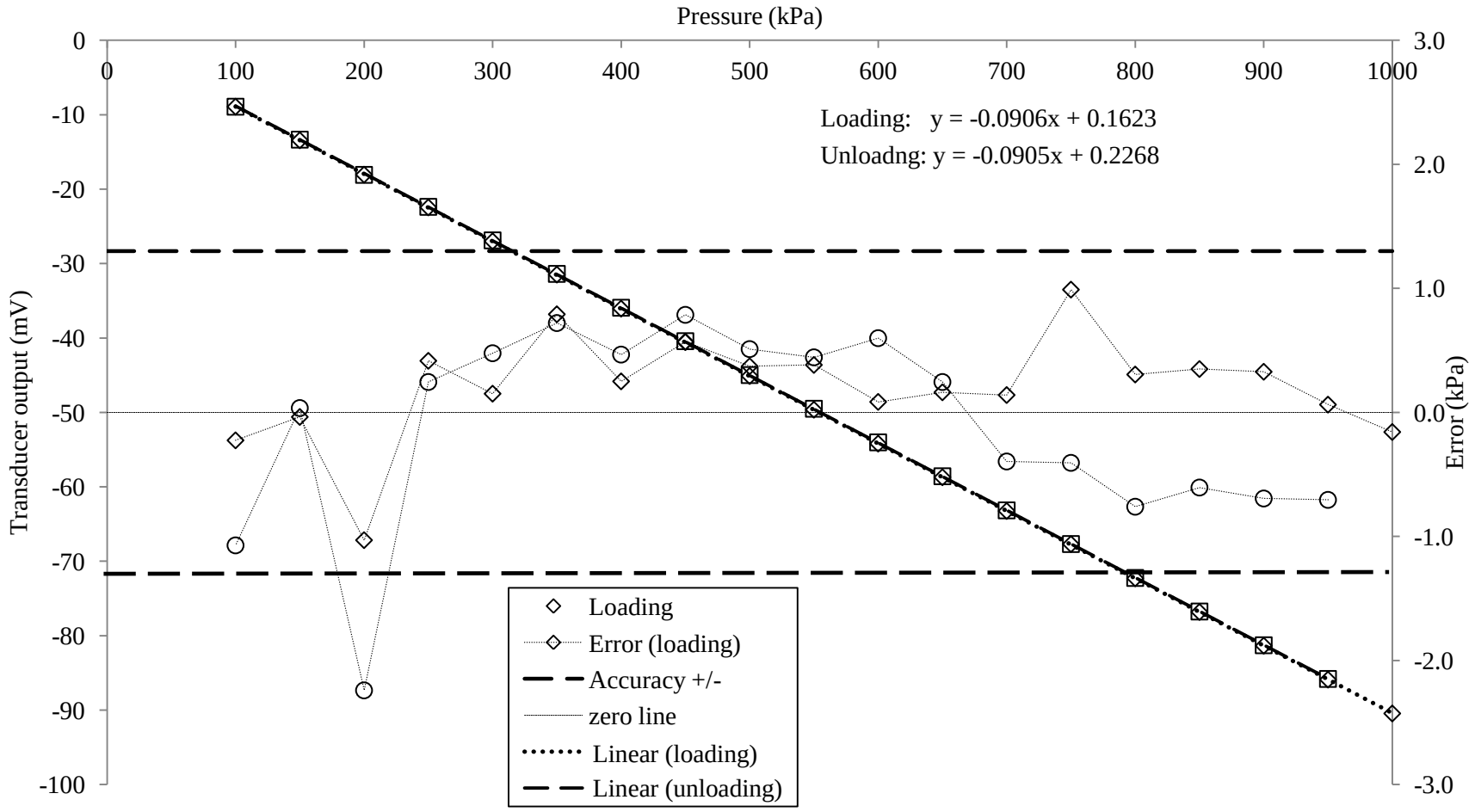

Figure 3.19: Cell pressure transducer calibration between 100kPa to 1000kPa with the Budenberg dead weight calibration equipment.

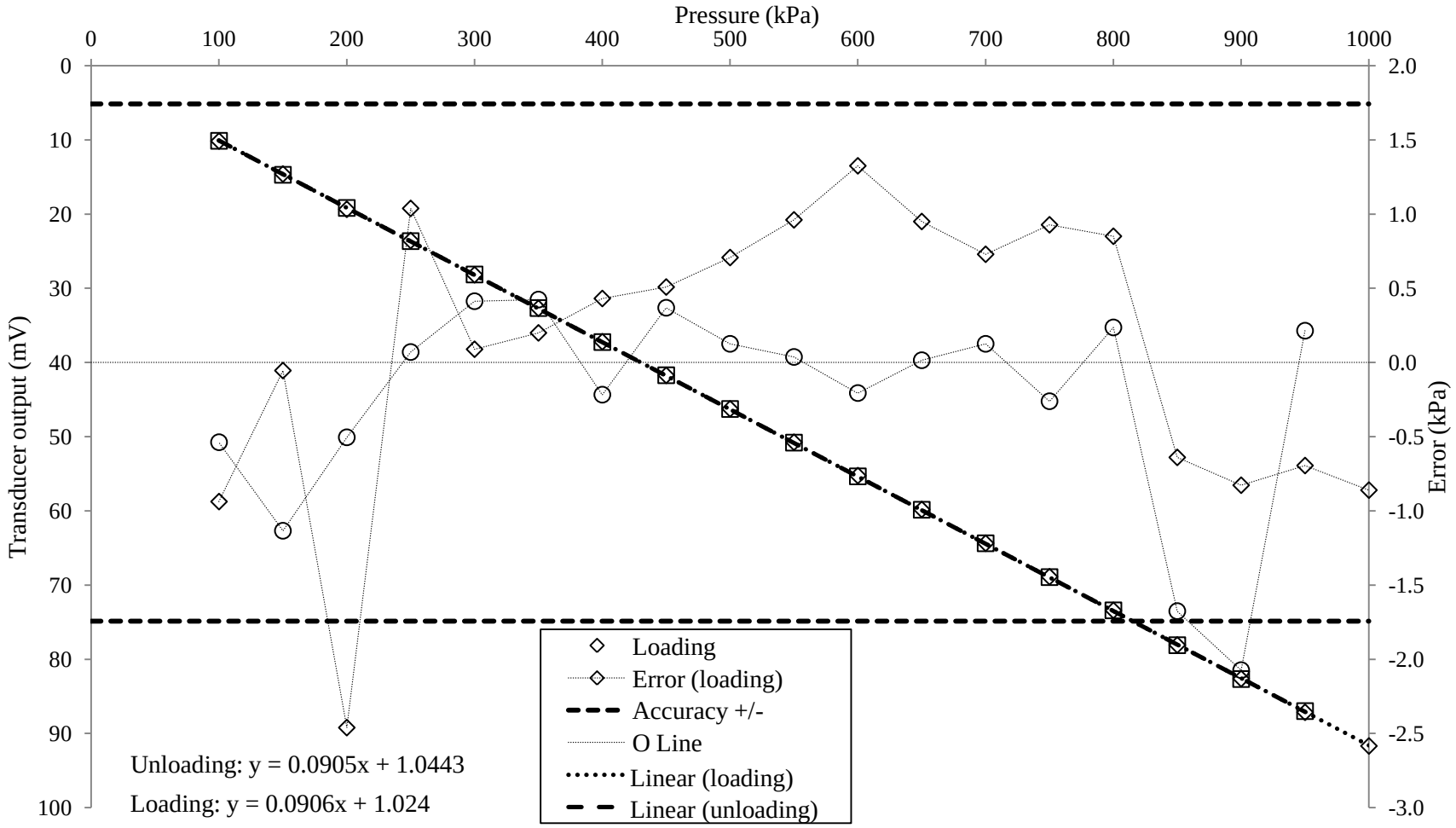

Figure 3.20: Air pressure transducer calibration between 100kPa to 1000kPa with the Budenberg dead weight calibration equipment.

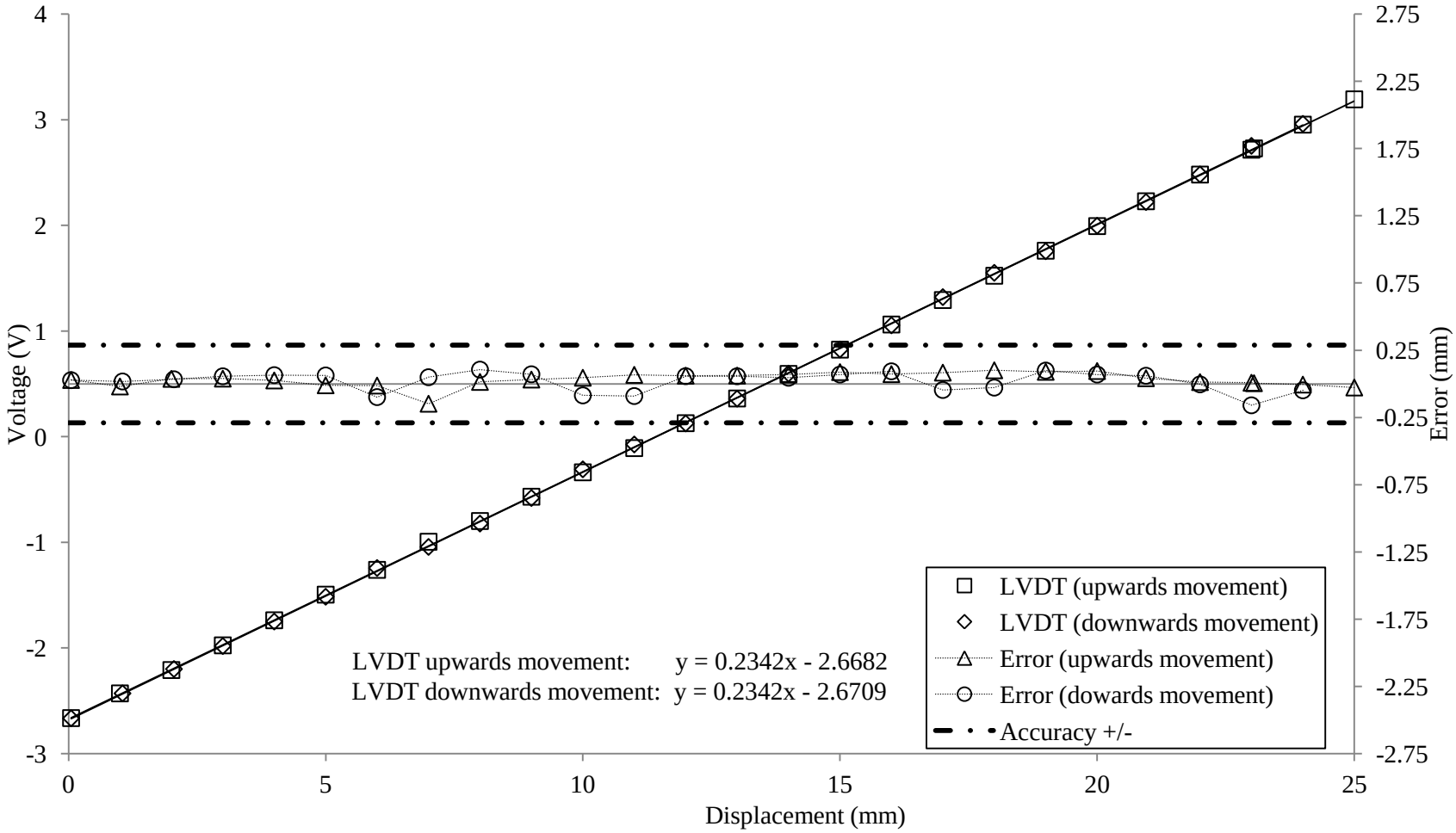

Figure 3.21: LVDT calibration.

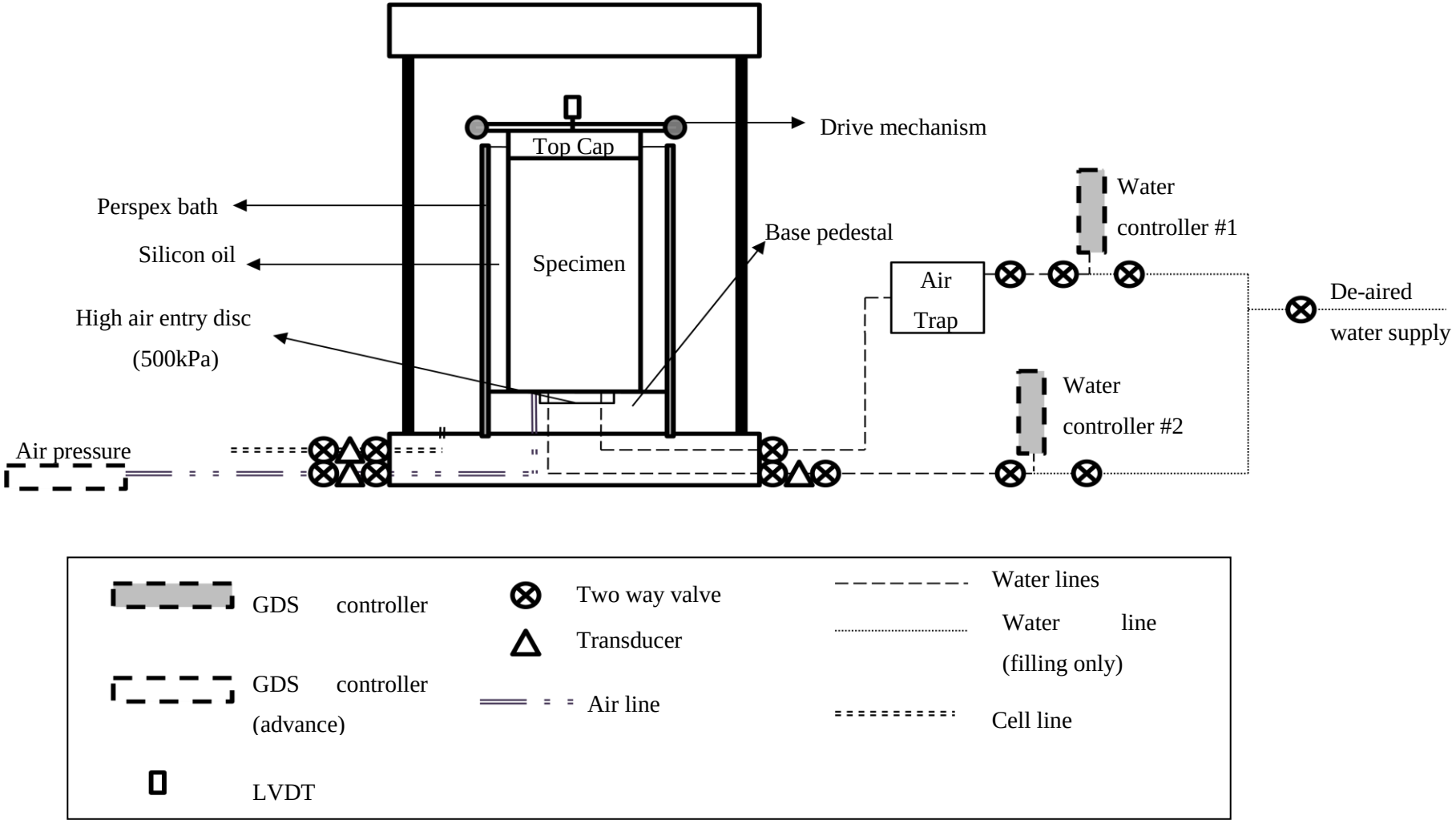

Figure 3.22: Configuration of resonant column apparatus to measure and control suction with the axis translation technique.

Chapter 4

Results and Discussion

This chapter firstly discusses the results of tests in which shear modulus and suction were simultaneously measured in the resonant column apparatus using axis translation. However, due to difficulties in achieving the simultaneous measurements, independent measurement of shear modulus and suction were undertaken. Thus, the majority of this chapter focuses on the independent tests and the resultant soil water characteristic curves obtained for each material using the pressure plate apparatus and filter paper technique. It concludes with a description of how suction influences the shear modulus, and its implications in practice.

Shear modulus and suction measurements were undertaken on specimens of material D and C, whilst only suction measurements were conducted on materials A and B. Testing predominantly focused on material D, as its particle size distribution coincides with the average grading for the formation material on the COALlink line (Figure 3.1) (Gräbe, 2002). As plasticity increases, suction at a given water content increases (Kim et al., 2003). As material C was the most plastic of the materials it was hypothesised that at a given dry density and water content it would have the largest suction. However, for saturated specimens at the same effective stress, shear modulus is typically lower for a clay than a sand specimen (Bui, 2009). Testing material C therefore allowed comparison of the suction/shear modulus behaviour for the different materials, but also how increased clay content influenced the shear modulus.

4.1. Axis translation technique

The axis translation technique is commonly employed for testing unsaturated soils. The resonant column apparatus was adapted as discussed in section 3.5 to apply cell and pore air pressure, whilst attempting to measure pore water pressure, in order to calculate the net normal stress and the matric suction of the specimen.

The shear modulus of a specimen of material D at a dry density of 2.11Mg/m^3 and water content of 4.22%, was initially measured (as detailed in Section 3.5.2) under a constant net normal stress (39kPa) for fifteen days, as the shear modulus of cohesive soil has been found to be dependent on confinement period (Anderson and Stokoe II, 1977) (Section 2.3.2). Although the measured undrained pore water pressure varied throughout this period, there was only a small linear increase in shear modulus with confinement period (Figure 4.1), probably resulting from secondary consolidation.

The specimen was then tested at a target net normal stress (40kPa) whilst cell and air pressures were increased simultaneously for each stage (stages 1 to 8:Table 4.1), with the pore water pressure line locked off (undrained). Although there were small changes in the net normal stress, as seen in Figure 4.2 the shear modulus throughout all stages continued to increase in the same linear manner with time as observed in the previous stage. These results suggest that the axis translation technique has negligible effect on a specimen's behaviour as deduced from its shear modulus.

During the simultaneous increase in cell and air pressure(s) the measured pore water pressure also changed although with a smaller magnitude. Assuming that the pore water phase is continuous, it should increase by the same amount that the air pressure is raised. If the measured pore water pressure were the real values, this indicates that the specimen's matric suction was increasing during translation, which would be expected to increase the shear modulus. To understand if the shear modulus and/or pore water pressure readings were incorrect, the net normal stress was varied (stages 9 to 17: Table 4.1). This led to an increase in shear modulus with an increase in net normal stress increase and decreased with a reduction in net normal stress, as seen in Table 4.1 and Figure 4.3a and b. This trend suggests that the shear modulus readings were correct, and the measured pore water pressure incorrect. Hence, the constant shear modulus during pressure translation suggests that the axis translation technique does not alter a specimen's properties and is therefore a valid testing technique.

An attempt was made to saturate the specimen by flushing water up through the high-air-entry disc, which achieved a B-value of 0.65. However, testing under the same net normal stress as shown in stage 17 (Table 4.1) the shear modulus reduced from 354MPa to 249MPa. This change in stiffness behaviour is linked to the saturation procedure which reduces the degree of suction within the specimen, suggesting that suction led to the change in behaviour.

It has been suggested that desaturation of the porous disc (Lourenco et al., 2008) caused by the period of time between the specimen coming into contact with the high-air-entry disc and raising the air pressure to measure a positive pore water pressure can lead to errors in measured matric suction. Even when this time was minimised, which improved the suction measured, the value of suction measured was still significantly less than that measured with the filter paper technique for a similarly prepared specimen. Due to the difficulties in measuring the pore water pressure using this set-up, along with the time constraints of this research, further work into addressing this issue was not conducted.

4.2 Soil water characteristic curves

To understand the suction inherent in the materials at different water contents, soil water characteristic curves were obtained using the filter paper technique and pressure plate apparatus (during drying) following the procedures discussed in sections 3.3.1 and 3.3.2. The following section focuses on the repeatability of these techniques, their differences, and the influence of the dry density and water content of these specimens on these curves when constructed.

4.2.1 Accuracy and repeatability

In order to understand and interpret experimental results correctly, it is fundamental to understand sources of error, accuracy and repeatability of a procedure. Accuracy relates to the ability to measure the true value, whilst repeatability is how precisely a given measurement can be repeated. The following discusses the assessment of the repeatability of measurements using the pressure plate and the filter paper techniques. Repeatability of the water content measurements, which is also relevant to the resonant column testing, is discussed first.

Gravimetric water content

Gravimetric water content was determined for the specimens and material mixes using a balance with a 0.01g resolution, from:

$$\text{Water content } (\%) = \frac{(M_1 - M_2)}{(M_2 - M_3)} \tag{4.1}$$

Where M_1 is the mass of the wet specimen and weighing container, M_2 is the mass of the dried specimen and weighing container and M_3 is the container mass. A number of moisture content tests were carried out to determine if the container used affected the measured gravimetric moisture content. The containers recommended in BS1377-2 (1990) were used

with and without lids along with metal trays described as baking tins in Table 4.2, since the specimens were too big for the recommended tins.

Table 4.2 highlights the results of these tests. It can be seen that apart from mix 1 set 5 good repeatability was achieved for a given container, with or without lids. For mix 1 and mix 3, a lower moisture content was measured than the target value of 8% and higher values for mix 2, although within a mix repeatability was good. The variation within a mix for different techniques was a maximum of 1.03% for all three mixes, with a variation of 0.02% for a technique (these values discount the anomaly highlighted above and the anomaly in mix 3 set 1). To ascertain whether the error was due to evaporation, water content variation within the mix, or due to weighing errors, tests were conducted replacing the soil with a metal weight.

Table 4.3 highlights the results of these tests showing the error associated with incorrectly weighing the tins gave a mean value of 0.02% for all sets with a maximum error of 0.15%. This suggests that weighing errors were negligible, and the major variation was due to evaporation and/or water content variation within the mix.

Filter paper water content

An analytical balance with a resolution of 0.0001g was used for determining water content. This accuracy of scale was required due to the small mass of a filter paper and the even smaller difference in mass between partially wet and dry filter papers due to absorbed water. To assess the accuracy in measurement of individual filter papers, the water content of six dried filter papers (placed in 105^0C oven for twenty four hours prior to any measurements) was determined, using the same procedure as highlighted in section 3.3.1 for measuring a specimen's suction. As an oven dried filter paper's water content should be zero, and this is used to derive the suction, theoretically the suction should also be zero. Therefore the difference between the measured oven dried filter paper's water content and the theoretical value provides a repeatability of the water content measurement but also the derived suction value. This was repeated twice more on the same filter papers with the same moisture tins, although due to damage some of the filter papers were discarded and not replaced between the sets of tests.

The measured gravimetric water contents for each test on supposedly dry filter paper are shown in Table 4.4, the water contents ranging for all tests between 0.5392% to 3.3446% with a mean value of 1.8851% and a standard deviation of 1.044%. The inaccuracy measured may occur due to a change in moisture of the filter paper during transfer, with the

magnitude depending on the water content of the filter paper. It is unrealistic and difficult to determine this change for each test but based on Chandler and Gutierrez (1986) assessment of both wetting and drying of on an initially oven-dried filter paper, it can be concluded that it is a contributing factor. Nevertheless, provided that the procedure is carried out as quickly as possible within their recommended thirty seconds it has been assumed to be insignificant (Chandler and Gutierrez, 1986).

Determination of suction from filter paper water content

Suction was determined, using Chandler et al. (1992) calibration curve (which is a further development of Chandler and Gutierrez (1986)). Two curves are given, with Equation 4.2 being used for a filter paper water content (w) less than 47%, and Equation 4.3 when w is greater.

$$\log_{10}(\text{suction}) = 4.8842 - 0.0622\text{w} \tag{4.2}$$

$$\log_{10}(\text{suction}) = 6.050 - 2.48\log\text{w} \tag{4.3}$$

The range of water content between 0.5392% to 3.3446% for the supposedly dry filter papers results in a suction range of 70902kPa to 46758kPa. As the filter paper's water content is used for determining suction the standard deviation error of 1.044% measured for the dried filter papers was added and subtracted from a range of filter paper tests, used to derive the soil water characteristic curves, to understand the effect this error had on the derived suction value. Table 4.5 summaries the results over the suction range encountered in this research.

Although the measured error is consistent throughout, the overall range of suction values at higher suctions is greater than that at low suction values (as seen in Table 4.5). This suggests that this technique is best suited for determining low suctions, where the possible error in suction values is low. However, given the difficulty in measuring large magnitude suctions using other techniques, such as pressure plate or osmotic methods, high suctions were still determined from filter paper water contents, as it proved a measure of these suctions.

Filter paper suction equilibrium period

A filter paper's water content is determined once the suction in the paper has reached equilibrium with the soil. ASTM D 5298-4 (1994) suggests this occurs after seven days. To assess this a number of specimens of material D at a dry density of 2.10Mg/m^3, air dried to

4% and 6% water content from a preparation water content of 8.13%, were tested with different equilibrium periods.

Table 4.6 shows the results from these tests. It can be seen that minor variations (0.5%) in moisture content occur for both specimens (equating to a suction difference of about 100kPa), with the same order of magnitude for the 6% specimen after 28 days as the 4% after 14 days with only minor variations occurring from day 5 and day 8 for the 4% and 6% specimens. The extension in equilibrium time therefore has not significantly influenced the suction and therefore seven days was taken as sufficient time to achieve suction equilibrium between a specimen and filter paper.

Although the smallest possible storage jars were used, the specimen may exchange moisture with the air in the jar, thus changing the suction (Ridley, 1995). The reduction in moisture content with extended storage seen in Table 4.6 seems to indicate this effect.

Pressure plate – pressure application

The pressure plate technique is reliant on accurately determining the water content of the specimen and setting of the required pressure (see section 4.2.1). The laboratory's compressed air supply (maximum pressure between 900 and 950kPa (compressor dependent)) was used to provide the pressure plates cell pressure (specimens air pressure). As two pressure plates were being used (500kPa and 1500kPa), slightly different arrangements were used for the air connection. In the 500kPa pressure plate the pressure gauge (a maximum pressure of 400kPa, with an accuracy of 0.25%) was situated before the apparatus with a valve to isolate the apparatus and the gauge. This ensured that the target pressure could be set. The 1500kPa apparatus had a Druck digital pressure gauge (DPI-104) (accuracy was ±0.1%). However, no valve was available to isolate the air line and the apparatus when raising the pressure; therefore if a higher pressure was inadvertently applied it was left at that value.

Pressure plate – suction equilibrium period

In this research, specimens were removed at regular intervals from the pressure plate during a test, one day for 500kPa pressure plate and four days for the 1500kPa pressure plate. A number of trial tests were conducted by removing specimens of material C at a dry density of 2.10Mg/m^3 subjected to a constant 400kPa pressure at daily intervals (Figure 4.4). Material C was used because it has the highest clay content of the materials, therefore assumed to have the lowest coefficient of permeability and hence it was assumed to take the longest to reach equilibrium. A test pressure of 400kPa was used for both pressure plates to

compare results. Coefficient of permeability within a specimen reduces with increasing suction since water transfer is only through the pore water phase and its volume reduces with increasing suction. The chosen test pressure would take the longest time to reach equilibrium in 500kPa pressure plate.

Figure 4.4 highlights the calculated water content for the specimens for different confinement times for both pressure plates. It can be seen that all three tests gave reasonably consistent water content measurements; although with time a slight reduction in water content was observed for all tests. For the 1500kPa test apparatus, smaller tests pressures of between 311kPa and 355kPa than the 400kPa target pressure for the second test were applied (due to the difference in test set up as highlighted above), however this change in pressure does not appear to influence the measured water content for these specimens. To quantify if the reduction in the specimens' water content was caused by evaporation or that the specimens had not reached suction equilibrium, a further test was conducted but with the ceramic disc covered with a plastic sheet to prevent water exchange between the specimens and ceramic porous disc.

The results shown in Figure 4.4, show that these specimens still lost moisture with time. As this water content change was slightly greater than in the other tests presented in Figure 4.4, it suggests that during long storage times in the pressure plate the application of pressure using compressed air led to a drying out of the specimens as the water content of the air and specimens came into equilibrium. Some of the water loss through evaporation may be compensated by water being taken out of the ceramic disc and into the specimen.

4.2.2 The effect of specimen preparation on the soil water characteristic curve

Changes in particle arrangement (fabric) for an unsaturated soil can alter the menisci shape of the pore water leading to different values of suction. This can occur due to specimens being prepared to different states (density or water content). Therefore, a soil water characteristic curve is only valid for specimens prepared at the same state or from the same specimen (Ng and Menzies, 2007). To investigate whether this was the case for these materials, the soil water characteristic curves were derived for specimens of materials C and D prepared at various water contents and dry densities (Table 4.7).

Variation in either water content (Figures 4.5 and 4.6) or density (Figure 4.7) did not result in different suctions for specimens of material D at suctions greater than 300kPa. A similar

pattern of behaviour is observed for material C, although the threshold for change is shifted to 500kPa suction (Figure 4.8). Measurements in this region (<300kPa and <500kPa suctions) were predominantly from pressure plate testing where the specimens were tested at their prepared state. As either the water content or density that a specimen is prepared at decreases, the void air volume increases (Figure 3.4), and therefore the higher its suction. The threshold for observed change is considered to be the 'as constructed' suction in the specimen or the air entry value of the specimen.

Below this value the application of pressure does not affect the water content as the inherent suction is controlling the menisci shape, thereby preventing flow of water out of the specimen. The low permeability of the high-air-entry disc and the short equilibrium period mean insufficient water is taken up by the specimen from the ceramic disc. As the applied pressure increases above the air entry value the applied pressure is able to change the menisci shape, increasing higher suctions, and therefore allowing water to flow out of specimen.

The air entry values are specific to a material constructed at a specific water content and dry density, as seen in Figure 4.5 to 4.8. As the water volume varies between the specimens, their suctions differ, with specimens with a higher water content having more water around the larger sized particles (larger pores), with water draining easier from the largest pores.

4.2.3 Comparison of suction measurement techniques

Pressure plate, filter paper and Ridley suction probe have been used to determine the suction of the specimens. The pressure plate applies suction directly to the specimen(s) whilst for the filter paper test suction is indirectly measured and relies on a derived calibration curve for the filter paper to determine the soils suction. A number of different calibration curves have been derived and extensive research undertaken to consider factors that influence the measured values (McQueen and Miller, 1968, Leong et al., 2002, Bulut and Wray, 2005, Bulut and Leong, 2007, Bicalho et al., 2010, 2011).

Suction measurements using a tensiometer were conducted by Dr. Andrew Ridley at Geo-observations on specimens of material D, prepared by the writer at the same densities and water contents as those tested in the resonant column apparatus. The specimen's properties for the tensiometer tests are detailed in Table 4.9 and extreme care was taken to limit any moisture loss from the prepared specimens during transit to Geo-observations laboratory and during testing.

For each specimen two distinct suction values as detailed in Table 4.9 were measured. Figures 4.9 (a to e) show the measured suction with time for each specimen; gaps within the data were due to logging difficulty whilst variations in measured suctions during a test were due to temperature fluctuations in the laboratory. Initial suction values were reached rapidly within twenty four hours of starting a test for each specimen. Suction continued to decrease before stabilising after about ten days for the higher water content specimens, compared with nearly three weeks for the lower water content specimens. In order to check evaporation wasn't an issue the 4.92% specimen was retested and gave an initial value slightly lower than the initial ≈170kPa of the first test almost instantly, and then continued to decrease to ≈200kPa suggesting that evaporation was not an issue.

The gradual reduction in suction from the initial twenty four hour time period to the end of testing is suggested to result, for a compacted clay soil, because the presence of clay clods resulting in a bi-modal structure with different suctions in the clay clods and the inter-pore spaces (Figure 4.10) which come into equilibrium over a long period of time (Ridley and Burland, 1994a). The initial suction values are thought to occur due to the pore water in the inter-aggregate pore space. The suction then continues to decrease as water moves within the specimen until suction equilibrium is established. In these specimens it was noted that during mixing small clay lumps (aggregates) formed, with the CT-scan highlighting (Figure 3.10) density variations within the sand regions due to more clay being present. The tensiometer measurements suggest that these regions had different suctions, and coefficients of permeability, as the less in-filled areas lead to a bi-modal structure. As the water content varied for each specimen, the water contents would differ within these regions between the specimens giving rise to different initial suction values for each specimen. Neither the pressure plate nor the filter paper measurements indicated a bimodal structure but this is expected as they measure a single suction value.

There was good correlation between the filter paper and pressure plate for material D (Figure 4.11). Although a similar trend was followed for material A, the pressure plate test gave slightly higher water contents than the filter paper (Figure 4.12).

Although all data has been presented in terms of matric suction it must be recognised that at suctions greater than 1000kPa, total rather than matric suction may be measured (Leong et al., 2002). At these magnitudes, the pore water is usually absorbed around the soils particles resulting in water exchange through the vapour phase. Filter paper tests were conducted in this range, however it is difficult to achieve accurate suction measurements in this range because of the small mass change in filter paper mass, (as discussed earlier), and the effect

of changes in relative humidity (Ridley, 1995, Lu and Likos, 2004). As water exchange with the filter paper is slower when through the vapour phase than direct contact, Leong et al. (2002) recommend the equilibrium time is increased to fourteen days. No extension was made in this research and therefore the suction measured in this range may have been overestimated.

In Figure 4.11, the suction from the filter paper tests were calculated using Chandler et al. (1992) calibration curve (Table 4.8). The pressure plate is only used to calibrate the filter paper at suctions less than 80kPa for this calibration curve, however there is correlation between the filter paper results and the pressure plate up to 400kPa (Figure 4.11).

Figure 4.13 shows the results of using different calibration curves (Table 4.8) for determining the filter paper suctions for material D. Two distinct patterns of behaviour can be identified: 1) good correlation using the calibration curve from Leong et al. (2002) and Chandler et al. (1992), while Hamblin (1981) gives significantly lower suctions for a given water content, 2) high degree of scatter for all calibration curves below 100kPa. Although Chandler et al. (1992) used the pressure plate to calibrate the low suction values; there were significant variations between 5kPa to 40kPa. In addition, smearing of clay on the filter paper at low suctions can lead to an overestimation of the filter paper's weight. Therefore, values of suction below 100kPa with the filter paper test have been discounted in this research. Furthermore, differences between the calibration curves may have arisen because of the varying equilibrium periods.

Figure 4.14 shows the results of the tensiometer measurements alongside results from filter paper tests for specimens constructed in a similar manner to those tested using the tensiometer. Also shown are results from earlier tests presented for material D. As seen in Figure 4.14 specimens A, D and E (Table 4.9) tensiometer measurement correspond with the lower suction measurements of the filter paper technique, with the pressure plate measurements lying above. The tensiometer measurements for specimens B and C (Table 4.9) underlie those values obtained from the filter paper test and the pressure plate test. Closer agreement between the filter paper and tensiometer values can be achieved if the Hamblin (1981) calibration is curve is used, although the behavioural pattern remains the same. It is also important to note the large scatter in suction values at a given water content for the different techniques; 6% water content has a range from 60 to 210kPa.

Tarantino et al. (2011) found that tensiometer measurements were lower than pressure plate measurements in the region of the air entry value where some of the pore-air is

discontinuous. This is likely caused by using the axis translation technique (in the pressure plate) which causes compression of the occluded air bubbles, hence a change in menisci shape and a higher suction magnitude (Marinho et al., 2008, Tarantino et al., 2011). However, whether this would be sufficient to cause such a large variation along with the agreement between specimens D and E (Table 4.9) and the filter paper measurements, but then disagreement for specimens B and C mean it is hard to conclude that this is the reason. It may be that differences in specimen fabric, or experimental technique, are the likely cause of the observed range in values of suction.

Factors such as the scale of measurement are also likely contributing factors to the measured suction values and equilibrium times. The tensiometer measures a very small area of the specimen (12 mm diameter) compared to the area of the filter paper (55mm diameter).

Given the same overall trend between the techniques, the similarity with these findings to those previously published, along with it being widely recognised that different techniques give different values of suction (Madsen et al., 1986, Tarantino et al., 2011) it can be concluded that these results are meaningful.

4.2.4 Curve fitting

To consider the general behaviour of the datasets, Fredlund and Xing (1994) equation (as discussed in section 2.2.3) was fitted to the data for material D. Fredlund and Xing (1994), suggest the use of a tangent to define the inflection point used to define the key parameters a, n, and m controlling the shape of the curve fit. However, it was difficult to define the inflection point as there was no clear air entry value. In addition, the indication of a high residual water content led to the above equation not fitting the data. Therefore, a further iterative process of redefining the inflection point and residual water content was undertaken until the curve fitted the data. This required the residual water content to be reduced to 1500kPa to fit the data. The resulting parameters used to curve fit the data are detailed in Table 4.10, with Figures 4.15 a to d showing the individual curve fits.

Figure 4.16 compares these individual curve fits, and although clearly illustrating the difference between the experimental techniques, along with Figures 4.15 a to d, it also illustrates the subjective nature of curve fitting especially where there is limited experimental data that does not cover the extremities of the transition region. Highlighting that when curve fitting with limited data that does not cover the whole suction range this can led to misinterpretation of the soils characteristics.

4.2.5 Comparison of the different materials soil water characteristic curves

Figure 4.17 presents the soil water characteristic curves for both material C and D. Material D gives a lower water content for the same suction than material C, along with an air entry value of 100kPa compared with around 300kPa for material C. This difference even though the specimens are at the same dry density (void volume), arises as a result of the different percentages of clay, silt and sand as discussed in Section 2.2. Considering Figure 4.19 (individual trend lines shown Figures 4.18 (a to d)), it can clearly be seen that the soil water characteristic curves are dominated by the clay fraction of the materials. Material A with the lowest clay content has the lowest suction, with suctions increasing with clay content, for a given water content (Figure 4.19).

4.3 Stiffness measurements from resonant column testing

This section discusses the results from resonant column testing. Tests on specimens of material D and C, where suctions were controlled through changes in the water content, were conducted to understand how suction changes influence stiffness.

4.3.1 Base line tests

A number of resonant column tests were conducted on specimens of Leighton Buzzard fraction E sand. Previous resonant column testing had been done on this grade of sand (Priest, 2004, Bui, 2009, Rees, 2009), and so allowed baseline tests to be conducted to ensure that the apparatus and testing procedure for the material mixes were robust.

A dry specimen (water content 0.24%) of Leighton Buzzard sand fraction E (LBE) was tapped with a resultant void ratio of 0.64 and dry density 1.61Mg/m^3. Testing included both loading and unloading of the specimen to determine changes in stiffness as a function of effective confining pressure (σ'). Figure 4.20 shows the response of the sand specimen during changes in confining pressure from 100kPa to 600kPa and similar unloading steps back down to 100kPa. It can be seen that the small strain maximum shear modulus G_0 (as detailed in section 2.3.2) increased with confining pressure. Shear modulus behaviour is dependent on confining pressures, and can be represented through Equation 4.4 (repeat of Equation 2.15):

$$G_0 = a\left(\frac{\sigma'}{1\text{kPa}}\right)^b \qquad (4.4)$$

(where a and b are constants).

The b exponent providing a measure of the contact stiffness and fabric change under isotopic stress (Cascante, 1996), tending to zero when there is no change in fabric or contact stiffness under loading, and generally tends to 0.5 at small strains (Clayton et al., 2010). The power fit of these data sets, leds to a b exponent of 0.57 and 0.58 which is close to the 0.4 to 0.6 range observed for pluviated sands (Clayton, 2011). It can be seen that good repeatability, on average 1% variation at a given confining pressure, was obtained between the loading and unloading steps, showing that the soil response was elastic with regard to changes in maximum shear modulus with confining pressure.

Figure 4.21, shows the comparison of the loading case with other tests conducted on LBE at a void ratio of 0.64. Although, the b exponent for all data sets lies within the 0.4 to 0.6 range, at a given effective confining pressure, there is variation between the measured shear modulus, on average 22.85% between the maximum and minimum measured values. There could be many contributing factors to cause this variation. Measurements may have been taken at different times, although as sands reach secondary consolidation rapidly unlike cohesive specimens this is likely to be a relatively small error. Different ways of defining the maximum shear modulus, repeatability of measurements between the researchers and the ability to produce identical specimens despite all preparing specimens by tamping.

Particle shape and size are known to influence shear modulus (Bui, 2009, Rees, 2009, Clayton et al., 2010). Therefore, base line tests were conducted on specimens of dry mixes of materials D and C (no appreciable water- no suction). Figure 4.22 shows the response of these mixes to changes in effective confining pressure. Also included is the response of LBE specimens shown in Figure 4.21, and other tests conducted on Leighton Buzzard sands. As shear modulus is also influenced by void ratio, the data in Figure 4.22 is normalised with respect to void ratio using Equation 2.16 to remove the influence of different void ratios in the data.

It can be seen that after accounting for void ratio differences, the shear modulus for materials C and D is considerably less than that of pure sand fractions and the sand and mica mixes. Although materials C and D sand fraction contains a high percentage of Leighton Buzzard sand fraction B (LBB), 32% and 47% respectively, they also contain significant silt and clay (46% material C and 27% material D). The stiffness of soils is related to the interaction of particles at the grain contacts. Bui (2009) showed that for a given effective stress, the stiffness of glass ballotini specimens reduced with reducing particle size. As the number of particle contacts increase, the stress at each contact reduces for a given global effective stress. In addition, soils which contain platy particles such as mica or clay show a

reduction in stiffness compared with materials of angular or round particles, as the addition of platy particles into a sand mix prevents direct contact between sand particles, thus leading to reduction of stiffness (Bui, 2009, Lee et al., 2010). This is illustrated through the higher b exponent for materials D and C than the pure sands (Figure 4.22). Although materials C and D have different values of clay, the overall stiffness is similar for both. This would suggest that once sufficient clay is present to prevent direct sand to sand grain contacts, additional clay just infills the pores space thus not influencing any further change in stiffness.

4.3.2 Material D

Twenty-one specimens of material D were prepared at various water contents at the same dry density (2.10Mg/m^3). As water content is related to suction this allowed the influence of suction on shear modulus to be evaluated.

Based on the derived soil water characteristic curve (Figure 4.19) specimens were prepared at water contents varying from 2% to 9.7%. Water contents between 2% to 8% covered the transition region where the most significant changes in suction and hence shear modulus would be expected to be observed (Mancuso et al., 2002). The 8% to 9.7% water contents covered the region above the air entry value (≈8% for this material), where suction changes theoretically should not influence the mechanical behaviour (Laloui and Nuth, 2008) and shear modulus should remain constant for same stress conditions. As seen in Table 4.11, the theoretical maximum water content of 9.7% (based on the zero air voids line Figure 3.4) was exceeded, resulting in the density of these specimens being lower than the target value. The water content varied on average ±5.34% with a maximum and minimum variation of ±20.32% and ±0.37% from the target value (Table 4.12). This error and the influence of compactive effort led to a dry density variation on average ±0.09Mg/m^3 (±4.10%) from the target of 2.10Mg/m^3 with a maximum and minimum variation of ±0.22Mg/m^3 (±10.48%) and ±0.01Mg/m^3 (±0.48%) (Table 4.12).

Tests were conducted under a variety of net normal stresses, representing the in-situ confining pressure that might be experienced in the field. Tests were generally conducted at net normal stresses of 10kPa, 20kPa, 50kPa, 100kPa and 150kPa as shown in Table 4.11. Testing was not conducted below 10kPa, due to difficulty of calibrating the transducers at these low pressures, and being lower than the applied pressure during specimen set-up. Also these pressures may not have been sufficient to provide adequate coupling between the specimen and the top cap and base pedestal (Hardin and Drnevich, 1972b).

Influence of the number of construction layers

Specimens were initially constructed in three layers and the compaction effort (number of blows) altered until the required layer depth was reached. In some cases, despite substantially increasing the compaction effort, this was not sufficient to reach the required depth and the number of construction layers was increased. CT scanning highlighted the issue of layering and density variation throughout the specimen, and therefore to minimise the extent of density variation (assumed a larger variation the greater the layer depth), all specimens were then constructed using ten layers.

Two specimens of material D tested under the same conditions, prepared at 8% water content to a dry density of 2.10Mg/m^3, but one constructed in three and the other in ten layers, were tested to consider the influence of the layering. At a given net normal stress the variation in the maximum shear modulus measured between the specimens was no greater than 7% (Table 4.13). Based on the base line tests this difference is within measurement repeatability, suggesting that variation in density through the specimen has a negligible effect on overall stiffness. It is hypothesised that the density variation did not influence the shear modulus as it's measurement in the resonant column apparatus is dependent on a specimen's overall density, which was consistent between the two specimens. Therefore, as the number of construction layers did not influence shear modulus, the results between specimens with different numbers of construction layers are directly compared in the following sections.

Influence of net normal stress

Each specimen was tested under various net normal stresses, equal to the applied cell pressure as the air line was continuously vented to atmosphere. This assumes that there was continuity between the pore air and atmosphere. However, the pore air is not always continuous hence this is not a reasonable assumption for near-saturated and saturated specimens where the pore air is assumed to be present as occluded bubbles. Here, increasing the cell pressure causes the pore air pressure to increase, only returning to the original pressure as air diffuses through the water and into the air bubble, which can take a long time. For each specimen, the maximum shear modulus was determined twenty four hours after the application of each net normal stress increment. As seen in Figure 4.23, the shear modulus reached a constant plateau within twenty four hours for both specimens where the pore air was assumed discontinuous. Determining the shear modulus for the near-saturated and saturated specimens at twenty four hours was therefore assumed acceptable.

Figure 4.24, shows the change in shear modulus with net normal stress for the specimens tested at all net normal stresses between 10kPa to 150kPa. Each dataset was fitted with a power law line and as seen in Figure 4.24, the b exponent (Equation 4.4) for the majority of specimens lies outside the expected range of 0.4 to 0.6 (Clayton, 2011) with a similar behavioural pattern observed for an unsaturated silty sand by Fleureau et al. (2002). For the 0.47% and 10.24% water content specimens which are essentially saturated and dry the b exponent's are within the expected range. Therefore, it suggests that the b exponent value is influenced by suction.

Matric suction induces a normal force at particle contacts and between clusters of particles, which is assumed to be constant during testing. In contrast, net normal stress affects both normal and tangential forces, and their magnitude increases with increasing net normal stress. At low net normal stresses, the forces arising due to suction are greater than those due to net normal stress, and therefore dominate the soils behaviour. As the net normal stress increases, suction forces remain constant; hence the influence of suction compared with those from net normal stress reduces. At high net normal stresses, suction forces no longer dominate the soil's behaviour, and eventually the forces arising due to net normal stress dominate. Figure 4.25 shows the measured shear modulus for these specimens at net normal stresses between 100kPa to 400kPa, the derived b exponent increases in all cases and lies within or is extremely close to the expected 0.4 to 0.6 range.

Influence of suction

The results of the dry mix specimen of material D (Figure 4.22), was used as a datum to compare with the other specimens to understand how suction influenced shear modulus.

At each target preparation water content the suction of a specimen made from the resonant column mix was determined using the filter paper technique. As seen in Figure 4.12, these suctions corresponded with those measured to derive the soil water characteristic curve. However, suction is not only dependent on a specimen's water content but also the distribution of water in the specimen, which depends on particle arrangement. Increasing net normal stress can cause a specimen to consolidate, changing the specimen's void ratio, and hence leading to changes in suction. For the test conducted on material D the axial deformation recorded consolidation during increases in net normal stress from 10kPa to 150kPa. For example specimens with a water content of 3.09% and 8.03% were 0.77mm and 0.91mm, respectively. As the deformation was generally less than a millimetre throughout testing it was therefore assumed that a change in a specimen's suction during testing was negligible.

Figures 4.26 to 4.30 show the results for tests conducted under a range of net normal stresses. It can be seen that the shear modulus was greater for the unsaturated specimens (specimens with added water to the mix) than for the dry specimen. As these specimens were prepared at the same dry density, and subjected to the same net normal stress, it can be assumed that the presence of suction has influenced the shear modulus of the specimens.

It can be seen in Figures 4.26 to 4.30 that the shear modulus initially increases with increasing water content reaching a maximum value around 4% to 6% depending on the net normal stress, and then decreases with increasing specimen water content. The general trend follows a bell shape curved at all net normal stresses. Although the bell shaped trend can clearly be seen, there is some scatter within the data, particularly at peak water content (4% to 6%) under net normal stresses of 10kPa and 20kPa. As the shear modulus was greater for a less dense specimen at a given water content, for example 6.16% water content specimen, this difference was assumed to be the influence of suction. The influence of suction is dependent on where the water resides. Minor variations in the distribution of water around the particles can cause subtle changes in shear modulus since the number of inter-particles contacts affected by the capillary (normal) force may alter, with the number of inter-particles contacts affected influencing the stability behaviour (shear modulus) of a soil (Wheeler et al., 2003). Although the specimens at the same water content may have been constructed in the same manner, the variation in measured shear modulus suggests that the proportion of bulk-water and menisci-water varied between the specimens leading to variations in the inter-particle forces and hence suction.

From Figure 4.31, it is clearly seen that the increase in shear modulus due to suction is most significant at low net normal stress. The maximum shear modulus was over five times greater than the dry specimen at 10kPa compared with two and a half times that at 50kPa. This clearly identifies the contribution of suction to shear modulus reducing with increasing net normal stress.

Figure 4.32, shows the ratio of maximum shear moduli for the unsaturated specimens to those of the dry specimen, against degree of saturation at net normal stresses of 10kPa and 100kPa with a trend line fitted to each data set. It can be seen that at 100kPa net normal stress the ratio of shear modulus is significantly less than at 10kPa. In addition, degree of saturation at which the maximum shear modulus occurs shifts to the left. Qian et al. (1991) observed this when particles less than 37μm were present. 25% of material D's particles are this size or less. The ratio of increase at a given net normal stress was however, significantly greater than observed by Qian et al. (1991). The fine particles of material D were platy

rather than spherical shaped like Qian et al.'s (1991) fine particles, which can lead to significantly higher peak normal forces between the particles (Gili and Alonso, 2002). This suggests that the higher observed shear modulus ratio is related to the shape of the fine particle.

The behaviour observed in Figure 4.32 is similar to that observed by Wu et al. (1984) and Qian et al. (1991) whom performed tests on compaction-controlled cohesionless specimens, including the localised minimum in shear modulus ratio for specimens close to saturation (water content from 0.67/0.75 to 0.9 (stress dependent)). As suggested by Wu et al. (1984) at or near total saturation the pore air was discontinuous and present as occluded air bubbles. Therefore, when net normal stress is applied these bubbles compress resulting in an increase in pore air pressure thereby giving a lower net stress than expected, based on just the applied confining pressure. The increase in shear modulus ratio after this point results from saturation and the correct net normal stress being applied.

At high degrees of saturation, the degree of suction is dominated by the bulk-water distributed throughout the soil, with minor suctions developing at the menisci-water contacts; hence the normal forces influencing stability throughout the specimen are low. As the degree of saturation reduces within the soil, the number of menisci-water contacts within the soil increases, leading to an increase in suction and shear modulus. As the degree of saturation reduces further a reduction in the peak shear modulus occurs. Although the model proposed by Fisher (1926) suggests an asymptotic normal force for a given particle contact as the degree of saturation reduces, the area of the contact over which this force acts, and possible number of contacts affected by menisci water distributed throughout the soil reduce, hence a reduction in shear modulus is seen.

Figure 4.33 plots changes in shear modulus with suctions, showing an observed peak in shear modulus around 400kPa. Mancuso et al. (2002, 2003) gave an asymptotic value of shear modulus value for their suction-controlled tests. However, in their tests the asymptotic value of shear was achieved at 400kPa suction, close to the value where maximum shear modulus is observed in the present for material D. Therefore, the limited range of suction measured in Mancuso's test would have prevented them seeing a reduction in shear modulus, thus leading to a limited understanding of the materials behaviour due to suction.

4.3.3 Stiffness of dried specimens

It has been stated by other researchers that comparing the suction/shear modulus relationship found through compaction-controlled testing is not valid as the use of different compaction

efforts and water contents to prepare the specimens results in fabric variations between the specimens which also influences the shear modulus (Mancuso et al., 2003). As observed for clay specimens (Romero et al., 1999, Romero and Simms, 2008), Delage et al. (1996) found for a silty clayey material with a 34% clay content that a dry of optimum specimen had a bi-modal structure whilst a wet of optimum specimen had a uniform particle distribution, regardless of these specimens being prepared at the same density. In order to understand if particle arrangement was also influencing the shear modulus, specimens of material D all prepared at a dry density of 2.10Mg/m^3 were completely dried from their preparation water content (6%, 7%, 8%, 9% and 10%) and tested at a variety of net normal stresses (10kPa, 20kPa, 50kPa, 100kPa, and 150kPa). As the specimens were all dry with the other contributing factors influencing shear modulus constant, it was expected that the shear modulus would be identical provided their particle arrangements were the same.

The shear modulus of these specimens was shown to be much greater than the initial dry mix specimen (Figure 4.34) and unsaturated specimens. In addition increased variability was observed in shear modulus between the specimens. Up to 40% between the maximum and minimum shear modulus was noted.

The shear modulus obtained for these dried specimens was very large (Figure 4.34), and it is recognised that there are difficulties with testing stiff soils/weak rocks in the resonant column apparatus (Kumar and Clayton, 2007). Drnevich (1978) detailed that the coefficient of friction may not be sufficient to maintain complete coupling between a stiff specimen and the base and top platen as strain increases, leading to a lower shear modulus and increased damping. Unless these specimens were dental plastered into position slippage occurred. Furthermore, their resonant frequency between 312Hz to 395Hz was outside the calibration range of the apparatus. It was assumed that the calibration of I_o could be extended and was valid in this region. Spurious resonant frequencies occurred due to system compliance (members of the apparatus vibrating (Avramidis and Saxena, 1990) as seen in Figure 4.35. There was no specific frequency that the spurious frequency occurred (Figures 4.35), consistent with Avramidis and Saxena (1990) finding variation between specimens, but it remained constant for a given specimen at different net normal stresses (Figures 4.36). However, the low amplitude of the spurious frequency meant that it was no longer apparent at high strains (Figures 4.37 and 4.38), which allowed confirmation that the correct frequency had been selected at the lower strains.

For specimens on the ‘dry’ side of the maximum dry density value (from the Proctor compaction curve) the shear modulus decreased with the reduction in as prepared water

content (Figure 4.34). In contrast, shear modulus increased for specimens prepared on the 'wet' side, whilst the shear modulus for specimens prepared at, or near, the optimum were reasonably similar.

Although the dried state at which the specimens were tested at was determined after their mass remained constant for a week, following daily changes during the initial stages of drying, their calculated water content, Table 4.14, indicated that water remained within the specimens. As this is greater than the amount required to form the absorbed (diffused double) layer around each clay particle (water content of $1.04x10^{-11}$%) it is not physico-chemical forces but suction, which has been assumed to act between the clay particles. It remains between the clay particles not only because of clays affiliation for water but as this is also the smallest pore space, with water draining from the largest pores first.

It was observed during preparation of the material mixes, that the clay particles formed lumps during mixing. At very low water contents, 2% and 3%, although lumps formed, due to the amount of water added there number was small with a large amount of the fines in a powered state. As the water content increased a greater number of lumps formed, however, at water contents on the 'wet' side of optimum, the mixes appeared homogeneous with no lumps visible; the water content sufficient to break down the suction within the lumps dispersing the clay throughout the mix. CT-scanning highlighted that there were regions where there was greater infill around the sand particles creating regions with a lower void space. It is believed that these regions arose from the lumps deforming under compaction, but not completely dispersing due to the suction between the clay particles, with the sand particles embedding into them as the lumps deformed during compaction. The distribution of the lumps around the sand particles, as seen in Figure 4.39, results in a different structure within the specimens regardless of being prepared at the same dry density.

When specimens prepared at 2% and 3% water content were dried although self supporting when constructed they started to crumble and were very brittle. During drying suction was assumed to develop/increase between the clay where water was present during preparation. If the sand particles are embedded in clay lumps (Figure 4.39) the increased suction in the clay acts as a support around the sand particles preventing slippage. Furthermore, Barden et al. (1973) suggested that when the water content is sufficient the clay is initially in suspension and during drying retreats with the menisci, forming clay buttresses between the sand particles, again preventing slippage at the sand contacts. At the low water contents there is not sufficient water to fill the void space and encompass the fines fraction within the void space, therefore during drying these particles remained within the void space, whilst the

small amount of sand particles embedded in clay lumps (Figure 4.39), and possibly smaller embedment area, results in limited support between the sand particles, hence collapse of the specimen. As the water content increases as seen in Figure 4.39, more sand particles are embedded in the clay. Even though the clay particles in void space may not recede during drying as there is greater support through more sand particles being embedded, the shear modulus increases. The formation of a particle arrangement where the sand particles are embedded is also supported by the higher shear modulus of the unsaturated specimens at low water contents (without drying) when not self supporting (which suggests suction was not acting between all the particles).

'Wet' of optimum the mixes were more homogeneous, and although the specimen prepared at 10% water content was able to be deformed/reshaped by hand when prepared, once dried it had the highest shear modulus (Figure 4.34). The deformability when prepared suggests that the suction was low and that the majority of the clay particles were in suspension in the void space around the sand particles as shown in Figure 4.39, with no suction acting between the clay particles. At these higher waters content there is significant water within the void space to encompass the fines fraction, thus during drying the clay particles recede with the menisci-water forming buttresses around the sand particles, along with suction between the clay particles increasing. The high shear modulus of 10% specimen when dried is postulated as due to the clay particles embedding around a greater number of sand particles evenly throughout the specimen compared with drying at lower water contents, in essence creating a more rigid lattice throughout the specimen.

These tests suggest that fabric variation between the specimens was also a contributing factor to the shear modulus behaviour.

Shear modulus variation with net normal stress

Each dried specimen was tested at a variety of net normal stress and as seen in Figure 4.40 there was minimal change in the shear modulus with an increase in net normal stress. Fitting a power line through each data set the b-exponent of Equation 4.4 varies between 0.02 and 0.05. This implies that there was no particle re-arrangement during testing, which is confirmed by the minimal axial deformation hence change in void ratio (Table 4.14). The fact that there was no deformation even at the larger net normal stresses (100kPa/150kPa), implies that the suction forces were large, with the material behaving like a cemented sand (Clayton et al., 2010).

In the derivation of the mathematical model to obtain shear modulus from resonant column tests, it is assumed that the base and top cap are rigidly fixed to the specimen. Even though the specimen was cemented into position, the very small changes in shear modulus at low net normal stress, 10kPa and 20kPa, indicates that the pressure applied improved the contact at these interfaces (Ashmawy and Drnevich, 1994, Clayton et al., 2009).

4.3.4 Material C

To understand how the variation in the clay fractions between the materials influenced shear modulus, tests were conducted on specimens of material C prepared at water contents of 3%, 4%, 6%, 7%, 9% and 10%, at a dry density of 2.10Mg/m^3. The following text examines the similarity and differences between their results and those obtained for material D.

As was noted in Figure 4.19 material C had larger suctions at a given water content. It was anticipated that specimens made with material C would have a larger shear modulus than material D. However, material D has a lower fines content and from the observations of dry specimens (Figure 4.22) where the shear modulus of material D is greater than material C, the shear modulus of material D might be expected to be greater, at given water contents.

Figure 4.41 shows the shear modulus variation between the unsaturated specimens and a dry specimen for materials C and D against water content. It can be seen that the shear modulus for material C is greater at water contents greater than 4%, with the overall increase in shear modulus due to suction being greater at any water content (Figure 4.42). Material C follows the bell-shape behaviour similar to that for material D, and like material D the shear modulus and the water content at which the maximum shear modulus occurs reduces with increasing net normal stress. The water content at which the maximum shear modulus occurred however is greater for material C than D.

Material C has a 27% clay content compared with 11% clay content for material D (Table 3.1). This results in the fines fraction remaining in a powdered state over a larger water content range than material D, with all the clay particles forming lumps at a higher water content, hence the shift in the water content at which the maximum shear modulus occurs. The greater clay content also means that the volume of clay under suction is greater than material D. This larger volume of clay results in a larger embedment area of sand particles in the clay, which encompasses a larger area around the sand contacts, or if not all sand contacts are covered within the specimen a more even distribution throughout the specimen. It is this greater stabilising effect at the sand contacts throughout the specimen that results in a greater increase in shear modulus than material D.

In preparing specimens of material C greater compactive effort was required to achieve the same density. This higher energy may have led to greater deformation of the clay lumps also creating a greater embedment area around the sand contacts.

The difference in shear modulus increase due to suction between materials C and D clearly illustrates that for sandy clayey materials it is not just contribution from the suction due to the water distribution between the particles but also the embedment of clay at the sand contacts throughout the specimen which is important to this increase. Therefore, based on these findings materials A and B would be expected to exhibit the same bell shape curve. For material A the maximum shear modulus would be expected to occur at a lower water content than all these materials, with the percentage increase in shear modulus due to suction being less, with the bell-shape curve occurring over a smaller water content range. For material B the behaviour would expect to lie between those observed between materials C and D.

4.3.5 Implications of the observed behaviour for formation material in-situ

The testing of reconstituted formation material has clearly shown that suction is beneficial to the small strain shear modulus but it is highly dependent on the water content/suction of the material. The following section evaluates the consequent of these results on future designs and maintenance of the structural integrity of existing railway formation.

Suction within railway formations from a review of monitoring in similar conditions are likely to vary between 10kPa and 800kPa (DeBruijn, 1965, Fredlund and Oloo, 1995, Blight and Harrison, 2000). As seen in Figures 4.43 and 4.44, these suctions coincide with the marked changes in shear modulus due to suction of the reconstituted specimens. Furthermore, the back calculated in-situ shear moduli of 70MPa to 140MPa for the COALlink formation (Gräbe and Clayton, 2003, Gräbe et al., 2005, Powrie et al., 2007) indicate that suctions were present in the formation.

It is the changes in shear modulus with suction variations which are important to structural integrity. Although different shear moduli may be sufficient to support the loading, if the variation results in different deformations occurring throughout the track length, then differential settlement or excessive deformation can occur, resulting in complete failure of the formation, or deterioration in ride quality, (Selig and Waters, 1994). Saturation of the formation, which could arise from more intense rainfall predicted in the winter months,

could also lead to deterioration through mud pumping and plastic shear failure (Selig and Waters, 1994, Brown, 1996, Gräbe and Clayton, 2003). Therefore, it is advisable that the water content and thus suction of the formation material is maintained at a constant level, achieved through providing adequate drainage and monitoring. Although the results of this research showed that suction has a beneficial influence on shear modulus, this reduces with confining pressure. This is not detrimental as although confining stresses increase with depth the shear stresses from loading reduce. Furthermore, as the relationship depends on a material's composition it is advisable that a material less susceptible to large shear modulus variations in the suction range expected to be encountered is specified.

Test stage	Target pressure values			Test stage duration	Measured values at the end of a test stage		
	Cell (kPa)	Air (kPa)	Water (kPa)	(cumulative) (days)	Net normal stress (kPa)	Matric suction (kPa)	G_0 (MPa)
1	50	10		15	39	22	137
2	150	110		16	53	103	141
3	250	210		17.5	56	190	148
4	350	310		18	63	149	150
5	350	310	Raised to 150 then returned to value at end of stage 4 and then left undrained	18.5	61	226	150
6	450	410		26	65	303	170
7	550	510		27	74	119	154
8	550	510	Raised to 257 then returned to value at end of stage 7 and then left undrained	30	75	173	172
9	550	410		31	168	119	351
10	550	360		32.5	216	96	413
11	550	310		34	263	64	439
12	550	270		35	308	59	469
13	550	310		36	260	106	456
14	550	360		37	213	137	437
15	550	410		38	166	167	415
16	550	460		39	119	202	385
17	550	510		40	73	199	354

Table 4.1: Test regime and measured values for material D tested using the axis translation technique.

	Gravimetric water content (%)								
	Set 1	Set 2	Set 3	Set 4	Set 5	Mean	Mean overall of mix	Standard deviation (%)	Overall standard deviation of mix (%)
Mix One									
British standard tins no lids	7.00	7.00	7.01	7.00	7.00	7.00	7.28	0.00	0.26
British standard tins with lids	7.48	7.49	7.50	7.50	6.79	7.35		0.28	
Baking tins	7.48	7.47	7.49	7.49	7.49	7.48		0.01	
Mix Two									
British standard tins no lids	8.99	8.98	8.99	8.98	8.98	8.98	8.39	0.00	0.44
British standard tins with lids	8.21	8.21	8.23	8.22	8.21	8.22		0.01	
Baking tins	8.00	7.99	7.99	7.98	7.96	7.98		0.01	
Mix Three									
British standard tins no lids	8.35	8.45	8.45	8.46	8.44	8.43	7.98	0.04	0.47
British standard tins with lids	7.55	7.54	7.53	7.53	7.54	7.54		0.01	

Table 4.2: Gravimetric water content variation between and with different weighing tins. Determined following BS1377-2 (1990).

	Water content caused by differences in weight measurement (%)					Mean water content (%)	Standard deviation (%)	Maximum water content change (%)	Minimum water content change (%)
Set 1	0.01	0.01	0.02	0.01	0.00	0.01	0.01	0.02	0.00
Set 2	-0.15	0.00	0.00	0.01	0.00	-0.03	0.07	0.15	0.00
Set 3	0.10	0.09	-0.03	0.09	0.11	0.07	0.06	0.11	-0.03
All Sets						0.02	0.06	0.15	0.00

Table 4.3: Gravimetric water content variation due to weighing errors. Assessed weighing identical weights in baking trays.

	Measured water content (%)					
Test 1	3.0820	0.9337	3.3058	1.6997	0.5392	0.7907
Test 2	3.3446	1.5052	0.8399	0.8821	1.4542	
Test 3	2.2094	2.7505	3.0549			

Table 4.4: Water content measured following the filter paper procedure on dried filter paper.

Measured suction (kPa)			Suction error range (kPa)
Determined from the filter paper's water content	Determined from the filter paper's water content + standard deviation error of 1.044%	Determined from the filter paper's water content- standard deviation error of 1.044%	
6	6	6	0
24	20	27	7
177	153	206	53
583	502	677	175
1203	1036	1397	361
1889	1627	2194	567
2643	2276	3070	794
5376	4629	6243	1614
5658	4872	6571	1699

Table 4.5: Suction error range determined accounting for the inherent accuracy of the filter paper water content determination.

Storage duration (days)	Average water content of the specimens (%)	Variation in water content between specimens (±water content)	Variation in water content between specimens (± percentage of average water content)	Average water content of the filter papers (%)	Variation in water content between filter papers (±water content)	Variation in water content between filter papers (± percentage of average water content)	Average suction (kPa)	Suction variation (±kPa)	Suction variation (± percentage of average suction)	Number of specimens
5	4.41	0.04	0.94	32.41	0.54	1.64	672	51	7.60	2
14	3.98	0.11	2.84	31.86	2.69	8.44	779	287	36.72	2
8	5.88	0.07	1.21	40.98	1.15	2.80	199	33	16.29	2
26	5.38	0.09	1.65	39.27	0.71	1.85	291	30	10.11	2

Table 4.6: Suction of filter paper specimens stored for different durations.

Target dry density (Mg/m^3)	Achieved dry density (Mg/m^3)	Variation from target dry density (±%)	Standard deviation from target dry density	Target water content (%)	Measured water content	Variation from target water content (±%)	Standard deviation from target water content
Material D							
2.10	2.10	0.00	0.00	2.00	2.21	10.50	0.00
2.10	2.10	0.00	0.00	4.00	4.25	6.25	0.00
2.10	2.03	3.33	0.00	6.00	6.60	10.00	0.00
2.10	2.11	0.00	0.03	8.00	7.98	6.00	0.27
2.10	2.12	0.95	0.12	9.00	8.84	4.33	0.33
2.10	2.10	0.00	0.00	10.00	9.42	15.00	0.60
1.70	1.82	9.41	0.07	4.00	4.18	4.50	0.00
1.70	1.83	14.12	0.06	6.00	6.36	6.00	0.00
1.70	1.96	22.35	0.08	8.00	8.11	1.38	0.00
Material C							
2.10	2.05	3.81	0.02	11.00	10.71	6.55	0.36
2.10	2.04	10.95	0.10	7.00	6.58	13.14	0.37
1.96	1.98	10.20	0.12	13.00	13.86	4.31	0.24

Table 4.7: Variation of dry density and water content from target values for filter paper and pressure plate specimens. (The values quoted above are the average values for both the pressure plate and filter paper specimens combined, prepared at a given target dry density and water content)

	Calibration curves		Calibration method
Chandler et al. (1992)	$\log_{10}(\text{suction}) = 4.842 - 0.0662w^*$ $\log10(\text{suction}) = 6.050 - 2.48\log w^*$	$w < 47\%$ $w > 47\%$	Pressure plate (≈0 to 80kPa) Oedometer cell (80 - 2000kPa) Salt solutions (6000kPa)
Hamblin (1981)	$\log_{10}(\text{suction}) = 8.022 - 3.683\log w^*$		Suction plate (up to 7kPa) Pressure plate (up to 70kPa) Pressure membrane (up to 1500kPa) Salt solutions (up to 5500kPa)
Leong et al. (2002)	$\log_{10}(\text{suction}) = 4.945 - 0.0673w^*$ $\log_{10}(\text{suction}) = 2.909 - 0.0229w^*$	$w < 47\%$ $w \geq 47\%$	Pressure plate (10-1500kPa) Salt solutions (≈0 to 9000kPa)

*w=water content (%)

Table 4.8: Filter paper calibration curves.

Specimen	Dry density (Mg/m^3)	Bulk density (Mg/m^3)	Gravimetric water content (%)	Suction measurement (kPa)	
				Initial response	Equilibrium value
A	2.02	2.1	4.31	550	600
B	2.05	2.15	4.92	170	200
C	2.06	2.09	6.16	60	89
D	2.11	2.27	7.29	25	57
E	1.99	2.14	7.96	15	38

Table 4.9: Tensiometer suction measurements and specimen properties.

	Dry density (Mg/m^3)	θ_s (%)	θ_i (%)	ψ_i (kPa)	ψ_p (kPa)	ψ_r (kPa)	s*	a (kPa)	m	n
Filter paper (Chandler et al. (1992))	2.1	9.7	7.40	150	770	1500	0.011935	150	0.993270	1.184100
Filter paper (Hamblin (1981))	2.1	9.7	6.00	170	700	1500	0.01132	170	1.762945	0.882817
Pressure plate	2.1	9.7	7.00	240	1000	1500	0.009211	240	1.197212	1.281639
Tensiometer	2.1	9.7	8.80	30	150	1500	0.073333	30	0.357363	3.406150

Table 4.10: Curve fitting parameters used for Fredlund and Xing (1994) equation.

Water Content (%)	Net normal stress (kPa)					e	Dry density (Mg/m^3)	Bulk density (Mg/m^3)	Sr
	10	20	50	100	150				
	G_0 (MPa)								
0.47	25	35	57	87	110	0.33	1.98	1.99	0.04
2.05	65	77	105			0.4	1.88	1.92	0.13
2.2			110	142	191	0.23	2.15	2.20	0.26
2.51	73	87	115	149	178	0.35	1.96	2.01	0.19
3.09	104	117	142	176	198	0.30	2.02	2.09	0.27
3.54	96	109	144			0.24	2.2	2.13	0.39
4.3			191	241		0.28	2.06	2.15	0.4
4.4			147	203		0.31	2.01	2.1	0.37
4.44	123	144	172			0.35	1.96	2.05	0.34
4.9	124	150	186	224	251	0.34	1.97	2.07	0.30
4.92	162	177	208	226	256	0.32	1.99	2.09	0.40
5.13	128	140	159	180	199	0.29	2.05	2.15	0.47
6.16	166	178	195			0.31	2.02	2.15	0.53
6.28			175	207	263	0.28	2.07	2.20	0.60
6.7			163	192		0.31	2.02	2.15	0.56
8.03	71	87	121	168	193	0.23	2.14	2.31	0.91
8.19			113	160		0.22	2.16	2.33	0.97
8.38	75	96	123			0.21	2.18	2.36	1.00
8.62						0.25	2.11	2.29	0.91
10.11			84			0.29	2.04	2.26	0.94
10.24	33	57	50	121	166	0.32	2.00	2.21	0.85

Table 4.11: Shear modulus (G_0) at a given net normal stress and basic specimen properties for material D.

Target water content (%)	Measured water content (%)	Deviation from target water content (%)	Target dry density (Mg/m^3)	Dry density (Mg/m^3)	Deviation from target dry density (%)
0.00	0.47	0.47	2.10	1.98	5.71
2.00	2.05	-2.50	2.10	1.88	10.48
2.00	2.2	9.09	2.10	2.15	-2.38
2.00	2.51	20.32	2.10	1.96	6.67
3.00	3.09	2.91	2.10	2.02	3.81
3.00	3.54	15.25	2.10	2.2	-4.76
4.00	4.3	6.98	2.10	2.06	1.90
4.00	4.4	9.09	2.10	2.01	4.29
4.00	4.44	9.91	2.10	1.96	6.67
5.00	4.9	-2.04	2.10	1.97	6.19
5.00	4.92	-1.63	2.10	1.99	5.24
5.00	5.13	2.53	2.10	2.05	2.38
6.00	6.16	2.60	2.10	2.02	3.81
6.00	6.28	4.46	2.10	2.07	1.43
7.00	6.7	-4.48	2.10	2.02	3.81
8.00	8.03	0.37	2.10	2.14	-1.90
8.00	8.19	2.32	2.10	2.16	-2.86
8.00	8.38	4.53	2.10	2.18	-3.81
8.00	8.62	7.19	2.10	2.11	-0.48
10.00	10.11	1.09	2.10	2.04	2.86
10.00	10.24	2.34	2.10	2.00	4.76

Table 4.12: Percentage variation of preparation water content and density from target value for specimens of material D.

Specimen water content (%)	Number of construction layers	Dry density (Mg/m^3)	Void Ratio	Degree of saturation		Net normal stress (kPa)			
						50	100	200	600
8.03	10	2.14	0.23	0.91	G_0 (MPa)	125	175	270	545
8.19	3	2.16	0.22	0.97		117	167	253	547
					Percentage difference in G_0	6.4	4.6	6.3	-0.4

Table 4.13: Variation in shear modulus (G_0) due to number of specimen construction layers (Material D - water content 8% dry density 2.1Mg/m^3).

	Net normal stress (kPa)					Net normal stress (kPa)								
	10	20	50	100	150	10	20	50	100	150				
Water content (%)	Axial Deformation (mm) (Cumulative(+ve indicates specimen contraction))					Void ratio change					Void ratio at start of testing	Dry density (Mg/m^3)	Dried water content (%)[1]	Volume change during drying (+ve expansion) (%)
6	0.01	0.02	0.03	0.07	0.09	0.32	0.32	0.32	0.31	0.31	0.32	2.00	1.16	0.24
7	0.03	0.02	0.03	0.05	0.06	0.29	0.29	0.29	0.29	0.29	0.29	2.05	0.47	0.18
8	0.01	0.00	0.00	0.02	0.04	0.32	0.32	0.32	0.32	0.32	0.32	2.00	0.98	0.55
9	0.02	0.00	0.00	0.00	0.01	0.32	0.32	0.32	0.32	0.32	0.32	2.00	1.81	-0.10
10	0.01	0.01	0.00	0.01	0.02	0.26	0.26	0.26	0.26	0.26	0.26	2.09	1.63	-1.26

[1]Water content calculated using the specimen's dried weight when tested and the 'target weight' at 0% water content at based on the specimen's weight when construction and its water content determined from the specimen's mix.

[2]Void ratio calculated assuming axial deformation same as radial deformation

Table 4.14: Cumulative axial deformation during increasing net normal of dried specimens of material D and their tested water content.

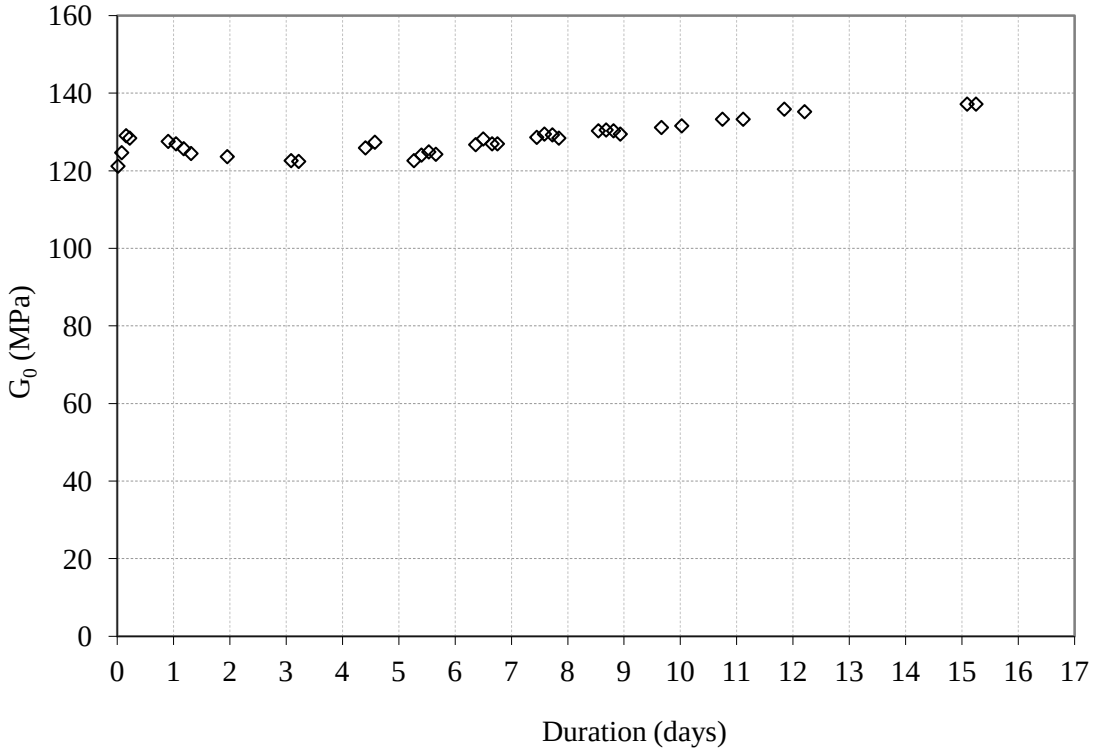

Figure 4.1: Shear modulus (G_0) variation with time under constant net normal stress (39kPa) for material D prepared to a dry density of 2.11Mg/m^3 and water content of 4.22%.

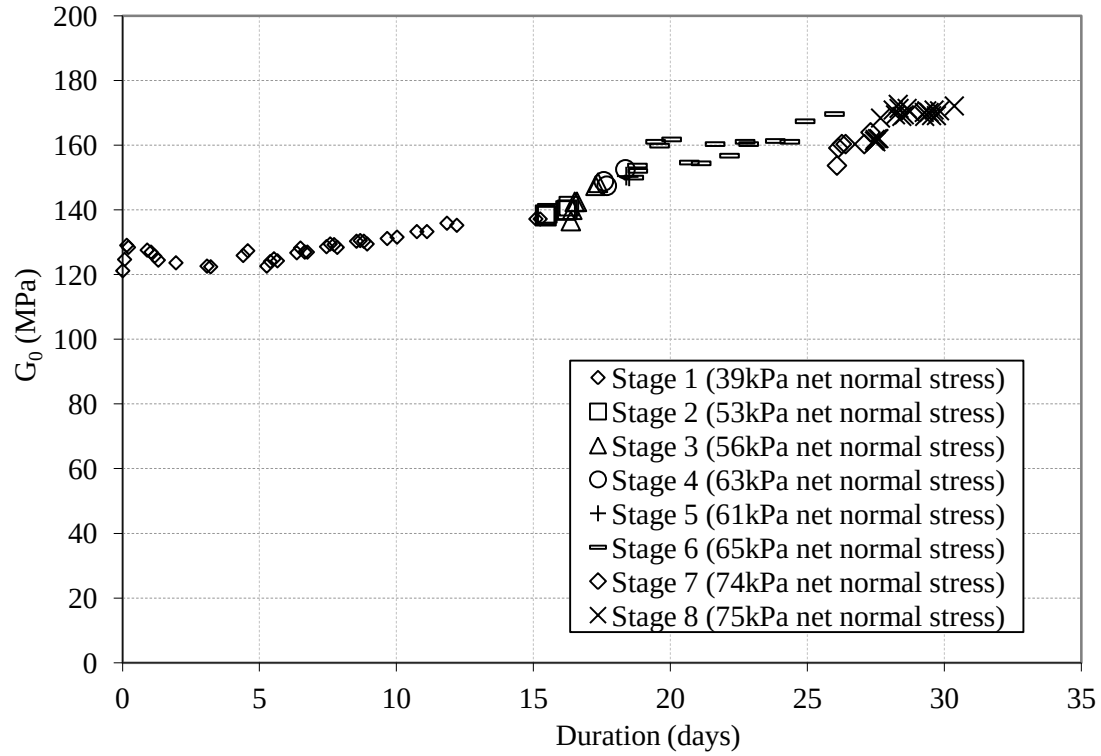

Figure 4.2: Shear modulus (G_0) variation with time under a target value of 40kPa net normal stress but different magnitudes of air and cell pressure (Material D: Dry density 2.11Mg/m^3 and water content of 4.22%).

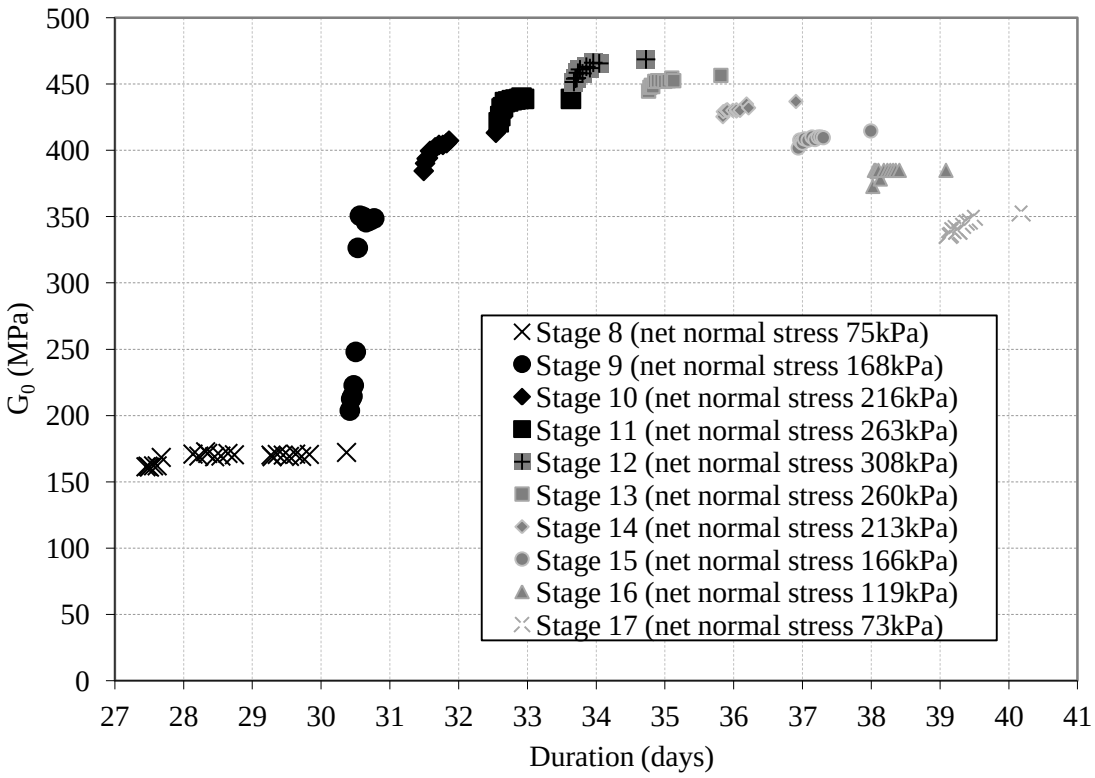

Figure 4.3a: Shear modulus (G_0) variation with time under varying net normal stresses (Material D: Dry density 2.11Mg/m^3 and water content of 4.22%).

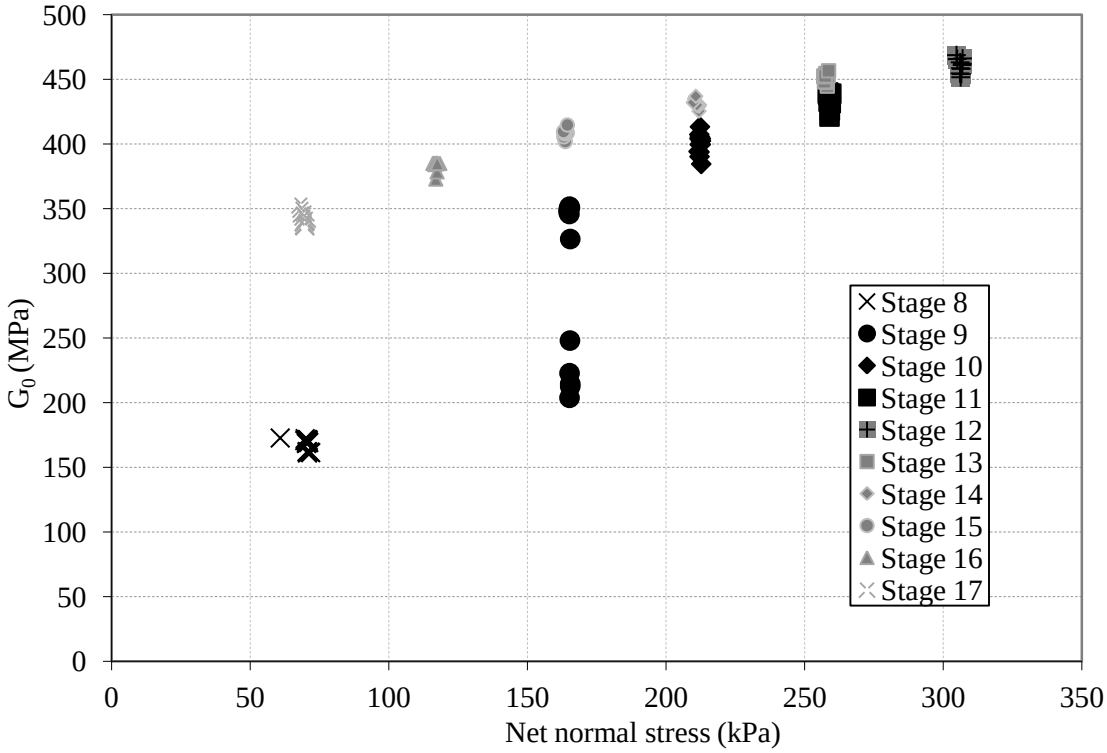

Figure 4.3b: Shear modulus (G_0) variation with net normal stress (Material D: Dry density 2.11Mg/m^3 and water content of 4.22%).

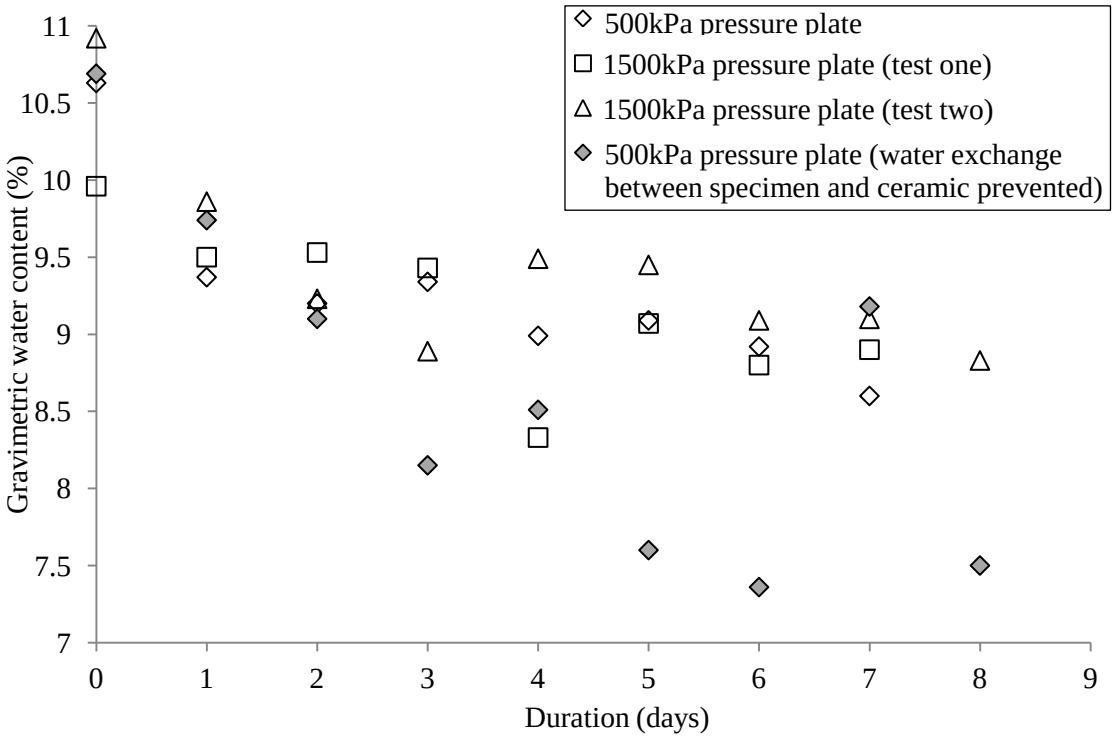

Figure 4.4: Water content variation with duration under constant pressure for material C in the pressure plate apparatus (500kPa and 1500kPa pressure plate apparatus).

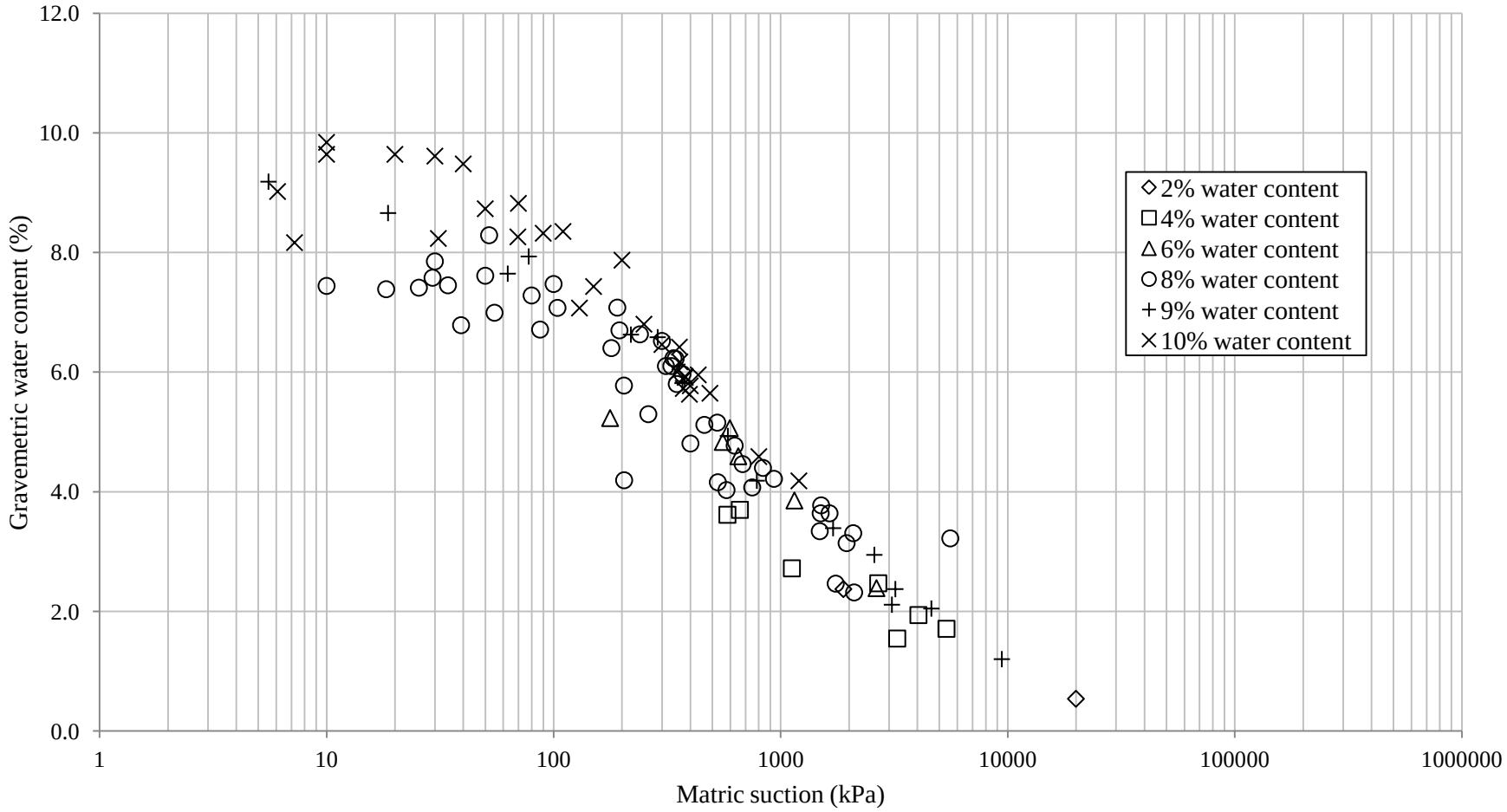

Figure 4.5: Soil water characteristic curve derived using the filter paper technique and pressure plate apparatus for material D prepared at various water contents to a dry density of 2.10Mg/m^3.

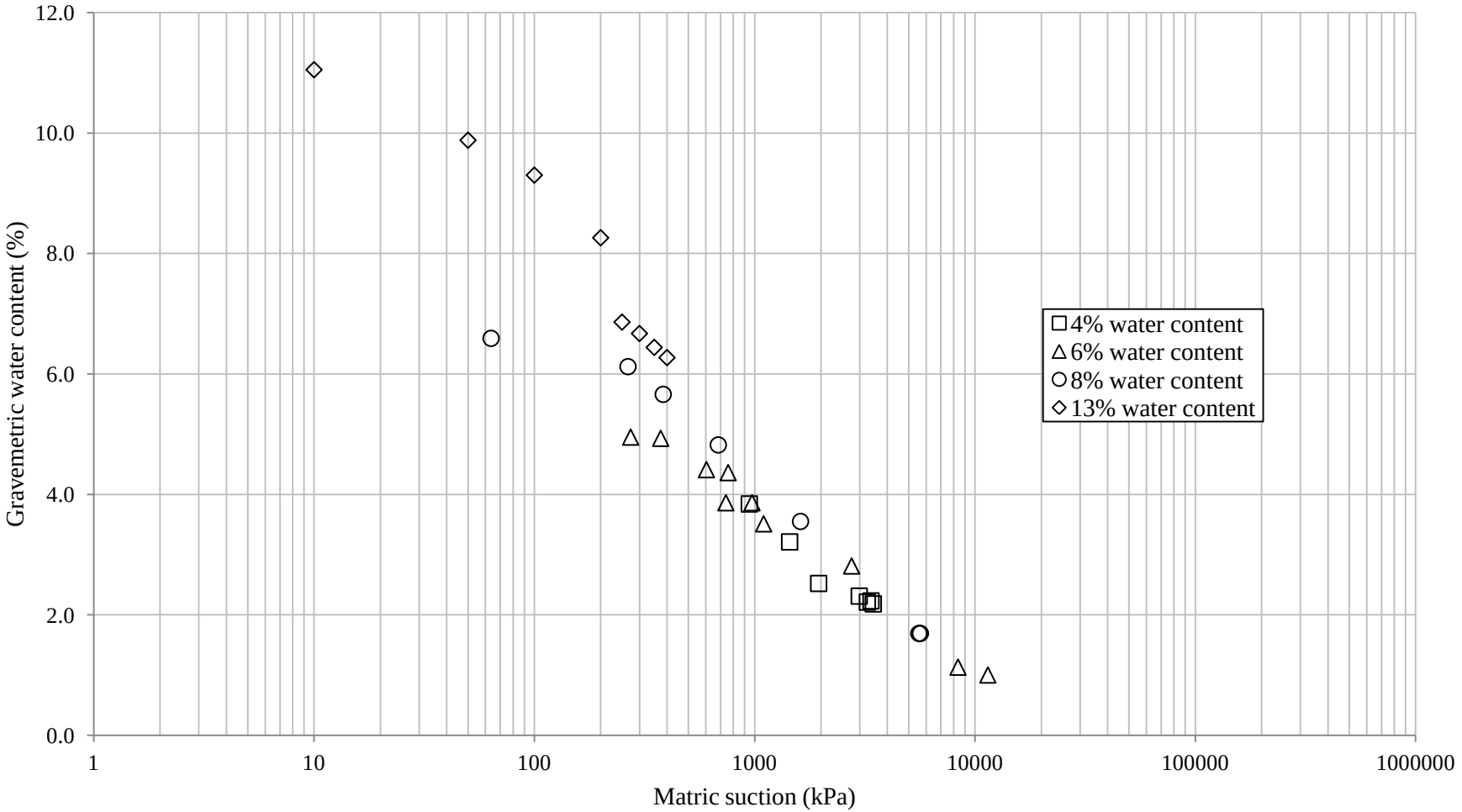

Figure 4.6: Soil water characteristic curve derived using the filter paper technique and pressure plate apparatus for material D prepared at various water contents to a dry density of 1.70Mg/m^3.

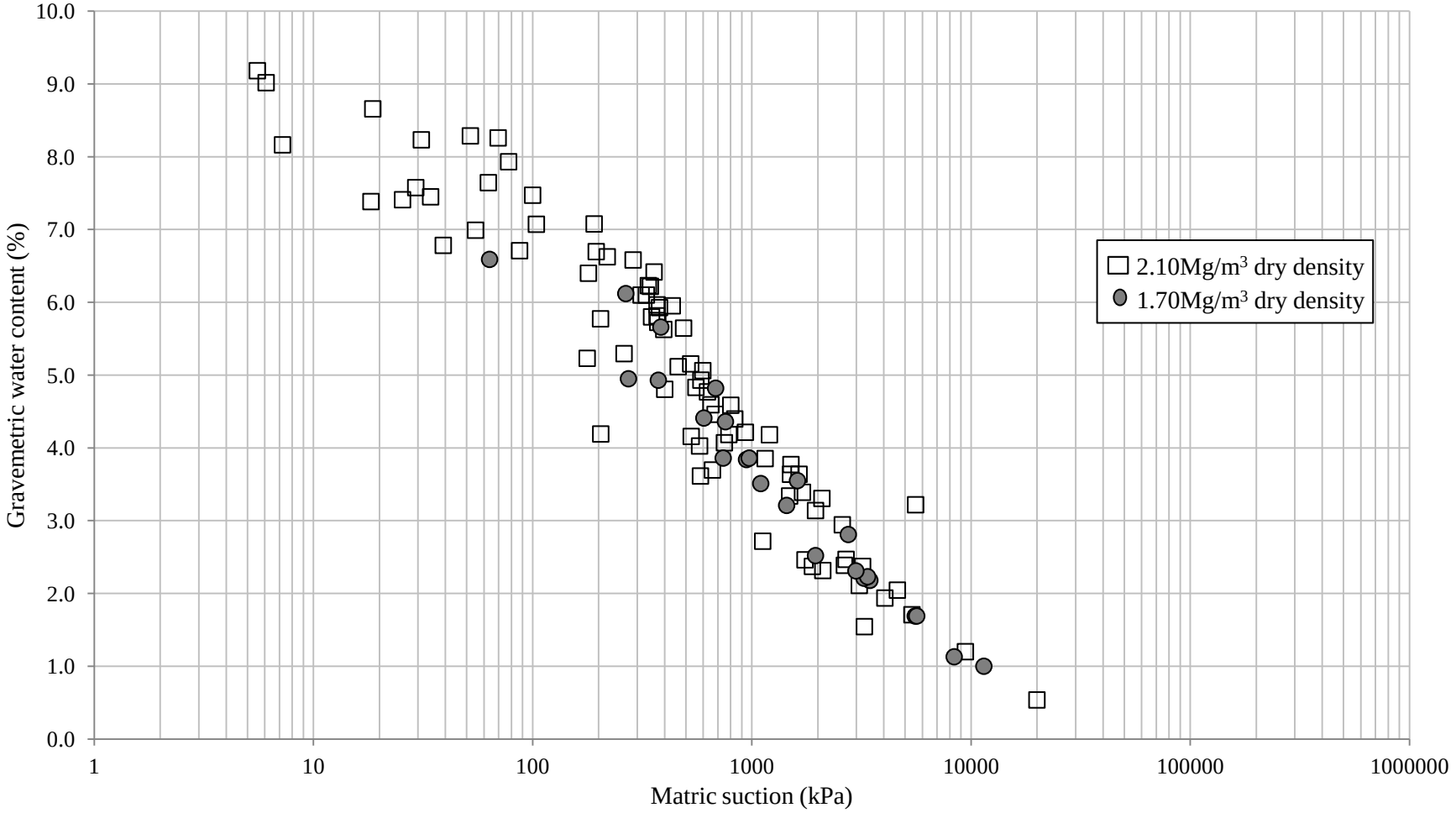

Figure 4.7: Soil water characteristic curve derived using the filter paper technique and pressure plate apparatus for material D prepared at various water contents to dry densities of 2.10Mg/m^3 and 1.70Mg/m^3.

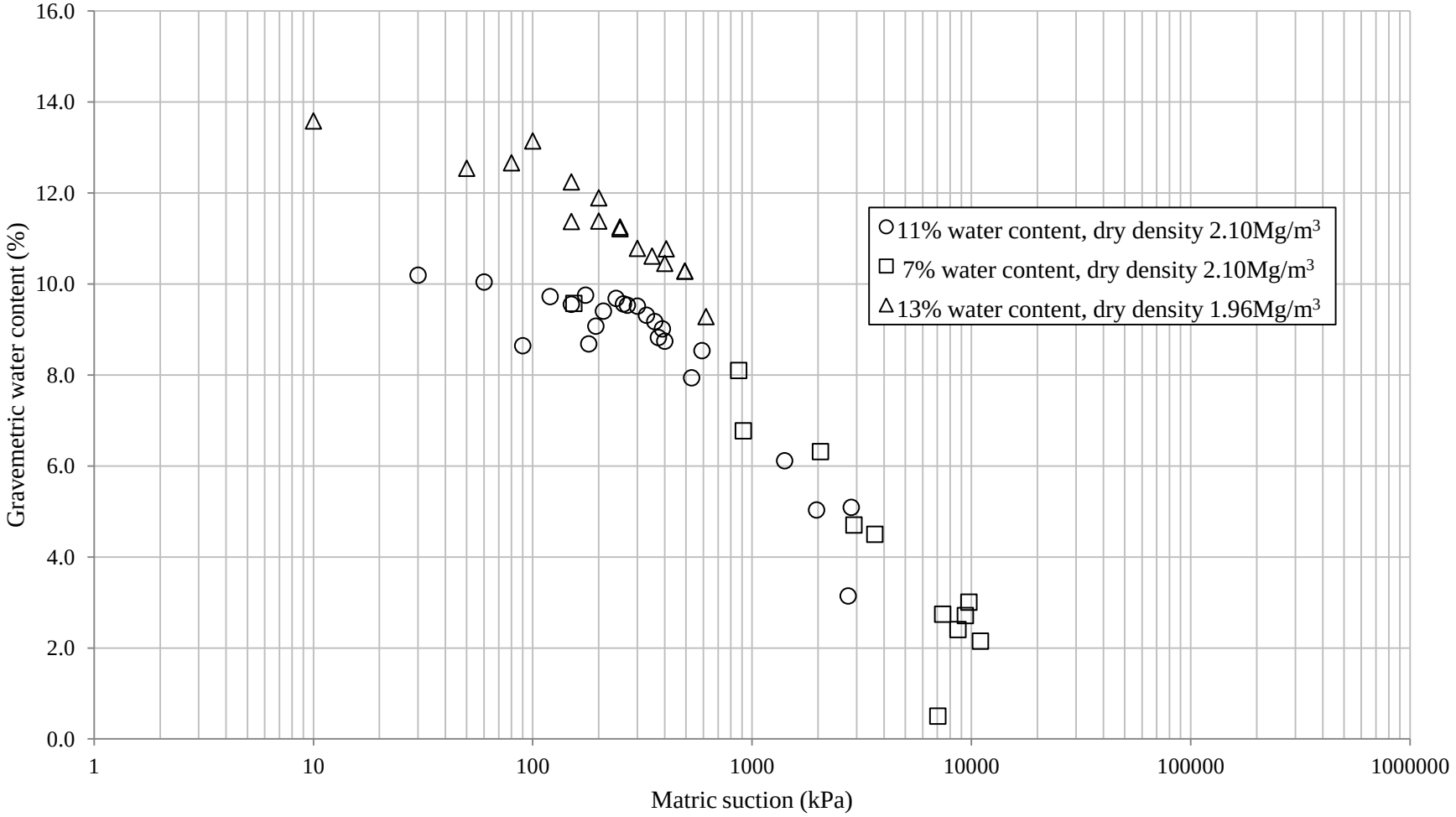

Figure 4.8: Soil water characteristic curve derived using the filter paper technique and pressure plate apparatus for material C prepared at various water contents and dry densities.

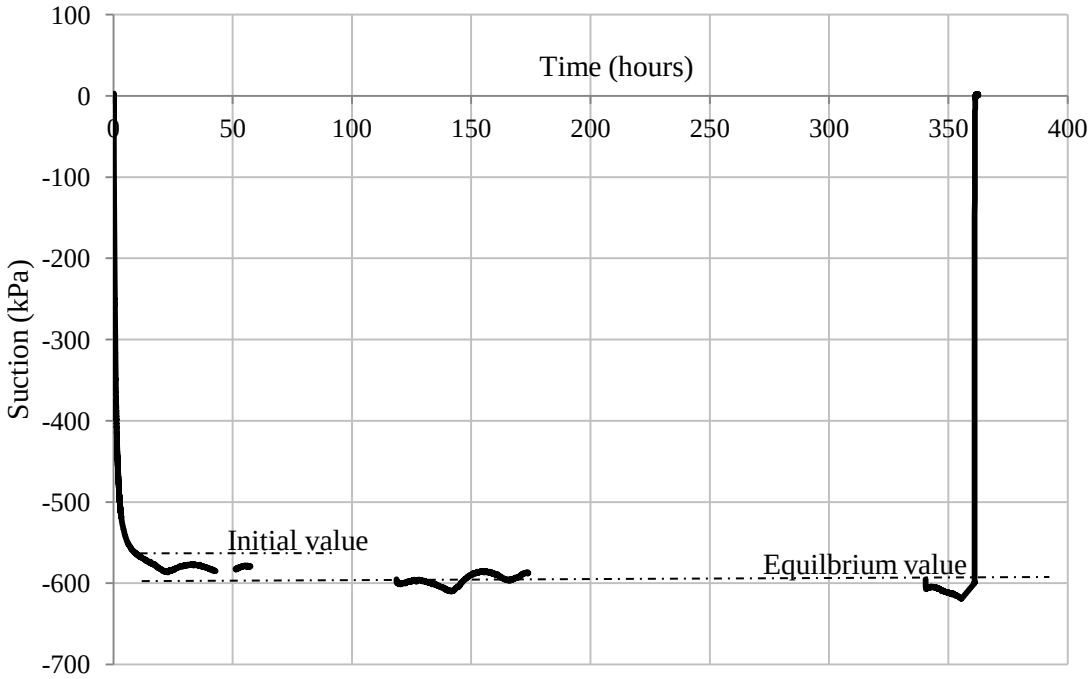

Figure 4.9 (a): Tensiometer measurement 4.31% water content specimen.

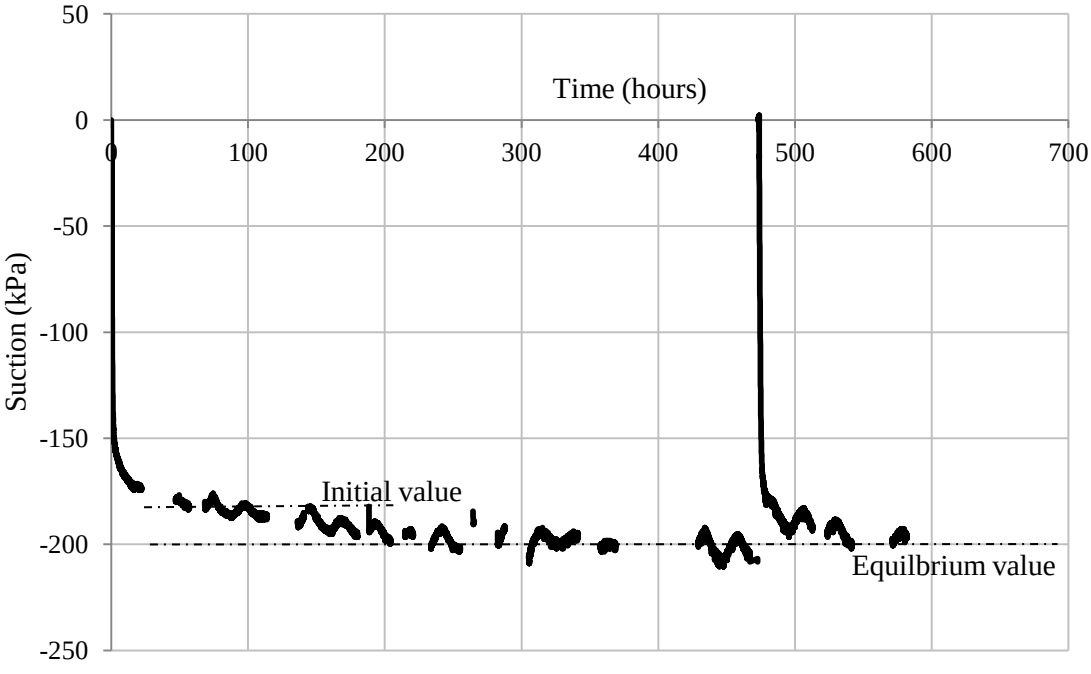

Figure 4.9 (b): Tensiometer measurement 4.92% water content specimen.

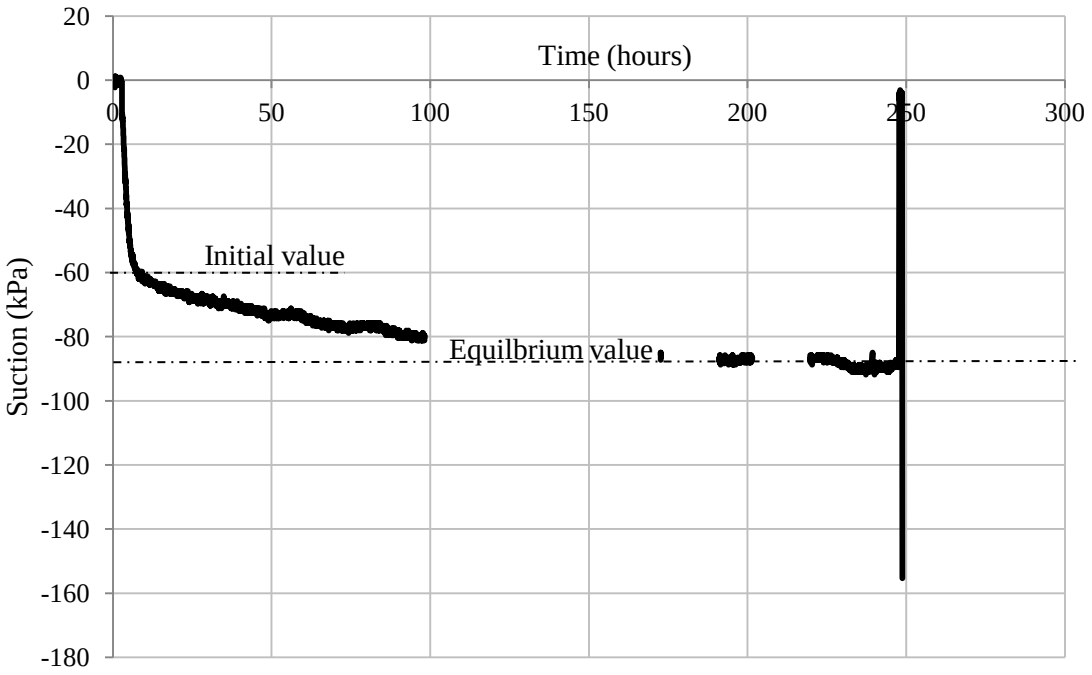

Figure 4.9 (c): Tensiometer measurement 6.16% water content specimen.

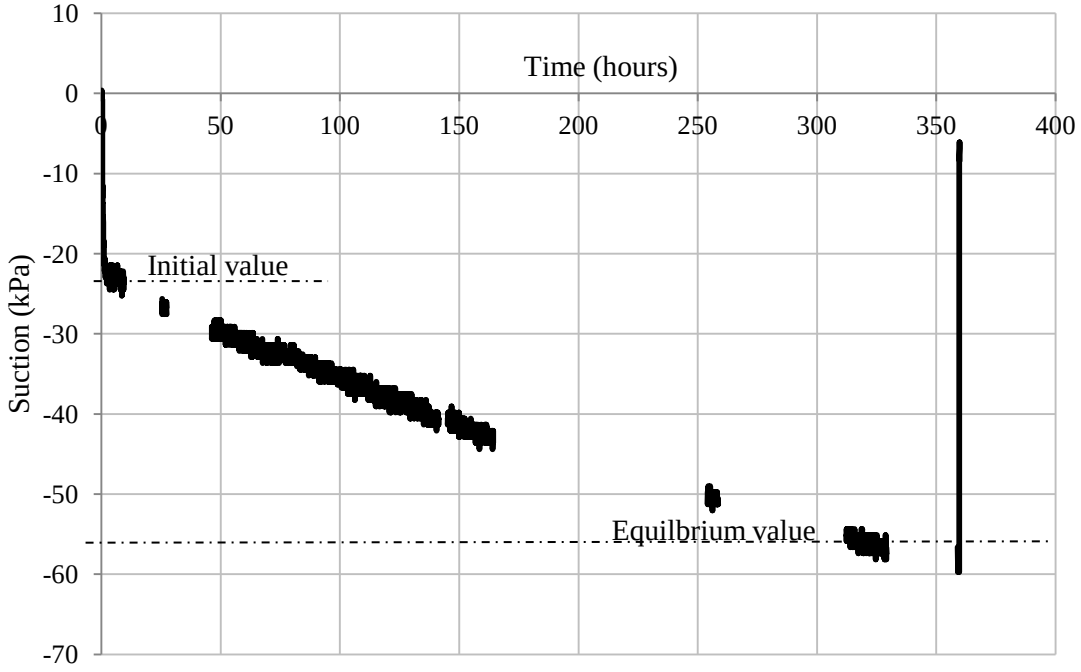

Figure 4.9 (d): Tensiometer measurement 7.29% water content specimen.

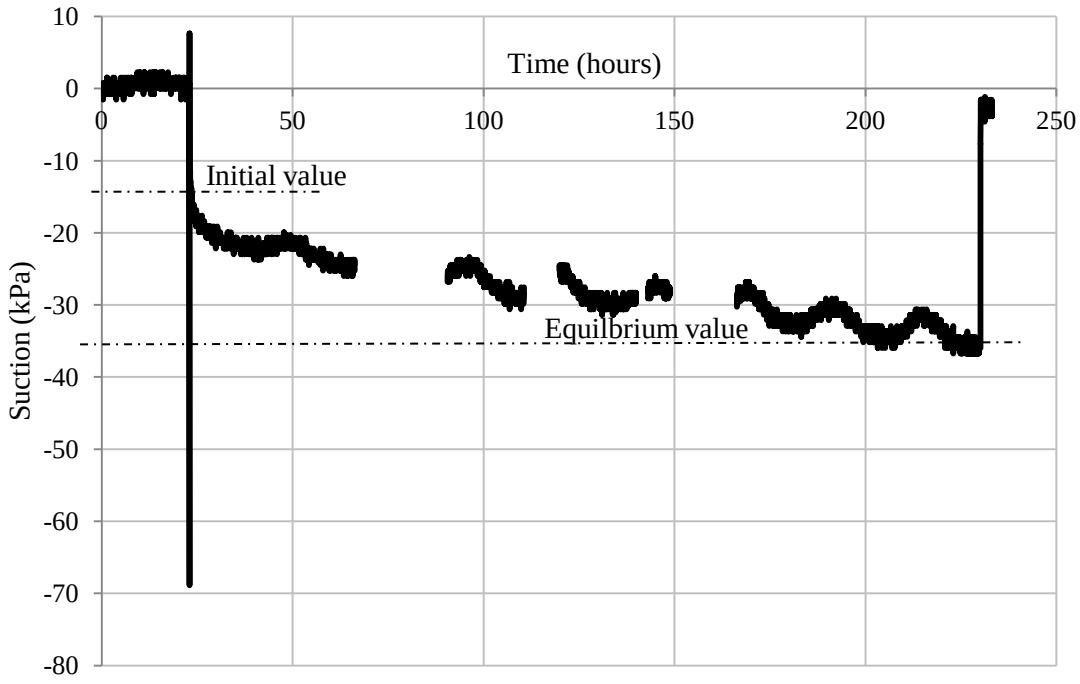

Figure 4.9 (e): Tensiometer measurement 7.96% water content specimen.

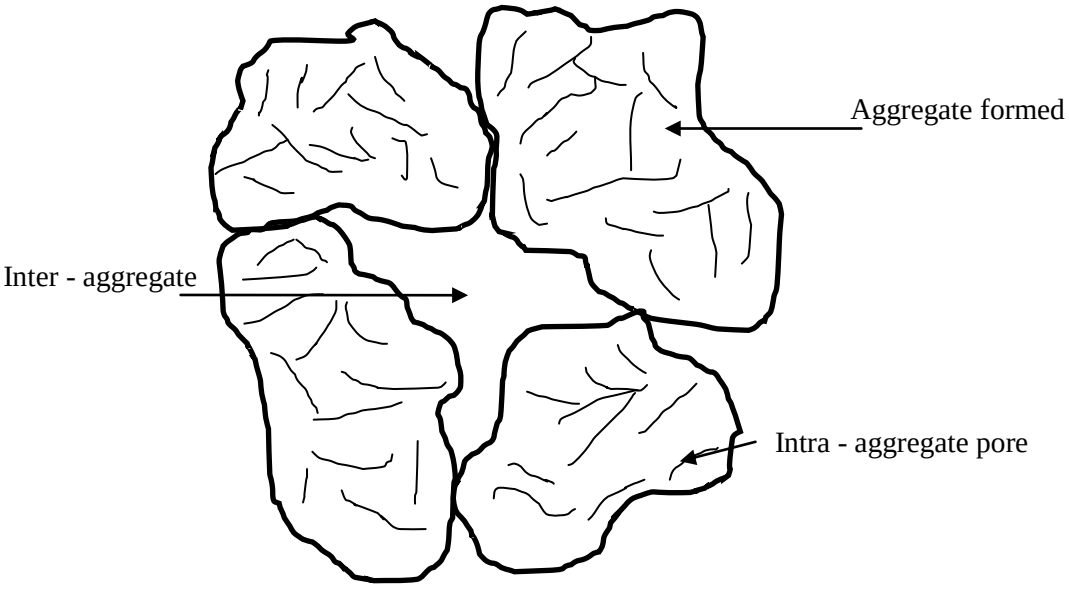

Figure 4.10: Aggregate structure formed by clay particles dry of optimum. Redrawn from Thom et al. (2007).

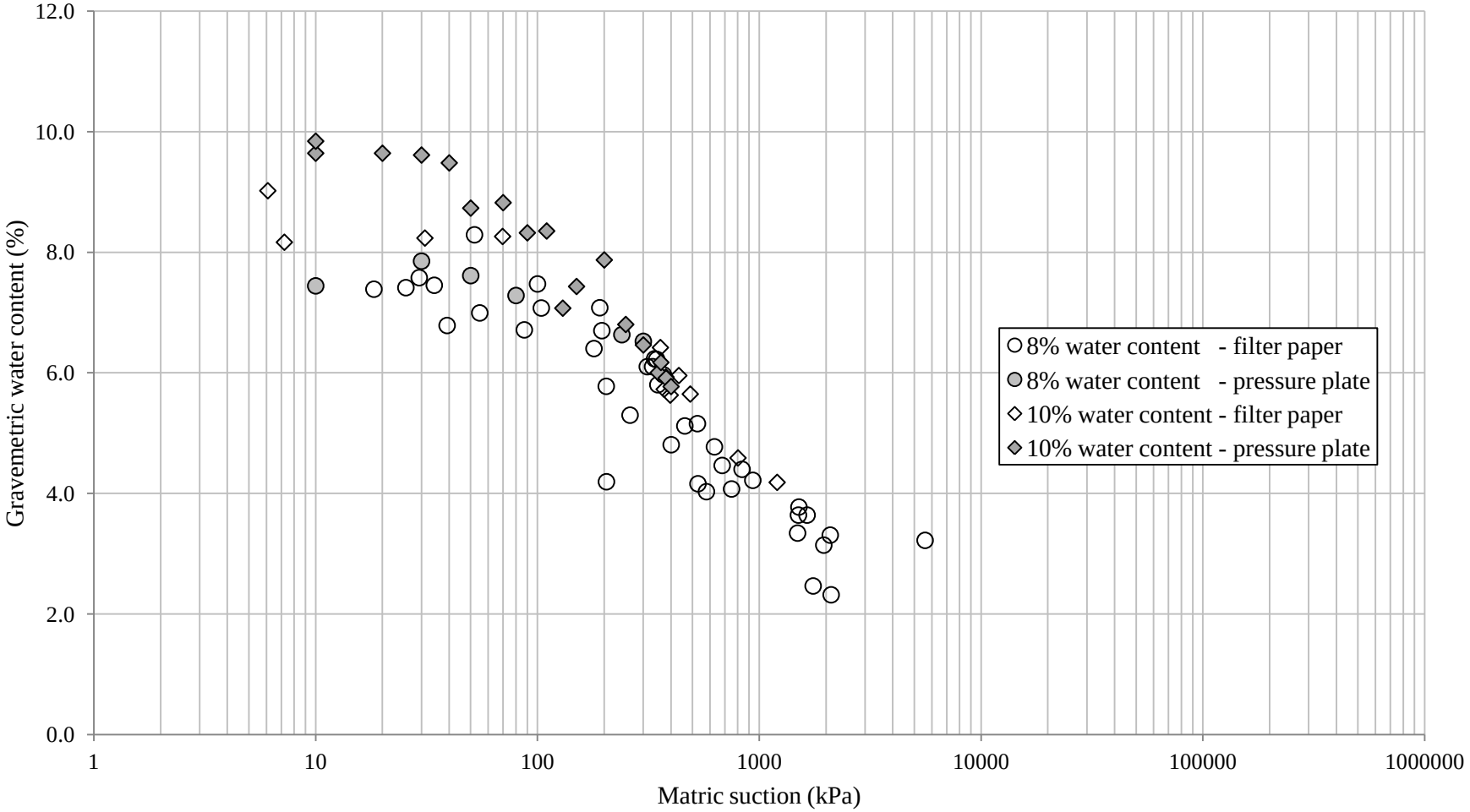

Figure 4.11: Comparison between filter paper technique and pressure plate apparatus used to derive the soil water characteristic curve for material D at a dry density of 2.10Mg/m^3.

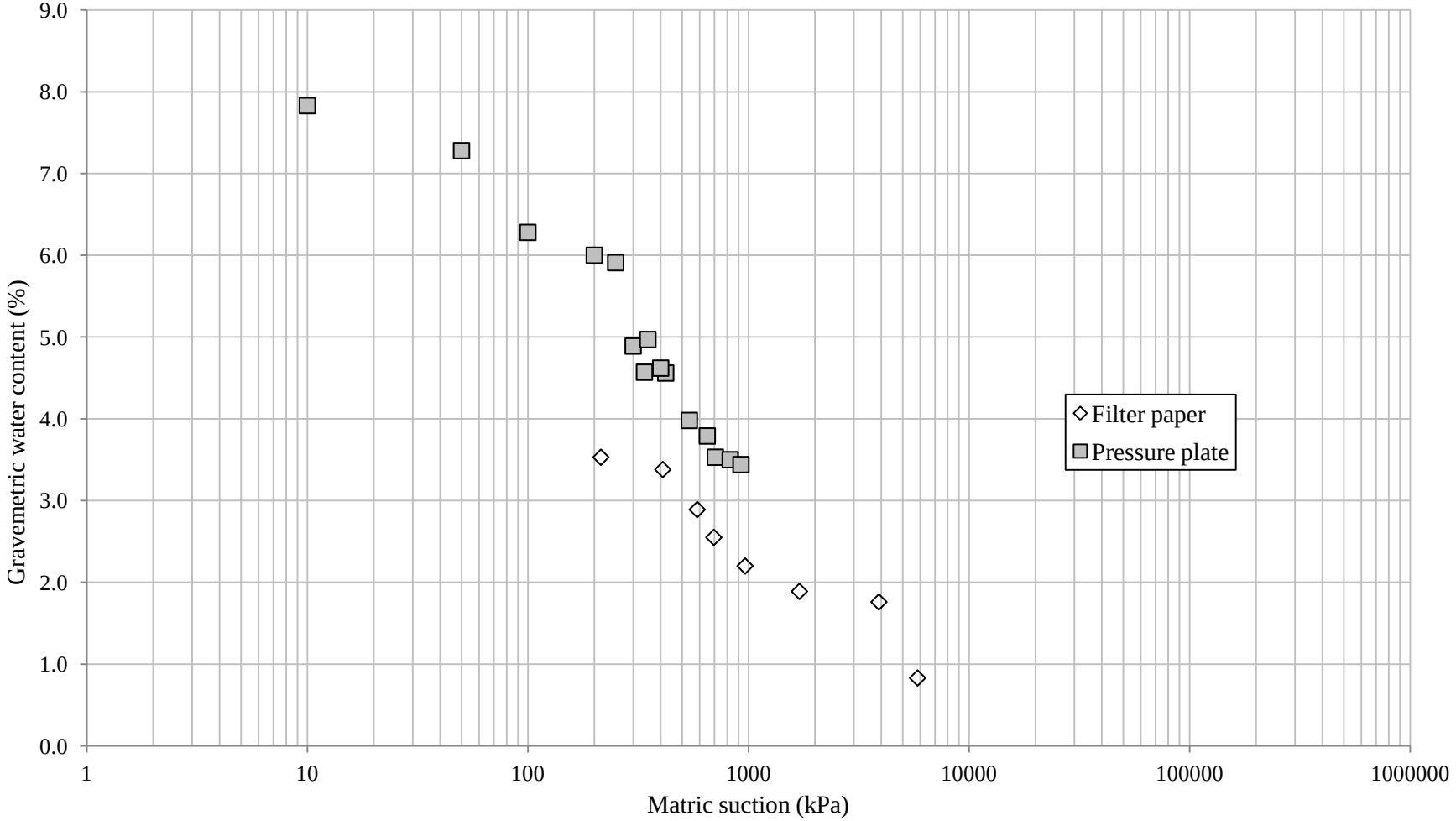

Figure 4.12: Comparison between filter paper technique and pressure plate apparatus used to derive the soil water characteristic curve for material A.

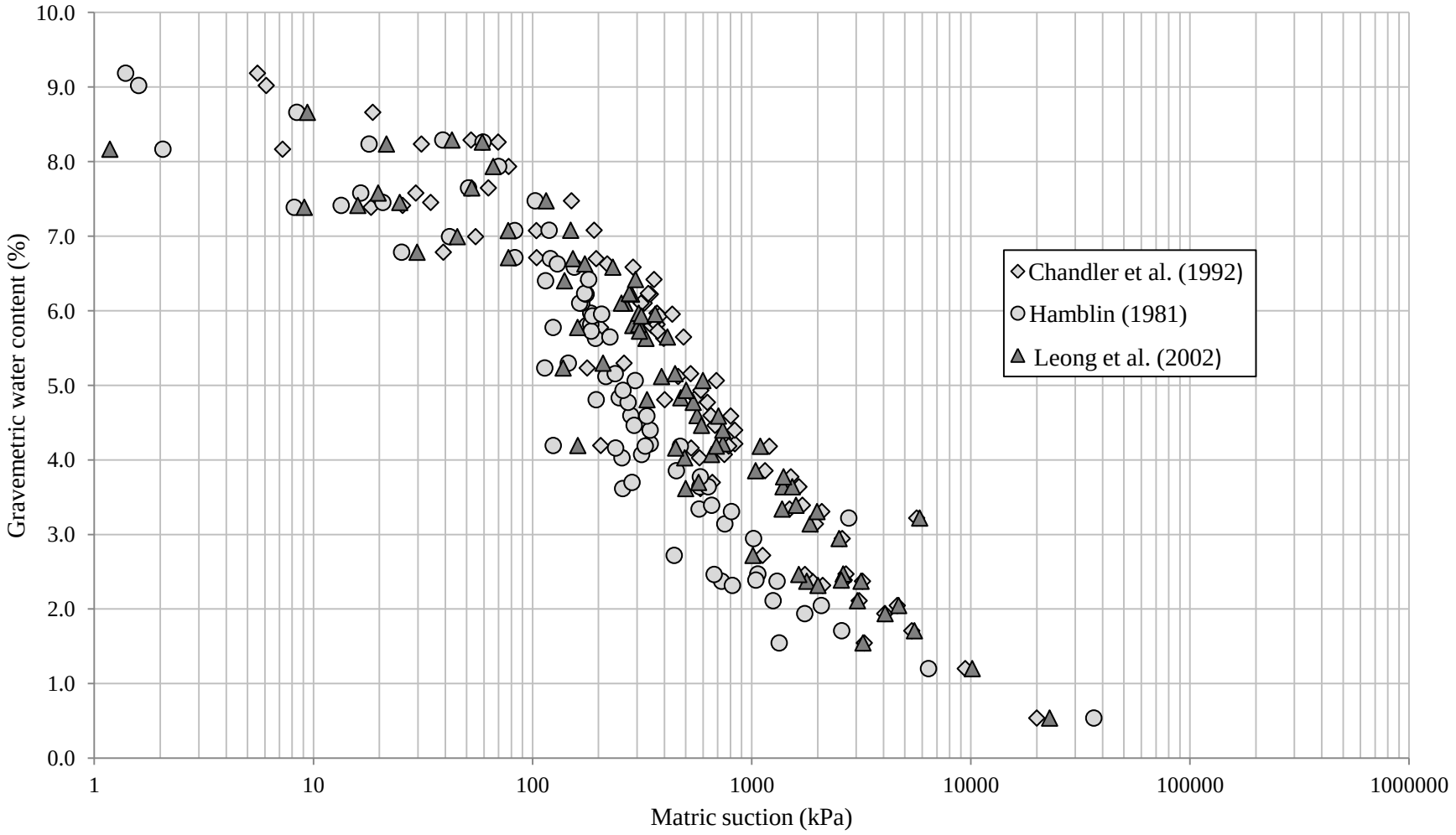

Figure 4.13: Comparison between filter paper calibration curves for material D at a dry density of 2.10Mg/m^3.

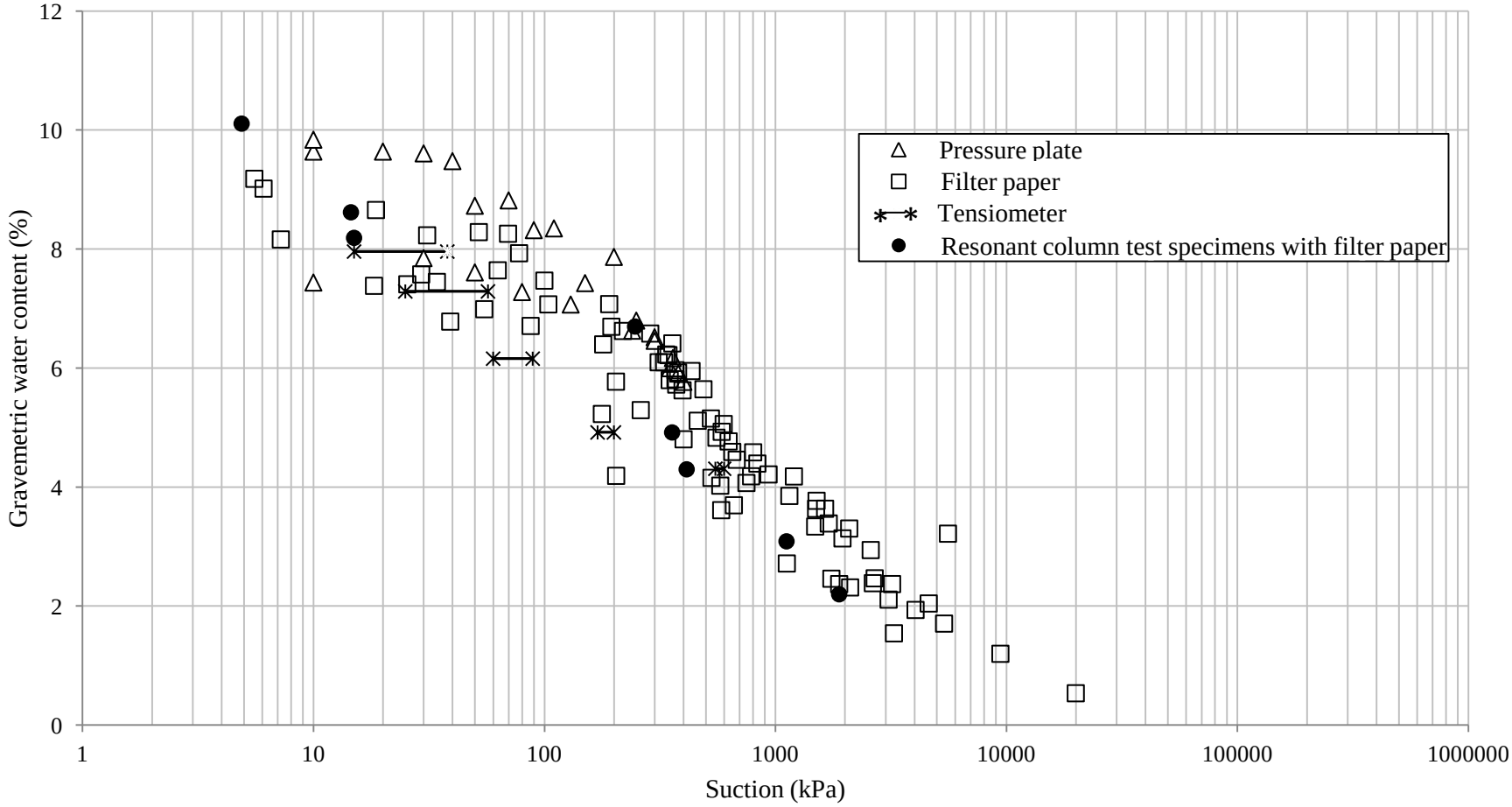

Figure 4.14: Soil water characteristic curve for material D (dry density of 2.10Mg/m^3) including tensiometer measurements and filter paper measurements conducted on resonant column specimens.

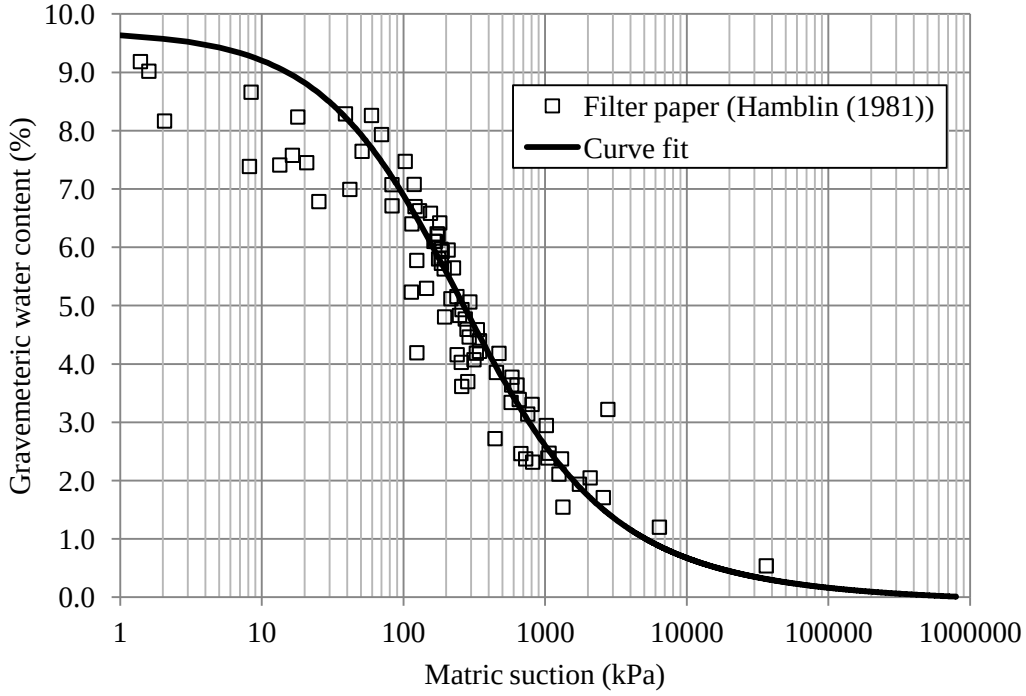

Figure 4.15 (a): Filter paper soil water characteristic curve data fitted with Fredlund and Xing (1994) equation for material D (dry density 2.10Mg/m^3). Suction calculated using Hamblin (1981) calibration equation.

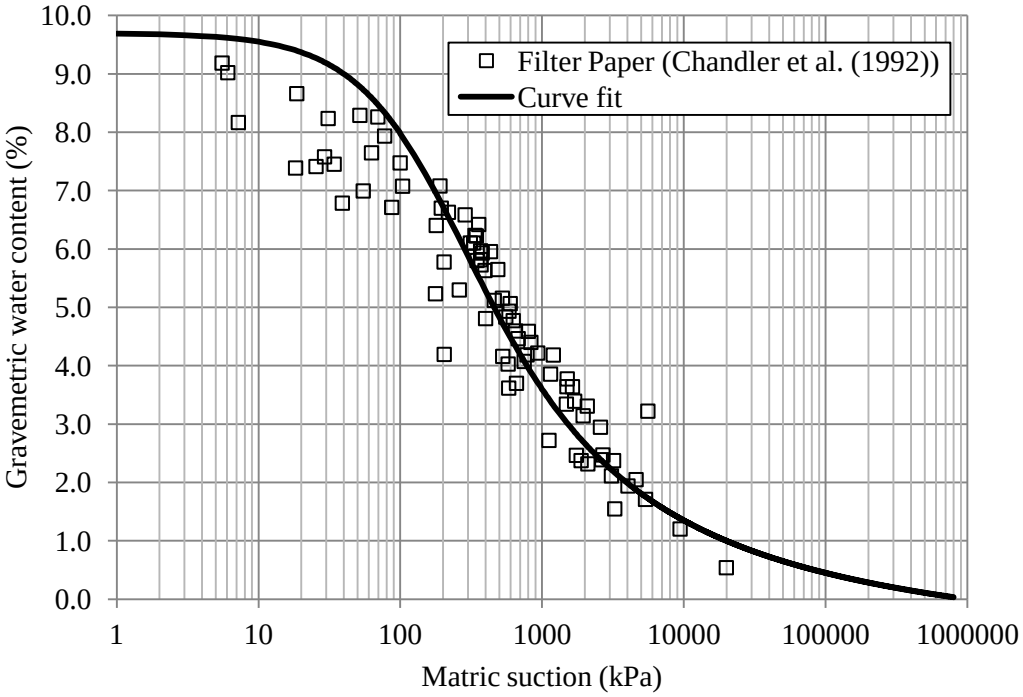

Figure 4.15 (b): Filter paper soil water characteristic curve data fitted with Fredlund and Xing (1994) equation for material D (dry density 2.10Mg/m^3). Suction calculated using Chandler et al. (1992) calibration equation.

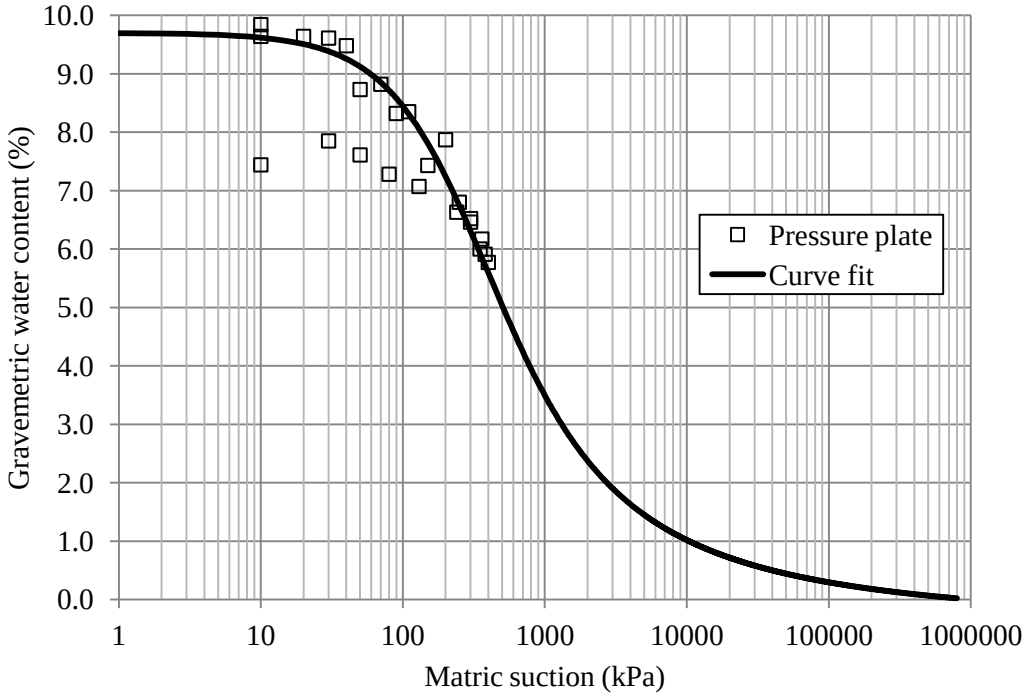

Figure 4.15 (c): Pressure plate soil water characteristic curve data fitted with Fredlund and Xing (1994) equation for material D (dry density 2.10Mg/m^3).

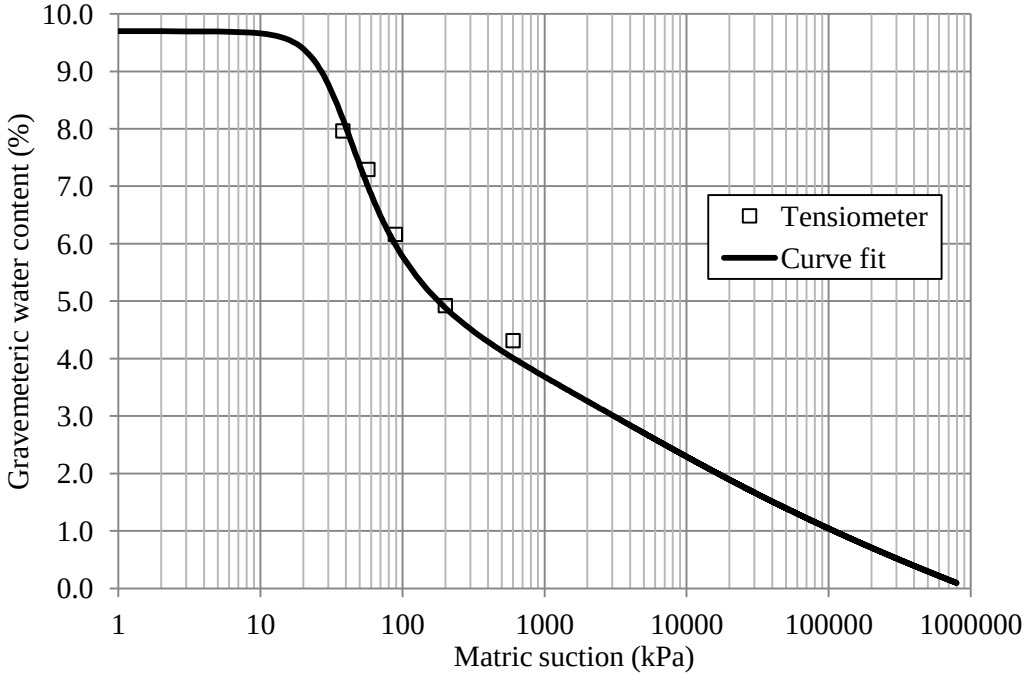

Figure 4.15 (d): Tensiometer soil water characteristic curve data fitted with Fredlund and Xing (1994) equation for material D (dry density 2.10Mg/m^3).

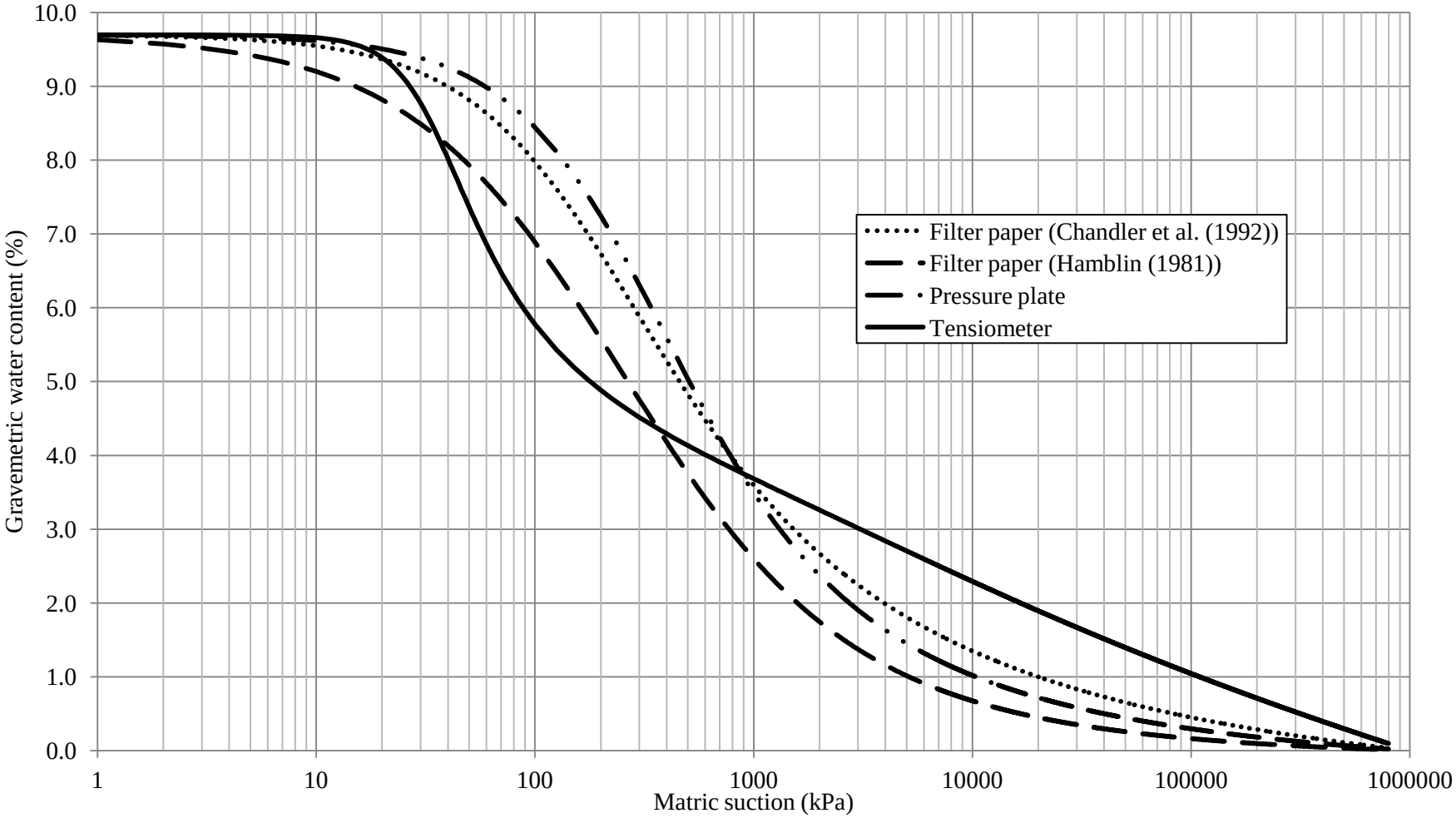

Figure 4.16: Soil water characteristic curve data fitted with Fredlund and Xing (1994) equation for material D (dry density 2.10Mg/m^3).

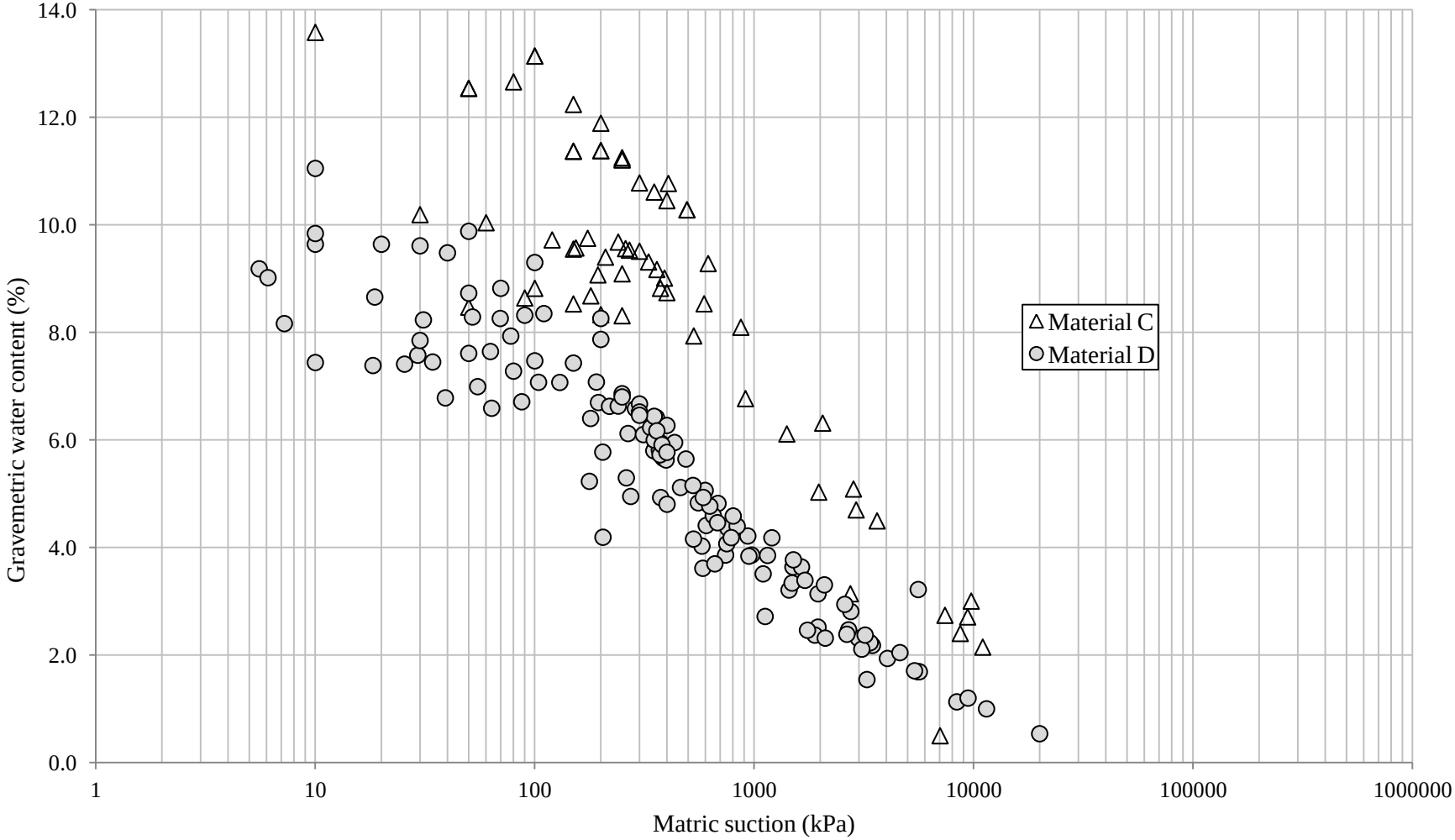

Figure 4.17: Soil water characteristic curves for material C and D

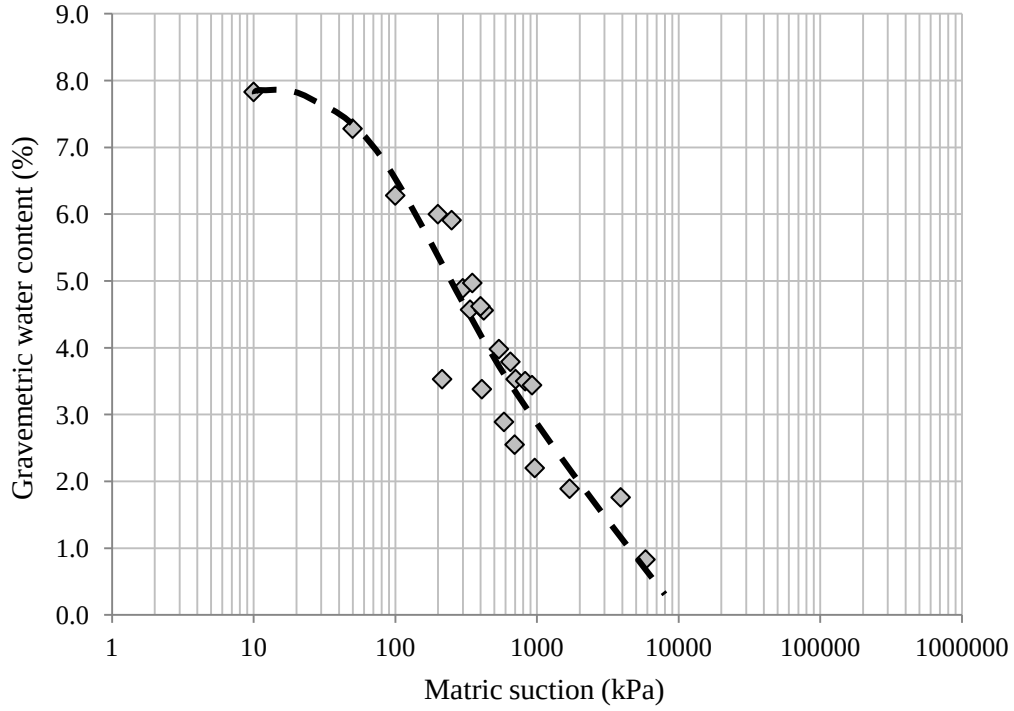

Figure 4.18 (a): Trend line through soil water characteristic curve data for material A.

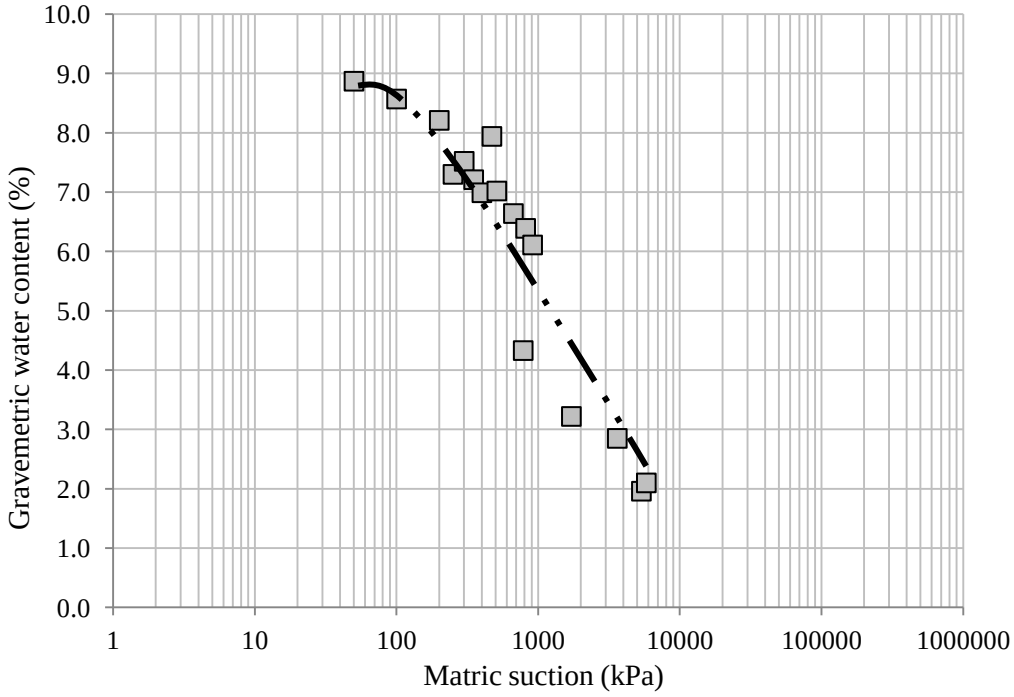

Figure 4.18 (b): Trend line through soil water characteristic curve data for material B.

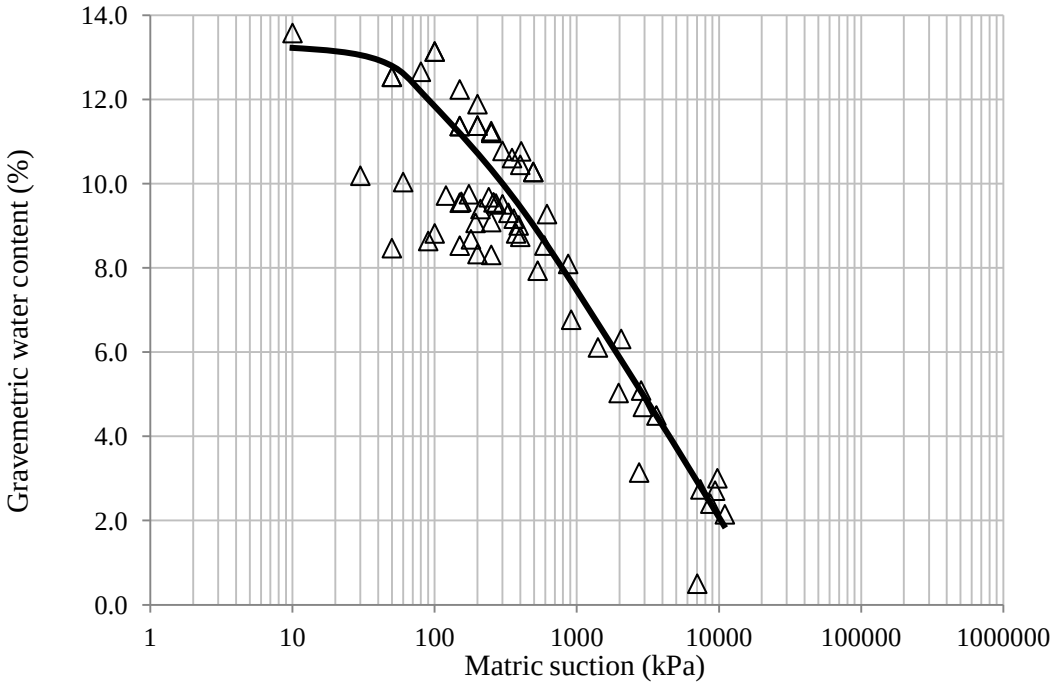

Figure 4.18 (c): Trend line through soil water characteristic curve data for material C.

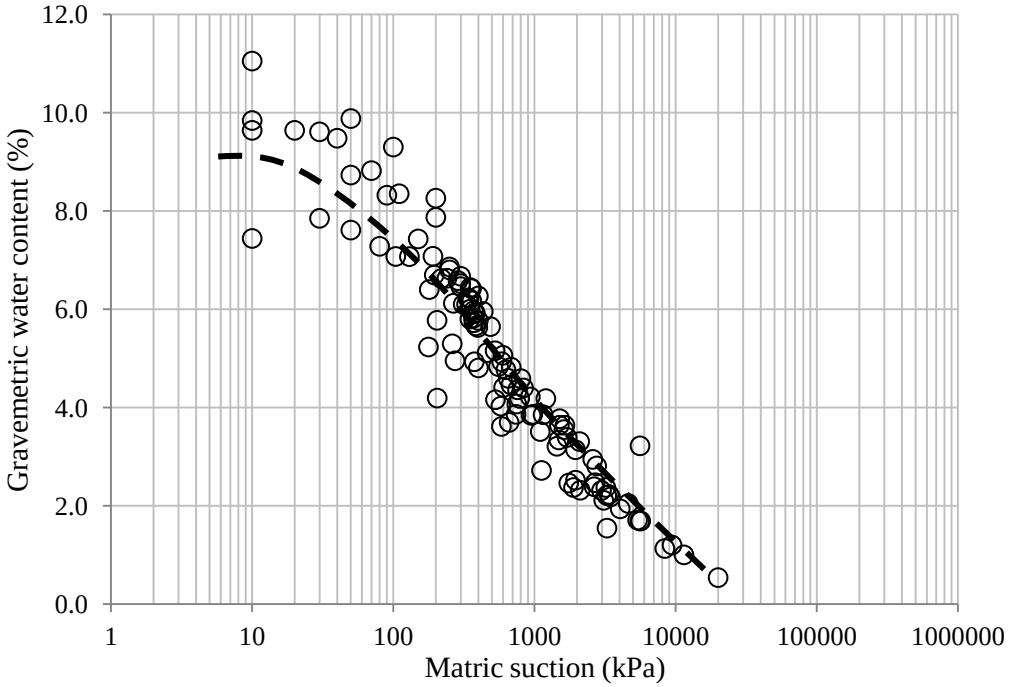

Figure 4.18 (d): Trend line through soil water characteristic curve data for material D.

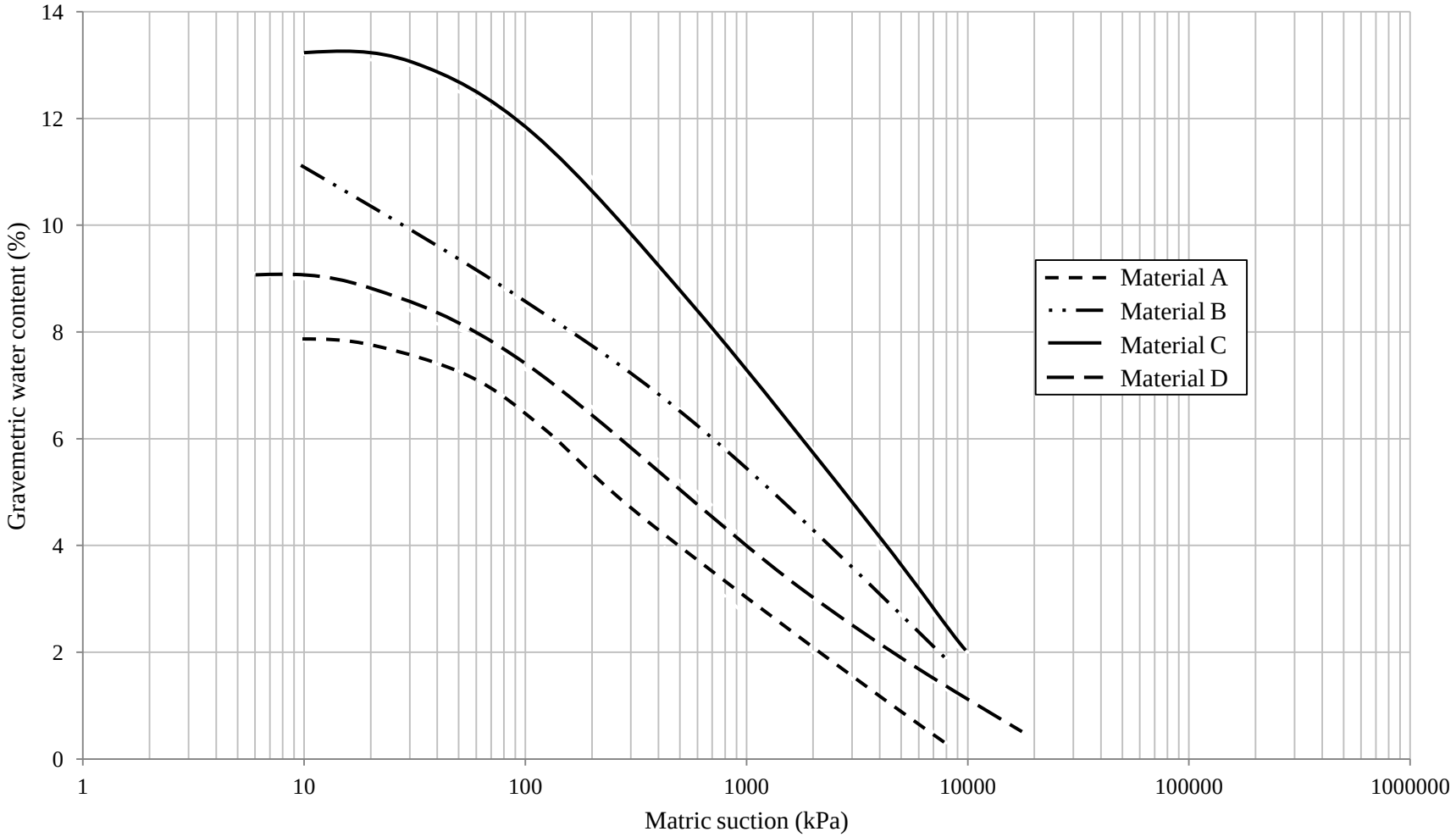

Figure 4.19: Soil water characteristic curve trend lines for materials A to D.

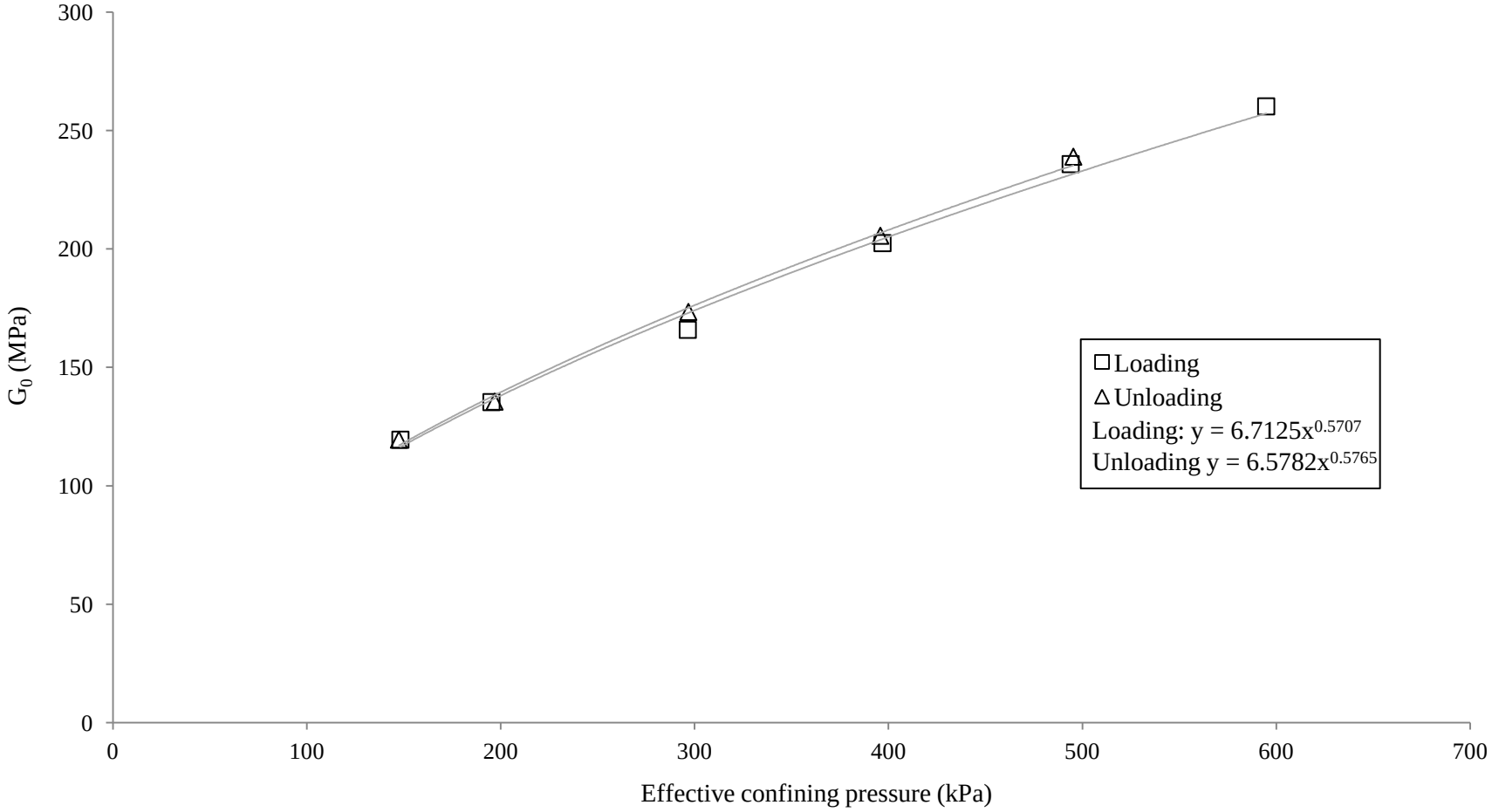

Figure 4.20: Comparison of small strain shear modulus (G_0) measurement during loading and unloading for Leighton Buzzard sand fraction E void ratio 0.64.

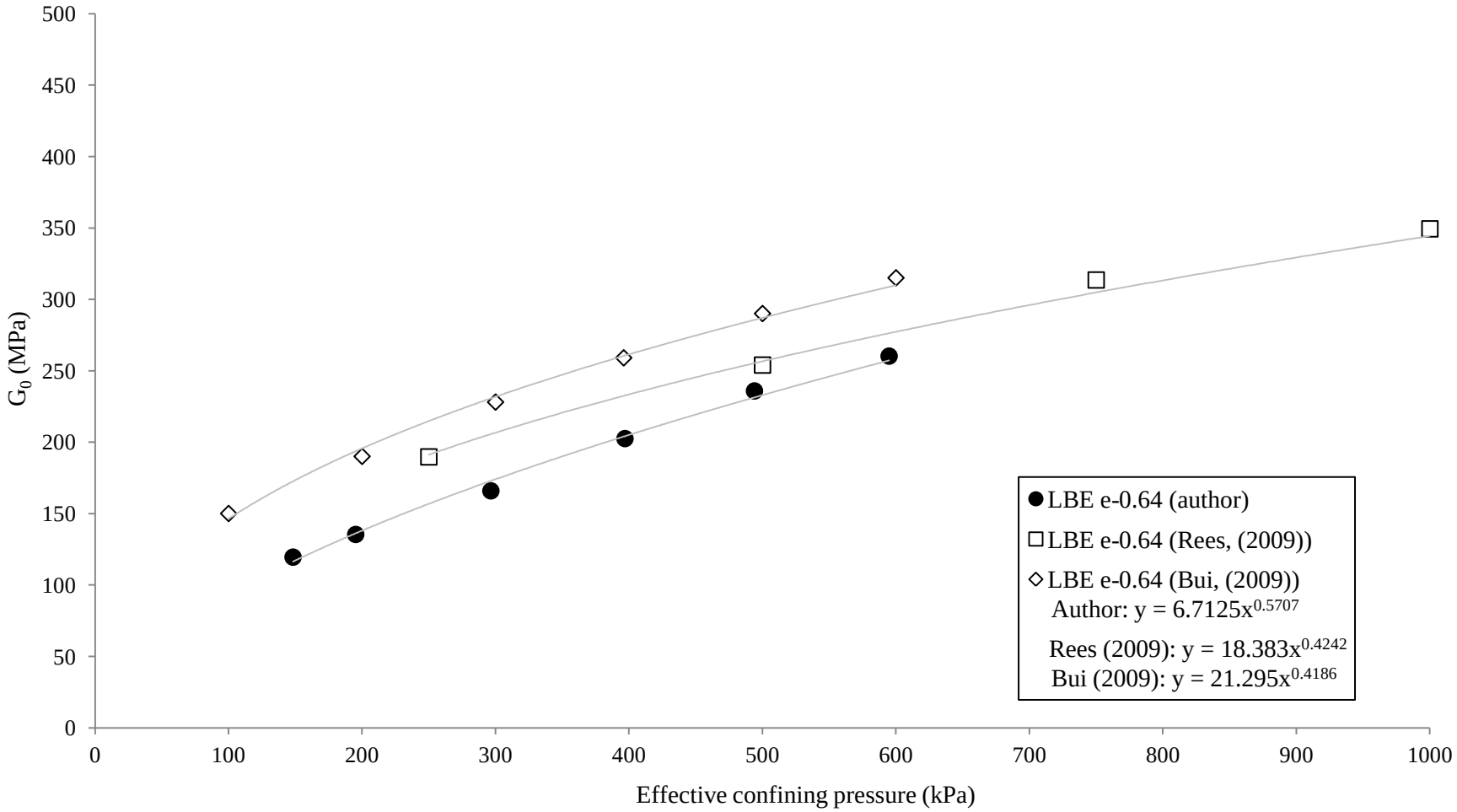

Figure 4.21: Comparison of shear modulus (G_0) measurement between different resonant column users for Leighton Buzzard sand fraction E at void ratio of 0.64 (graph drawn using the following data sources Rees (2009) Figure 4.25; and Bui (2009) Figure 6.5).

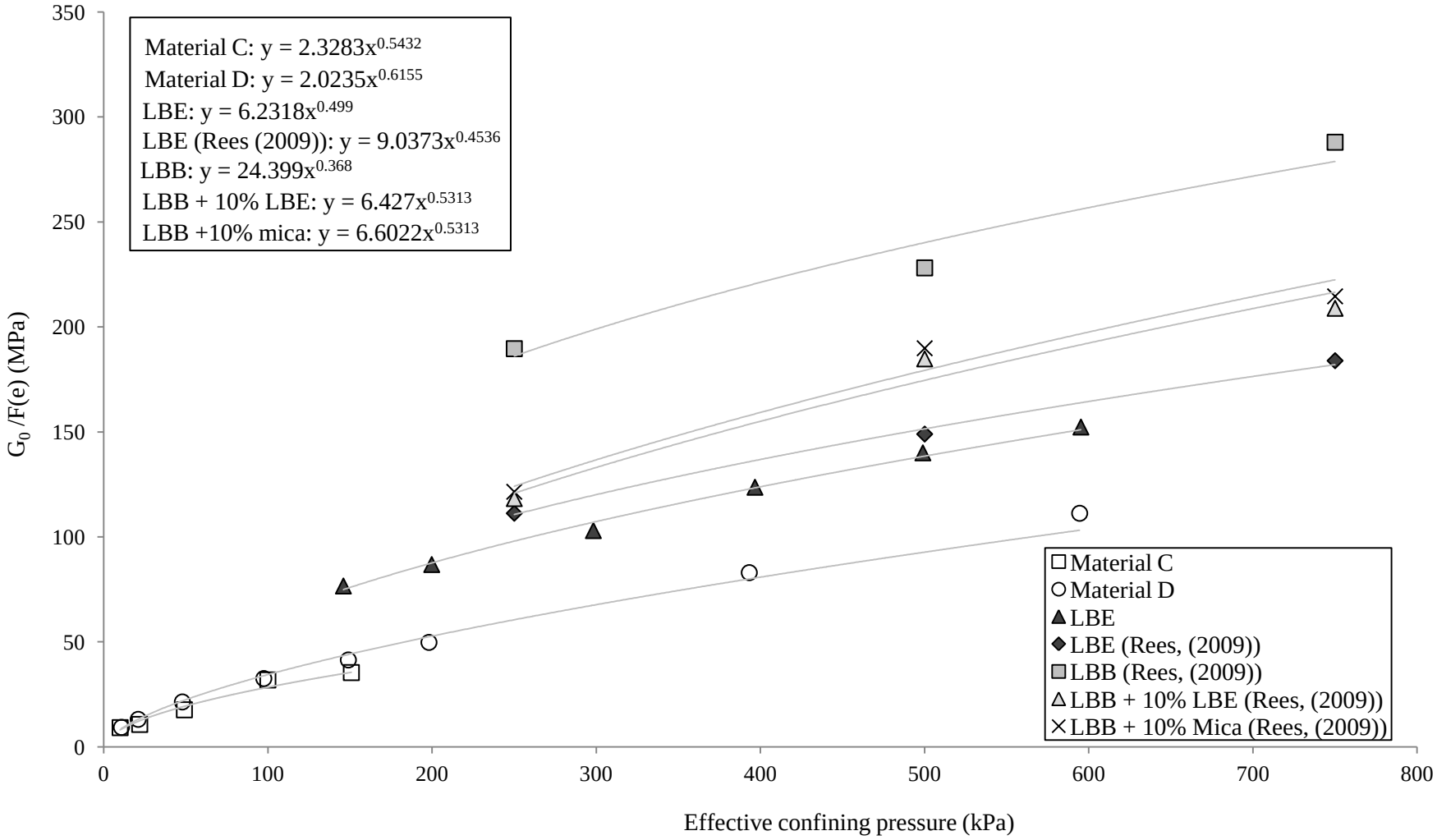

Figure 4.22: Shear modulus (G_0) comparison between different materials corrected for void ratio using Hardin (1978) correction factor (Equation 2.16).

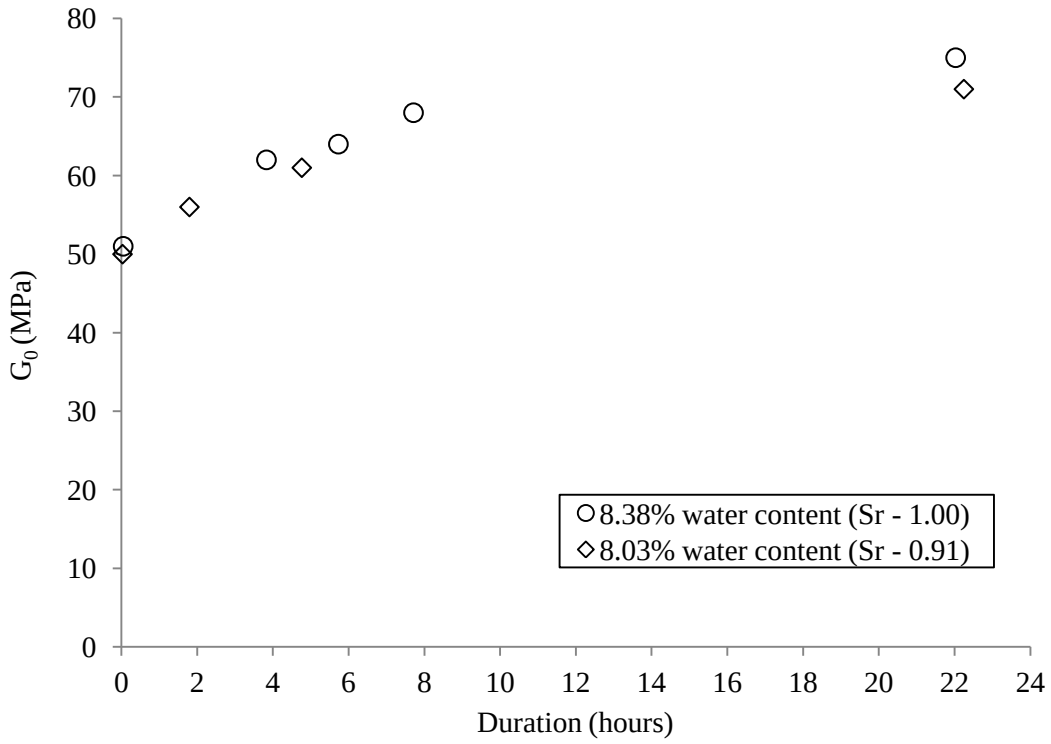

Figure 4.23: Shear modulus (G_0) variation with duration for specimens with a degree of saturation greater than 0.85 hence air phases assumed discontinuous at a net normal stress of 10kPa.

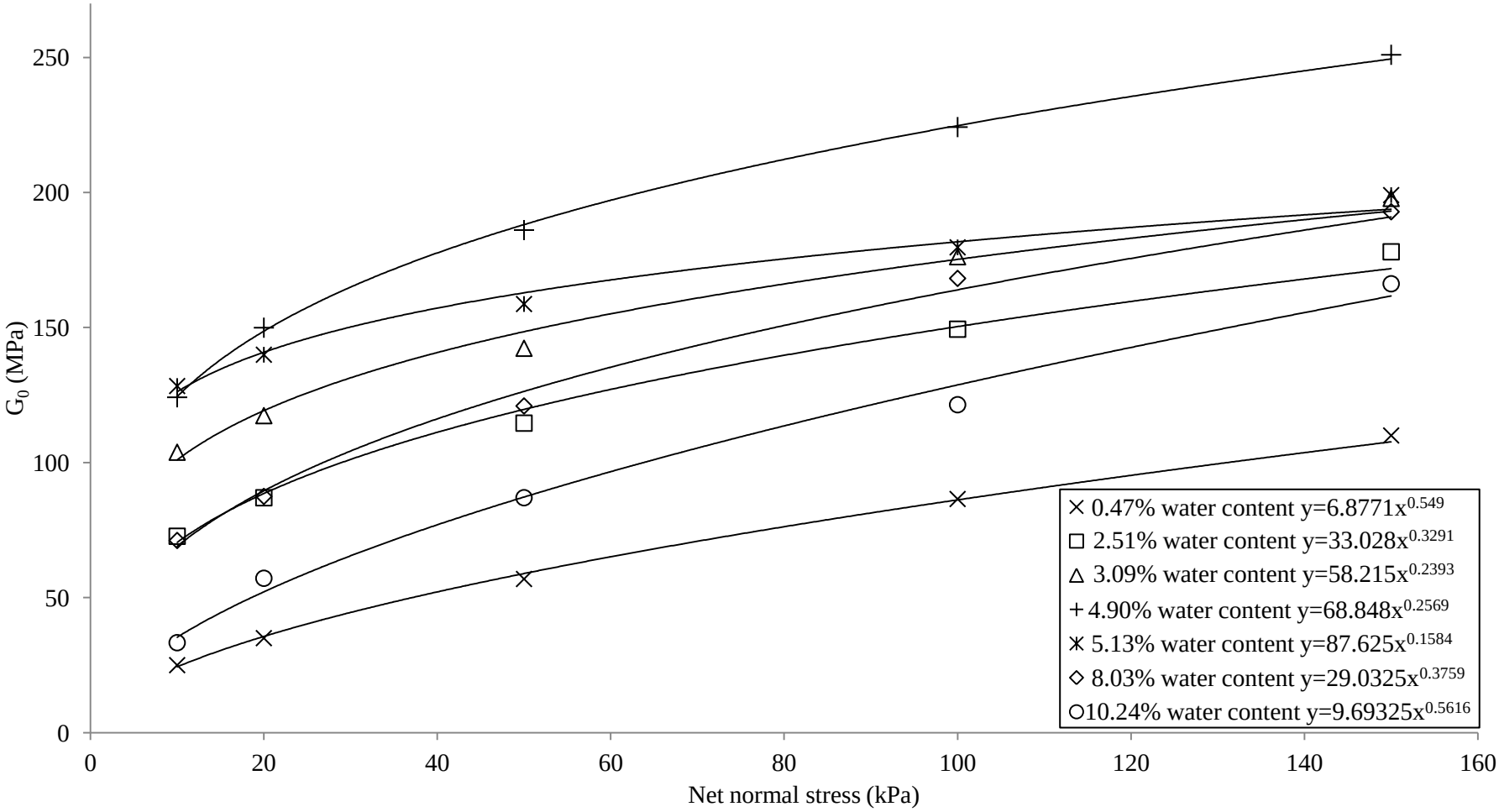

Figure 4.24: Shear modulus (G_0) variation with net normal stress between 10kPa and 150kPa for different water content specimens of material D.

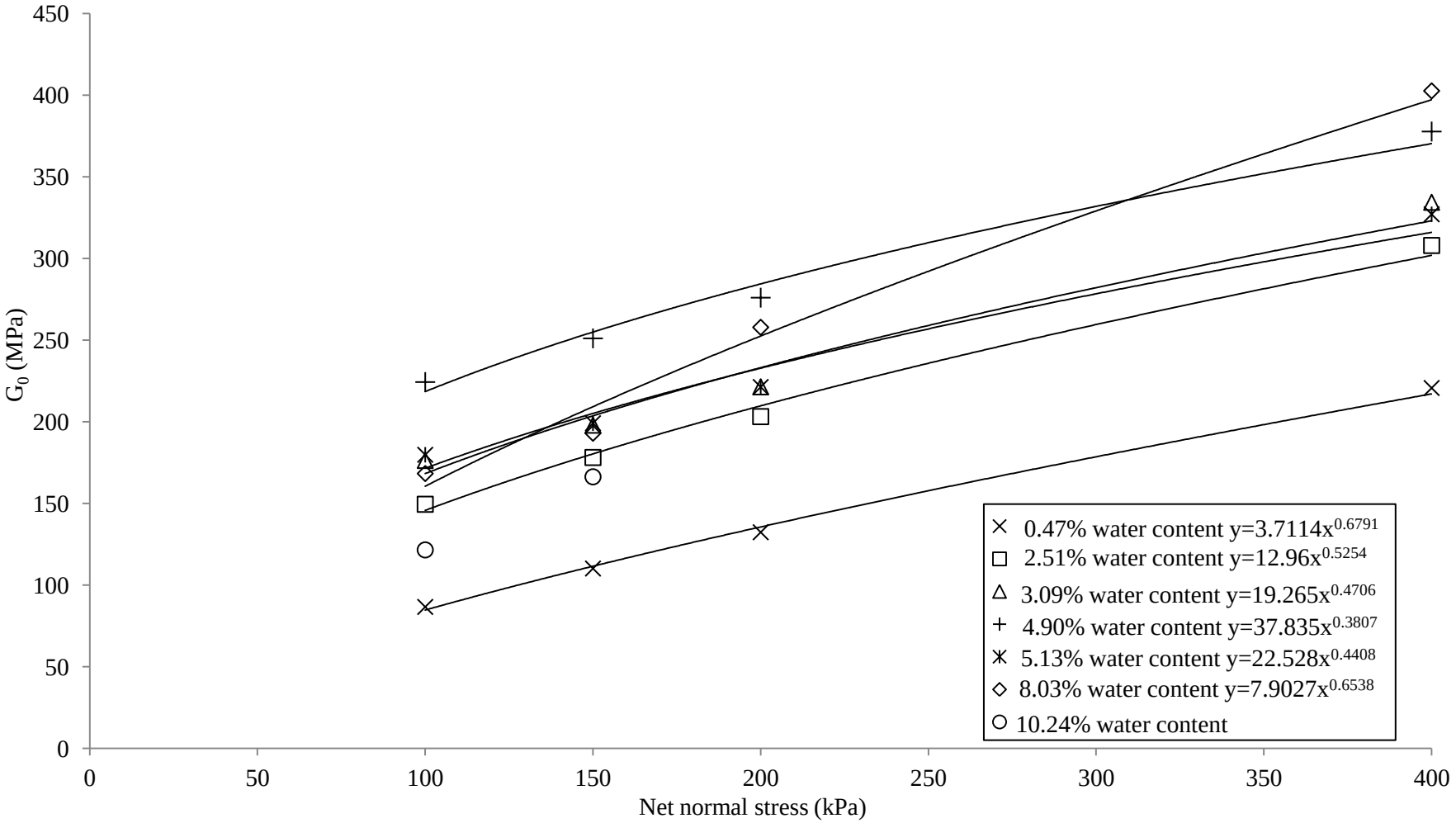

Figure 4.25: Shear modulus (G_0) variation with net normal stress between 100kPa and 400kPa for different water content specimens of material D.

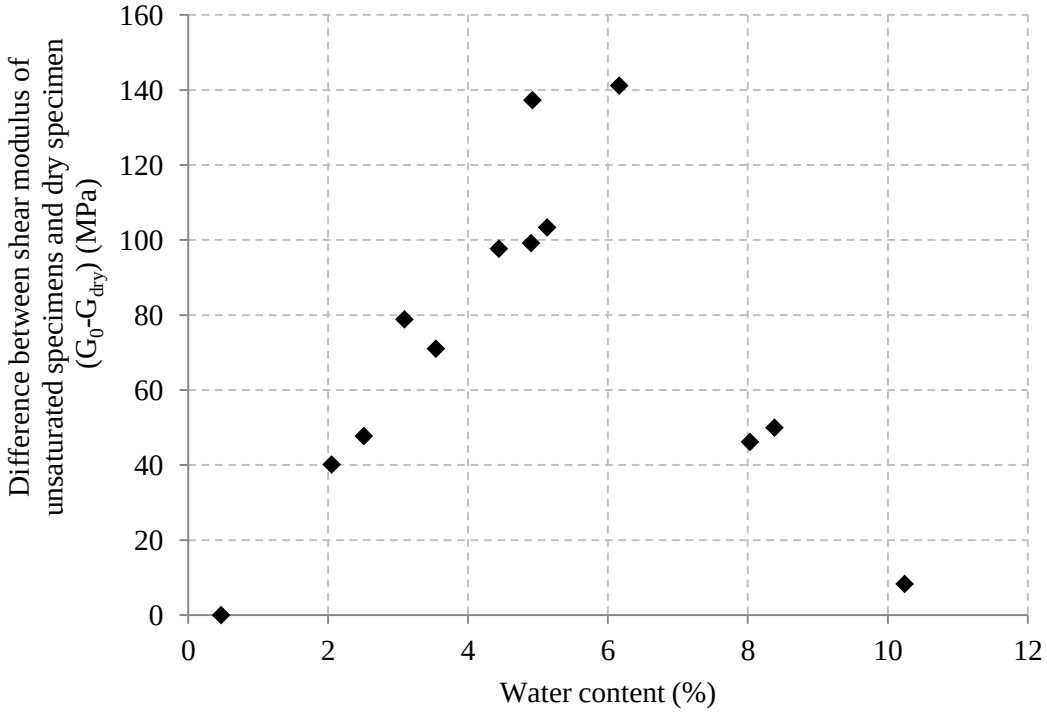

Figure 4.26: Shear modulus (G_0) variation compared with a dry specimen with water content for specimens of material D at 10kPa net normal stress.

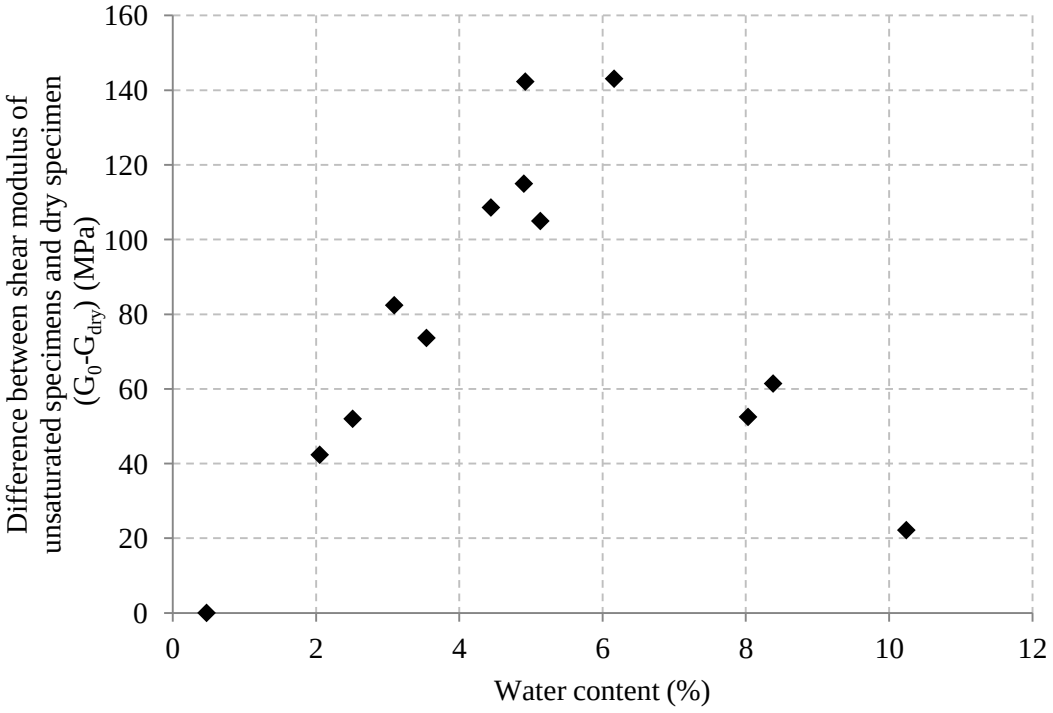

Figure 4.27: Shear modulus (G_0) variation compared with a dry specimen with water content for specimens of material D at 20kPa net normal stress.

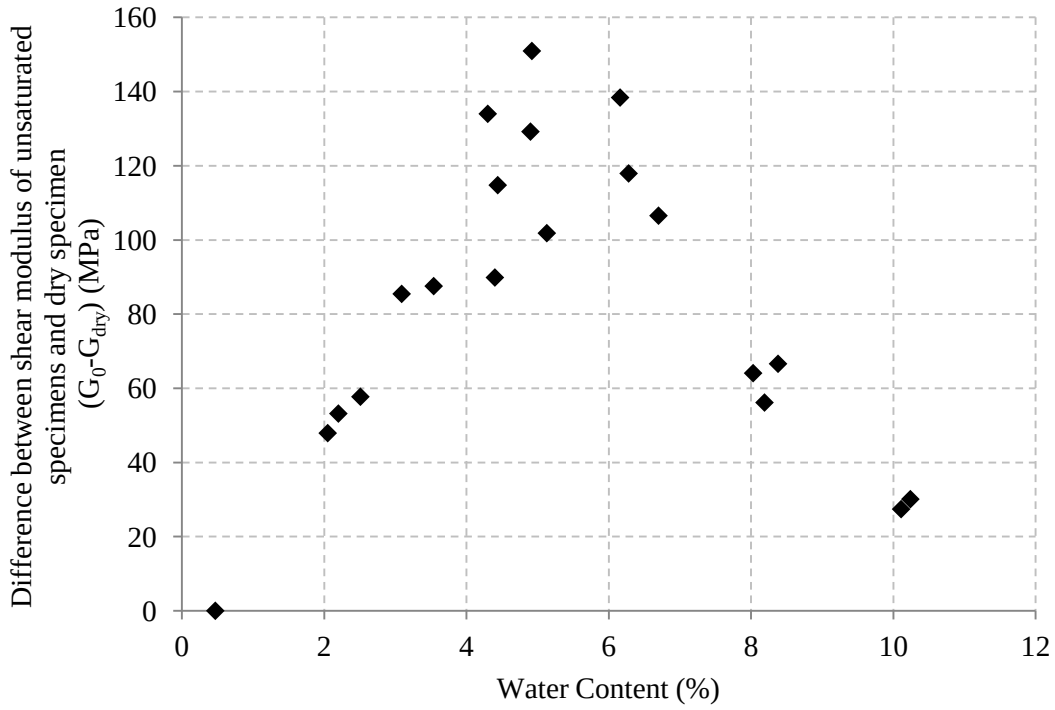

Figure 4.28: Shear modulus (G_0) variation compared with a dry specimen with water content for specimens of material D at 50kPa net normal stress.

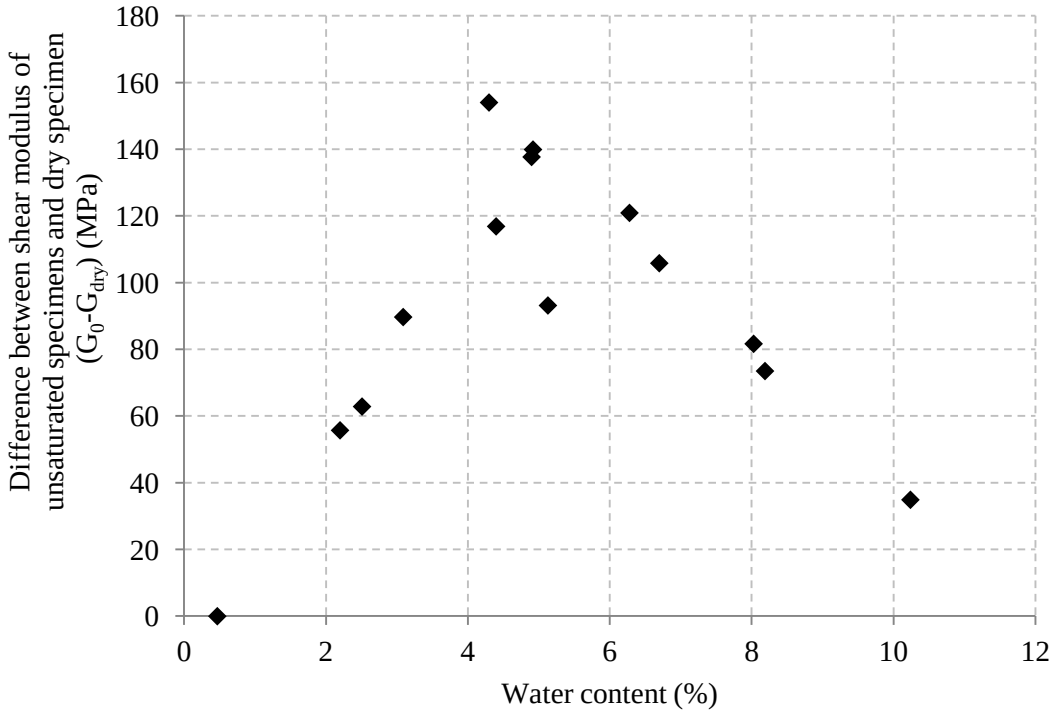

Figure 4.29: Shear modulus (G_0) variation compared with a dry specimen with water content for specimens of material D at 100kPa net normal stress.

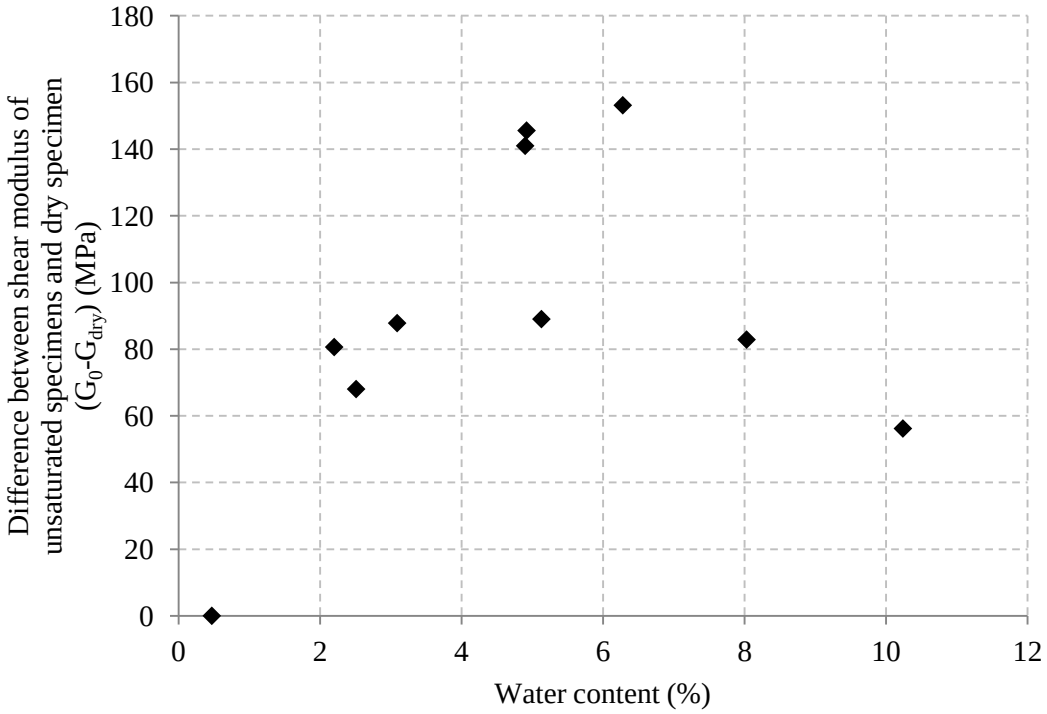

Figure 4.30: Shear modulus (G_0) variation compared with a dry specimen with water content for specimens of material D at 150kPa net normal stress.

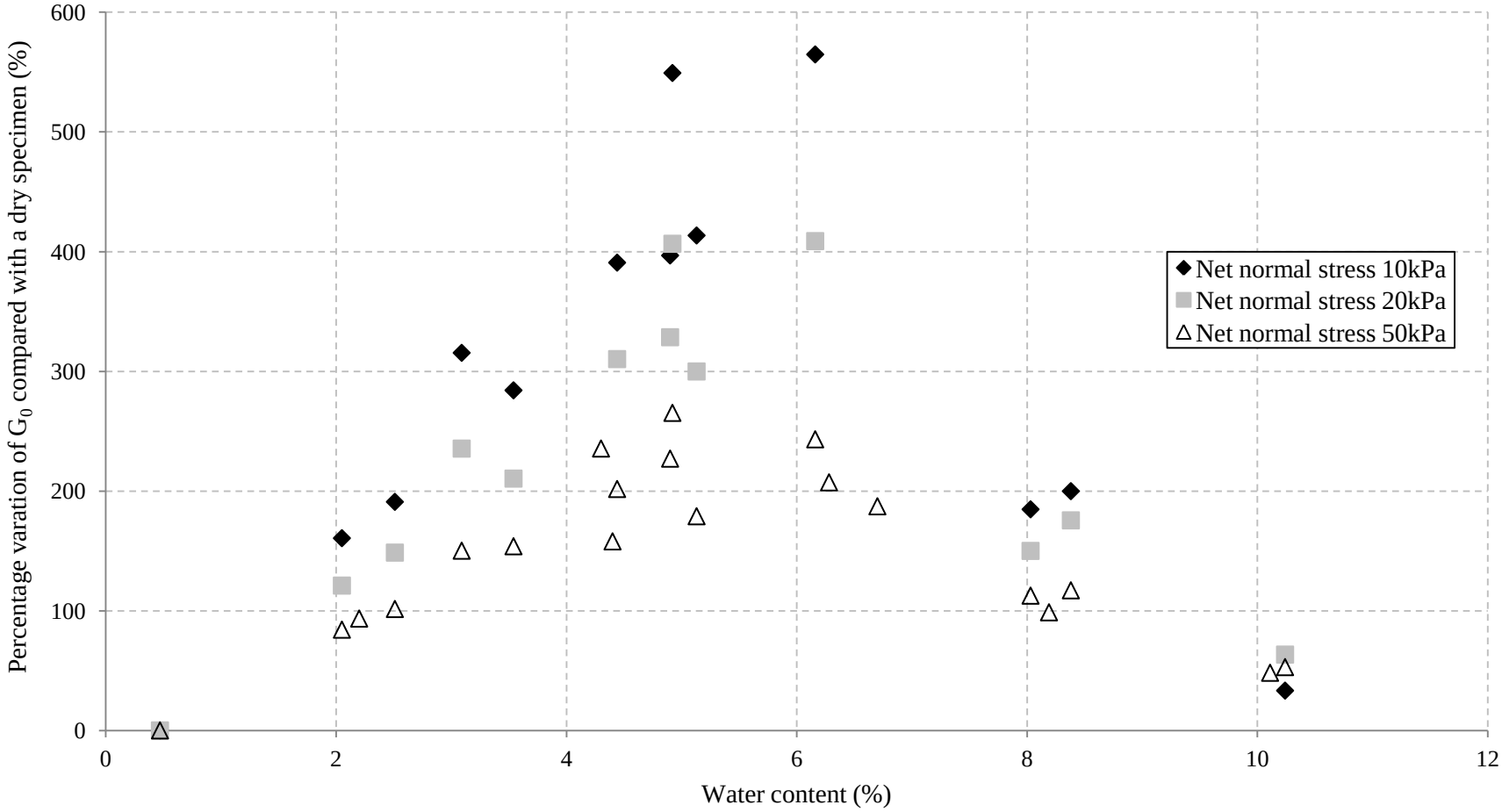

Figure 4.31: Percentage variation in shear modulus (G_0) compared with a dry specimen with water content for specimens of material D at 10kPa, 20kPa and 50kPa net normal stress.

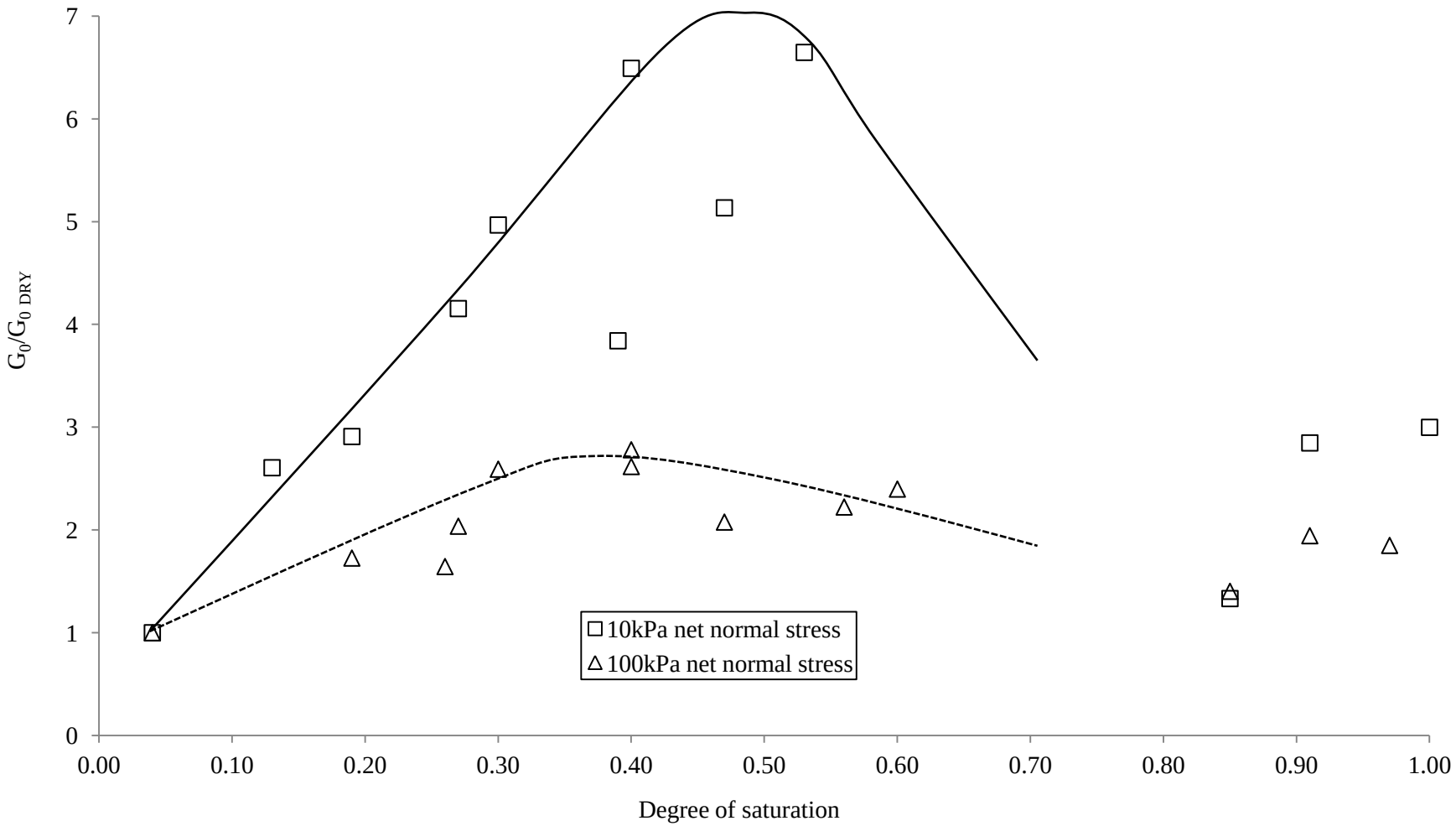

Figure 4.32: Influence of suction on the shear modulus (G_0) of material D at 10kPa and 100kPa net normal stress at various degrees of saturation with a trend line through each data set.

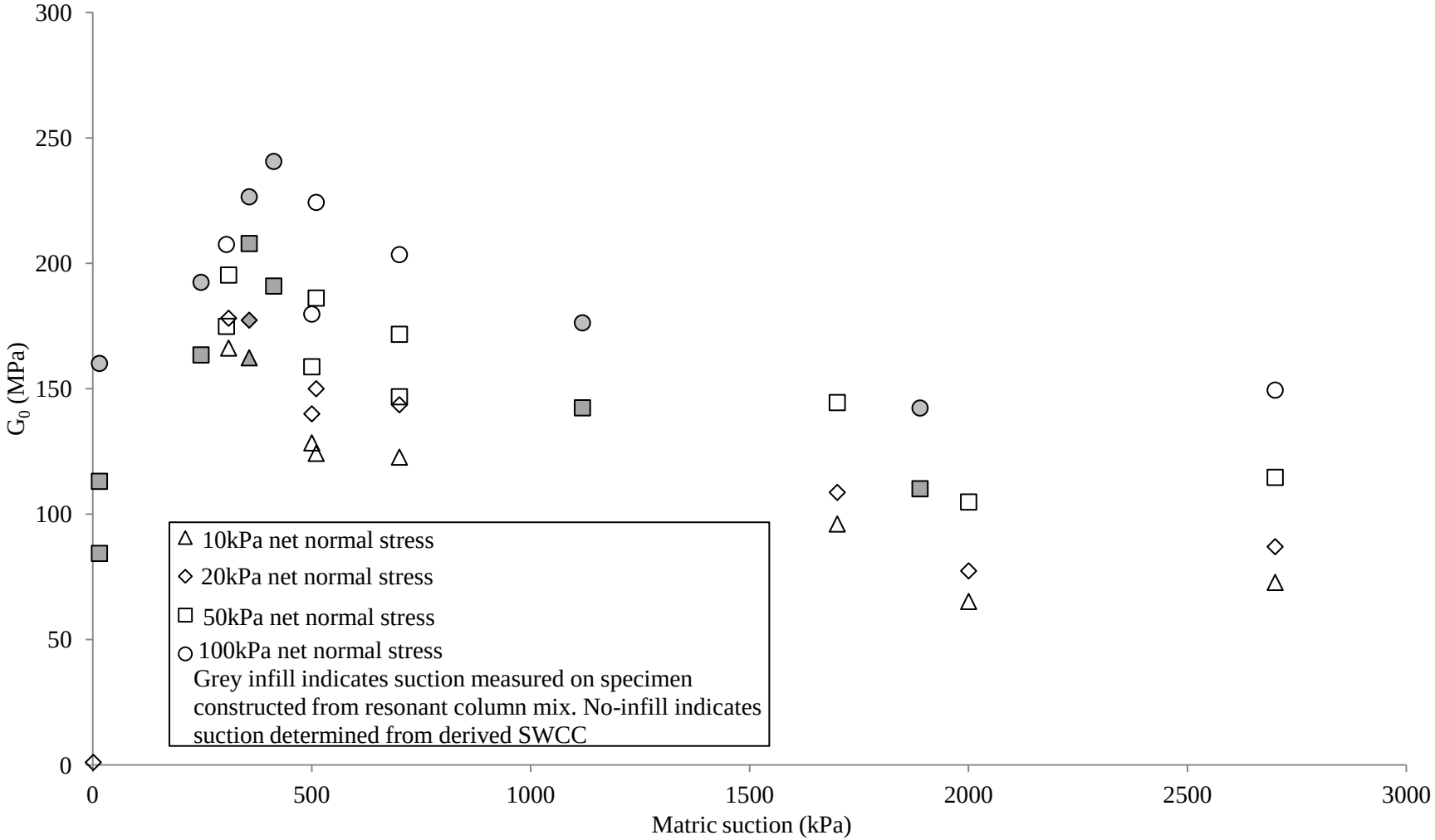

Figure 4.33: Shear modulus (G_0) with suction for specimens of material D at various net normal stresses.

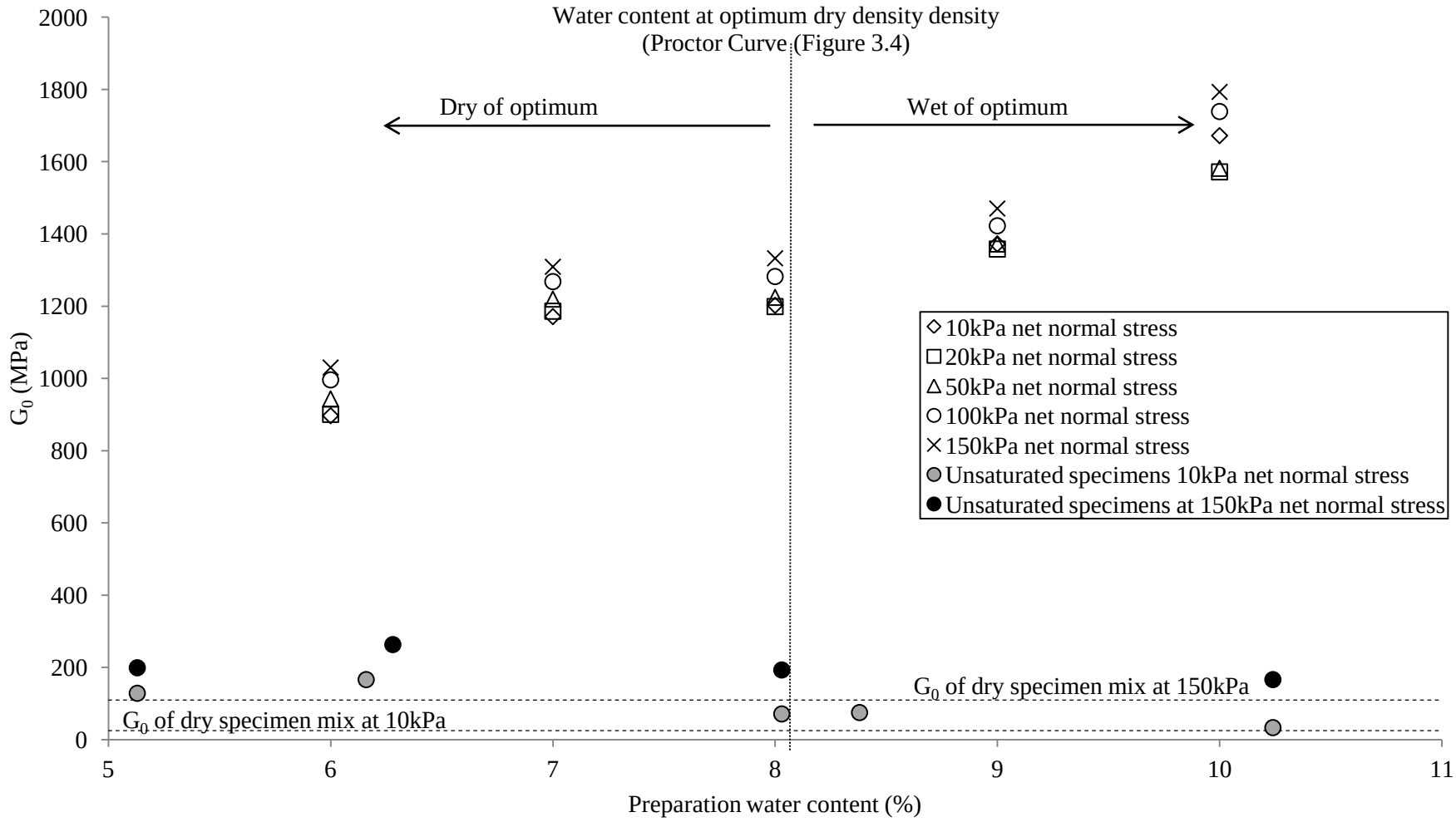

Figure 4.34: Shear modulus (G_0) of dried specimens of material D in relation to their preparation water content.

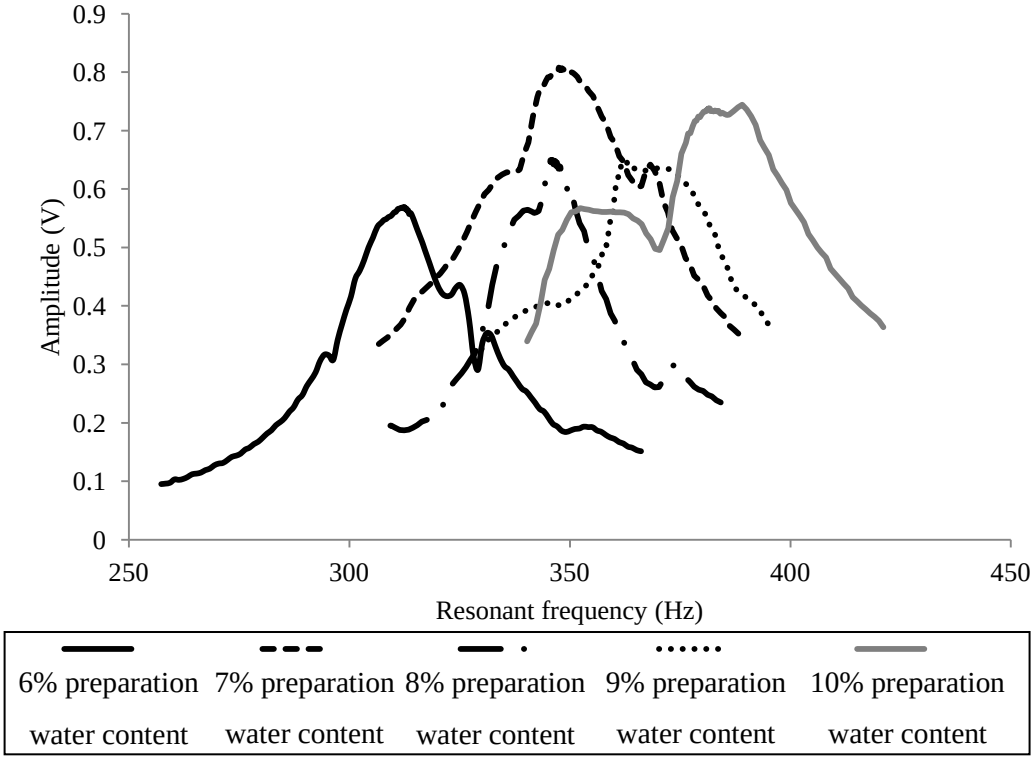

Figure 4.35: Resonant frequency of dried specimen's of material D at a strain of 0.0002% and net normal stress of 10kPa.

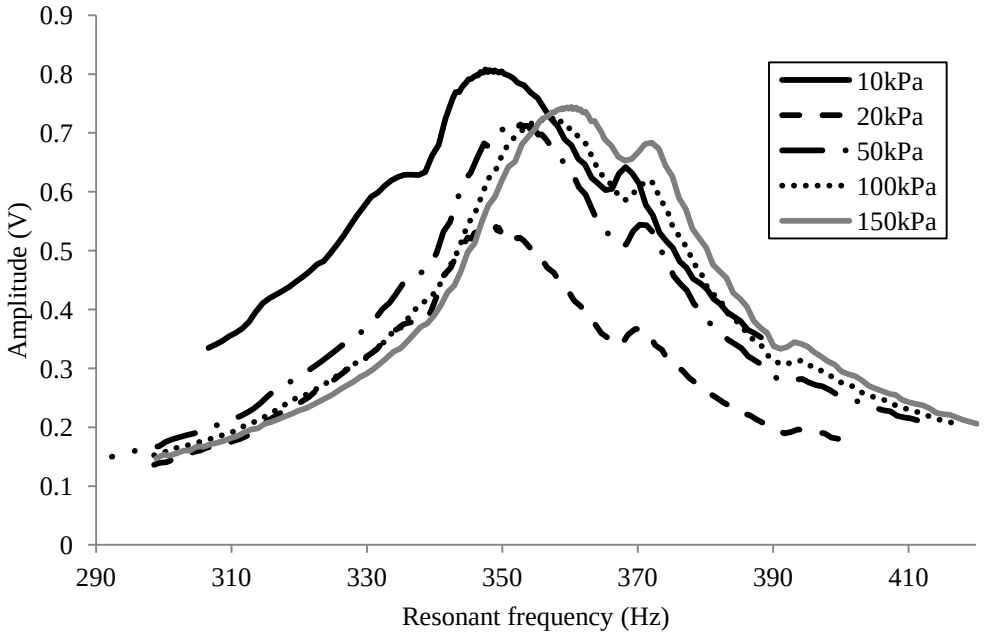

Figure 4.36: Resonant frequency at different net normal stress at a strain of 0.0002% for the dried specimen of material D prepared at 7% water content.

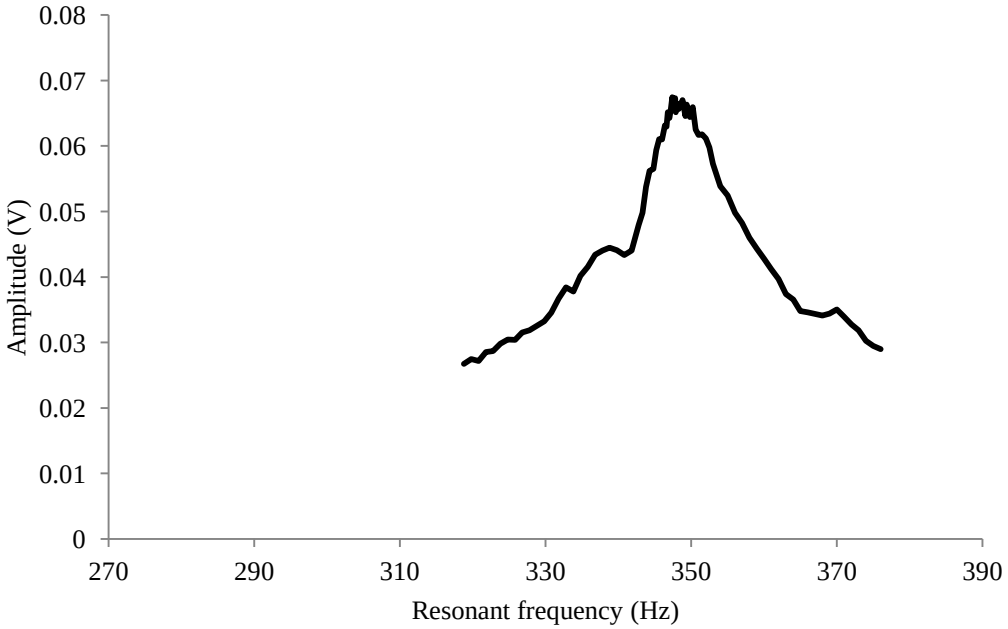

Figure 4.37: Spurious resonant frequency for the dried specimen of material D prepared at 10% water content at a strain of 0.00002%, net normal stress 10kPa.

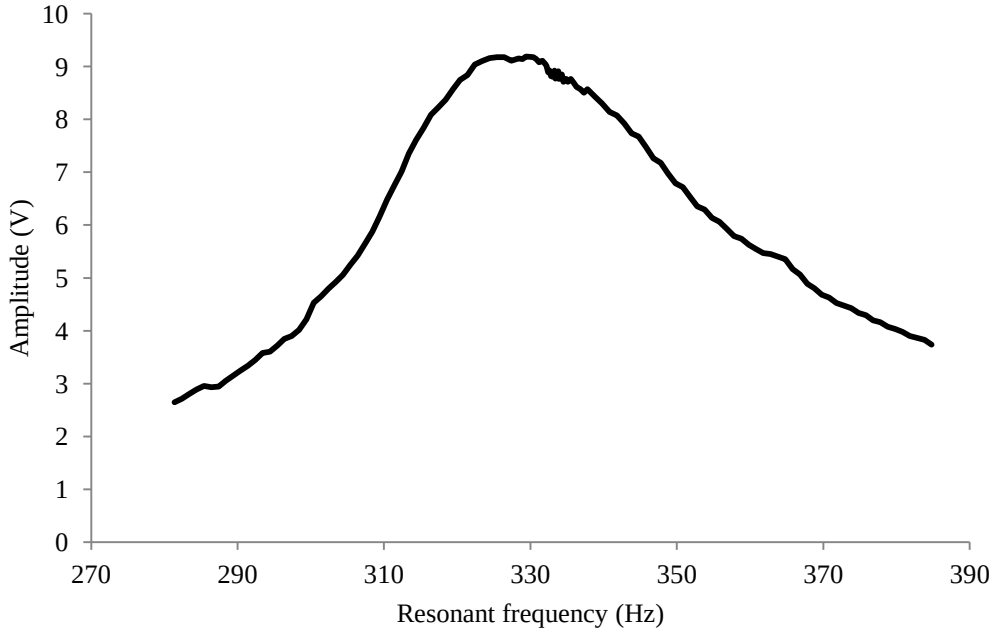

Figure 4.38: Spurious resonant frequency for the dried specimen of material D prepared at 10% water content at a strain of 0.003%, net normal stress 10kPa.

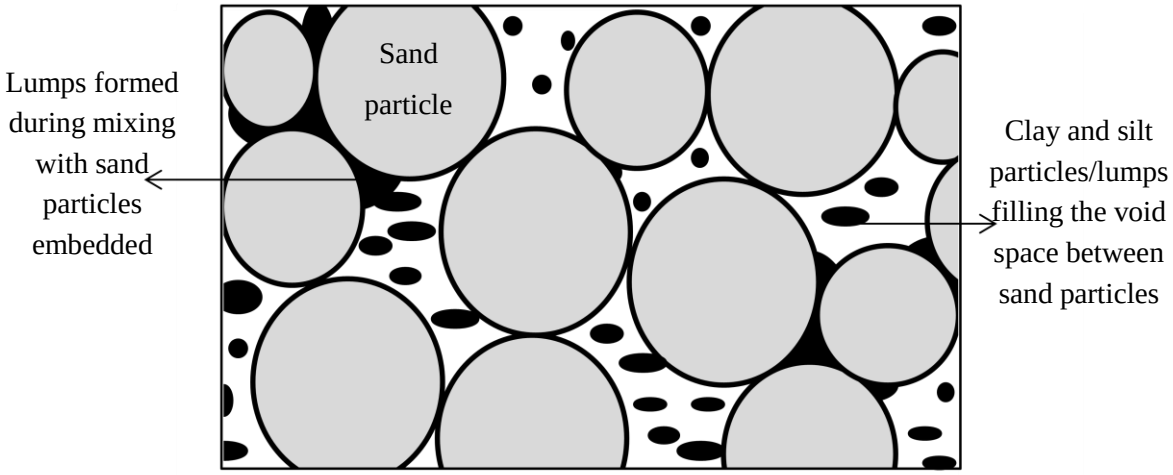

Visualisation of soil structure at low water contents where lumps are present in the material mix but with large amount of fines constituents in a powdered

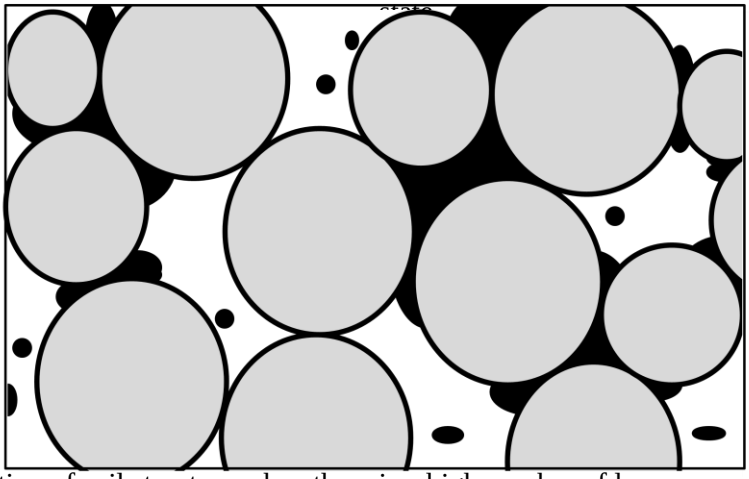

Visualisation of soil structure when there is a high number of lumps present in the material mix but a very small amount of fines constituents in a powdered state

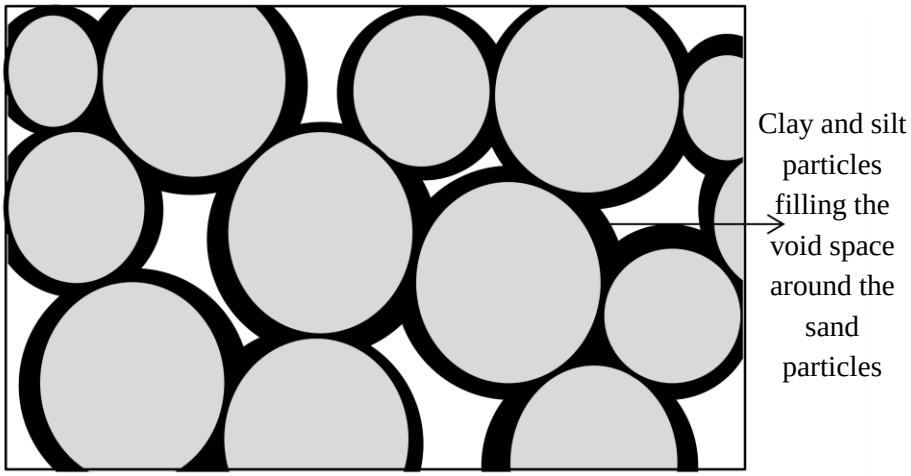

Visualisation of soil structure when are no lumps present in the material mix and the fully wetted fines constituents homogeneous throughout

Figure 4.39: Visualisation of particle arrangement following preparation at different water contents.

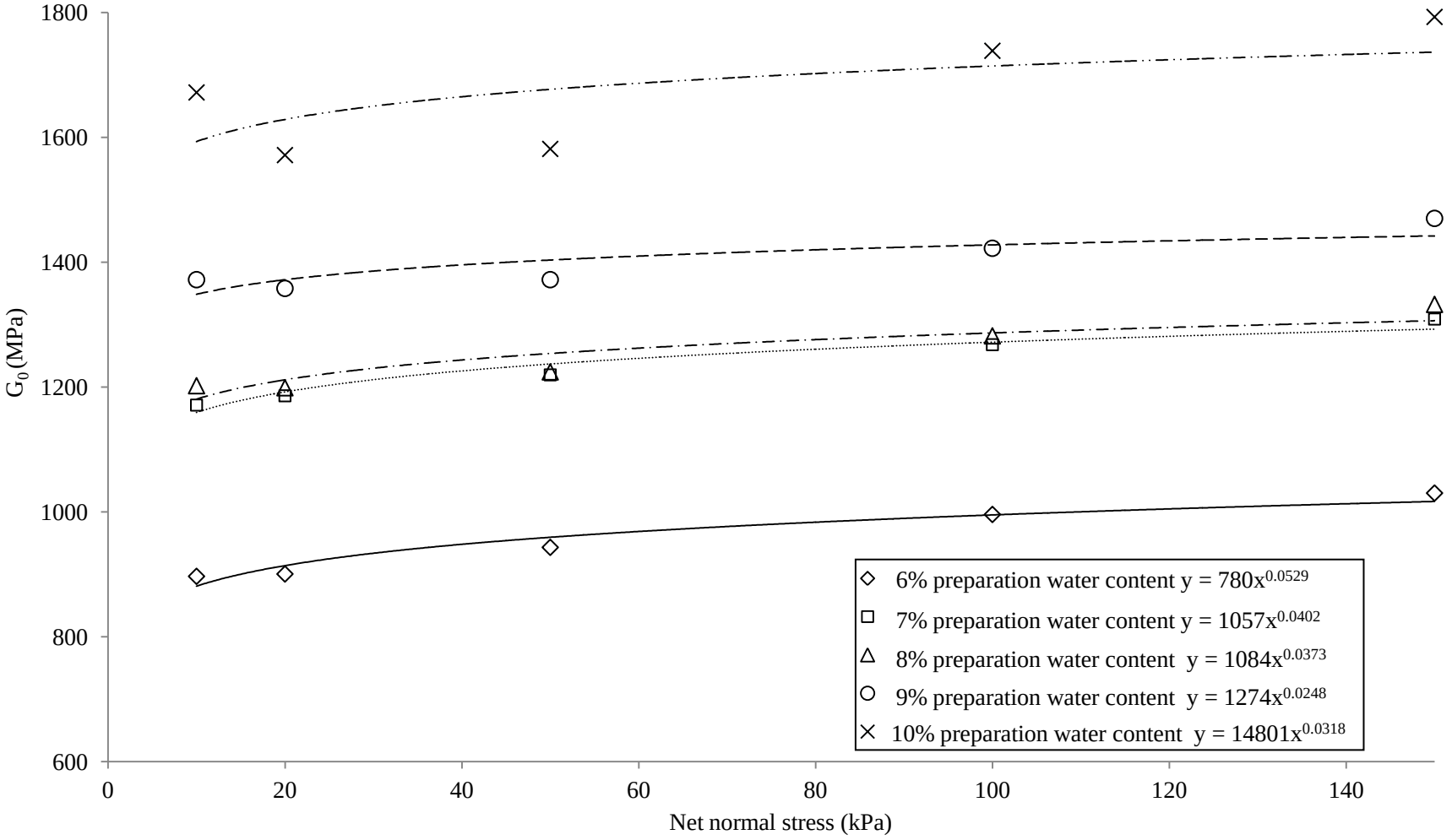

Figure 4.40: Variation of shear modulus (G_0) of the dried specimens of material D with net normal stress.

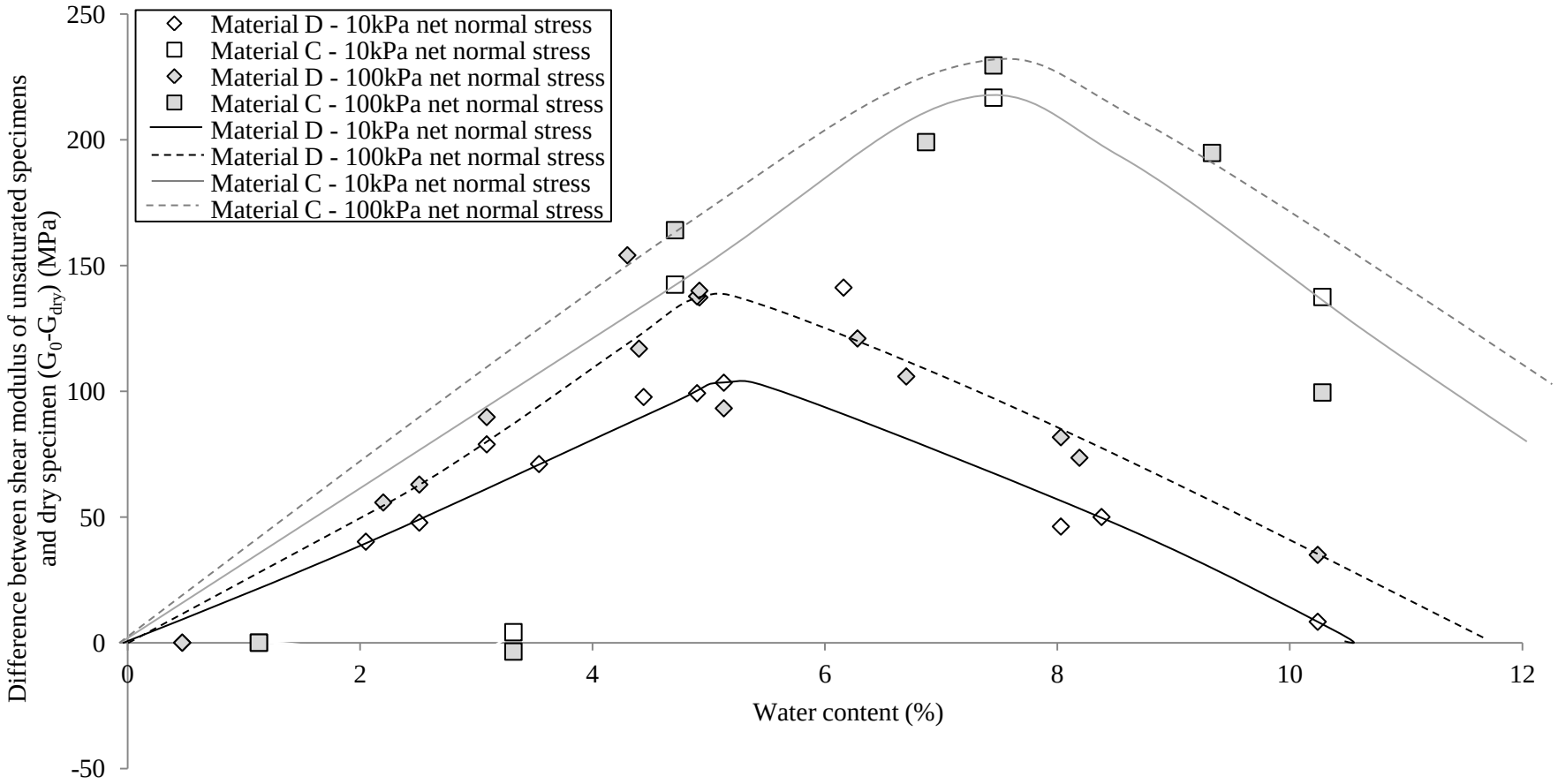

Figure 4.41: Shear modulus (G_0) variation compared with a dry specimen with water content for material C and D at net normal stresses of 10kPa and 100kPa with a trend line through each data set.

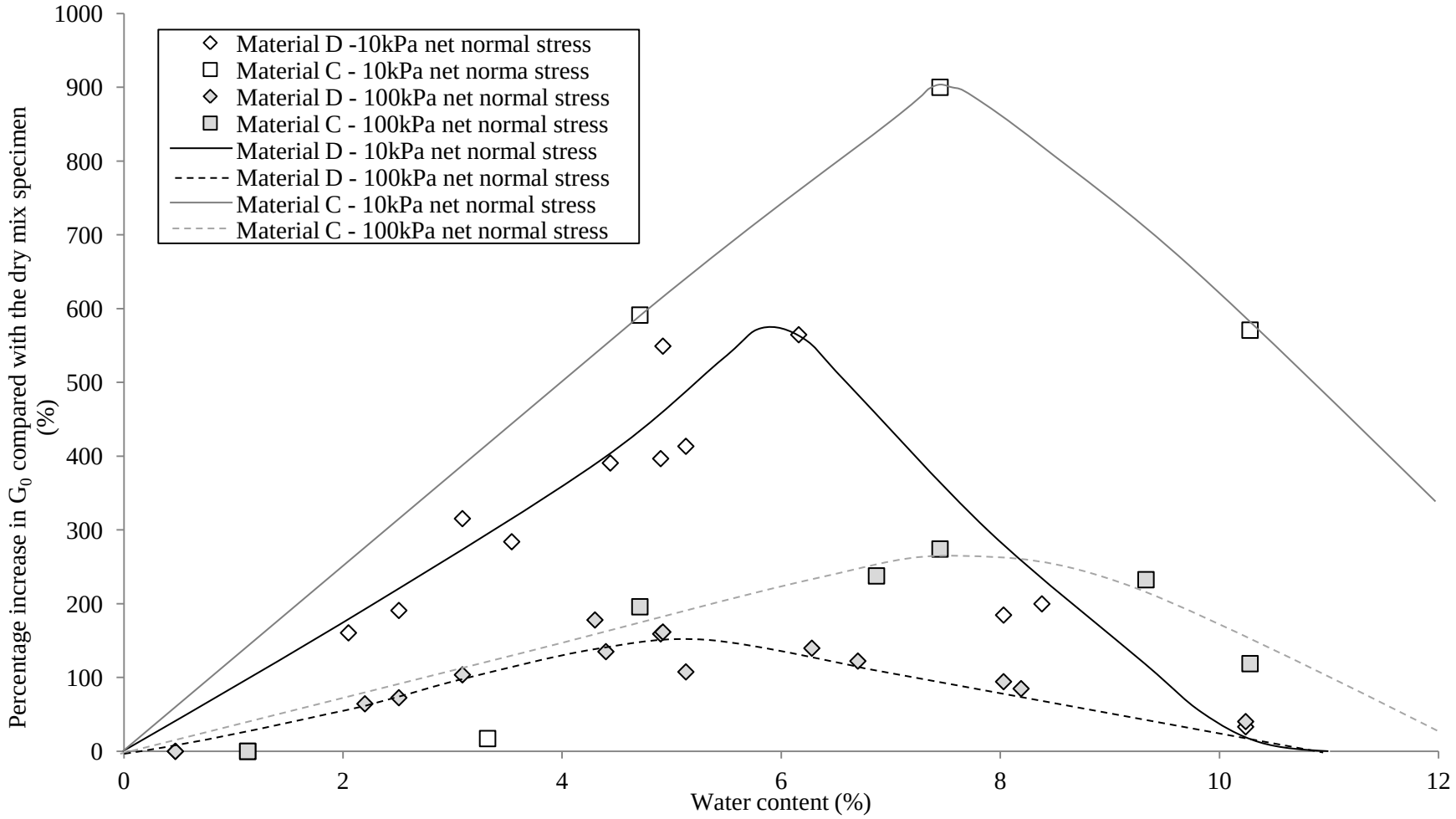

Figure 4.42: Percentage increase in shear modulus (G_0) compared with dry mix specimen versus water content for material C and D at net normal stresses of 10kPa and 100kPa with a trend line through each data set.

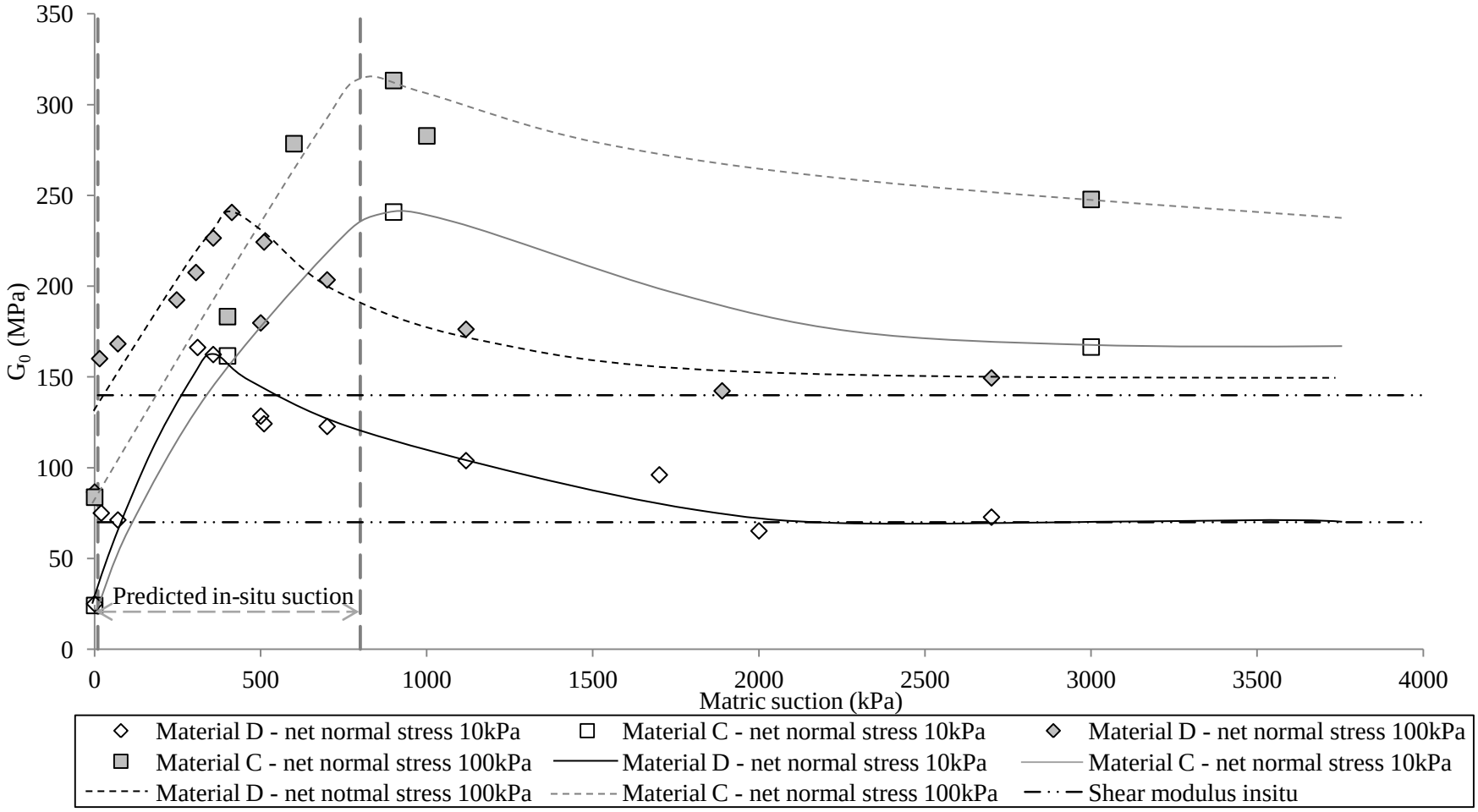

Figure 4.43: Shear modulus (G_0) versus water content for material C and D at net normal stresses of 10kPa and 100kPa with a trend line through each data set.

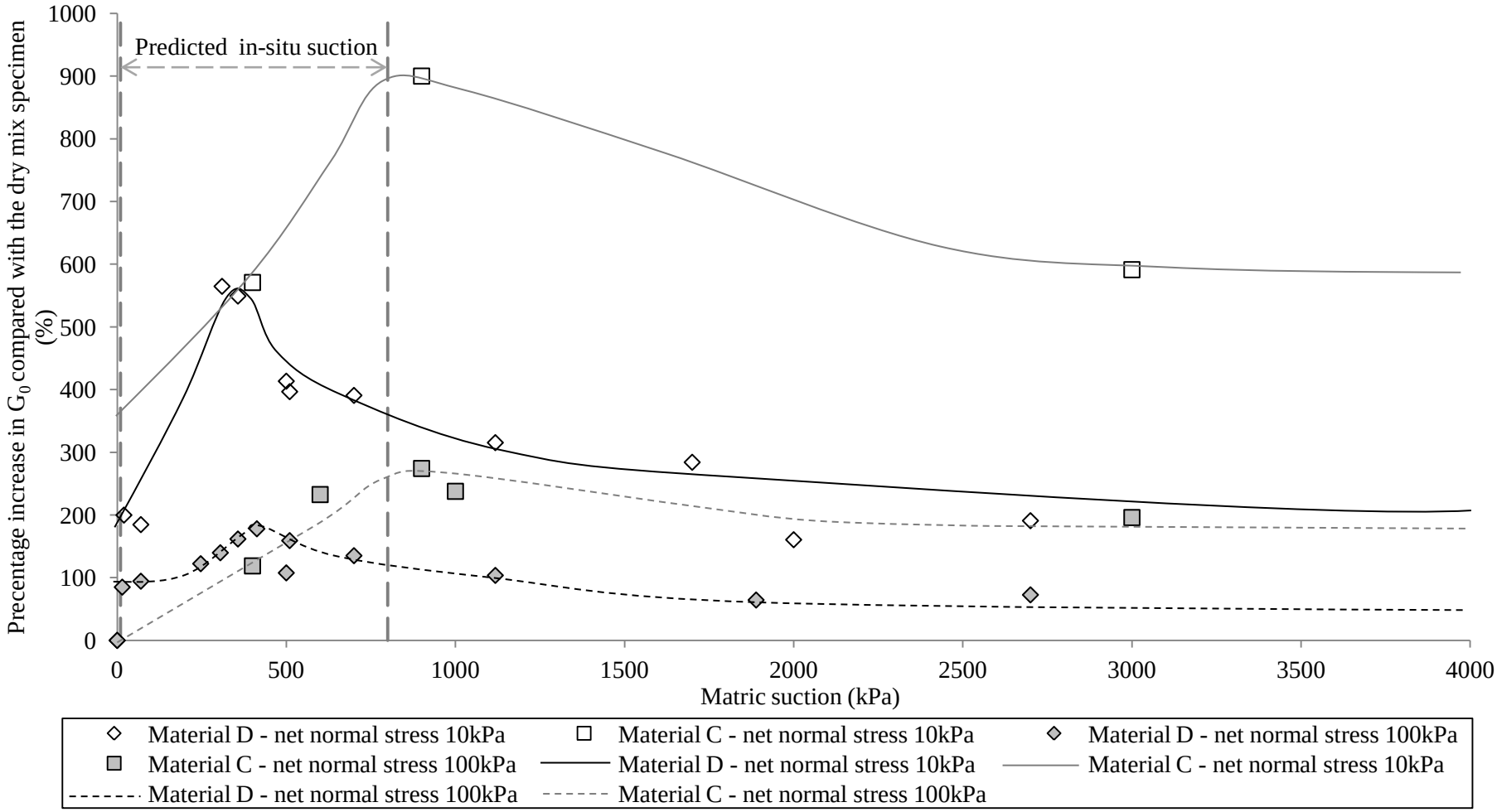

Figure 4.44: Percentage increase of shear modulus (G_0) due to suction for material C and D at a net normal stress of 10kPa and 100kPa with a trend line through each data set.

Chapter 5

Conclusions and Recommendations for Further Work

The differences between stiffness measured in the laboratory, and that back-calculated from field monitoring has suggested that suction may significantly increase stiffness of railway formation material.

Railway formations are generally compacted and founded at a shallow depth and are therefore usually unsaturated and subjected to low confining pressures. Prior to this research, a literature review showed that no assessment had been made of the degree of suction or the influence of seasonal changes on these materials. Furthermore, despite stiffness being a key design parameter, used to assess performance, it has rarely been measured, especially under cyclic conditions or in the small strain region.

This thesis, therefore, has reported both stiffness in the small strain region and the suction behaviour of four materials representative of railway formation under in-situ stress conditions.

5.1 Specimen preparation issues

Specimens were prepared, using a modification of the Proctor technique, from four material mixes comprising sand, silt and clay. Gräbe (2002) had previously identified these as representative of formation material on a heavy haul line in South Africa. Suction was varied by preparing each material at different pre-determined water contents.

Despite significant care in specimen preparation, heterogeneity between and within specimens occurred. CT-scanning showed that horizontal compaction caused vertical density variation within each layer, as well as throughout the specimen. Furthermore, the water contents of the specimens deviated from their target value, which, as the compactive effort was not altered, led to deviation from the target density. However, shear modulus measurements (conducted with the resonant column apparatus) showed good repeatability despite the density variation.

5.2 Determination of the soil water characteristic curves

Soil water characteristic curves were determined for each material using both the pressure plate apparatus and the filter paper technique. The pressure plate apparatus was used at suctions less than 1000kPa and the filter paper at suctions greater than 100kPa. Tensiometer measurements were also conducted on material D.

Suction changed significantly with water content throughout the range investigated, decreasing with increasing water content. The suction at any given water content was always greatest for the material with the largest clay content, reducing sequentially with clay content reduction.

Neither preparation density nor water content influenced the soil water characteristic curve once the suction of the test specimen was exceeded. Measurements in this region were predominately obtained using the pressure plate apparatus. Before the test specimen's suction was exceeded the curve was dependent on preparation water content, with the water content remaining constant despite different suctions being applied in the pressure plate. The air entry value of these materials was therefore dependent on preparation water content and density, and the pressure plate testing procedure.

The pressure plate procedure developed in this research involved removing specimens, which were not pre-saturated, at regular intervals; results compared favourably with the filter paper technique. For material D, at any given suction greater than 50kPa the water content of the tensiometer measurements was lower than both these techniques.

This difference between suction measured with the tensiometer and using other techniques agreed with the findings of other researchers. Tarantino et al.'s (2011) hypothesis suggests that part of this difference results from pressure elevation in the pressure plate altering the suction of these specimens. Differences in specimen fabric and experimental technique were

also likely contributory factors. For the filter paper technique, differences between calibration curves must also be considered.

5.3 Shear modulus measurements

The shear moduli of materials C and D were measured using a Stokoe resonant column apparatus and were therefore determined in the small strain region under cyclic conditions. For a given specimen, measurements were conducted at low net normal stresses, generally from 10kPa to 150kPa, to represent the low stress levels experienced by formations.

Three different testing regimes were undertaken. Firstly, measuring a specimen's shear modulus and its suction using the axis translation technique, in the resonant column apparatus. Experimental difficulties however, led to shear modulus and suction being measured separately. The second testing regime therefore only measured the shear modulus, of specimens prepared to the same dry density but at different water contents, at various net normal stresses in the resonant column apparatus. As a result of preparing these specimens at different water contents, particle arrangement within specimens may have differed, also influencing the measured shear modulus. In order to explore this possibility, a series of specimens were prepared at different water contents but to the same density, and tested once air dried.

Axis translation technique

Shear modulus remained constant under the application of a constant net normal stress (40kPa) whilst translating the magnitude of cell and air pressure applied, despite pore water pressure not translating by the same amount.

Varying the net total stress then applied to the specimen, led to an increase in shear modulus with an increase in net normal stress and a reduction with a decrease in net normal stress. This suggested the shear modulus readings were correct, and the difficulty lay with measuring suction through correctly measuring the pore water pressure. The axis translation technique therefore has negligible effect on a specimen's structure or its shear modulus behaviour.

Reducing the specimen's suction, by saturating the specimen, and testing under a constant net normal stress led to a reduction of over twenty five percent in the shear modulus. Suction therefore influences shear modulus.

Specimens tested at preparation water content

Net normal stress was applied by raising the cell pressure to the required value whilst the pore air line was vented to atmosphere, with the pore air pressure assumed zero. This assumption is only valid when the specimen's air phase is continuous, which is not the case for specimens which are saturated or near saturation. Here, an increase in the cell pressure causes the pore air pressure to increase and the measured shear modulus to relate to a lower net normal stress than assumed. This was hypothesised as the reason why there was a localised minimum in shear modulus, in relation to degree of saturation, for specimens close to saturation.

Shear modulus in the small strain region was uniquely dependent on specimen water content, given constant density. It was greater for unsaturated specimens than for a dry mix specimen of the same material. For material D, the maximum shear modulus was over five times greater than that of the dry mix specimen at 10kPa net normal stress. Shear modulus was therefore significantly influenced by suction. However, the suction/shear modulus relationship was complex. The shear modulus increased with increasing water content (suction) until an optimum, and then decreased.

No asymptotic value of shear modulus was reached as suction increased and water content reduced, in line with previous resonant column findings using the axis translation technique to control suction. This is due to the limited range of suctions they investigated, with the reduction in shear modulus only seen at extremely high suctions as the area of the contact over which the normal force acts, and possible number of contacts affected by menisci water distributed throughout the soil reduce.

The shear modulus was similar for specimens compacted at very low and high water contents. Although greater than for the dry mix specimen, it was still significantly lower than in specimens prepared at water contents near the maximum shear modulus. Therefore, very large and small suctions do not significantly increase shear modulus.

Shear modulus increased with net normal stress. However, for material D at a net normal stress of 100kPa, the maximum shear modulus was almost twice that of the dry mix specimen. Thus, suction's contribution to shear modulus reduced with increasing confining stress. As confining stresses increase with formation depth, whilst stresses from loading reduce, the maximum increase in shear modulus due to suction coincides with the pressures where increases in shear modulus are most beneficial to the performance.

Material C, which had a higher clay content than material D, (24% compared with 11%), showed the same overall suction/shear modulus behavioural pattern. However, the optimum water content at which the maximum shear modulus occurred increased. The shear modulus due to suction was greater at any given water content, regardless of net normal stress. It was postulated that the shear modulus was greater than material D as the number of clay lumps, hence regions of sand particles embedded by clay increased.

Air-dried specimens

In order to explore the possibility that the particle arrangement within specimens may have differed as a result of preparation at different water contents, a series of specimens of material D were prepared, at different water contents but to the same density, and air dried. Although they reached a constant weight they were not completely dry, with water contents between 0.47% and 1.81%.

The shear moduli of the air dried specimens differed. This was smallest for the specimens dried from the lowest preparation water content, then increased with increasing preparation water content, plateaued either side of the Proctor optimum, and then continued to increase with increasing preparation water content. Particle arrangement, therefore, cannot be discounted as influencing the suction/shear modulus relationship.

The significantly higher shear moduli of the air dried specimens, compared to the dry and unsaturated specimens, arises due to the development or increase in the suction in the clay lumps embedding the sand particles. Additionally, if the water content is sufficient in the void space the clay particles also re-distribute with the menisci-water during drying, retreating around the sand particles, and acting as buttresses preventing deformation.

5.4 Relevance for practice

This research has illustrated that suction can significantly influence the small strain shear modulus of railway formations. A review of the literature suggested that the likely suction, and variations due to climatic conditions, are likely to produce significant changes in shear modulus.

The implication of not considering these changes, especially as changes in suctions are unlikely to be the same throughout the track length, is deterioration in ride quality, or in the worst case loss of structural integrity, as variations in shear modulus could lead to excessive deformation or differential settlement under loading. Saturation of the formation, which

could arise from the more intense rainfall predicted in the winter months, could also lead to deterioration through mud pumping (Selig and Waters, 1994).

The suction/shear modulus relationship is dependent upon material composition, therefore a formation's material properties must be considered. It is advisable that materials are specified which are less susceptible to large shear modulus changes due to variation in suction.

5.5 Suggestions for future work

It is recommended, based on the work presented in this thesis, that the following is undertaken to build upon the work presented in this thesis:

The shear modulus at various suctions was only measured for two different materials in this research. Therefore, to confirm the hypothesis of the influence of a materials composition on the suction/shear modulus relationship, resonant column testing as conducted in this research should now be undertaken on materials A and/or B.

As the suction/shear modulus relationship presented was found to also be influenced by particle arrangement, suction-controlled testing on specimens prepared at the in-situ preparation state for each material should be conducted.

The dried specimen's results led to the hypothesis of different particle arrangements between specimens prepared at different water contents, and that during drying if the preparation water content was sufficient to encompass the fines in the void space, that during drying they retreated with the menisci-water buttressing around the sand particles. Therefore, visual examination and mercury intrusion porosimetry should be undertaken to verify the particle arrangement when constructed and once dried.

Measuring a specimen's suction using the axis translation technique in the resonant column apparatus was not resolved in this research. Therefore, it should be investigated further.

To-date suctions have not been measured in railway formations. This needs to be conducted to verify the magnitude and variation in suction postulated in this research.

References

Adwan Chemicals. (2011). Silica Flour [Online], Available from: http://www.adwanchem.com/Silica_Flour.htm, March 2010.

Aitchison, G. D. (1961). Relationship of moisture and effective stress function in unsaturated soils. *Pore pressure and suction in soils conf. organized by the British National Soc. of the Int. Soc. of Soil Mechanics and Foundation Engineering, London,* 47-65.

Aitchison, G. D., Russam, K., Richards, B. G., Donaldson, G. W., Williams, A. B. & Kassiff, G. (1965). Statement of the review panel: Engineering concepts of moisture equilbria and moisture changes in soils. *A symposium in print moisture equilibria and moisture changes in soils beneath covered areas., Australia,* 7-21.

Al-Khafaf, S. & Hanks, R. J. (1974). Evaluation of the filter paper method for estimating soil water potential. *Soil Science,* 117 (4): 194-199.

Allberry, E. C. (1950). On the capillary forces in an idealized soil. *Journal of Agricultural Science,* 40 (1-2): 134-142.

Anderson, D. G. & Stokoe II, K. H. (1977). Shear Modulus: A time-dependent soil property *Dynamic Geotechnical Testing ASTM STP 654.* 66-90.

Ashmawy, A. K. & Drnevich, V. P. (1994). A general dynamic model for the Resonant Column/Quasi-Static Torsional Shear Apparatus. *Geotechnical Testing Journal* 17 (3): 337-347.

ASTM-D4015 (1995). Standard test methods for modulus and damping of soils by the resonant-column method, *ASTM,* Philadelphia.

ASTM-D5298-94 (1994). Standard test method for measurement of soil potential (suction) using filter paper: In 1994 annual book of ASTM standards, *ASTM,* Philadelphia.

ASTM-D6836-02 (2003). Standard test methods for determination of the soil water characteristic curve for desorption using a hanging column, pressure extractor, chilled mirror hygrometer and/or centrifuge, *ASTM,* Philadelphia.

Atkinson, J. H. & Sallfors, G. (1991). Experimental determination of stress-strain-time characteristics in laboratory and in situ tests. General report to session 1. *Proc. 10th Eur. Conf. Soil Mech. Found. Engineering,* 3, 915-956.

Avramidis, A. S. & Saxena, S. K. (1990). The modified "stiffened" drnevich resonant column apparatus. *Japanese Society of Soil Mechanics and Foundation Engineering,* 30 (3): 53-68.

Barden, L., McGown, A. & Collins, K. (1973). The collapse mechanism in partly saturated soil. *Engineering Geology,* 7 (1): 49-60.

Bicalho, K. V., Marinho, F. A. M., Fleureau, J. M. & Gomes Correia, A. (2011). Evaluation of filter paper calibrations for indirect determination of soil suctions of unsaturated soils. *Proc. of 5th Int. Conf. on Unsaturated Soils, Barcelona,* 1, 609-613.

Bicalho, K. V., Nunes, G. W., Marinho, F. A. M., Fleureau, J. M., Gomes Correia, A. & Ferreira, S. (2010). Evaluation of filter paper calibrations for laboratory estimating of soil suctions. *Proc. of the 4th Asia Pacific Conf. on Unsaturated Soils, Newcastle, Australia,* 1, 215-219.

Biglari, M., D'Onfrio, A., Mancuso, C., Jafri, M. K. & Shafiee, A. (2011). Stress path effects on shear stiffness, damping ratio and volumetric behaviour of normally consolidated unsaturated compacted clay. *Proc. of 5th Int. Conf on Unsaturated Soils, Barcelona* 1, 199-204.

Biglari, M., d'Onofrio, A., Mancuso, C., Shafiee, A. & Jafari, M. K. (2010). Small strain behaviour of unsaturated plastic material in suction control RCTS test. *Proc. of the 4th Asia Pacific Conf. on Unsaturated Soils, Newcastle, Australia,* 1, 33-38.

Bishop, A. W. (1959). The principle of effective stress. *Teknisk ukeblad,* 106 (39): 859-863.

Bishop, A. W. & Blight, G. E. (1963). Some aspects of effective stress in saturated and partly saturated soils. *Géotechnique,* 13 (3): 177-197.

Bittelli, M. & Flury, M. (2009). Errors in water retention curves determined with pressure plates. *Soil Science Soc. of America Journal,* 73 (5): 1453-1460.

Blight, G. E. (1965). A Study of Effective Stresses for Volume Change. IN Aitchison, G. D. (Ed.) *A symposium in print: Moisture equilibria and moisture changes in soils beneath covered areas.* Australia: Butterworth, 259-269.

Blight, G. E. & Harrison, B. A. (2000). A comparison of in-situ soil suction measurements. *Unsaturated Soils for Asia, Singapore,* 281-285.

Bocking, K. A. & Fredlund, D. G. (1980). Limitations of the axis-translation technique. *Proc. of 4th Int. Conf. on Expansive Soils, Denver, Colorado,* 1, 117-135.

Brown, S. F. (1996). Soil mechanics in pavement engineering. *Géotechnique,* 46 (3): 383-426.

BS1377-2 (1990). Methods of test for soils for civil engineering purposes Part 2: Classification tests, *British Standard Institution,* London.

BS1377-2:1990 (1990). Methods of test for soils for civil engineering purposes Part 2: Classification tests, *British Standard Institution,* London.

BS1377-4 (1990). Methods of test for soils for civil engineering purposes - Part 4: Compaction-related tests, *British Standard Institution,* London.

BS13286-2 (2004). Unbound and hydraulically bound mixtures, *British Standard Institution,* London.

Bui, M. T., (2009). Influence of some particle characteristics on the small strain response of granular materials, *PhD Thesis,* Civil Engineering, University of Southampton.

Bulut, R. & Leong, E. C. (2007). Indirect measurement of suction. *Journal of Geotechnical and Geological Engineering,* 26 (6): 633-644.

Bulut, R. & Wray, W. K. (2005). Free energy of water-suction-in filter papers. *Geotechnical Testing Journal,* 28 (4): 355-364.

Burland, J. B. (1964). Effective stresses in partially saturated soils discussion of "some aspects of effective stress in saturated and partly saturated soils " by G.E.Bight and A.W. Bishop. *Géotechnique,* 14 (1): 63-68.

Burrow, M. P. N., Bowness, D. & Ghataora, G. S. (2007). A comparison of railway track foundation design methods. *Proc. IMechE Part F. J. Rail and Rapid Transit,* 221 (1): 1-12.

Cascante, G., (1996). Propagation of mechanical waves in particulate materials, *PhD Thesis,* University of Waterloo.

Casini, F., Desideri, A., Mancuso, C. & Vassallo, R. (2008). Application to a compacted soil of a Cam Clay model extended to unsaturated conditions. *Proc. of 1st European Conf. on Unsaturated Soils, Durham,* 609-615.

Chandler, R. J., Crilly, M. S. & Montogomery-Smith, G. (1992). A low-cost method of assessing clay desiccation for low-rise building. *Proc. Institution of Civil Engineers Geotechnical Engineering (Civil Engineering),* 92 (2): 82-89.

Chandler, R. J. & Gutierrez, C. I. (1986). The filter-paper method of suction measurement - Technical note. *Géotechnique,* 36 (2): 265-268.

Cho, G. C. & Santamarina, J. C. (2001). Unsaturated particulate materials - particle level studies. *Journal of Geotechnical and Geoenvironmental Engineering,* 127 (1): 84-96.

Chung, R. M., Yokel, F. Y. & Drnevich, V. P. (1984). Evaluation of dynamic properties of sands by resonant column testing. *Geotechnical Testing Journal,* 7 (2): 60-69.

Clayton, C. R. I. (2011). Stiffness at small strain: research and practice. *Géotechnique,* 61 (1): 5-37.

Clayton, C. R. I., Gräbe, P. J. & Powrie, W. (2006). Ground investigation and monitoring for track formation problems. *Railway Foundations Proc. of 1st Int. Conf. on Railway Foundations.* Birmingham, University of Birmingham Press.

Clayton, C. R. I., Matthews, M. C. & Simons, N. E. (1995). *Site Investigation,* Oxford, Blackwell Science.

Clayton, C. R. I., Priest, J. A., Bui, M. T., Zervos, A. & Kim, S. G. (2009). The Stoke resonant column apparatus: Effects of stiffness, mass and specimen fixity. *Géotechnique,* 59 (5): 429-437.

Clayton, C. R. I., Priest, J. A. & Rees, E. V. L. (2010). The effects of hydrate cement on the stiffness of some sands. *Géotechnique,* 60 (6): 435-445.

Clayton, C. R. I., Theron, M. & Vermeulen, N. J. (2004). The effect of particle shape on the behaviour of gold tailings. *Advances in geotechnical engineering: The Skempton conference, London,* 393-404.

Croney, D. (1952). The movement and distribution of water in soils. *Géotechnique,* 3 (1): 1-16.

D'Onza, F., D'Onofrio, A. & Mancuso, C. (2008). Effects of unsaturated soil state on the local seismic response of soil deposits. *Proc. of 1st European Conf. on Unsaturated Soils, Durham,* 531-536.

DeBruijn, C. M. A. (1965). Some observations on soil moisture conditions beneath and adjacent to tarred roads and other surface treatments in South Africa. IN Aitchison, G. D. (Ed.) *Moisture Equilibria and moisture changes in soils beneath covered areas.* Australia: Butterworths, 135-142.

Delage, P., Audiguier, M., Cui, Y.-J. & Howat, M. B. (1996). Microstructure of a compacted silt. *Canadian Geotechnical Journal,* 33 (1): 150-158.

Delage, P., Romero, E. & Tarantino, A. (2008). Recent developments in techniques of controlling and measuring suction in unsaturated soils. *Proc. of 1st European Conf. on Unsaturated Soils, Durham,* 33-52.

Drnevich, V. P. (1978). Resonant column testing - problems and solutions. *Dynamic Geotechnical Testing, ASTM STP 654.* 384-398.

Dyvik, R. (2010). Understanding the measurement of soil dynamic properties [Online], Available from: https://workspace.imperial.ac.uk/geotechnics/public/2.%20R%20Dyvik's%20talk%2017%20March%202010.pdf, 2011

Fisher, R. A. (1926). On the capillary forces in an ideal soil correction of formulae given by W.B.Haines. *Journal of Agricultural Science* 16 (3): 492-505.

Fisher, R. A. (1928). Further note on the capillary forces in an ideal soil. *Journal of Agricultural Science,* 18 (3): 407-410.

Fleureau, J. M., Hadiwardoyo, S., Dufour-Laridan, E., Langlois, V. & A.G., C. (2002). Influence of suction on the dynamic properties of a silty sand. *Proc. of 3rd Int. Conf. on Unsaturated Soils, Recife, Brazil,* 2, 463-471.

Fredlund, D. G., Fredlund, M. D. & Wilson, G. W. W. (2002). Use of the grain-size distribution for estimation of the soil-water characteristic curve. *Canadian Geotechnical Journal,* 39 (5): 1103-1117.

Fredlund, D. G., Fredlund, M. G. & Wilson, G. W. (1997). Prediction of the soil-water characteristic curve from grain-size distribution and volume-mass properties. *Proc. of 3rd Brazilian Symposium on Unsaturated Soils, Rio de Janeiro,* 13-23.

Fredlund, D. G. & Morgenstern, N. R. (1977). Stress state variables for unsaturated soils. *Journal of the Geotechnical Engineering Division,* 103 (GT5): 447-466.

Fredlund, D. G. & Oloo, S. Y. (1995). Matric suction monitoring in an expansive soil subgrade in Kenya. *Proc. of 1st Int. Conf. on Unsaturated Soils, Paris,* 1, 631-635.

Fredlund, D. G. & Rahardjo, H. (1993). *Soil mechanics for unsaturated soils,* New York, John Wiley & Sons Inc.

Fredlund, D. G. & Xing, A. (1994). Equations for the soil-water characteristic curve. *Canadian Geotechnical Journal,* 31 (3): 521-532.

Fredlund, D. G., Xing, A. & Huang, S. (1994). Predicting the permeability function for unsaturated soils using the soil-water characteristic curve. *Canadian Geotechnical Journal,* 31 (3): 533-546.

Frost, J. D. & Park, J. Y. (2003). A critical assessment of the moist tamping technique. *Geotechnical Testing Journal,* 26 (1): 57-70.

Fung, Y. C. (1994). *A first course in Continuum Mechanics,* 3rd. New York, Prentice Hall.

Gallipoli, D., Wheeler, S. J. & Karsunen, M. (2003). Modelling the variation of degree of saturation in a deformable unsaturated soil. *Géotechnique,* 53 (1): 105-112.

Geo-observations. (2011). Geotechnical Observations [Online], Available from: http://www.geo-observations.com/Equipment/index.html, 22nd March 2011.

Gili, J. A. & Alonso, E. E. (2002). Microstructural deformation mechanisms of unsaturated granular soils. *Int. Journal for Numerical and Analytical Methods in Geomechanics,* 26 (5): 433-468.

Gräbe, P. J., (2002). Resilient and permanent deformation of railway foundations under principal stress rotation, *PhD Thesis,* Civil Engineering, University of Southampton.

Gräbe, P. J. & Clayton, C. R. I. (2003). Permanent deformation of railway foundations under heavy axle loading. *Proc. of Int. Heavy Haul Conf.,* 325-333.

Gräbe, P. J. & Clayton, C. R. I. (2009). Effects of principal stress rotation on permanent deformation in rail track foundation. *Journal of Geotechnical and Geoenvironmental Engineering,* 135 (4): 555-565.

Gräbe, P. J., Clayton, C. R. I. & Shaw, F. J. (2005). Deformation measurement on a heavy haul track formation. *Proc. 8th Int. Heavy Haul Conf.* Rio de Janeiro, Brazil: 287-295.

Haines, W. B. (1925). Studies in the physical properties of soils II. A note on the cohesion developed by capillary forces in an ideal soil. *Journal of Agricultural Science,* 15 (4): 529-535.

Haines, W. B. (1927). Studies in the physical properties of soils IV. A further contribution to the theory of capillary phenomena in soil. *Journal of Agricultural Science,* 7 (12): 264-290.

Hamblin, A. P. (1981). Filter-paper method for routine measurement of field water potential. *Journal of Hydrology,* 53 (3/4): 355-360.

Hardin, B. O. (1978). The nature of stress-strain behaviour of soils. *Proc. of ASCE special conf. on Earthquake Engineering and Soil Dynamics, Pasadena,* 1, 3-90.

Hardin, B. O. & Black, W. L. (1968). Vibration modulus of normally consolidated clay. *Journal of Soil Mechanics and Foundation Division,* 94 (2): 353-369.

Hardin, B. O. & Drnevich, V. P. (1972a). Shear modulus and damping in soils: design equations and curves. *Journal of Soil Mechanics and Foundation Division,* 98 (SM7): 667-691.

Hardin, B. O. & Drnevich, V. P. (1972b). Shear modulus and damping in soils: measurement and parameter effects. *Journal of Soil Mechanics and Foundation Division,* 98 (SM6): 603-624.

Hardin, B. O. & Richart, F. E. J. (1963). Elastic wave velocities in granular soils. *Journal of Soil Mechanics and Foundation Division,* 89 (SM1): 33-65.

Hardin, K. O., Drnevich, V. P., Wang, J. & C.E., S. (1994). Resonant column testing at pressures up to 3.5MPa (500psi). IN Ebelhar, R. J., Drnevic, V. P. & Kutter, B. L. (Eds.) *Dynamic Geotechnical Testing II ASTM STP213.* Phaladelphia: American Society of Civil Engineers, 222-233.

Hilf, J. W., (1956). An investigation of Pore-Water pressure in compacted cohesive soils, *PhD Thesis,* Bureau of Reclamation Design and Construction Division, Technical Memorandum 654, United States Department of the Interior.

Hillel, D. & Mottes, J. (1966). Effect of plate impedance, wetting method, and aging on soil moisture retention. *Soil Science,* 102 (2): 135-139.

Imery Ceramics. (2005). Imerys data sheet silica flour [Online], Available from: http://www.hamgil.com/assets/documents/MSDS-HymodPrima.pdf, March 2010.

Indraratna, B. & Wadud, S. (2005). *Mechanics of ballasted rail tracks: A geotechnical perspective,* London, Taylor & Francis Group plc.

IPCC (2007). Summary for policymakers. IN Solomon, S., Qin, D., Manning, M., Chen, Z., Marquis, M., Averyt, K. B., Tignor, M. & Miller, F. (Eds.) *Climate change 2007: The physical science basis. Contribution of working group I to the fourth assessment report of the intergovernmental panel on climate change* Cambridge and New York, Cambridge University Press.

Janz, M. (2001). Technique for measuring moisture storage capacity at high moisture levels. *Journal of Materials in Civil Engineering,* 13 (5): 364-370.

Jennings, J. E. (1961). A revised effective stress law for use in the prediction of the behaviour of unsaturated soils. *Pore pressure and suction in soils conf. organized by the British National Soc. of the Int. Soc. of Soil Mechanics and Foundation Engineering, London,* 26-30.

Jennings, J. E. & Burland, J. B. (1962). Limitations to the Use of Effective Stresses in Partly Saturated Soils. *Géotechnique,* 12 (2): 125-144.

Kaye, G. W. C. & Laby, T. H. (1973). *Tables of Physical and Chemical Constants,* 14th. London, Longmans.

Khoury, N. N. & Zaman, M. M. (2004). Correlation between resilient modulus, moisture variation, and soil suction for subgrade soils. *Transportation Research Record,* 1874 99-107.

Kim, D.-G., Seo, W.-S. & Lee, S.-H. (2006). Development of modulus: Soil moisture model for subgrade soils using suction control testing system. *Pavement mechanics and performance Proc. of sessions of GeoShanghai, Shanghai, China,* 256 -263.

Kim, D.-S., Kweon, G.-C. & Lee, K.-W. (1997). Alternative method of determining resilient modulus of compacted subgrade soils using free-free resonant column test. *Transportation Research Record,* 1577 62-69.

Kim, D.-S., Seo, W.-S. & Kim, M.-J. (2003). Deformation characteristics of soils with variations of capillary pressure and water content. *Soils and Foundations Japanese Geotechnical Society,* 43 (4): 71-79.

Kim, D.-S. & Stokoe II, K. H. (1994). Characterization of resilient modulus of compacted subgrade soils using resonant column and torsional shear tests. *Transportation Research Record,* 1369 83-91.

Kim, T. C. & Novak, M. (1981). Resonant column technique for dynamic testing of cohesive soils. *Canadian Geotechnical Journal,* 18 (3): 448-455.

Krawczyk, J. V. (1969). An examination of methods of determining the specific gravity of soils. *Road Research Laboratory Report No. LR 272.* Crowthorne, Berkshire, Road Research Laboratory Ministry of Transport.

Kumar, J. & Clayton, C. R. I. (2007). Effect of sample torsional stiffness on resonant column test results. *Canadian Geotechnical Journal,* 44 (2): 221-230.

Kweon, G.-C. & Kim, D.-S. (2000). Deformational Characteristics of Subgrade Soils in Korea. *KSCE Journal of Civil Engineering,* 4 (2): 83-90.

Ladd, R. S. (1978). Preparing test specimens using undercompaction. *Geotechnical Testing Journal,* 1 (1): 16-23.

Laloui, L. (2010). *Mechanics of unsaturated geomaterials,* London, John Wiley & Sons.

Laloui, L. & Nuth, M. (2008). Effective stress concept in unsaturated soils: Clarification and validation of a unified framework. *Int. Journal for Numerical and Analytical Methods in Geomechanics,* 32 (7): 771-801.

Lambe, T. W. & Whitman, R. V. (1969). *Soil mechanics,* New York, John Wiley & Sons.

Lee, J. Y., Francisca, F. M., Santamarina, J. C. & Ruppel, C. (2010). Parametric study of the physical properties of hydrate-bearing sand, silt, and clay sediments: small-strain mechanical properties. *Journal of Geophysical Research,* 115 (B11104): 1-9.

Leong, E. C., He, L. & Rahardjo, H. (2002). Factors affecting the filter paper method for total and matric suction measurements. *Geotechnical Testing Journal,* 25 (3): 322-333.

Leong, E. C. & Rahardjo, H. (1997). Review of soil-water characteristic curve equations. *Journal of Geotechnical and Geoenvironmental Engineering,* 123 (12): 1106-1117.

Likos, W. J. & Lu, N. (2002). Filter paper technique for measuring total soil suction. *Transportation research record,* 1786 120-128.

Lourenco, S. D. N., Gallipoli, D., Toll, D. G., Augrade, C. E., Evans, F. D. & Medero, G. M. (2008). Calibrations of a high-suction tensiometer. *Géotechnique,* 58 (8): 659-668.

Lu, N. & Likos, W. J. (2004). *Unsaturated soil mechanics,* Hoboken, New Jersey, John Wiley & Sons.

Lu, N. & Likos, W. J. (2006). Suction stress characteristic curve for unsaturated soil. *Journal of Geotechnical and Geoenvironmental Engineering,* 132 (2): 131-142.

Madsen, H. B., Jensen, C. R. & Boysen, T. (1986). A comparison of the termocouple psychrometer and the pressure plate methods for determination of soil water characteristic curves. *Journal of Soil Science,* 37 (3): 357-362.

Mancuso, C., Silvestri, F. & Vinale, F. (1993). Stress-strain behaviour of a dam core material by field and laboratory dynamic tests. IN Anagnostospoulos, A., Frank, R., Kalteziotis, N. & Schlosser, F. (Eds.) *Proc. of Int. Symposium on Geotechnical Engineering of Hard Soils and Soft Rocks.* Athens, Brookfield

Mancuso, C., Vassallo, R. & D'Onofrio, A. (2002). Small strain behavior of a silty sand in controlled-suction resonant column torsional shear tests. *Canadian Geotechnical Journal,* 39 (1): 22-31.

Mancuso, C., Vassallo, R. & D'Onofrio, A. (2003). Small strain behaviour of soils in controlled suction conditions. *Proc. of 3rd Int. Conf. on Unsaturated Soils, Recife, Brazil,* 3, 917-928.

Marinho, F. A. M., Take, W. A. & Tarantino, A. (2008). Measurement of matric suction using tensiometric and axis translation techniques. *Journal of Geotechnical and Geological Engineering,* 26 (6): 615-631.

McQueen, I. S. & Miller, F. (1968). Calibration and evaluation of a wide-range gravimetric method for measuring moisture stress. *Soil Science,* 106 (3): 225-231.

Merchán, V., Vaunat, J. & Romero, E. (2010). The influence of drying on the small strain shear modulus for static compacted boom clay. *Proc. of 4th Asia-Pacific Conf. on Unsaturated Soils, Newcastle Australia,* 1, 141-145.

Mitchell, J. (2005). *Fundamentals of soil behaviour,* 3rd edn. John Wiley and Sons.

Mondolfo, L. F. (1976). *Aluminum alloys: structure and properties,* Butterworths, London.

Monroy, R., Zdravkovic, L. & Ridley, A. M. (2010). Evolution of microstructure in compacted London Clay during wetting and loading. *Géotechnique,* 60 (2): 105-119.

Munoz-Castelblanco, J. A., Pereira, J.-M., Delage, P. & Cui, Y.-J. (2011). Suction measurements on natural unsaturated soil: A reappraisal of the filter paper method. *Proc. of 5th Int. Conf. on Unsaturated Soils, Barcelona, Spain,* 707-712.

Murphy, J. M., Sexton, D. M. H., Jenkins, G. J., Boorman, P. M., Booth, B. B. B., Brown, C. C., Clark, R. T., Collins, M., Harris, G. R., Kendon, E. J., Betts, R. A., Brown, S. J., Howard, T. P., Humphrey, K. A., McCarthy, M. P., McDonald, R. E., Stephens, A., Wallace, C., Warren, R., Wilby, R. & Wood, R. A. (2009). *UK climate projections science report: Climate change projections*. Met Office Hadley Centre, Exeter.

Murray, E. J. & Sivakumar, V. (2010). *Unsaturated soils - A fundamental interpretation of soil behaviour,* 1st Edn. London, Wiley-Blackwell.

Ng, C. W. W. & Menzies, B. (2007). *Advanced unsaturated soil mechanics and engineering,* 1st Edn. New York, Taylor and Francis.

Ng, C. W. W. & Pang, Y. W. (2000). Influence of stress state on soil-water characteristics and slope stability. *Journal of Geotechnical and Geoenvironmental Engineering,* 26 (2): 157-166.

Olson, R. E. & Langfelder, L. J. (1965). Pore water pressures in unsaturated soils. *ASCE: Journal of the Soil Mechanics and Foundations Division*, 91 (SM4): 127-149.

Pineda, J. A., Lima, A. & Romero, E. (2008). Influence of hydraulic paths on the low-strain shear modulus of a stiff clay. *Proc. of the 1st European Conf. on Unsaturated Soils, Durham,* 519-523.

Powrie, W., Yang, L. A. & Clayton, C. R. I. (2007). Stress changes in the ground below ballasted railway track during train passage. *Proc. IMechE Part F. J. Rail and Rapid Transit,* 221 (2): 247-262.

Priest, J. A., (2004). The effects of methane gas hydrate on the dynamic properties of sand, *PhD Thesis,* Civil Engineering, University of Southampton.

Priest, J. A., Powrie, W., Yang, L., Clayton, C. R. I. & Gräbe, P. J. (2010). Measurements of transient ground movements below a ballasted railway line. *Géotechnique,* 60 (9): 667-677.

Proctor, R. R. (1933). The design and construction of rolled-earth dams. *Engineering New Record,* 111 (9): 245-248.

Qian, X., Gray, H. D. & Woods, R. D. (1991). Resonant column tests on partially saturated sands. *Geotechnical Testing Journal,* 14 (3): 266-275.

Qian, X., Gray, H. D. & Woods, R. D. (1993). Voids granulometry: Effects on shear modulus of unsaturated sands *Geotechnical Testing Journal,* 199 (2): 295-314.

Rees, E. V. L., (2009). The effect of natural and synthesised methane gas hydrate on the stiffness of some sediments, *PhD Thesis,* Civil Engineering, University of Southampton.

Ridley, A. M. (1995). Discussion on "Laboratory filter paper suction measurements" by Sandra L. Houston, William N. Houston, and Anne-Marie Wagner. *Geotechnical Testing Journal,* 18 (3): 391-396.

Ridley, A. M. & Burland, J. B. (1993). A new instrument for the measurement of soil moisture suction. *Géotechnique,* 43 (2): 321-324.

Ridley, A. M. & Burland, J. B. (1994a). Discussion: A new instrument for the measurement of soil moisture suction. *Géotechnique,* 44 (3): 551-556.

Ridley, A. M. & Burland, J. B. (1994b). A new device for the direct measurement of soils suction over a wide range. IN Fookes, P. G. & Parry, R. H. G. (Eds.) *Engineering Characteristics of Arid Soils.* Rotterdam: A.A.Balkema, 289-301.

Ridley, A. M. & Burland, J. B. (1999). Use of the tensile strength of water for the direct measurement of high soils suction: Discussion. *Canadian Geotechnical Journal,* 36 (1): 178-180.

Ridley, A. M., Dineen, K., Burland, J. B. & Vaughan, P. R. (2003). Soil matrix suction: some examples of its measurement and application in geotechnical engineering. *Géotechnique,* 53 (2): 241-253.

Romero, E., Facio, J. A., Lloret, A., Gens, A. & Alonso, E. E. (1997). A new suction and temperature controlled triaxial apparatus. *Proc. 14th Int. Conf. on Soil Mechanics and Foundation Engineering, Balkema,* 1, 185-188.

Romero, E. E., Gens, A. & Lloret, A. (1999). Water permeability, water retention and micorstructure of unsaturated compacted Boom Clay. *Engineering Geology,* 54 (1): 117-127.

Romero, E. E. & Simms, P. H. (2008). Microstructure investigation in unsaturated soils: A review with special attention to contribution of mercury intrusion porosimetry and environmental scanning electron microscopy. *Journal of Geotechnical and Geological Engineering,* 26 (6): 705-727.

Selig, E. T. & Waters, J. M. (Eds.) (1994). *Track geotechnology and structure management,* London, Thomas Telford Publications.

Sherwood, P. T. (1970). The reproducibility of the results of soil classification and compaction tests. *Road Research Laboratory Report No. LR 339.* Crowthorne, Berkshire, Road Research Laboratory Ministry of Transport.

Sherwood, P. T. & Ryley, M. D. (1968). An examination of cone-penetrometer methods for determining the liquid limit of soils. *Road Research Laboratory Report No. LR233.* Crowthorne, Berkshire, Road Research Laboratory Ministry of Transport.

Sibelco Minerals and Chemicals LTD (2000a). Oakamoor HPF4 silica flour specification (issue 3).

Sibelco Minerals and Chemicals LTD (2000b). Oakamoor HPF5 silica flour specification (issue 3).

Sivakumar, V., Sivakumar, R., Murray, E. J., Mackinnon, P. & Boyd, J. (2010). Mechanical behaviour of unsaturated kaolin (with isotropic and anisotropic stress history) Part 1: wetting and compression behaviour. *Géotechnique,* 60 (8): 581-594.

Tarantino, A., Gallipoli, D., Augrade, C. E., De Gennaro, V., Gomez, R., Laloui, L., Mancuso, C., El Mountassir, G., Munox, J. J., Pereira, J.-M., Peron, H., Pisoni, G., Romero, E., Raveemdoraraj, A., Rojas, J. C., Toll, D. G., Tombolato, S. & Wheeler, S. J. (2011). Benchmark of experimental techniques for measuring and controlling suction. *Géotechnique,* 61 (4): 303-312.

Terzaghi, K. (1936). The shearing resistance of saturated soils and the angle between the planes of shear. *Proc. of 1st Int. Conf. on Soil Mechanics and Foundation Engineering,* 1, 54-56.

The kaolin and ball clay association.UK. (2011). Ball Clay/Plastic Clay [Online], Available from: http://www.kabca.org/what-is-ball-clay-.php, 27th August 2011.

Thom, R., Sivakumar, R., Sivakumar, V., Murray, E. J. & Mackinnon, P. (2007). Pore size distribution of unsaturated compacted kaolin: the initial states and final states following saturation. *Géotechnique,* 57 (5): 469-474.

Tinjum, J. M., Benson, C. H. & Blotz, L. R. (1997). Soil water characteristic curves for compacted clays. *Journal of Geotechnical and Geoenvironmental Engineering,* 123 (11): 1060-1069.

Toll, D. G. (1990). A framework for unsaturated soil behaviour. *Géotechnique,* 40 (1): 31-44.

Transport and Road Research Laboratory (1973). *Soil mechanics for road engineers,* Her Majesty's Stationery Office.

Van Genuchten, M. T. (1980). A closed-form equation for predicting the hydraulic conductivity of unsaturated soils. *Soil Science*, 44 (5): 892-892.

Vanapalli, S. K., Sillers, W. S. & Fredlund, M. G. (1998). The meaning and relevance of residual state to unsaturated soils. *51st Canadian Geotechnical Conf., Edmonton, Alberta*, 1, 101-108.

Vassallo, R., Mancuso, C. & Vinale, F. (2006). Effects of stress-strain history on the initial shear stiffness of an unsaturated compacted silt. *Proc. of 4th Int. Conf. on Unsaturated Soils, Carefree, Arizona*, 1, 1145-1156.

Vassallo, R., Mancuso, C. & Vinale, F. (2007a). Effects of net stress and suction history on the small strain stiffness of a compacted clayey silt. *Canadian Geotechnical Journal*, 44 (4): 447-462.

Vassallo, R., Mancuso, C. & Vinale, F. (2007b). Modelling the influence of stress-strain history on the initial shear stiffness of an unsaturated compacted silt. *Canadian Geotechnical Journal*, 44 (4): 463-472.

Vinale, F., D'Onofrio, A., Santucci de Magistric, F. & Tatsuoka, F. (2001). The pre-failure behaviour of soils as construction materials. *Proc. of 2nd Int. Conf. on Pre-Failure Deformation Characteristics of Geomaterials, Torino, Italy*, 2, 995-1007.

Wang, X. & Benson, C. H. (2004). Leak-free pressure plate extractor for measuring the soil water characteristic curve. *Geotechnical Testing Journal*, 27 (2): 1-9.

Wheeler, S. J., Sharma, R. S. & Buisson, M. S. R. (2003). Coupling of hydraulic hysteresis and stress-strain behaviour in unsaturated soils. *Géotechnique*, 53 (1): 41-54.

Wu, S., Gray, H. D. & Richart, F. E. (1984). Capillary effects on dynamic modulus of sands and silts. *Journal of Geotechnical and Geoenvironmental Engineering*, 110 (9): 1188 - 1203.

Wu, S., Gray, H. D. & Richart, F. E. (1985). Capillary effect on shear modulus at high strains. *Proc. of 11th Int. Conf. on Soil Mechanics and Foundation Engineering, San Francisco*, 2, 1091-1094.

Yang, D. Q., Rahardjo, H. & Alonso, E. E. (1998). Modelling the volumetric behaviour of an unsaturated expansive soil. *Proc. 2nd Int. Conf. on Unsaturated Soils, Beijing*, 2, 977-983.